CANADIAN THESES ON MICROFICHE

I.S.B.N.

THESES CANADIENNES SUR MICROFICHE

National Library of Canada
Collections Development Branch

Canadian Theses on
Microfiche Service

Ottawa, Canada
K1A 0N4

Bibliothèque nationale du Canada
Direction du développement des collections

Service des thèses canadiennes
sur microfiche

NOTICE

The quality of this microfiche is heavily dependent upon the quality of the original thesis submitted for microfilming. Every effort has been made to ensure the highest quality of reproduction possible.

If pages are missing, contact the university which granted the degree.

Some pages may have indistinct print especially if the original pages were typed with a poor typewriter ribbon or if the university sent us a poor photocopy.

Previously copyrighted materials (journal articles, published tests, etc.) are not filmed.

Reproduction in full or in part of this film is governed by the Canadian Copyright Act, R.S.C. 1970, c. C-30. Please read the authorization forms which accompany this thesis.

AVIS

La qualité de cette microfiche dépend grandement de la qualité de la thèse soumise au microfilmage. Nous avons tout fait pour assurer une qualité supérieure de reproduction.

S'il manque des pages, veuillez communiquer avec l'université qui a conféré le grade.

La qualité d'impression de certaines pages peut laisser à désirer, surtout si les pages originales ont été dactylographiées à l'aide d'un ruban usé ou si l'université nous a fait parvenir une photocopie de mauvaise qualité.

Les documents qui font déjà l'objet d'un droit d'auteur (articles de revue, examens publiés, etc.) ne sont pas microfilmés.

La reproduction, même partielle, de ce microfilm est soumise à la Loi canadienne sur le droit d'auteur, SRC 1970, c. C-30. Veuillez prendre connaissance des formules d'autorisation qui accompagnent cette thèse.

THIS DISSERTATION
HAS BEEN MICROFILMED
EXACTLY AS RECEIVED

LA THÈSE A ÉTÉ
MICROFILMÉE TELLE QUE
NOUS L'AVONS REÇUE

NL-339 (r. 82/08)

Canada

0-315-19394-8

National Library of Canada
Bibliothèque nationale du Canada

Canadian Theses Division
Division des thèses canadiennes

Ottawa, Canada
K1A 0N4

67302

PERMISSION TO MICROFILM — AUTORISATION DE MICROFILMER

• Please print or type — Écrire en lettres moulées ou dactylographier

Full Name of Author — Nom complet de l'auteur

ANNA MARIA VENEZIA - FLORIANO

Date of Birth — Date de naissance
15 / 4 / 1954

Country of Birth — Lieu de naissance
ITALY

Permanent Address — Résidence fixe

UNIVERSITY OF ALBERTA CHEMISTRY DEPARTMENT

Title of Thesis — Titre de la thèse

CHEMICAL AND THRESHOLD IONIZATION EFFECTS IN PHOTOELECTRON AND AUGER SPECTRA OF MOLECULES

University — Université

UNIVERSITY OF ALBERTA

Degree for which thesis was presented — Grade pour lequel cette thèse fut présentée

Ph. D

Year this degree conferred — Année d'obtention de ce grade
1984

Name of Supervisor — Nom du directeur de thèse
R. G. CAVELL

Permission is hereby granted to the NATIONAL LIBRARY OF CANADA to microfilm this thesis and to lend or sell copies of the film.

The author reserves other publication rights, and neither the thesis nor extensive extracts from it may be printed or otherwise reproduced without the author's written permission.

L'autorisation est, par la présente, accordée à la BIBLIOTHÈQUE NATIONALE DU CANADA de microfilmer cette thèse et de prêter ou de vendre des exemplaires du film.

L'auteur se réserve les autres droits de publication; ni la thèse ni de longs extraits de celle-ci ne doivent être imprimés ou autrement reproduits sans l'autorisation écrite de l'auteur.

Date
August 16 1984

Signature
Anna Maria Venezia Floriano

NL-91 (4/77)

THE UNIVERSITY OF ALBERTA

CHEMICAL AND THRESHOLD IONIZATION EFFECTS IN PHOTOELECTRON AND AUGER SPECTRA OF MOLECULES

by

© ANNA MARIA VENEZIA-FLORIANO

A THESIS

SUBMITTED TO THE FACULTY OF GRADUATE STUDIES AND RESEARCH

IN PARTIAL FULFILMENT OF THE REQUIREMENTS FOR THE DEGREE

OF DOCTOR OF PHILOSOPHY

DEPARTMENT OF CHEMISTRY

EDMONTON, ALBERTA

FALL, 1984

T H E U N I V E R S I T Y O F A L B E R T A

RELEASE FORM

NAME OF AUTHOR ANNA MARIA VENEZIA-FLORIANO

TITLE OF THESIS CHEMICAL AND THRESHOLD IONIZATION EFFECTS IN PHOTOELECTRON AND AUGER SPECTRA OF MOLECULES

DEGREE FOR WHICH THESIS WAS PRESENTED Ph.D.

YEAR THIS DEGREE GRANTED 1984

Permission is hereby granted to THE UNIVERSITY OF ALBERTA LIBRARY to reproduce single copies of this thesis and to lend or sell such copies for private, scholarly or scientific research purposes only.

The author reserves other publication rights, and neither the thesis nor extensive extracts from it may be printed or otherwise reproduced without the author's written permission.

Anna Maria Venezia Fl.

(Signed)

PERMANENT ADDRESS:

Via Duca Degli Abruzzi 2
Palermo
Italy

DATED August 16 1984

THE UNIVERSITY OF ALBERTA

FACULTY OF GRADUATE STUDIES AND RESEARCH

The undersigned certify that they have read, and recommend to the Faculty of Graduate Studies and Research, for acceptance, a thesis entitled

CHEMICAL AND THRESHOLD IONIZATION EFFECTS IN PHOTOELECTRON AND AUGER SPECTRA OF MOLECULES.

submitted by Anna Maria Venezia-Floriano

in partial fulfilment of the requirements for the degree of Doctor of Philosophy

R.G. Cavell (Supervisor)

S. Huzinaga

M. Keil

J. Takats

R. Egerton, Dept. of Physics

G.M. Bancroft (External Examiner)
University of Western Ontario

DATE August 2, 1984

To my parents and my husband

ABSTRACT

Germanium $L_{2,3}M_{2,3}M_{4,5}$ and $L_{2,3}M_{4,5}M_{4,5}$ Auger spectra excited by Al $K\alpha_{1,2}$ radiation were measured in a series of Germanium compounds. Energies and intensities were calculated by theoretical models based on a mixed coupling scheme using jj coupling for the initial state and LS coupling for the final state. Relaxation contributions were evaluated and shown to vary with the polarizabilities of the molecules.

Excitation of the same levels of Germanium by Mg $K\alpha_{1,2}$ radiation, which has an energy close to the Ge L_2 binding energy threshold, yielded spectral effects known as the Post Collision Interaction (PCI) effects which are due to the interaction of slow ejected electrons with the fast Auger electron. A spectator satellite arising from excitation of a core electron to a bound outer level of the molecule was also observed. A pronounced dependence of the Auger final state configuration was shown to occur by comparison of the $L_{2,3}M_{4,5}M_{4,5}$ and $L_{2,3}M_{2,3}M_{4,5}$ spectra.

Tin $M_{4,5}N_{4,5}N_{4,5}$ Auger spectra in Tetramethyltin and Hexamethylditin were measured and compared to that of metallic Tin. Energies and intensities were in agreement with theory based on a mixed coupling scheme with jj

coupling for the initial state and intermediate coupling in the final state.

The valence Auger spectra of Oxygen and Fluorine in OF_2 and Boron and Fluorine in BF_3 were also measured. Intensities and energies of these spectra were analyzed according to a simplified Molecular Orbital treatment. The calculated intensities reproduced reasonably well the experimental shape of the spectra, but large discrepancies appeared between the calculated and experimental energies. Values for the energies of the doubly charged ions OF_2^{2+} and BF_3^{2+} were obtained from the highest energy normal Auger line of these valence Auger spectra.

Chlorine $KL_{2,3}L_{2,3}(^1D_2)$ Auger and Chlorine $2p_{3/2}$ photoelectron energies were measured in Chloromethane and Chlorosilane derivatives to evaluate the relative contribution of initial and final state effects to photoelectron and Auger processes in molecules wherein the central atom bonding may involve d orbitals. These effects, expressed by the differences in potential contributions, ΔV and in relaxation contributions, ΔR, were obtained from the differences of core photoelectron and Auger shifts. The Transition Potential Model (TPM) provided a satisfactory interpretation of chemical shifts in both series and no evidence of d-orbital participation from Silicon in chemical bonding was apparent.

ACKNOWLEDGEMENTS

The author wishes to thank her supervisor Professor R.G. Cavell for his help and guidance during the course of this study. She also thanks the other members of the research group, in particular Dr. J. Väyrynen and especially Dr. C. Pua. Thanks are also due to the staff in the departmental workshops for their capable assistance.

Appreciation is due to Annabelle Wiseman for the typing of this thesis.

The author also acknowledges her gratitude to her husband Antonio for his invaluable help and encouragement.

TABLE OF CONTENTS

LIST OF TABLES

LIST OF FIGURES

CHAPTER I

INTRODUCTION

A. General Introduction

Ionization of a medium by radiation leads to the production of photoelectrons and Auger electrons.

Photoelectron Spectroscopy (PES) and Auger Electron Spectroscopy (AES) each involve the experimental determination of the energy distribution of photoelectrons and Auger electrons respectively. Photoelectrons are produced in the photoionization process according to Einstein's law[1]

$$E_k = h\nu - E_B \qquad \text{I-1}$$

E_k is the kinetic energy of the ejected electron which is the measured quantity in the experiment, $h\nu$ is the energy of the radiation, E_B is the ionization energy (or binding energy) for the electron from a particular level. A feature of the experiment is that, provided the photon is sufficiently energetic, many different levels in the

species may be ionized, thus a spectrum is produced which reveals all accessible energy levels as a distribution of photoelectrons with kinetic energies governed by equation I-1 for each molecular level.

Auger electrons are produced when a molecule containing an inner shell vacancy or hole undergoes a radiationless decay in competition to the radiative decay (X-ray fluorescence).

B. Historical Aspects

The two phenomena, photoionization and Auger emission, have been known for a long time; in 1905 Einstein[1] explained the photoelectric effect, while Pierre Auger[2] discovered in 1923 the effect now named after him. However, the field of photoelectron spectroscopy did not grow immediately after the discovery of the physical phenomenon. The reason for the delay was the inadequate technology which did not allow high resolution measurements of the electron energies. The study of beta ray spectra of atoms, requiring the accurate measurement of the discrete energies of electrons ejected during internal conversion, gave impetus for the improvement of the techniques of electron spectroscopy.

Present day high-resolution PES, grew out of two parallel developments that occurred principally in Uppsala, Sweden and at the Imperial College in London, England. The thrust of the Uppsala research was the determination of electron binding energies from the atomic shells by photoelectron spectroscopy. As a result of this program it was discovered that the binding energies of the core electrons were dependent on the chemical environment.[3] To study these changes in binding energy a spectrometer capable of measuring electrons with approximately 1 keV energy with a resolution better than 0.1% is necessary. The beta ray (electron) spectrometers developed for nuclear physics research easily met this requirement. Meanwhile, Turner and Al-Jobury[4] in England were using photoelectron spectra excited by low energy sources such as He^{I} resonance lamps to study the binding energies of the electrons in valence orbitals. The lower energies of the electrons place less stringent requirements on the analyzer (but stray magnetic fields can be more damaging to the instrumental capability).

Depending on the energy of the radiation used as the excitation source, PES is often subdivided into XPS (X-ray Photoelectron Spectroscopy) or ESCA (Electron Spectroscopy for Chemical Analysis) and UPS (Ultraviolet Photoelectron

Spectroscopy). XPS, in which the incident radiation is in the X-ray energy range, probes the non-bonding core electrons which have energies characteristic of a particular chemical element. UPS, in which the incident radiation is in the vacuum ultraviolet energy range, probes the energy distribution of valence electrons. PES allows investigation of electronic structure, providing a direct picture of molecular orbitals for gas phase species and valence bands (densities of states) in the solid state.

In this thesis XPS and AES have been applied to the study of various aspects of atomic and molecular properties of different chemical compounds. For clarity, this thesis is organized in separate chapters, each consisting of Introduction, Experimental, Results and Conclusions sections. In this first introductory chapter only a general description of the processes is given and a more detailed discussion of the theoretical aspects will be found in the subsequent chapters.

C. Description of the Various Processes

In Figure I-1 are shown the different processes which can occur in electron spectroscopy. Both X-rays (K, L, M, ...) and orbital (1s, 2s, 2p, ...) notations for the

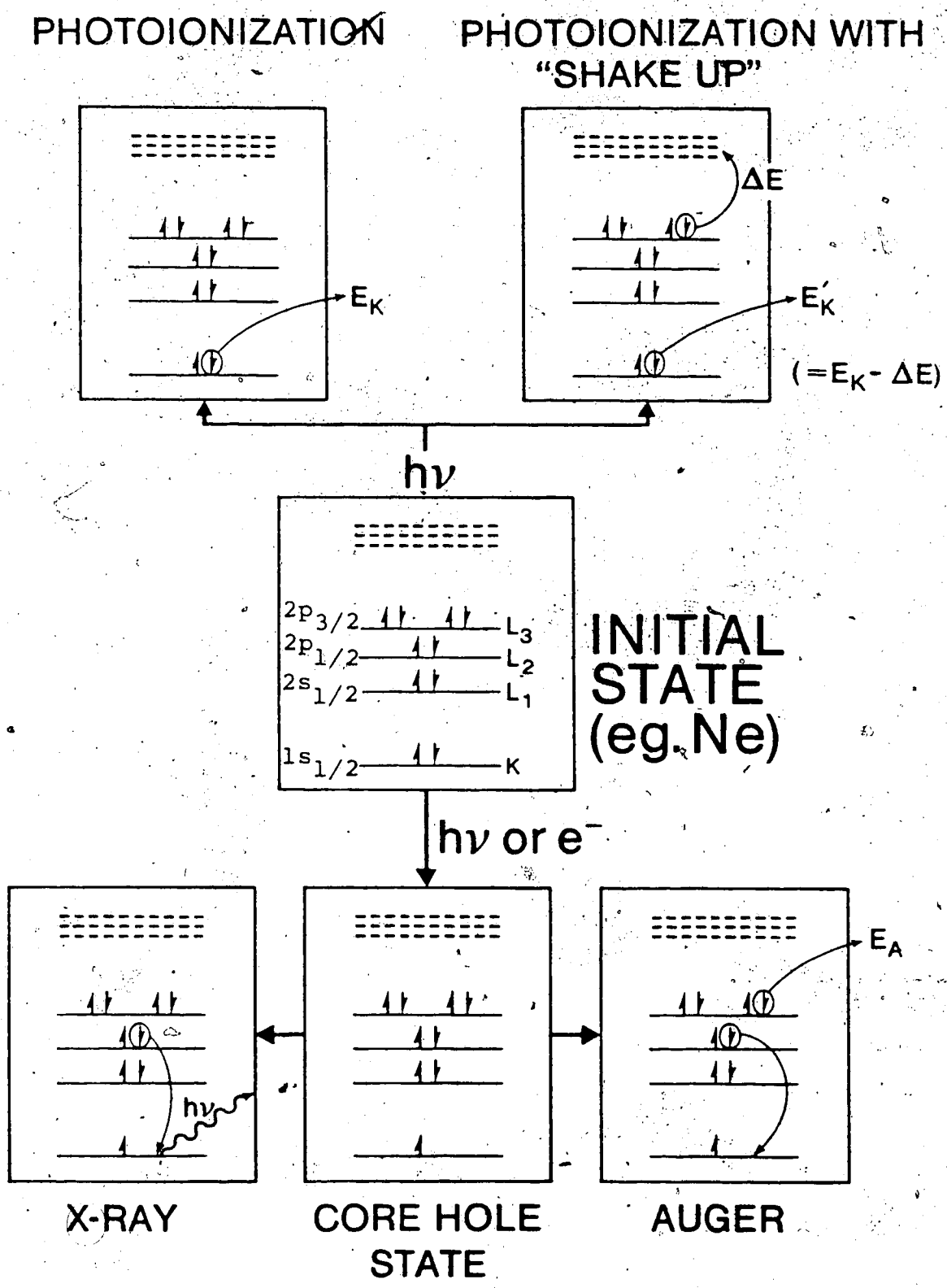

Figure I-1. Processes involved in electron spectroscopy.

electron energy levels are used in the figure to show the correspondences in nomenclature.

1. Photoionization

When a molecule or atom A is bombarded with photons of energy $h\nu$, the simplest process that can occur is a transition from the initial state to a final state constituted by an ion A_k^+ with a hole in a level k plus a free electron.

$$h\nu + A \rightarrow A_k^+ + e^- \qquad \text{I-2}$$

Conservation of energy dictates that the energy of the ion relative to that of the molecule plus the kinetic energy of the electron is equal to the energy of the incident photon. The recoil energy of the ion is considered to be zero because the mass of the ion is three orders of magnitude larger than that of the electron, and by conservation of energy and momentum, it can be shown that its recoil energy is negligible. The energy balance relative to the process described by equation I-2 is the following:

$$h\nu - E_k = E(A_k^+) - E(A) \equiv E_B \qquad \text{I-3}$$

where E_k is the kinetic energy of the photoelectron, and E_B is the binding energy of a level k. This binding energy is equal to the difference between the total energy of the initial state (the molecule) E(A) and that of the final ion state $E(A_k^+)$.

In quantum mechanical terms the probability for the occurrence of the process described in equation I-2 is proportional to the square of the transition moment integral[5]

$$M = \langle \phi'' | \Sigma p | \phi' \rangle \qquad \text{I-4}$$

where p is the dipole moment operator. The sum extends over all electrons and nuclei. ϕ'' and ϕ' are the wave functions associated with the initial state and the final state respectively. The Born-Oppenheimer approximation allows separation of the wavefunctions into the product of electronic and nuclear functions. Neglecting the rotational contribution to the nuclear function because in PES, rotational structure is unresolved, equation I-4 becomes

$$M = \int \phi_v''^*(R)\phi_v'(R)dR \int \phi_e''^*(r;R) | \Sigma p_e | \phi_e'(r;R)dR \qquad \text{I-5}$$

where p_e is the electronic dependent part of the dipole moment. The first integral is related to the so-called Franck-Condon factor and it is responsible for the relative intensities of the vibrational bands in photoionization transitions. In XPS, however, the vibrational structure is not observed because the vacancies are produced in core levels, and in general transitions occur to the ground state vibrational level of the ion. Furthermore, lifetime effects (and excitation linewidths) lead to bands in which the small vibrational contributions are obscured. The second integral in equation I-5 is the matrix element of the electric dipole moment for a given nuclear configuration (R). For a photoelectron transition to be allowed, this integral must be non-zero. The transition from the initial state of molecule plus photon, to ion plus electron, is restricted by the dipole selection rules $\Delta L=\pm 1$, $\Delta S=0$ but because the free electron can leave the ion carrying whatever angular momentum is needed to satisfy these rules, the photoionization process can be considered to have no selection rules and the analysis of the principal peaks can be carried out within the framework of a one-electron transition model.

The photoelectron spectrum of a material yields several kinds of information. Most obviously, it provides a series of ionization energies relating to various states of the singly ionized system. In addition, the intensity distribution reveals information concerning the photoionization cross-section, or the probability of the process, and the angular distribution of the photoelectrons.[6] The photoionization cross-section of a material is the total probability of ionizing it with a photon of given energy. It is a function of the photon energy. The sum of the intensities (that is areas) of the PE bands provides a proportional measure of the photoionization cross-section, while individually the PE band intensities give a measure of the partial photoionization cross-section for each of the different ionization processes that are energetically possible. The spatial distribution of photoelectrons is usually highly anisotropic. If θ is the angle between the direction of propagation of the photons (which are assumed to be unpolarized) and the direction of the outgoing electrons, then the angular variation of the intensity of a photoelectron peak is of the form[5]

$$I(\theta) \propto 1 + \frac{1}{2}\beta\left(\frac{3}{2}\sin^2\theta - 1\right) \qquad \text{I-6}$$

β is called the asymmetry parameter; it depends on the nature of the given molecular orbital and its value ranges from +2 to -1. For a spherical symmetric distribution of charge, such as for an atomic s orbital, the value of β is +2, the emergent photoelectron has a preferred orientation direction at a 90° angle to the photon beam. The β value provides an important clue as to the nature of the molecular orbitals. For $\theta = 54°44'$, the angular term vanishes and the intensity distribution is independent of the asymmetry parameters.

Auger emission from an excited (core-hole) molecular state in free molecule is not dependent on the orientational properties of the excitation source.

This thesis is not however concerned with the aspects of photoionization cross-section or angular dependences in photoelectron spectroscopy but only with the kinetic energy analysis of photoelectrons and Auger spectroscopy.

2. Multielectron Excitation

The photoionization with "shake up" illustrated in Figure I-1 is a two electron transition in contrast to the one electron transition we have considered above. The process is the result of a sudden change in the central potential of an atom felt by an outer shell electron when

a vacancy is suddenly produced in one of the inner shells by photoelectron ejection. Two types of two-electron transition can be distinguished, depending upon whether the outer shell electron, as a consequence of this change of potential, is excited to a higher bound-state (shake-up)[7,8] or to an unbound continuum state (shake-off).[9,10] The first process (shake-up) will appear as a discrete satellite photoelectron line at a kinetic energy lower than the main line by the difference between the ground and excited states of the ion with the core vacancy. The shake-off will appear as a continuous spectrum rising smoothly from a lower kinetic energy to a threshold whose energy distance for the main peak is equal to the ionization potential for the ground state of the ion with a core vacancy.

These kinds of transitions result in an ionic state of the same angular momentum as the primary hole state and a continuum function with an angular momentum that yields an overall state symmetry required by the dipole selection rules. Recently,[11] it has become apparent that these satellites arise from a configuration interaction with the primary hole state, and they can be treated as the primary photoionization process because they are fundamentally equivalent. They both involve a one electron dipole transition but to two different final states.

3. X-ray Fluorescence and the Auger Process

When a vacancy is formed in one of the inner shells of an atom, it may be filled by either a radiative (X-ray fluorescence) or a non-radiative (Auger) transition (Figure I-1). In X-ray fluorescence, the excess energy is released in the form of a photon, whereas in the Auger process the excess energy is carried away by an electron. Comparison of the relative transition probabilities of these two competing processes have been made.[12] If we have N_K K-vacancies, we have then a number of K-series X-ray quanta = $N_{\gamma K}$ and a number of K-series Auger electrons = N_{AK}. The corresponding transition probabilities are $P_{\gamma K}$ and P_{AK}. Defining the K-shell fluorescence yield, ω_K and the K-shell Auger yield a_K:

$$\omega_K = \frac{N_{\gamma K}}{N_K} = \frac{P_{\gamma K}}{P_{\gamma K} + P_{AK}} \qquad \text{I-7}$$

$$a_K = \frac{N_{AK}}{N_K} = \frac{P_{AK}}{P_{AK} + P_{\gamma K}} \qquad \text{I-8}$$

with $\omega_K + a_K = 1$.

In the case of L shell the Coster-Kronig yield, $f_{L_i L_k}$, must be added. These transitions[13] are of the types $L_i L_k X_q$, $M_i M_p X_q$ and so on, involving an electron

transition between two L, M, ... subshells, the released energy being carried away by an electron from an outer shell. The $f_{L_iL_k}$ is defined by: $f_{L_iL_k} = N_{L_iL_k}/N_{L_i}$ where $N_{L_iL_k}$ is the number of Coster-Kronig transitions L_iL_kX.

Figure I-2 shows the experimental fluorescence yield ω_K as a function of the atomic number Z. The strong dependence on atomic number Z arises from the expression of the propability $P_{\gamma K}$ for emission of radiation

$$P_{\gamma K} \propto \nu^3 |\langle f|r|i\rangle|^2 \qquad \text{I-9}$$

ν being the transition frequency. In the hydrogenic approximation the transition energy $h\nu$ is proportional to Z^2 and the dipole matrix element $\langle f|r|i\rangle$ depends on Z as $\langle f|r|i\rangle \sim \frac{1}{Z}$, therefore

$$P_{\gamma K} = KZ^6 \cdot \frac{k'}{Z^2} = aZ^4 \qquad \text{I-10}$$

In the same hydrogenic limit, the probability for Auger transitions is independent of Z, i.e. $P_{AK} = b$. This gives

$$\omega_K = \frac{aZ^4}{b + aZ^4} \qquad \text{I-11}$$

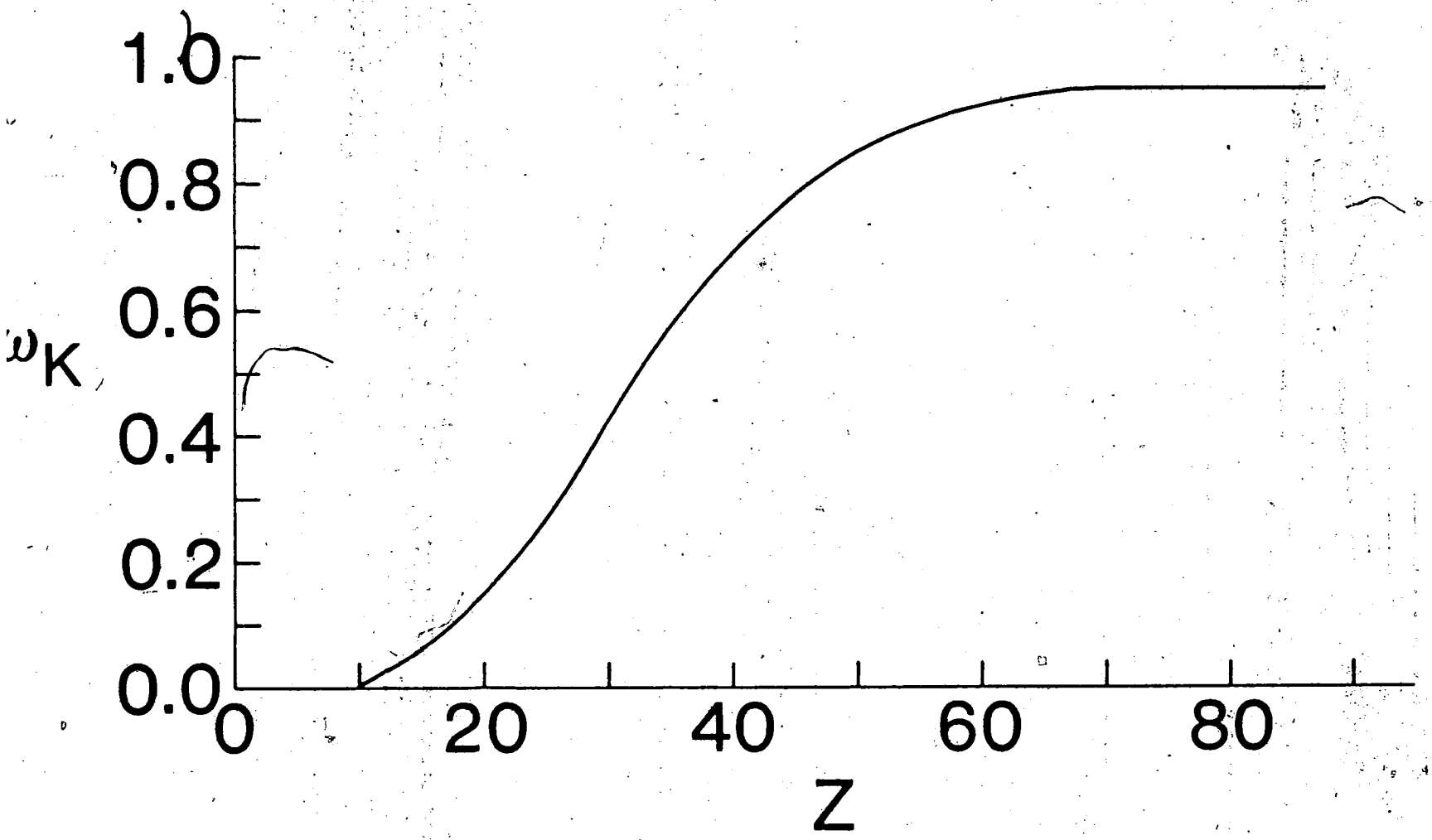

Figure I-2. Experimental fluorescence yield ω_K as a function of atomic number Z.[14]

The general result is that the greater the transition energy the more likely is the radiative transition and vice versa. At E ≈ 10 keV both processes have about the same probability. Because X-ray fluorescence is not measurable with the equipment used in this work, only a brief discussion will be provided to show the relation of XRF to the Auger process.

The selection rules governing X-ray transitions are the dipole rules $\Delta L = \pm 1$ $\Delta J = 0, \pm 1$ with $J = 0 \nleftrightarrow J = 0$. Thus transitions from L_2 to K ($K\alpha_2$) and L_3 to K ($K\alpha_1$) are allowed but the transition from L_1 to K is forbidden. The energy of the emitted X-ray corresponds to the difference between the energies of the two levels involved in the transition and, as a first approximation, the shifts for the core levels of a molecule are very similar. Thus shifts in the X-ray line in a series of molecules should be very similar. This limits the use of X-ray emission for the study of the chemical environment.

The Auger transitions are caused by the Coulomb interaction between the atomic electrons. We can express the probability for a given Auger transition as[15]

$$P_{i\to f} = \frac{2\pi}{\hbar}|\langle\phi_f(S_f L_f M_f J_f)|V|\phi_i(S_i L_i M_i J_i)\rangle|^2 \rho(E)_f \ s^{-1} \qquad \text{I-12}$$

where $V = \sum_{i \neq j} e^2/r_{ij}$ and $\phi_i(S_iL_iM_iJ_i)$ and $\phi_f(S_fL_fM_fJ_f)$ are the initial and final state wave functions characterized by their quantum numbers S, L, M, J and $\rho(E)_f$ is the density of the final states for the energy that satisfies conservation of energy. Normalizing to one electron per atomic unit of energy, and measuring the transition rate per atomic unit of time $\tau_o = \hbar a_o/e^2 = 2.42 \times 10^{-17}$ sec

$$P_{i\to f} = 2\pi \left| \langle \phi_f(S_fL_fM_fJ_f) \left| \sum_{i>j} \frac{1}{r_{ij}} \right| \phi_i(S_iL_iM_iJ_i) \rangle \right|^2 \quad \text{I-13}$$

The wave functions ϕ_f and ϕ_i can be expressed in terms of the two hole states

$$\begin{aligned} \phi_f &= \phi_Y(1)\ \phi_Z(2) \\ \phi_i &= \phi_K(1)\ \phi_\lambda(2) \end{aligned} \qquad \text{I-14}$$

where ϕ_K is the initial core hole function, ϕ_Y and ϕ_Z are the final state hole functions and ϕ_λ is the continuum wave function of the outgoing electron. The initial and final state $S_iL_iM_iJ_i$ and $S_fL_fM_fJ_f$ values are thus defined in terms of s, ℓ, m, j of the two holes in each of the final states. Note that the Auger processes KYZ and KZY are indistinguishable.

The transition probability may also be written as

$$P_{i\to f} = 2\pi|D-E|^2 \qquad \text{I-15}$$

where D is the direct matrix element

$$D = \int\int \phi_Y^*(1)\ \phi_Z^*(2)\left|\frac{e^2}{\vec{r}_1-\vec{r}_2}\right|\phi_K(1)\ \phi_\lambda(2)\ d\tau_1\ d\tau_2 \qquad \text{I-16}$$

and E is the exchange matrix element

$$E = \int\int \phi_Z^*(1)\ \phi_Y^*(2)\left|\frac{e^2}{\vec{r}_1-\vec{r}_2}\right|\phi_K(1)\ \phi_\lambda(2)\ d\tau_1\ d\tau_2 \qquad \text{I-17}$$

Equation I-13 and also equation I-15 are non zero only if the selection rules for the Coulomb interaction e^2/r_{ij} are fulfilled. These rules are for pure LS coupling:[16] $S_i = S_f$; $L_i = L_f$; $M_{S_i} = M_{S_f}$; $M_{L_i} = M_{L_f}$ and always $J_i = J_f$; $M_i = M_f$; $\pi_i = \pi_f$. The parity π of the total system is given by $\pi = (-1)^{\Sigma \ell_i}$. These selection rules are not very restrictive because there is usually a choice of quantum numbers for the outgoing electron which satisfies all selection rules.

The energy of an Auger transition KYZ where the initial state has a vacancy in the K shell and the final state has two vacancies, one in the Y and one in the Z shell of the system A is given by

$$E_{KYZ} = E_{A^+(K)} - E_{A^{++}(YZ)} \qquad \text{I-18}$$

where $E_{A^+(K)}$ and $E_{A^{++}(YZ)}$ are the total energies of the initial hole state and the final hole state. The Auger process KYZ can be written as the algebric sum of three simple steps.

$$A \rightarrow A^+(K) + e^- \qquad E(K) \qquad \text{I-19a}$$

$$A \rightarrow A^+(Y) + e^- \qquad E(Y) \qquad \text{I-19b}$$

$$A^+(Y) \rightarrow A^{++}(YZ) + e^- \qquad E(Z(Y)) \qquad \text{I-19c}$$

The energy of each process is written on the right.

Instead of calculating the total energies for initial and final states, it is convenient to express the Auger energies in terms of the experimental binding energies of the levels involved.

$$E_{KYZ} = E(K)-E(Y)-E(Z(Y))$$
$$= E(K)-E(Y)-E(Z)-F(YZ; X) \qquad \text{I-20}$$

where E(K), E(Y), E(Z) are the binding energy of electrons K, Y, Z in the neutral system, E(Z(Y)) is the binding energy of electron Z in an atom already ionized in shell Y, and

$$F(YZ;\ X) = E(Z(Y)) - E(Z) \qquad \text{I-21}$$

Asaad and Burhop[17] attributed the term F(YZ; X) to an electrostatic interaction between the two holes in the final state giving rise to different Auger transition components. This can be calculated using multiplet coupling theory.[18] This electrostatic term is indicated as F(YZ; X) where X is the term designation of the two hole final state. The Hamiltonian for a N-electron system is given by:

$$H = H_O + H_C + H_{SO} \qquad \text{I-22}$$

where $H_O = \sum_{i=1}^{N} \left(-\frac{1}{2}\nabla_i^2 - \frac{Z}{r_i}\right) = \Sigma h_i$ is the pure hydrogenic Hamiltonian

$H_C = \sum_{i>j} \frac{1}{r_{ij}}$ is the Coulombic interaction of the electron pairs

$H_{SO} = \sum_i \xi(r_i)\,(\vec{\ell}_i \vec{s}_i)$ is the spin-orbit interaction

When dealing with closed shell atoms in the neutral state, the fine structure arising from the holes in the final

state can be easily discussed with the use of the equivalence principle of holes and electrons,[19] which states that the level separation for a shell lacking $N<4\ell+2$ electrons is the same as for a shell with N electrons present, only the absolute energies are displaced by a constant value. The spin-orbit energies for a configuration of $4\ell + 2-N$ electrons are the negative of those for a configuration of N electrons.

The state of the final vacancies depends strongly on the coupling scheme. The different coupling schemes are determined by the relationship between the coulombic interaction H_C and the spin-orbit interaction H_{SO} which is different for different ranges of atomic number Z.

$H_C >> H_{SO}$:	LS-coupling	$Z < 18$
$H_C << H_{SO}$:	jj-coupling	$Z > 36$
$H_C \approx H_{SO}$:	intermediate coupling	$18 < Z < 36$

In the L-S coupling regime the spin angular momenta s of each of the electrons involved are coupled to give a total spin angular momentum, S, of the system, and similarly the orbital angular momenta, ℓ, couple to give a total orbital angular momentum L. Total spin and orbital momenta couple to give the total angular momentum J of the

system. The resultant state is designated as $^{2S+1}L_J$ where 2S+1 is the multiplicity, J is the total angular momentum and L is the total orbital angular momentum which is designated by letters S, P, D, F, etc. for L = 0, 1, 2, 3, respectively. States with different J but with the same L and S quantum numbers are degenerate. In jj coupling, the spin-orbit interaction dominates and the s and ℓ momenta of each electron couple to form a total angular momentum j, for each electron. Thus each electron is described by a j value. This gives the $2s_{1/2}(L_1)$ $2p_{1/2}(L_2)$, $2p_{3/2}(L_3)$ electrons, and the Auger component is indicated as KL_1L_2, KL_1L_3, etc. In intermediate coupling (IC) the double vacancy state is characterized by L, S and J; the degeneracy with respect to J is removed by the spin-orbit perturbation.[16] The Auger component is indicated for example as KL_1L_2 ($^1P_1$). The terms F(YZ;X) are expressed as the sum of Slater direct (F) and exchange (G) integrals[18] appropriate to each term arising from a particular configuration of the two holes in the final state (X).

It has been found that equation I-20 with accurately calculated values for the electrostatic term F(YZ;X) does not reproduce the experimental Auger energies.[50] The discrepancy is believed to arise from the neglect of the

relaxation of passive electron orbitals in the doubly charged final state. This relaxation, indicated as R(YZ), increases the Auger electron energy. It is called often "static relaxation", and it represents the amount by which the binding energy of the electron in step I-19c is reduced because its potential is made more repulsive when the passive electrons relax toward the hole left by the electron in step I-19b. It is called static relaxation to distinguish it from the "dynamic relaxation"[50] which arises from the acceleration of the outgoing electron produced by the collapse of the occupied outer orbitals toward the hole during the emission process and which is accounted for by the use of empirical binding energies in equation I-20.

The equation for the Auger energy therefore becomes

$$E_{KYZ} = E(K)-E(Y)-E(Z)-F(YZ;X)+R(YZ) \qquad I-23$$

The relaxation term R(YZ) thus determines the change of the Auger electron energy with the chemical environment and therefore makes the analysis of these electrons potentially useful sources of information on molecular properties. It is quite important from the experimental point of view that the energy of the Auger electron

(equation I-23) depends only on the energies of the levels involved and not on the excitation source. As a consequence of this feature the linewidth of the source does not affect the linewidth of the Auger peak, and either photon or electron excitation can be used to produce the Auger spectrum.

4. Different Types of Auger Processes

Besides the processes illustrated in Figure I-1 some other transitions, with usually low intensity, may occur and appear in the "normal" Auger spectrum. When an initial vacancy created without additional excitation is filled by an Auger transition, the process is referred to as normal or diagram Auger. However, as we have seen in the photoionization case, there is a finite probability for the occurrence of an excitation, or ionization, "shake-up"[8] or "shake-off",[9,10] accompanying the initial photoionization. The non-radiative readjustment to a state formed by the shake-up process usually results in high energy satellite lines,[7] whereas , readjustments to shake off result in the formation of low energy satellite Auger electrons.[7]

Additional high energy satellite peaks can occur as the result of an autoionization process.[12] An autoionization state is formed by the resonance absorption

of a photon which places an inner-shell electron into an unoccupied molecular orbital. Decay of an autoionization state by a non-radiative transition in which the initial core vacancy becomes filled by an atomic electron, and the electron in a bound outer orbital becomes expelled, results in high energy Auger satellite electrons. If photon excitation is used, the energy of the radiation must match the energy of the electronic transition. In the case of electron excitation during the collision of the electron beam with the molecule the high energy electrons impart to the system only the energy necessary for the transition. Therefore autoionization processes are observed more often with electron excitation. Additional low energy satellites can be due to the so-called double Auger process,[20] consisting in the ejection of an additional electron accompanying the emission of the Auger electrons. These processes however are difficult to resolve because they appear as a continuous distribution of energy below the normal Auger lines.

The charge on the resulting ion following the Auger transition is characteristic of the different processes: normal processes produce ions with charge of +2; high energy satellite processes produce ions with charge of +1 from autoionization and charge of +2 from "shake-up"

processes; low energy satellite processes produce ions with charge of +3 from "shake-off" and from double Auger transitions.

D. Purpose of the Work

The main aim of the work described in this thesis was to obtain information on chemical properties of molecules through the analysis of their Auger spectra.

In Chapter III it is shown that there is a large dependence of the Auger energy on the so-called "final state effect" which is associated with a relaxation process suffered by the molecule when it loses two electrons. This effect can be evaluated from the experimental binding energy and Auger energy shifts.

Chapter IV and VI describe the Auger spectra involving only inner shells of Germanium and Tin atoms respectively, in different chemical environment. Analysis of intensity and energy is based on an atomic model.

The effect of the excitation energy near the ionization energy threshold of the Ge $2p_{1/2}$ orbital on Germanium $L_2M_{2,3}M_{4,5}$ and $L_2M_{4,5}M_{4,5}$ Auger Spectra is described in Chapter V. Mg $K\alpha_{1,2}$ radiation was used to study threshold effects and the spectra excited by this radiation were compared to those excited by $AlK\alpha_{1,2}$ which

provides a photon energy well in excess of the threshold ionization potential.

In Chapter VII Auger transitions from small molecules in which the final state has two holes in the valence orbitals are discussed. In this case the energy as well as the intensities depend very much on the molecular environment and a theoretical estimate of both is based on a molecular orbital model.

CHAPTER II

GENERAL EXPERIMENTAL

A. Electron Spectrometer

The electron spectrometer used for this work was a McPherson ESCA 36 consisting of an X-ray source for photoionization, a scanning electron energy analyzer, and an electron detector. The spectrometer control and data acquisition were implemented by a small computer (PDP-8). A turbomolecular pumping system gave an oil free vacuum required for the experiment. In Figure II-1 are illustrated the main components of the instrument.

The electron energy analyzer (scanning monochromator) consisted of two sections of concentric spheres having a mean radius of 36 cm, and a gap spacing of 80 mm. The electrons produced in the target chamber entered the analyzer through a slit. Inside the analyzer, the electrons were separated according to their kinetic energies by the electric field applied to the spheres. The electrons reached the detector through a second slit located at 180° from the first, where they were then

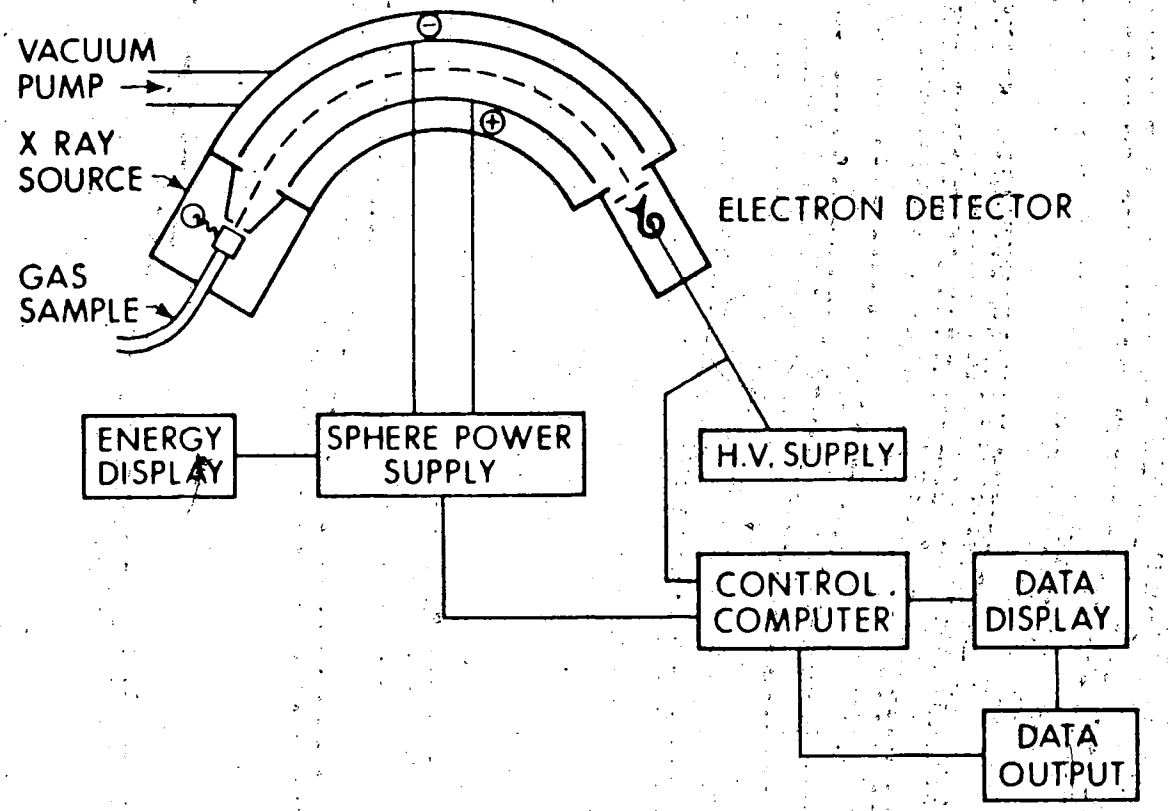

Figure II-1. Schematic of the electron spectrometer.

counted. The electron detector was a single channel electron multiplier mounted on a carriage behind the exit slit. It could achieve a gain of 10^7. The detector and the exit slit could be moved along the electron optical path for focusing purposes. The entrance and exit slits defined the resolution of the spectrometer, together with a pair of adjustable baffles that permitted the selection of instrumental resolution at any time during instrument operation. The resolution of the spectrometer was energy dependent. The 36 cm spheres could achieve a resolution of 0.02% of the analyzing energy. For example at 100 eV, the smallest interval of energy that could be distinguished was 0.02 eV; at 1000 eV this energy was 0.2 eV. While traveling in the region between the electrostatic spheres, the electrons moved through a magnetic field free space ($<2 \times 10^{-4}$ Gauss). To obtain this field free space, the earth's and stray magnetic fields were cancelled by two mu-metal shields. The inner shield was inside the vacuum and enclosed the spheres. A second shield was mounted externally to the vacuum tank.

An instrument constant in the computer program related the desired electron kinetic energy value to the proper voltage on the spheres automatically. Scanning was achieved by digitally stepping the power supply through

the desired energy range and in the required voltage steps within the power supply resolution.

B. Excitation Sources

The excitation sources used were either an X-ray tube or a high current electron gun.

1. X-ray Tube

The X-ray tube consisted of a cathode which was a thoriated tungsten filament at a negative potential and a water cooled anode at a positive potential, surrounded by a shield held at ground potential. The Copper anode was capped with the metal required to produce the desired radiation. The X-rays entered the sample cell through a 0.003 mm Aluminum window. This window removed the low energy Brehmsstrahlung from the X-ray beam and also kept the gas sample away from the X-ray region. The radiations used in this work were, Al $K\alpha_{1,2}$ (1486.6 eV),[21] Mg $K\alpha_{1,2}$ (1253,64)[22] and $AgL\alpha_1$ (2984.34 eV).[23] In all cases the X-ray source was operated at a power of approximately 300-400 Watts given by a potential difference of 10 kV between the cathode and anode, and by a filament emission current of 30-40 millamperes.

2. Electron Gun

The electron gun is shown in Figure II-2. It was constructed by Dr. J. Väyrynen during his stay in this laboratory. The main structure of the gun consisted of a tungsten filament 0.15 mm in diameter, modelled on a hair pin or simple spiral tip form, and a cylinder electrically connected to the filament by a resistence of 100 kΩ and which was then maintained at a negative potential with respect to the filament. This potential difference partially focussed the charge cloud emitted from the filament into the anode hole. A three element electron lens focussed the beam so as to relay the maximum electron beam to the target region. The voltage of the middle element was varied in order to maximize the beam current, whereas the other two elements were held at ground. The power supply for the filament of the electron gun was HV-isolated and stabilized to give a constant current through the filament. Typical voltage and current values across the filament were 3 V and 3 A respectively. The maximum beam current of the gun was approximately 2 mA by the accelerating voltage of about 2.5 kV.

3. Sample Handling

All the samples were obtained from commercial sources. The liquids were first degassed in vacuum by a

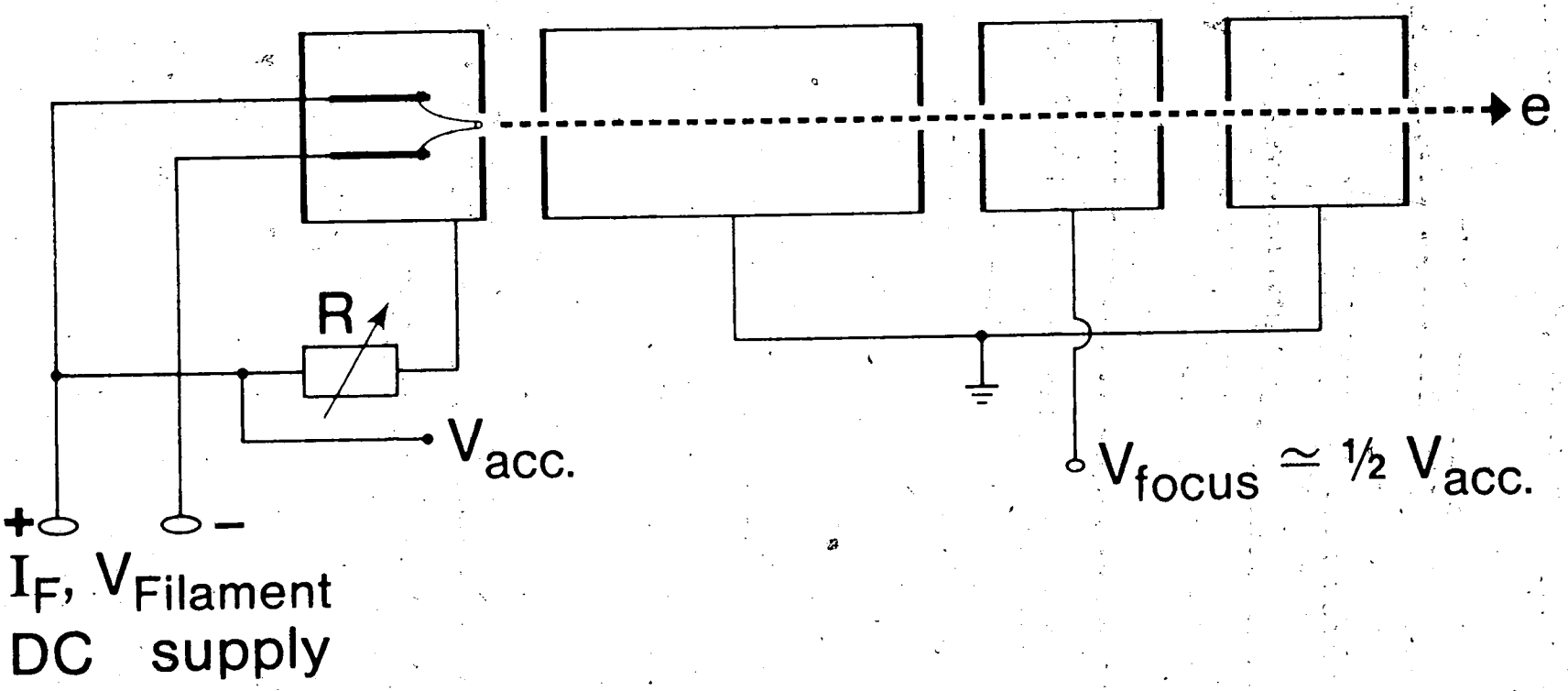

Figure II-2. Schematic of the electron gun.

freeze-thaw technique. The samples (except solid GeO_2) were studied in the vapor phase at a constant pressure during a given run. The gas pressures in the target chamber were approximately 150-200 micron in the case of X-ray excitation, much lower (about 1 μ) in the case of electron gun excitation. The pressure inside the analyzer was approximately 10^{-2} μ. The sample pressure was monitored by a MKS Baratron Pressure gauge.

4. Energy Calibration

The kinetic energy of the electron was calculated from the equation

$$KE = k\Delta V \qquad \text{II-1}$$

where ΔV is the potential difference between the analyzer spheres and k is the experimentally determined instrument constant. In order to compensate for any possible variations with time in the measured energies (due to alteration of external fields, pressure differences, charge differences, etc.) and for the non-linearity of the kinetic energy and potential difference relationship at high kinetic energy where relativistic effects are noticeable, the spectral lines were calibrated with two

accurately known rare gas lines. Calibrations were done on a mixture of sample and rare gas. In order to use Ar 2s as a reference line, which is not a primary standard, it was calibrated with respect to Neon $KL_{2,3}L_{2,3}(^1D_2)$ Auger line (804.557(17) eV kinetic energy)[24] and Argon $2p_{3/2}$ (248.62(8) eV binding energy)[25] photoelectron line. The value of 326.37(5) eV was obtained, in agreement with the value given in literature.[24] Kr $L_2M_{4,5}M_{4,5}(^1G_4)$ Auger line which is not a primary standard was also accurately calibrated with respect to Ne 1s (870.312(17) eV binding energy)[24] photoelectron line and Ne $KL_{2,3}L_{2,3}(^1D_2)$ Auger lines. The value of 1513.73(10) eV was obtained and used subsequently as reference line.

The spectra were recorded digitally and analyzed by means of a locally adapted version of a least squares programme[26] which fitted the data to either a Lorentzian or Gaussian function. Count rates were corrected for transmission of the analyzer by the function 1/E before applying the fitting procedure.

CHAPTER III

EFFECT OF CENTRAL ATOM ON TERMINAL CHLORINE $KL_{2,3}L_{2,3}(^1D_2)$ AUGER AND CORE IONIZATION ENERGIES

A. Introduction

In this chapter the experimental Chlorine $KL_{2,3}L_{2,3}(^1D_2)$ Auger energies and Chlorine 2p binding energies in Chloromethanes, Fluorochloromethanes, Methylchloromethanes and in Chlorosilanes and Methylchlorosilanes are discussed. Binding energies and Auger energies are compared to evaluate relative contributions of initial state effects and final state effects in molecules wherein the central atom bonding may involve 'd' orbitals. These effects, which are expressed by the differences in potential contribution ΔV and differences in relaxation contributions ΔR can be obtained from the difference of core photoelectron and Auger energy shifts. The ΔV and ΔR terms obtained from experimental results are compared with the corresponding values obtained from potential models utilizing potentials from CNDO/2 calculations.

B. Experimental

All compounds: CCl_4, $CHCl_3$, CH_2Cl_2, CH_3Cl, $CFCl_3$, CF_2Cl_2, CF_3Cl, CH_3CCl_3, $(CH_3)_2CCl_2$, $(CH_3)_3CCl$, $SiCl_4$, $SiHCl_3$, SiH_2Cl_2, CH_3SiCl_3, $(CH_3)_2SiCl_2$, $(CH_3)_3SiCl$ were obtained from commercial sources; the Methane derivatives from Aldrich, the Silane derivatives from Aldrich, Pierce and Peninsular Chem. Research. The purity of the samples varied from practicum grade (>95%) for $SiHCl_3$ to purissimum grade (>99%) for the other compounds. The different purity grades of the liquids did not affect the measurements of the respective vapors, since clean peaks were recorded. The Auger line Cl $KL_{2,3}L_{2,3}(^1D_2)$ was excited by Ag $L\alpha_1$ radiation (2984.34(2) eV)[23] and calibrated with respect to the Ne 1s (870.312(17) eV binding energy)[24] and Ar 1s (326.37(5) eV binding energy)[25] photoelectron lines. The Cl 2s, Cl 2p, Si 2p lines were excited by Mg $K\alpha_{1,2}$ radiation (1253.64 eV)[21]. Cl 2s and Cl 2p lines were calibrated with respect to the Ar $2p_{3/2}$ (248.62(8) eV binding energy)[25] and Ar 2s (326.37(5) eV binding energy)[25] photoelectron lines, Si 2p was calibrated with respect to the Kr $3p_{3/2}$ (214.55(15) eV binding energy)[25] and Kr $3d_{5/2}$ (93.80(10) eV binding energy)[25] photoelectron lines.

C. Theory

As described in Chapter I, XPS yields directly electron binding energies which depend on the chemical environment. The difference between the experimentally determined binding energy for a particular electron level in a given molecule and that for the same level in another molecule taken as reference is called "chemical shift". Binding energy shifts arise from changes in electronic and nuclear charge distribution between one molecular species and another. They are, therefore, closely related to properties of chemical interest.

As was described by equation I-3 the electron binding energy is equal to the transition energy for a molecule from the initial state A to the final state A_k^+ and it is given by the difference between the total energy of the initial neutral state A and the final hole state A_k^+. Rather accurate total energies are obtained by self consistent field (SCF) calculations within the Hartree-Fock formalism[27] with different levels of approximation. The binding energies are calculated as differences of these total energies. This is known as the ΔE_{SCF} method. The rigorous evaluation of chemical shifts involves four total energy calculations, two for each

molecular species. This method can be quite time consuming depending on the various levels of approximation and sophistication used, such as the extent of the basis set and inclusion of configuration interaction. Also some difficulty arises in calculating the hole states because they do not always satisfy the conditions required by the variational principle. A quite drastic simplification to this method is introduced by the "sudden" approximation wherein it is considered that the ionization process occurs so quickly that the remaining electrons in the molecule (passive electrons) do not have time to adjust to the new situation with a core hole, and so they can be represented by the same wavefunctions of the ground state. From this assumption it follows that the ionization energy E_B of a kth orbital is just equal to the orbital energy ε_k.

$$E_B = E(A_k^+) - E(A) = -\varepsilon_k \qquad \text{III-1}$$

This result is known as Koopmans' theorem[28] and it involves only one calculation for each system. Koopmans' energies, however, overestimate the experimental values especially for inner shells.

Hedin and Johansson[29] formulated a correction that relates the Koopmans' energies to the energies obtained from complete hole state calculations. This correction, which is called the relaxation energy, is obtained by evaluating the expectation value of a "relaxation potential" V_R:

$$V_R = \sum_{j \neq k} (V_j^* - V_j) \qquad \text{III-2}$$

in the kth state. V_j and V_j^* represent both the Coulomb plus exchange potentials due to the jth occupied orbital in the initial neutral state and in the final ionic state with a hole in the kth orbital respectively. The relaxation energy $E_R(k)$ is

$$E_R(k) = \frac{1}{2} \langle k|V_R|k\rangle \qquad \text{III-3}$$

where $\langle k|V_R|k\rangle$ is given by a combination of Coulomb and exchange integrals.[29] The relaxed binding energy therefore becomes

$$E_B = -\varepsilon_k - \frac{1}{2} \langle k|V_R|k\rangle \qquad \text{III-4}$$

Equation III-4 still requires hole-state calculations in order to evaluate V_j^*, the potential due to the relaxed jth passive orbitals, for each value of j. To avoid these difficult calculations, the "equivalent cores approximation"[30,31] is introduced. The essence of this approximation derives from the realization that one electron in an inner orbital will (almost completely) shield an outer electron from one unit of nuclear charge. Thus an outer orbital in an atom of nuclear charge Ze with a hole in an inner shell can be approximated by the corresponding outer orbital in the ground state of the next element of atomic number Z+1. All the hole state integrals for the element with atomic number Z required in equation III-2 are replaced by the corresponding ground-state integrals of the element with atomic number Z+1. Good agreement between experimental binding energies and calculated energies has been obtained with this approach and the chemical shifts predicted from differences in these binding energies agree with the experiment to ~1 eV or better depending on the basis sets used for the calculations. The method discussed above, however, even with the simplifying approximations used is still difficult and expensive especially for large molecules.

By inferring the physical origins of the chemical shifts, it has been possible to formulate an electrostatic potential model which allows the calculation of the shifts directly without need for the total energies of the neutral molecule and ion.[32] According to this model, the binding energies are considered to be determined by two factors: the electrostatic potential experienced by the core electron in the ground state before ionization and which is often referred to as "initial state effect", and the relaxation potential energy that arises from the redistribution of the electronic charge during ionization and which is referred to as the "final state effect". Consideration of only the first factor leads to formulation of a Ground-state Potential Model (GPM).[32] If both factors are considered, the Relaxation Potential Model (RPM)[32] is obtained.

Basch[33] and Schwartz[34] showed that the shifts in the orbital energy of level i and in its potential energy are quite accurately related by

$$\Delta\varepsilon^i \cong \Delta V^i \qquad \text{III-5}$$

where ΔV^i includes interaction between the core electron i under consideration and the valence electrons and

interaction between the core electron i with the nucleus and core electrons on other atoms. The core electrons on other atoms effectively screen an equal amount of nuclear charge and may be considered as shrunk into their respective nuclei. The interaction of the core electron i with the nucleus and core electrons on other atoms may consequently be considered as between point charges. Basch[33] also collapsed the core orbital of interest into the corresponding nucleus, reducing in this way all the two-electron integrals to one-electron integrals over the valence electrons. Then, instead of calculating the potential energy shifts of the core electron i according to III-5, shifts in the potential energy at the nucleus ΔV_n created by the valence electrons of the atom of interest treating the other atoms in the molecule as point charges can be used

$$\Delta\varepsilon^i \cong \Delta V_n \qquad \text{III-6}$$

Then, by application of Koopmans' theorem (equation III-1)

$$\Delta E_B{}^i \cong -\Delta V_n \qquad \text{III-7}$$

The potential term ΔV_n involves no core orbitals and may be evaluated from semiempirical calculations such as

CNDO[35] which does not use core orbitals in the basis set. When the relaxation potential energy (equation III-3) is included, the use of the equivalent cores approximation[30,31] gives the following expression

$$\Delta E_B = -\Delta V_n(Z) - \Delta R \qquad \text{III-8}$$

where ΔR is the relaxation energy shift relative to a reference molecule. Using

$$\Delta R = \frac{1}{2}[\Delta V_n(Z+1) - \Delta V_n(Z)] \qquad \text{III-9}$$

the (RPM) expression for the chemical shift is

$$\Delta E_B = -\frac{1}{2}[\Delta V_n(Z+1) + \Delta V_n(Z)] \qquad \text{III-10}$$

where $\Delta V_n(Z)$ and $\Delta V_n(Z+1)$ are the nuclear potentials calculated for the atoms of nuclear charge Z and Z+1 respectively. In CNDO, the equivalent cores approximation is introduced by replacing the ionized atom with an atom of the next higher atomic number (thus Argon for Chlorine) and repeating the calculations using the same molecular geometry but increasing the net molecular charge by one unit to equate the number of electrons in the two species

(Z and Z+1) and to preserve the closed shell configuration. The Relaxation Potential Model requires two calculations, one for the Z atom and one for the Z+1 atom in the molecule.

The Transition Potential Model (TPM)[36] has been suggested as a method of evaluating shifts and, if only shift predictions are needed, only one calculation per molecule is required. In this approach the ionized atom in the molecule is replaced by a pseudo-atom of effective charge $Z^* = Z+\frac{1}{2}$ with the assumption of a linearity between charges and potentials. The parameters used for this atom in semiempirical calculations are interpolated between those appropriate to the Z and Z+1 atoms, so equation III-8 becomes

$$\Delta E_B = -\Delta V_n(Z^*) \qquad \text{III-11}$$

Expressions analogous to equations III-7, III-9, III-10 may be derived for Auger electron energy shift.[37]

$$\Delta E_{Au} = \Delta V_n(Z+1) \qquad \text{(GPM)} \qquad \text{III-12}$$

$$\Delta E_{Au} = \frac{1}{2}[\Delta V_n(Z+1) + \Delta V_n(Z+2)] \qquad \text{(RPM)} \qquad \text{III-13}$$

$$\Delta E_{Au} = \Delta V_n(Z+3/2) \qquad \text{(TPM)} \qquad \text{III-14}$$

These expressions allow the estimation of the Auger shifts from potentials at the nucleus obtained from CNDO calculations. However for Chlorine in particular RPM and TPM models require calculations on a Z+2 and Z+3/2 atoms which are beyond Argon and for which the CNDO parameterization is not available.

The Auger shifts involving core levels can be expressed[38] as a function of the potential and relaxation terms analogous to those used for the photoelectron shifts. From equation I-23 and from equation III-8 the following expression for the Auger energy shift is obtained

$$\Delta E_{KYZ} = \Delta V(Y) - \Delta R(Y) + \Delta R(YZ) \qquad \text{III-15}$$

assuming that the potential shift at the nucleus is the same for any core electron regardless of whether a K or L shell electron is involved. $\Delta R(Y)$ and $\Delta R(YZ)$ are the changes in relaxation energy which consists of a readjustment of the electronic charge accompanying the creation of a single hole and a double hole respectively.

The readjustment of electrons from the same atom which undergoes the process (intraatomic relaxation)[39] is

assumed to be almost constant from one molecule to the other. So the contribution from these electrons to the relaxation energy changes is zero. $\Delta R(Y)$ and $\Delta R(YZ)$ in equation III-15 are due to contributions from all the other atoms in the molecule and they are called extraatomic relaxation energies.[39] This kind of relaxation consists in the polarization of the electron clouds on adjacent atoms which increases the kinetic energy of the outgoing electron.[40] From the classical electrostatic treatment of the polarization energy of an ion in a dielectric solid it arises that the extraatomic relaxation is proportional to the square of the ion charge.[41]

In the case of photoionization the charge of the ion is +1; in the case of the Auger process the charge is +2 and therefore the $\Delta R(YZ)$ in equation III-15 differs by a factor of four from the relaxation $\Delta R(Y)$.

$$\Delta E_{Au} = \Delta V(Y) - \Delta R(Y) + 4\Delta R(Y) \qquad \text{III-16}$$

$$\Delta E_{Au} = \Delta V(Y) + 3\Delta R(Y) \qquad \text{III-17}$$

Combining equation III-8 and equation III-17 the relation between photoelectron and Auger energy shifts is obtained

$$\Delta E_{Au} + \Delta E_B = 2\Delta R(Y) \quad . \qquad \text{III-18}$$

The relationship, given by equation III-18, between the Auger shift ΔE_{Au} and the binding energy ΔE_B has been defined as the Auger parameter, $\Delta\alpha$.[42]

$$2\Delta R = \Delta\alpha. \qquad \text{III-19}$$

Using equations III-8 and III-17 it is possible then to calculate the effect of the initial state potential ΔV and of the final state relaxation ΔR if the binding energy shifts and Auger energy shifts are measured.

D. Results and Discussion

In Table III-1 are listed the experimental Chlorine $2p_{3/2}$, Chlorine 2s, Carbon 1s photoelectron energies, and the Chlorine $KL_{2,3}L_{2,3}(^1D_2)$ Auger energies in a series of Carbon based molecules. In Table III-2 are reported the corresponding values for analogous Silicon compounds. The Cl $2p_{3/2}$ binding energy and Cl $KL_{2,3}L_{2,3}(^1D_2)$ Auger energy shifts in the two series of compounds relative to CCl_4 and $SiCl_4$ are given in Table III-3 and Table III-4

Table III-1. Cl $2p_{3/2}$, Cl 2s, C 1s Binding Energies and Cl $KL_{2,3}L_{2,3}(^1D_2)$ Auger Kinetic Energies for Methane Series[a]

Compound	Cl $2p_{3/2}$ (eV)	Cl 2s (eV)	Cl $KLL(^1D_2)$ (eV)	C 1s (eV)
CCl_4	207.09	277.98	2374.45	296.35
$HCCl_3$	206.96	277.85	2374.29	295.24
H_2CCl_2	206.76	277.61	2373.88	293.91
H_3CCl	206.30	277.20	2373.45	292.46
CH_3CCl_3	206.60	277.52	2374.75	295.05[b] 291.71[c]
$(CH_3)_2CCl_2$	206.15	276.96	2375.02	293.69[b] 291.29[c]
$(CH_3)_3CCl$	205.47	276.27	2375.51	291.15
$FCCl_3$	207.23	278.21	2373.87	297.58
F_2CCl_2	207.68	278.51	2373.17	298.91
F_3CCl	207.83	278.80	2372.25	300.35

a. The values are the averages of at least three measurements. The maximum deviation is 0.05 eV.

b. C 1s binding energy of the central Carbon atom.

c. C 1s binding energy of the Methyl Carbon atom.

Table III-2. Cl $2p_{3/2}$, Cl 2s, Si 2p Binding Energies and Cl KLL($^1D_2$) Auger Kinetic Energies for Silane Series[a]

Compound	Cl $2p_{3/2}$ (eV)	Cl 2s (eV)	Cl KLL($^1D_2$) (eV)	Si 2p (eV)
$SiCl_4$	206.84	277.82	2373.68	110.11
$HSiCl_3$	206.60	277.54	2373.62	109.33
H_2SiCl_2	206.44	277.26	2373.60	108.52
CH_3SiCl_3	206.17	277.03	2374.10	108.91
$(CH_3)_2SiCl_2$	205.56	276.61	2374.48	107.82
$(CH_3)_3SiCl$	205.27	276.20	2374.95	106.82

a. The values are the averages of at least three measurements. The maximum deviation is 0.05 eV.

Table III-3. Cl $2p_{3/2}$ Binding Energy Shifts and Cl $KL_{2,3}L_{2,3}(^1D_2)$ Auger Energy Shifts Calculated Relative to CCl_4 ($\Delta E = E_{compd} - E_{CCl_4}$)

Compound	$\Delta E_{Cl\ 2p_{3/2}}$ (eV)	$\Delta E_{Cl\ KLL(^1D_2)}$ (eV)
CCl_4	0.0	0.0
$HCCl_3$	-0.13	-0.16
H_2CCl_2	-0.33	-0.57
H_3CCl	-0.79	-1.00
CH_3CCl_3	-0.49	0.30
$(CH_3)_2CCl_2$	-0.94	0.57
$(CH_3)_3CCl$	-1.62	-1.06
$FCCl_3$	0.14	-0.58
F_2CCl_2	0.59	-1.28
F_3CCl	0.74	-2.20

Table III-4. Cl $2p_{3/2}$ Binding Energy Shifts and Cl $KL_{2,3}L_{2,3}(^1D_2)$ Auger Energy Shifts Calculated Relative to $SiCl_4$ ($\Delta E = E_{compd} - E_{SiCl_4}$)

Compound	$\Delta E_{Cl\ 2p_{3/2}}$ (eV)	$\Delta E_{Cl\ KLL(^1D_2)}$ (eV)
$SiCl_4$	0.0	0.0
$HSiCl_3$	-0.24	-0.06
H_2SiCl_2	-0.40	-0.08
CH_3SiCl_3	-0.67	0.42
$(CH_3)_2SiCl_2$	-1.28	0.80
$(CH_3)_3SiCl$	-1.58	1.27

respectively. Some of the photoelectron and Auger energies listed in Table III-1 had been reported by other workers;[43,44] the values obtained in this work are in good agreement with literature values with the exception of some of the Cl $KL_{2,3}L_{2,3}(^1D_2)$ Auger energies which are about 1.2 eV smaller than those reported by Aitken et al.[43] This discrepancy may be due to the use of different calibration procedures. Two calibrant lines both on the low kinetic energy side of the unknown line were used in the previous study whereas in this work two peaks bracketing the unknown line were used.

All the values reported are the averages of at least three measurements. The maximum deviation was 0.05 eV. Peak positions were determined by a least squares fit curve of a Gaussian lineshape to the data.[26] Chlorine 2p was fitted with two Gaussians separated by the spin-orbit splitting of 1.8 eV. The spin-orbit splitting of the Silicon 2p level was not resolved. The Silicon $2p_{1/2}$-$2p_{3/2}$ energy difference has been reported to be about 0.6 eV.[45] However, it was not possible to fit two Gaussian components separated by this amount to the experimental peak because of convergence problems so the Si 2p lines were fitted with a single Gaussian of greater full width at half maximum (FWHM). Presuming, as seems

reasonable, that the spin-orbit splitting is essentially a constant, this procedure will not affect shift values.

From Tables III-1 and III-2 it can be seen that the energies do not change drastically from one compound to the other. However there are some definite trends in agreement with chemical environment consideration.

Plots of the experimental Chlorine $2p_{3/2}$ binding energy shifts versus the experimental Chlorine $KL_{2,3}L_{2,3}(^1D_2)$ Auger shifts for Carbon compounds and Silicon compounds are shown in Figures III-1 and III-2, respectively. The sign of the Auger shifts has been changed because the binding energy axis and the kinetic energy axis, which are used for the Auger energies, have opposite directions. In both series of compounds the points lie on different lines. The slopes of these lines change with the environment of the Chlorine and none of them is unity which would correspond to equal absolute value of the shifts. For the Methyl substituted compounds in the Carbon and Silicon series, the Auger shifts are smaller than the photoelectron shifts whereas the Chlorofluorocarbons have much larger Auger shifts as compared to the photoelectron shifts. For the Hydrocarbons in both series, the shifts of the binding energies are in opposite direction with respect to the

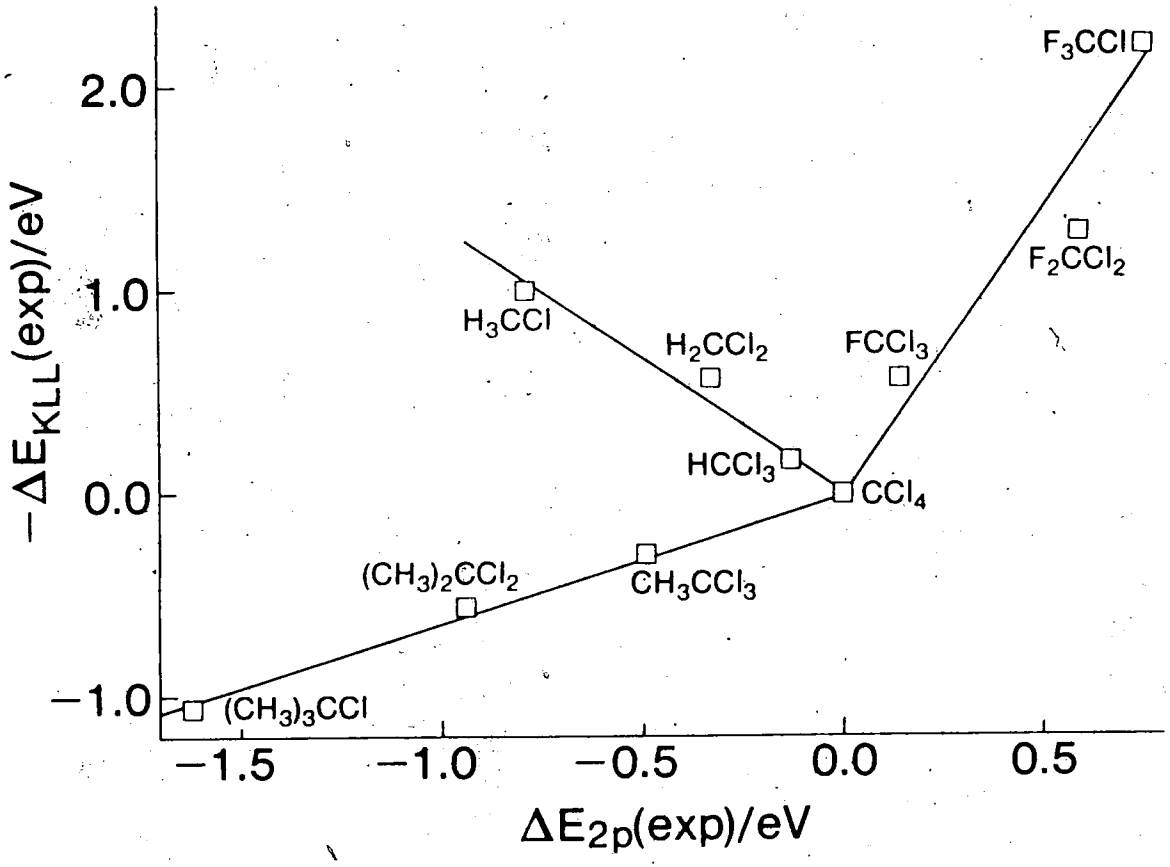

Figure III-1. Experimental Cl $KL_{2,3}L_{2,3}(^1D_2)$ Auger energy shifts, $-\Delta E_{KLL}$, versus Cl $2p_{3/2}$ binding energy shifts, ΔE_{2p}, for Methane derivatives.

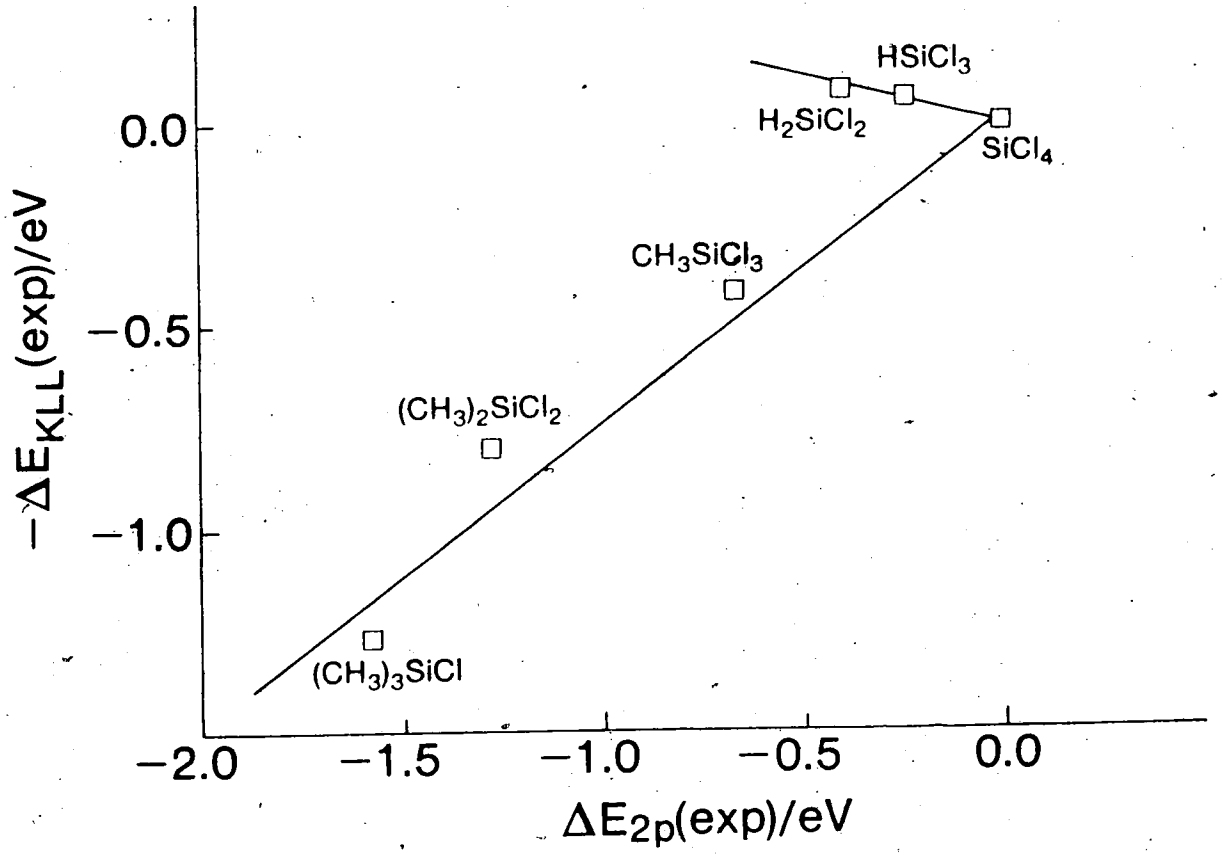

Figure III-2. Experimental Cl $KL_{2,3}L_{2,3}(^1D_2)$ Auger energy shifts, $-\Delta E_{KLL}$, versus Cl $2p_{3/2}$ binding energy shifts, ΔE_{2p}, for Silane derivatives.

shifts in Auger energies. Differences in magnitude of the Auger energy shifts and binding energy shifts have previously been observed[46] for Si 2p and Si $KL_{2,3}L_{2,3}$ in different series of compounds. Also in that case the Methylchlorosilanes $(CH_3)_x SiCl_{4-x}$ gave smaller Si KLL Auger shifts than Si 2p binding energy shifts. For the molecules lying on the same line in Figures III-1 and III-2 it can be assumed that

$$\Delta E_{Au} = -k \Delta E_B \qquad \text{III-20}$$

where the constant k, given by the slope, takes different values depending on the groups present in the molecules. From Tables III-3 and III-4 it can be seen that the Auger shifts in the H_xSiCl_{4-x} series are small compared to the corresponding series in Carbon compounds.

The various potential models were used to calculate Chlorine 2p binding energy shifts. The potentials at the nucleus have been obtained from CNDO/2 semi-empirical calculations, using the original parameterization of Pople et al.[35] with the exception of Cl for which revised (I+A)/2 parameters[47] were used. Calculations have been performed with and without inclusion of d orbitals in the basis set. Values of Chlorine $2p_{3/2}$ binding energy

shifts, ΔE_{2p}, calculated using GPM potential differences according to equation III-7 from CNDO/2 calculations without d orbitals in the basis set are plotted against the corresponding experimental values in Figures III-3 and III-4 for Carbon and Silicon compounds, respectively. If the model reproduced the experimental results, a linear plot with slope of unity would be expected. The lines in the figures have been calculated by least squares analysis and the parameters of the fit are given in Table III-5. Deviations from ideality are observed in all cases. All the points corresponding to molecules with the same kind of chemical environment follow one line characterized by a unique slope which is determined by the kind of substituents in the molecules. The negative and small value of the slope obtained for the line correlating Chlorofluorocarbons F_xCCl_{4-x} is quite peculiar. The Relaxation Potential Model was also applied for these compounds. The Chlorine $2p_{3/2}$ binding energy shifts, calculated using RPM potential differences according to equation III-10 and without d orbitals in the basis set for CNDO/2 calculations, are plotted against the corresponding experimental values in Figures III-5 and III-6 for Carbon and Silicon compounds, respectively. The parameters of the least squares fit are given in Table

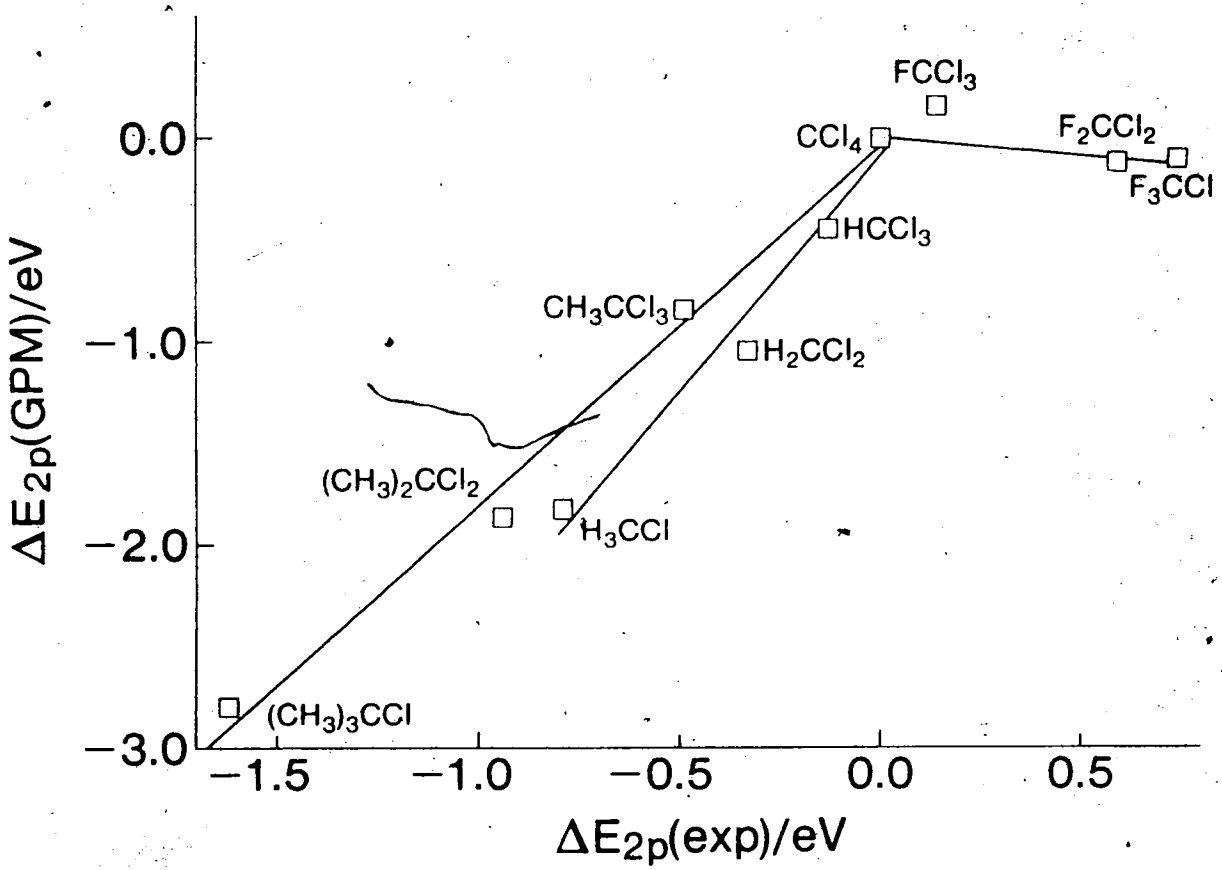

Figure III-3. Plot of calculated, ΔE_{2p}(GPM), versus experimental, ΔE_{2p}(exp), Cl $2p_{3/2}$ binding energy shifts for Methane derivatives. Calculated shifts were obtained from the Ground Potential Model (GPM) using CNDO/2 point charge potentials without d orbitals.

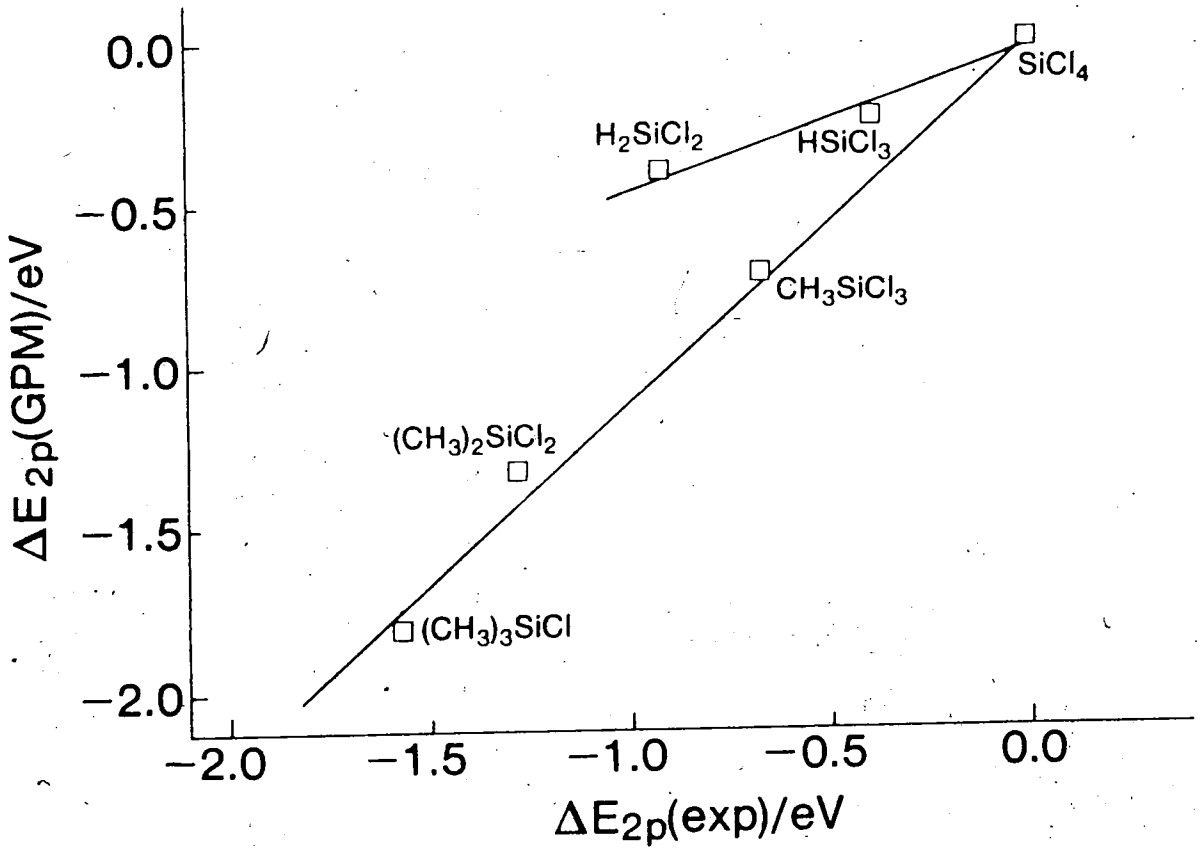

Figure III-4. Plot of calculated, ΔE_{2p}(GPM), versus experimental, ΔE_{2p}(exp), Cl $2p_{3/2}$ binding energy shifts for Silane derivatives. Calculated shifts were obtained from the Ground Potential Model (GPM) using CNDO/2 point charge potentials without d orbitals.

Table III-5. Parameters from Least-Squares Fit of Data in Figures III-3 and III-4 (GPM)

Compound[a]	Slope	Intercept	Corr.[b]
$(CH_3)_xCCl_{4-x}$	1.76	-0.04	1.00
H_xCCl_{4-x}	2.24	-0.13	0.98
F_xCCl_{4-x}	-0.28	0.08	0.75
$(CH_3)_xSiCl_{4-x}$	1.12	0.02	1.00
H_xSiCl_{4-x}	0.43	-0.03	0.98

a. x = 0 to 4; H_3SiCl is missing from the series.

b. Correlation factor of the fit.

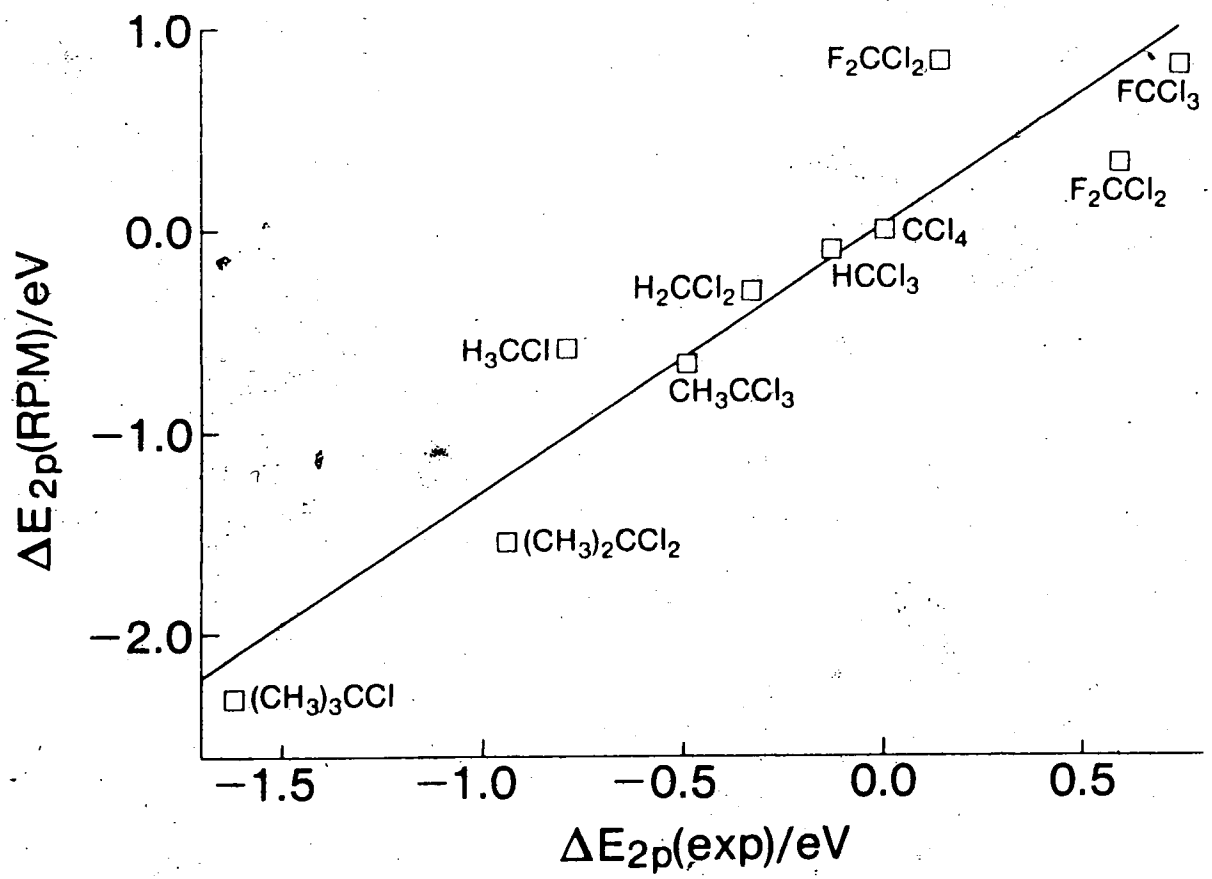

Figure III-5. Plot of calculated , ΔE_{2p}(RPM), versus experimental, ΔE_{2p}(exp), Cl $2p_{3/2}$ binding energy shifts for Methane derivatives. Calculated shifts were obtained from the Relaxation Potential Model (RPM) using CNDO/2 point charge potentials without d orbitals.

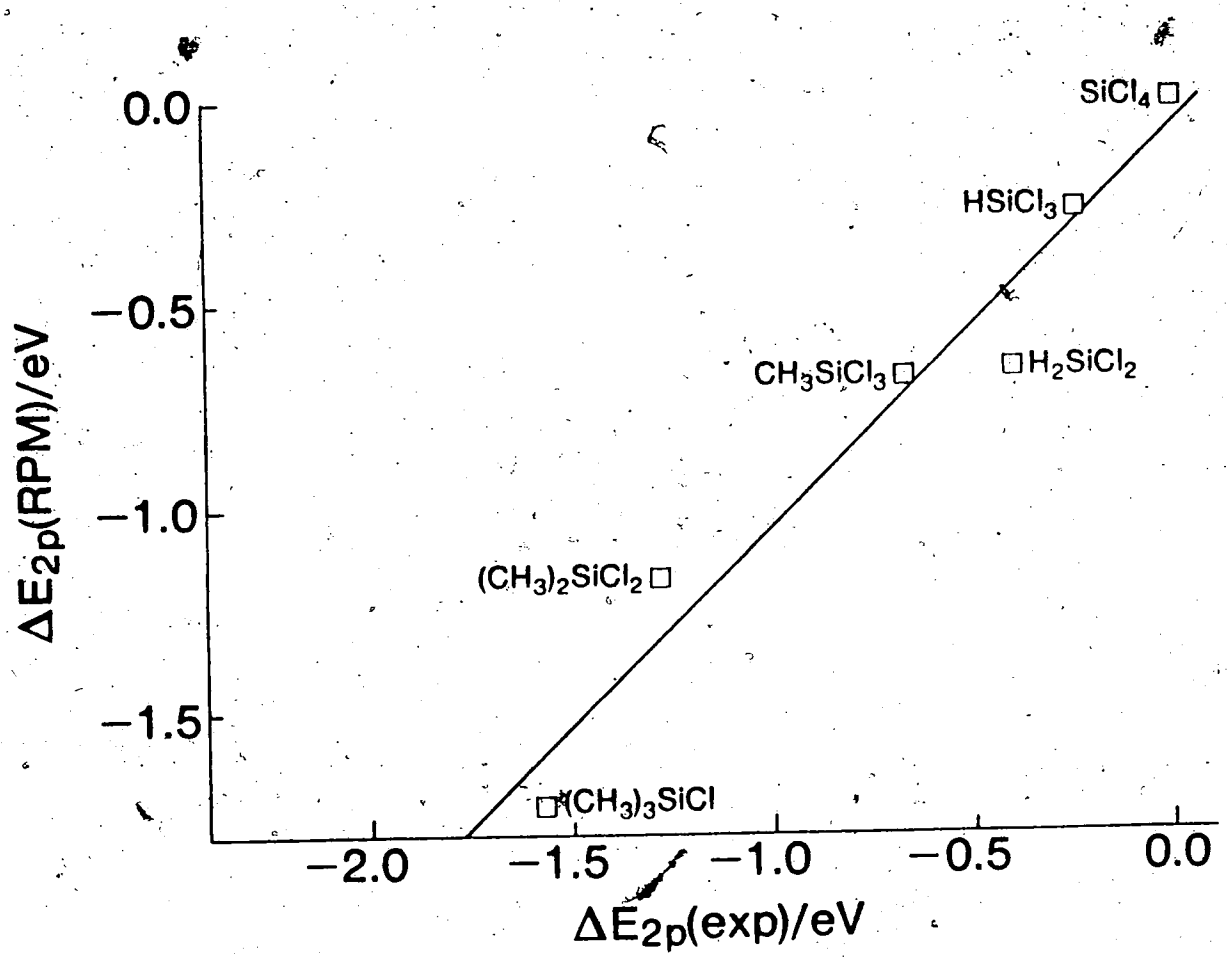

Figure III-6. Plot of calculated , ΔE_{2p}(RPM), versus experimental, ΔE_{2p}(exp), Cl $2p_{3/2}$ binding energy shifts for Silane derivatives. Calculated shifts were obtained from the Relaxation Potential Model (RPM) using CNDO/2 point charge potentials without d orbitals.

III-6. In this case all Carbon compounds correlate with each other with a slope >1 and likewise all Silicon compounds correlate but with a slope of approximately unity. Also the points relative to F_xCCl_{4-x} series are scattered about the line with positive slope. These results show that the RPM approximation, which accounts for that part of the chemical shift which is due to the relaxation of the molecule accompanying the photoionization process, is a better model than GPM. The Transition Potential Model, which is an alternate model equivalent to the RPM, was also applied to Cl $2p_{3/2}$ binding energy shifts. Equation III-11 was used without d orbitals included in the basis set of the CNDO/2 calculations. The plots obtained from TPM potential differences are shown in Figures III-7 and III-8 for Carbon and Silicon compounds respectively. As expected the results are similar to those obtained from the RPM. The parameters of the least squares fit are given in Table III-7. When the d orbitals were included in the basis set of the CNDO/2 calculations, within the TPM approximation, the results shown in Figures III-9 and III-10 for Carbon and Silicon compounds were obtained respectively. No relevant change is observed for the Carbon series compared to the results obtained without d orbitals. For the

Table III-6. Parameters from Least- Squares Fit of Data in Figures III-5 and III-6 (RPM)

Compound[a]	Slope	Intercept	Corr.[d]
L_xCCl_{4-x}[b]	1.31	0.02	0.94
$YSiCl_{4-x}$[c]	0.99	-0.06	0.98

a. x from 0 to 4; H_3SiCl is missing from the series.

b. L = H, CH_3, F.

c. Y = H, CH_3.

d. Correlation factor of the fit.

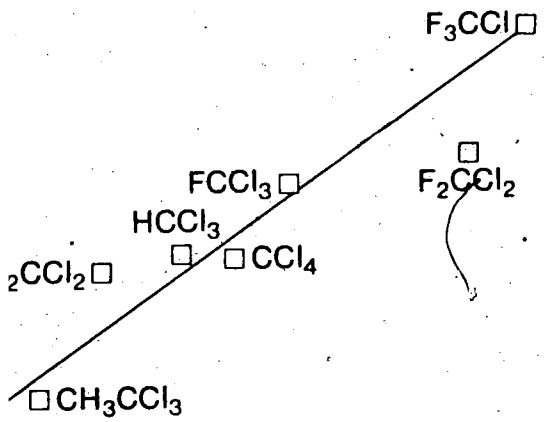

Cl_2

without d orbitals

0.5 0.0 0.5

(exp)/eV

versus experimental, ΔE_{2p}(exp), Cl $2p_{3/2}$

Calculated shifts were obtained from the

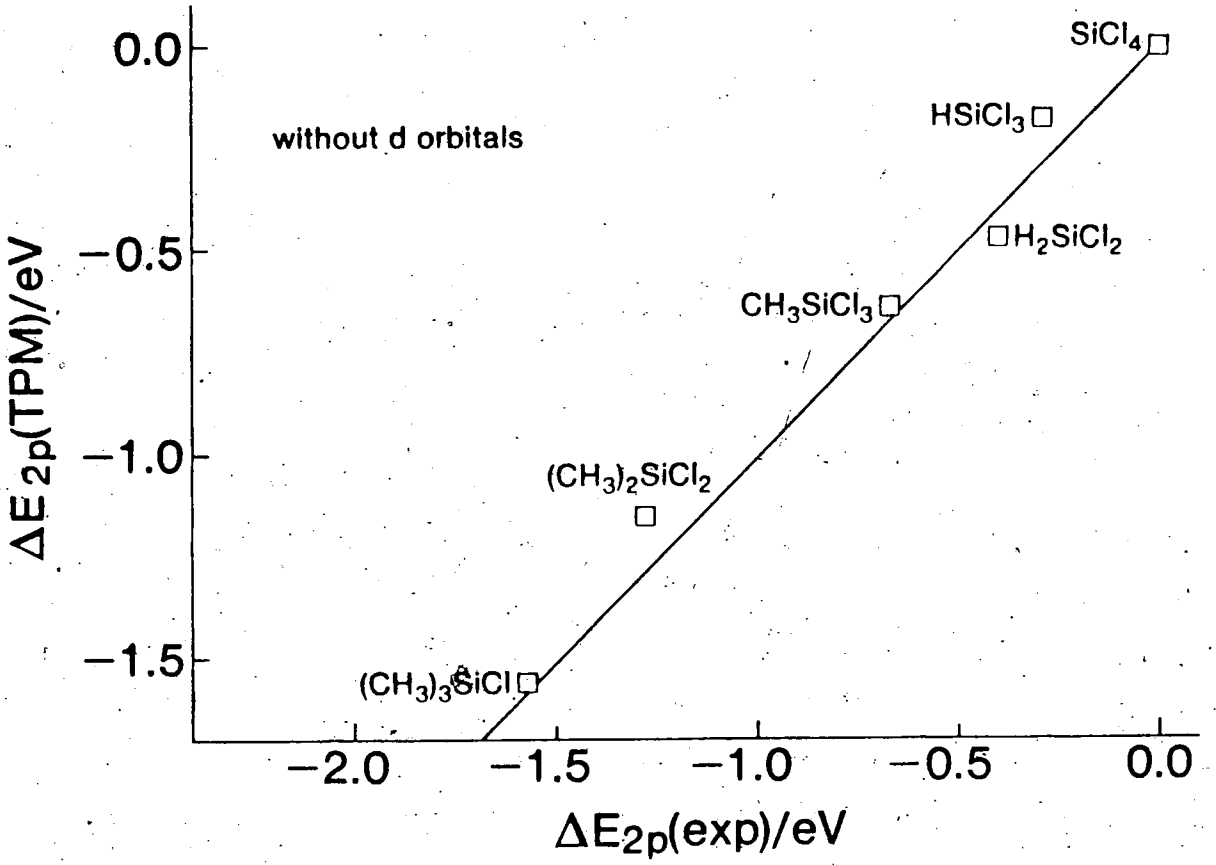

Figure III-8. Plot of calculated, $\Delta E_{2p}(TPM)$, versus experimental, $\Delta E_{2p}(exp)$, Cl $2p_{3/2}$ binding energy shifts for Silane derivatives. Calculated shifts were obtained from the Transition Potential Model (TPM) using CNDO/2 point charge potentials without d orbitals.

Table III-7. Parameters from Least-Squares Fit of Data in Figures III-7 and III-8 (TPM)

Compound[a]	Slope	Intercept	Corr.[d]
L_xCCl_{4-x}[b]	1.36	0.11	0.94
Y_xSiCl_{4-x}[c]	1.03	0.01	0.99

a. x from 0 to 4; H_3SiCl is missing from the series.

b. L = H, CH_3, F.

c. Y = H, CH_3.

d. Correlation factor of the fit.

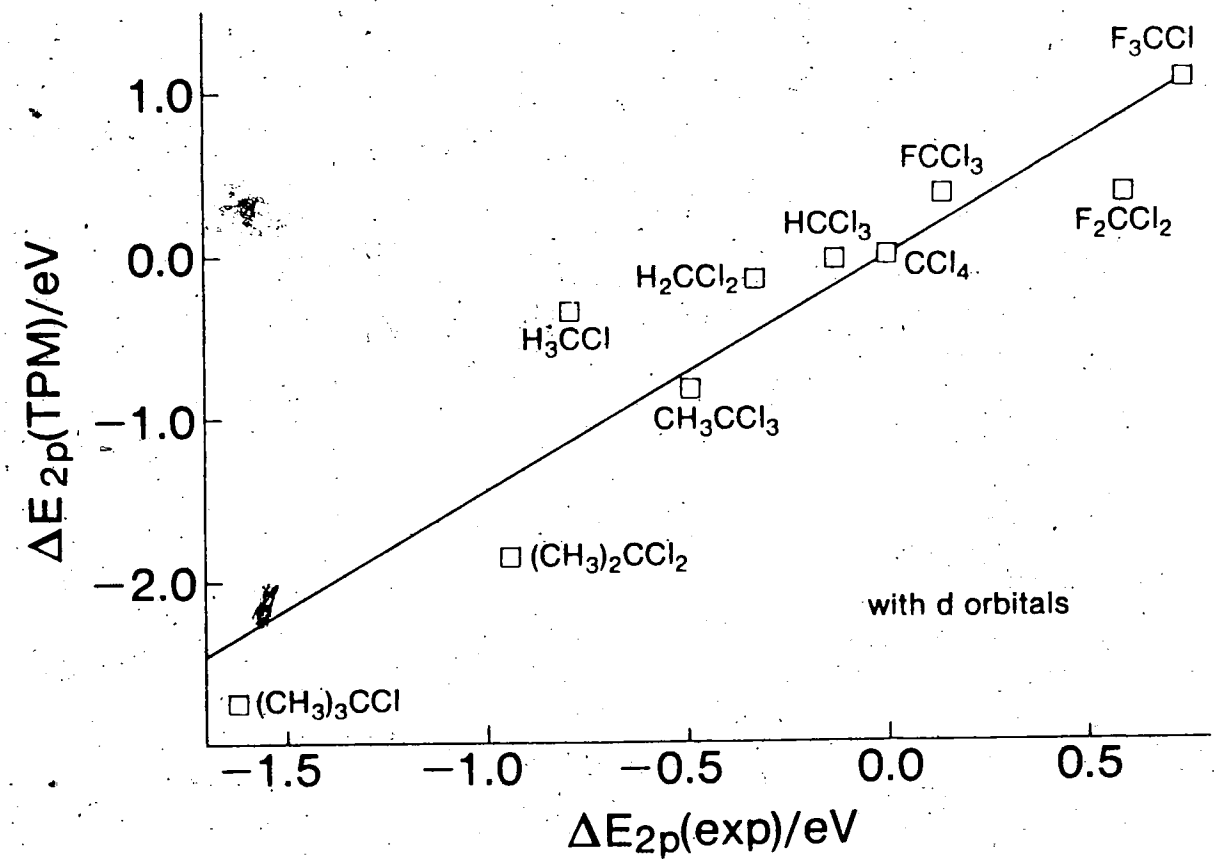

Figure III-9. Plot of calculated, ΔE_{2p}(TPM), versus experimental, ΔE_{2p}(exp), Cl $2p_{3/2}$ binding energy shifts for Methane derivatives. Calculated shifts were obtained from the Transition Potential Model (TPM) using CNDO/2 point charge potentials with d orbitals.

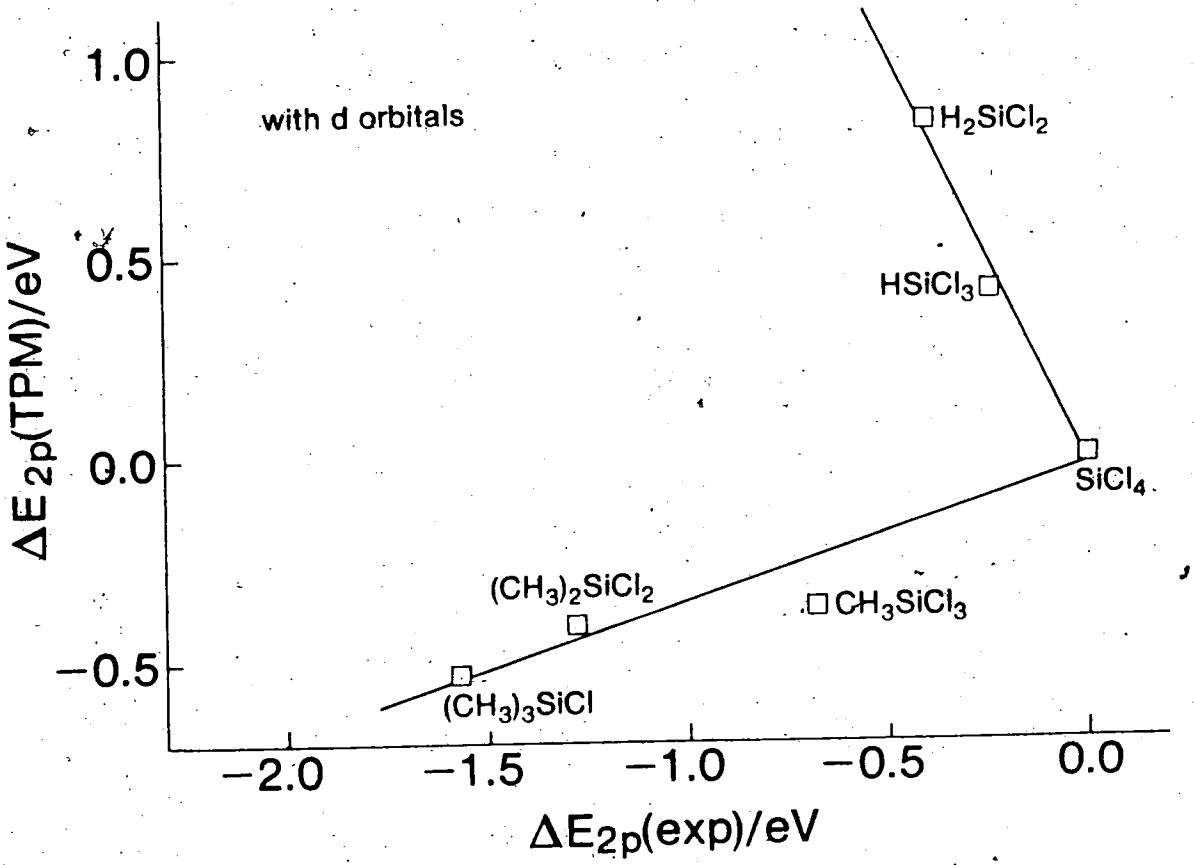

Figure III-10. Plot of calculated, $\Delta E_{2p}(TPM)$, versus experimental, $\Delta E_{2p}(exp)$, Cl $2p_{3/2}$ binding energy shifts for silane derivatives. Calculated shifts were obtained from the Transition Potential Model (TPM) using CNDO/2#point charge potentials with d orbitals.

Silicon series two different lines, one with a positive slope for the $(CH_3)_xSiCl_{4-x}$ sub-series and another with negative slope for the H_xSiCl_{4-x} sub-series were obtained. The parameters of the least squares fit relative to the TPM results with d orbitals included in the CNDO/2 basis set are given in Table III-8. The drastic change obtained for the Silicon series and shown in Figure III-10 could be due to an improper parameterization for the Silicon d orbitals.

Returning to the question of possible d orbital involvement in Silicon compounds that might have been shown by this experiment, it can be concluded, from the fact that the RPM and TPM models applied to the chemical shifts of Carbon and Silicon compounds produced similar results, that the effects which determine the Chlorine energy shifts are the same in Silicon and Carbon series and there is no evidence of "d orbital participation" in Silicon bonding.

Using equations III-8, III-17 and III-18 it is possible to estimate the magnitude of the relaxation and initial state potential effects directly from experimental results and compare them with the corresponding values obtained from CNDO calculations according to equations III-7 and III-9. The results are reported in Tables III-9

Table III-8. Parameters from Least-Squares Fit of Data in Figures III-9 and III-10 (TPM)

Compound[a]	Slope	Intercept	Corr.[b]
L_xCCl_{4-x}	1.48	0.08	0.94
$(CH_3)_xSiCl_{4-x}$	0.31	-0.05	0.95
H_xSiCl_{4-x}	-2.05	-0.02	0.99

a. x = 0 to 4; H_3SiCl is missing from the series.

b. Correlation factor of the fit.

Table III-9. Relaxation Energies and Initial State Potentials Derived from Experimental Shifts and CNDO Potentials, Relative to CCl_4 ($\Delta R = R_{compd} - R_{CCl_4}$, $\Delta V = V_{compd} - V_{CCl_4}$)

Compound	ΔR_{exp} (eV)	ΔR(CNDO) (eV)	ΔV_{exp} (eV)	ΔV(CNDO) (eV)
CCl_4	0.0	0.0	0.0	0.0
$HCCl_3$	-0.14	-0.34	0.28	0.44
H_2CCl_2	-0.45	-0.73	0.78	1.04
H_3CCl	-0.89	-1.23	1.68	1.81
CH_3CCl_3	-0.09	-0.18	0.58	0.85
$(CH_3)_2CCl_2$	-0.18	-0.31	1.12	1.86
$(CH_3)_3CCl$	-0.28	-0.50	1.90	2.82
$FCCl_3$	-0.22	-0.68	0.08	-0.16
F_2CCl_2	-0.34	-0.45	-0.25	0.12
F_3CCl	-0.73	-0.93	-0.01	0.11

and III-10. There are discrepancies between the experimental and the calculated values. However, except for the Fluorine derivatives, the trend in both series is reproduced. In agreement with other studies,[43] the relaxation within the series of compounds H_xCCl_{4-x} and H_xSiCl_{4-x} shows the effect of replacing Chlorine by Hydrogen. The high polarizability of Chlorine as compared to Hydrogen results in a decrease in relaxation energy from CCl_4 to CH_3Cl which is regular through the series. Chlorine is more electronegative than Hydrogen, and so the negative electrostatic potential at the Chlorine nucleus of interest increases in the H_xCCl_{4-x} series from CCl_4 to CH_3Cl. The effect of replacing Chlorine with Fluorine is shown by the series F_xCCl_{4-x}. The relaxation energies decrease with replacement of Chlorine by the less polarizable Fluorine. There is, however, no definite trend for ΔV, thus, as the small values observed for $FCCl_3$ and F_3CCl suggest, exchanging Fluorine for Chlorine does not have an appreciable effect on the potential term. A similar result has been found by Smith and Thomas[48] for a series of Halogenated Carboxylic acids (CH_2XCOOH) substituted by Chlorine, Bromine and Fluorine.

Table III-10. Relaxation Energies and Initial State Potentials Derived from Experimental Shifts and CNDO Potentials, Relative to $SiCl_4$ ($\Delta R = R_{comp} - R_{SiCl_4}$, $\Delta V = V_{compd} - V_{SiCl_4}$)

Compound	ΔR_{exp} (eV)	ΔR(CNDO) (eV)	ΔV_{exp} (eV)	ΔV(CNDO) (eV)
$SiCl_4$	0.0	0.0	0.0	0.0
$HSiCl_3$	-0.15	-0.11	0.39	0.39
H_2SiCl_2	-0.24	-0.25	0.64	0.91
CH_3SiCl_3	-0.12	-0.02	0.79	0.71
$(CH_3)_2SiCl_2$	-0.24	-0.06	1.52	1.33
$(CH_3)_3SiCl$	-0.15	-0.08	1.73	1.81

CNDO calculations reveal also that the ΔV term for these compounds is small. The series $(CH_3)_xCCl_{4-x}$ and $(CH_3)_xSiCl_{4-x}$ show that replacing Chlorine by CH_3 yields a slight decrease in the relaxation energy. The positive ΔV terms indicate that the electrostatic potential on Chlorine increases on replacing the electron acceptor Chlorine by the electron donor Methyl.

A direct comparison between the behavior of Silicon and Carbon compounds is provided by the relaxation energy shifts and the potential energy shifts for each Silicon compound relative to the corresponding Carbon compound. The results are given in Table III-11. The negative sign of the relaxation energy shifts means that the relaxation energy decreases upon replacement of the Carbon atom by the Silicon atom without other alterations to the molecule. The positive potential terms are in agreement with the more electropositive nature of Silicon relative to Carbon. Silicon tends to donate more negative charge to Chlorine increasing the potential at the Cl nucleus.

Auger energy shifts can be estimated from equation III-17 using ΔV and ΔR terms obtained from potential differences given by CNDO/2 calculations. The results are listed in the second column of Tables III-12 and III-13 for Carbon and Silicon compounds respectively. The

Table III-11. Relaxation Energy Shifts and Initial Potential Shifts Derived from Experimental Shifts and CNDO Potentials

($\Delta R = R_{L_xSiCl_{4-x}} - R_{L_xCCl_{4-x}}$,

$\Delta V = V_{L_xSiCl_{4-x}} - V_{L_xCCl_{4-x}}$; L = H, CH_3)

Compound	ΔR_{exp} (eV)	ΔR(CNDO) (eV)	ΔV_{exp} (eV)	ΔV(CNDO) (eV)
$SiCl_4$	-0.51	-0.71	0.76	0.80
$HSiCl_3$	-0.51	-0.48	0.87	0.75
H_2SiCl_2	-0.30	-0.23	0.62	0.67
CH_3SiCl_3	-0.54	-0.55	0.97	0.66
$(CH_3)_2SiCl_2$	-0.56	-0.37	1.15	0.08
$(CH_3)_3SiCl$	-0.38	-0.29	0.58	-0.20

Table III-12. Auger Energy Shifts $\Delta E_{Cl\ KL_{2,3}L_{2,3}(^1D_2)}$ Calculated According to Equations III-17 (CNDO) and III-22 (Semiempirical) and Experimental Auger Energy Shifts, Relative to CCl_4

Compound	ΔE_{KLL}(CNDO) (eV)	ΔE_{KLL}(semiemp) (eV)	ΔE_{KLL}(exp) (eV)
CCl_4	0.0	0.0	0.0
$HCCl_3$	-0.58	-0.18	-0.16
H_2CCl_2	-1.15	-0.59	-0.57
H_3CCl	-1.88	-1.20	-1.00
$(CH_3)CCl_3$	0.31	0.49	0.30
$(CH_3)_2CCl_2$	0.93	1.19	0.57
$(CH_3)_3CCl$	1.32	1.76	1.06
$FCCl_3$	-2.20	-1.28	-0.58
F_2CCl_2	-1.23	-1.01	-1.28
F_3CCl	-2.68	-2.28	-2.20

Table III-13. Auger Energy Shifts $\Delta E_{Cl\ KL_{2,3}L_{2,3}(^1D_2)}$ Calculated According to Equations III-17 (CNDO) and III-22 (Semiempirical) and Experimental Auger Shifts Relative to $SiCl_4$)

Compound	ΔE_{KLL}(CNDO) (eV)	ΔE_{KLL}(semiemp) (eV)	ΔE_{KLL}(exp) (eV)
$SiCl_4$	0.0	0.0	0.0
$HSiCl_3$	0.06	0.02	-0.06
H_2SiCl_2	0.16	0.18	-0.08
CH_3SiCl_3	0.65	0.45	0.42
$(CH_3)_2SiCl_2$	1.15	0.79	0.80
$(CH_3)_3SiCl$	1.57	1.43	1.27

experimental Auger energy shifts are given in the fourth column of the same tables. As shown in the tables, differences exist between the two sets of values. In equation III-17 the Auger energy shift is expressed as a function of a potential term $\Delta V(Y)$ and a relaxation term $\Delta R(Y)$ associated with the formation of a single core hole in the level Y. Equation III-13 represents the Relaxation Potential Model for the Auger shifts and can not be used for Chlorine because of the limitations of the CNDO parameterization. If equation III-17 is subtracted from equation III-13 and ΔR is expressed as in equation III-9, equation III-20 is obtained.

$$\Delta E_{Au}(\text{eq. III-13}) - \Delta E_{Au}(\text{eq. III-17}) =$$

$$\frac{1}{2}[\Delta V_n(Z+2)-\Delta V_n(Z+1)] - \frac{1}{2}[\Delta V(Z+1)-\Delta V(Z)] =$$

$$= \Delta R^* - \Delta R \qquad \text{III-20}$$

The second term in brackets is ΔR which represents the relaxation energy shift associated with the formation of a single core hole. The first term in brackets, which is indicated as ΔR^*, represents the relaxation energy shift associated with the formation of a double core hole from a

single core hole. The validity of expression III-17 is based on the assumption that the change in potential is related linearly to the core charge and therefore $\Delta R=\Delta R^*$. This does not seem to be always true. Adams[37] showed that the correlation between the relaxation term ΔR, obtained from ab initio LCAO SCF MO calculations, and the experimental Auger parameter $\Delta\alpha$, defined in equation III-19, improves if in equation III-18 the relaxation energy associated with the formation of the double core hole, ΔR^*, is considered instead of ΔR yielding

$$\Delta E_{Au} + \Delta E_B = 2\Delta R^* \qquad \text{III-21}$$

Combining equations III-8 and III-21 the following equation is obtained

$$\Delta E_{Au} = \Delta V + \Delta R + 2\Delta R^* \qquad \text{III-22}$$

It was not possible to compute potentials for the nuclear charge of Z+2, therefore ΔR^* was obtained from the experimental energy shifts according to equation III-21 and values of ΔV and ΔR were obtained from CNDO/2 calculations. In order to distinctively label these new calculations, the attribution "semiempirical" has been

attached to these values. The results are shown in the third column of Tables III-12 and III-13. In both series of compounds, a better agreement between experimental shifts and calculated shifts results from this correction. The discrepancies for the H_xSiCl_{4-x} may be due to the very small experimental shifts which confer larger proportionate experimental errors. The smaller Auger shifts for these compounds as compared to the H_xCCl_{4-x} (Tables III-3 and III-4) seem to be the only appreciable difference between Carbon and Silicon derivatives. However, if the small relaxation for Silicon compounds, which determines the magnitude of the Auger shifts, was due to a participation of the d orbitals of Silicon in a $(p\rightarrow d)\pi$ bonding with the Chlorine, this would increase from $SiCl_4$ to H_2SiCl_2 and would have decreased the capability of the Chlorine and Silicon charge to relax. The calculated values of ΔR should therefore have been less negative than the experimental ones because the model that was used cannot accommodate this effect. On the other hand, considering the way ΔR is calculated, as difference of potential terms, it is possible that a fortuitus cancellation of errors arose to yield relaxation terms comparable with the experimental ones.

E. Conclusion

The application of the Relaxation Potential Model and Transition Potential Model to the Cl 2p chemical shifts in substituted Chloromethanes and Chlorosilanes gives better results than the ground state GPM scheme. The inclusion of d orbitals in the CNDO calculations did not alter the correlation in the Methane series but the correlation between calculated predictions and experimental results for the Silane series was poorer, probably due to an inadequate parameterization for the d orbitals. No evidence of d orbital participation in Silicon bonding is shown from these results. The relaxation of the molecule accompanying the photoionization is different from the relaxation accompanying the Auger process, and depending on the kind of substituents in the compound, the relaxation affects differently the photoelectron and Auger electron energies. A better estimation of the Auger shifts is obtained if the relaxation associated with the formation of a double core hole from a single core hole is considered instead of the relaxation associated with the formation of a single core hole from the ground state.

CHAPTER IV

GERMANIUM $L_{2,3}M_{4,5}M_{4,5}$ AND $L_{2,3}M_{2,3}M_{4,5}$ AUGER SPECTRA OF GERMANIUM COMPOUNDS

A. Introduction

To analyze the influence of the chemical environment on inner shell Auger spectra, Ge $L_{2,3}M_{2,3}M_{4,5}$ and $L_{2,3}M_{4,5}M_{4,5}$ spectra have been measured in a variety of Germanium compounds. In this case the Auger process is referred to as inner shell because it involves only core electrons; the valence electrons are not specifically involved in the transitions. For Germanium and the other elements of the third period, the ionization probability of the L levels by Al $K\alpha_{1,2}$ or Mg $K\alpha_{1,2}$ X-ray is high.[7b] Ionization of L_2 and L_3 levels leads predominantly to LMM rather than LMN or LNN Auger spectra.[7b] Ionization of the L_1 level by Al $K\alpha_{1,2}$ X-rays is only between 15% to 40% as probable as $L_{2,3}$ ionization and furthermore this vacancy leads predominantly to $L_1L_{2,3}M$ Coster-Kronig Auger transitions.[7] In addition, transitions involving the M_1 level are usually very weak so the $L_{2,3}M_1M_{2,3}$ and the

$L_{2,3}M_1M_{4,5}$ transitions play a minor role in the LMM Auger spectra,[49] in agreement with a small transition probability value (see equation I-12). As a result Ge Auger spectra are dominated by the $L_{23}M$ spectra where the M components of high angular momentum dominate.

Most peaks of the LMM Auger spectra are broad and do not show much structure because of the large number of final states with different terms and energies. The term splittings are small, only a few electron volts, and are comparable to the lifetime broadening of the Auger transitions. As it will be seen for the Germanium case, the $L_{2,3}M_{4,5}M_{4,5}$ term splittings are more easily resolvable than the $L_{2,3}M_{2;3}M_{4,5}$ term splittings.

In this work the experimental energies and intensities of the Auger spectra are compared with the theoretical calculations.

Atomic Germanium has an open shell ground state electronic configuration ($3d^{10}4s^24p^2$) so that coupling of the 4p electrons with the final state holes in the 3d or 3p shell resulting from the $L_{2,3}M_{4,5}M_{4,5}$ and $L_{2,3}M_{2,3}M_{4;5}$ Auger transitions gives rise to additional energy level splittings. However, the molecules provide a closed shell configuration with filled molecular orbitals. The total coupling between final state holes of the Auger process

and valence orbitals is therefore zero. This greatly simplifies the analysis of the spectra. Calculations were based on the intermediate coupling (IC) and Russell-Saunders (LS) coupling schemes. Relaxation contributions were evaluated from Auger and core level measurements.

B. Experimental

The $L_{2,3}M_{2,3}M_{4,5}$ and $L_{2,3}M_{4,5}M_{4,5}$ Auger spectra of Germanium in gaseous GeH_4, $Ge(CH_3)_4$, $Ge(C_2H_5)_4$, $GeCl_4$, GeF_4, and solid GeO_2 were measured. GeO_2 and $GeCl_4$ were obtained from Aldrich Chemical Company; GeH_4 from Matheson; GeF_4 from Ozark Mahoning, $Ge(CH_3)_4$ and $Ge(C_2H_5)_4$ from Alfa Inorganics. Al $K\alpha_{1,2}$ radiation (1486.6 eV)[21] was used to excite the Auger spectra. The spectra were calibrated with Ar $2p_{3/2}$ photoelectron line (248.62(8) binding energy)[25] and Ne $KL_{2,3}L_{2,3}(^1D_2)$ Auger line (804.557(17) eV kinetic energy)[24]. The Ge $2p_{1/2}$, Ge $2p_{3/2}$ photoelectron lines were excited by Ag $L\alpha_1$ radiation with energy of 2984.34(2) eV[23] and calibrated by comparison with the Kr $L_2M_{4,5}M_{4,5}$ Auger line (1513.73(10) eV kinetic energy see Chapter II) and Ne 1s photoelectron line (870.312(17) eV binding energy).[24] The Ge 3d, Ge 3p photoelectron lines were also obtained with Al $K\alpha_{1,2}$ radiation and were calibrated with respect to Ne 2s (48.42

eV[25] binding energy) photoelectron line and Ne $KL_{2,3}L_{2,3}(^1D_2)$ Auger lines. For solid GeO_2, the Auger spectra and the photoelectron lines were calibrated with respect to the Fermi level using Au $4f_{7/2}$ photopeak (83.8(2) eV binding energy)[25] originating from a small spot evaporated onto the surface of the sample.

C. Theory

To obtain a theoretical estimate of the energies in a group of Auger diagram lines the scheme proposed by Shirley[50] can be used. Accordingly the energy of LMM Auger electron transitions can be written as

$$E(L_aM_bM_c; X) = E(L_a) - E(M_b) - E(M_c) - F(M_bM_c; X) + R_S^T(M_bM_c) \quad \text{IV-1}$$

$E(L_a)$, $E(M_b)$, $E(M_c)$ are the experimental core level binding energies which are determined by XPS. $F(M_bM_c; X)$ and $R_S^T(M_bM_c)$ are the coulombic interaction energy and the static relaxation energy respectively which have already been described in Chapter I. Combining the core electron binding energies and the Auger energies, the following relation is obtained

$$E(L_a)-E(M_b)-E(M_c)-E(L_aM_bM_c;\ X) = F(M_bM_c;\ X)-R_S^T(M_bM_c) \quad \text{IV-2}$$

The expression on the left side of equation IV-2 which is composed of only experimentally determined quantities is the Auger parameter ξ as defined by Lang and Williams:[51]

$$\xi = E(L_a)-E(M_b)-E(M_c)-E(L_aM_bM_c;\ X) \quad \text{IV-3}$$

From equations IV-2 and IV-3 it follows that the Auger parameter is equal to the coulombic term minus the relaxation term.

$$\xi = F(M_bM_c;\ X) - R_S^T(M_bM_c) \quad \text{IV-4}$$

and if the term $F(M_bM_c;\ X)$ can be estimated, equation IV-4 allows the determination of $R_S^T(M_bM_c)$.

The value of the coulombic interaction energy depends on the coupling scheme employed.[18] In pure LS coupling the d^{-2} hole state configuration corresponding to the final state of the $L_{2,3}M_{4,5}M_{4,5}$ Auger process gives rise to 5 levels: ^1S, ^1G, ^3P, ^1D, ^3F. The $p^{-1}d^{-1}$ hole state configuration corresponding to the $L_{2,3}M_{2,3}M_{4,5}$ process gives rise to 6 levels: ^1P, ^3P, ^1D, ^3D, ^1F, ^3F. In Intermediate Coupling the levels arising from the configuration d^{-2} are split according to the J value,

yielding 9 states. The six levels arising from the configuration $p^{-1}d^{-1}$ are split into 12 states. The general expressions for $F(M_b M_c; X)$ are given in ref. 52 in terms of Slater's integrals.[53] The energies of each final state belonging to the d^{-2} configuration are, in LS coupling:

$$E(^1G_4) = 2E_{M_{4,5}} + F^0(3d3d) + \frac{4}{49}F^2(3d3d) - \frac{1}{441}F^4(3d3d)$$

$$E(^3F_{432}) = 2E_{M_{4,5}} + F^0(3d3d) - \frac{8}{49}F^2(3d3d) - \frac{1}{49}F^4(3d3d)$$

$$E(^1S_o) = 2E_{M_{4,5}} + F^0(3d3d) + \frac{2}{7}F^2(3d3d) - \frac{2}{7}F^4(3d3d) \qquad \text{IV-5}$$

$$E(^3P_{210}) = 2E_{M_{4,5}} + F^0(3d3d) + \frac{1}{7}F^2(3d3d) - \frac{4}{21}F^4(3d3d)$$

$$E(^1D_2) = 2E_{M_{4,5}} + F^0(3d3d) - \frac{3}{49}F^2(3d3d) + \frac{4}{49}F^4(3d3d)$$

Because of the quite large spin-orbit splitting in the initial state ($2p_{1/2}$-$2p_{3/2}$≈30 eV)[54] and the small spin-orbit splitting in the final state ($3d_{3/2}$-$3d_{5/2}$≈0.7 eV)[54], the mixed coupling scheme[55,56] was used for the calculation of the relative intensities of the line components. This scheme applies jj coupling for the initial state and intermediate coupling or LS coupling for

the final state. For intermediate coupling, the spin-orbit interaction matrices of Condon and Shortley[16] were used. The numerical value of the 3d spin-orbit parameter was obtained from the theoretical calculations of Huang et al.[57] The relaxation term $R_S^T(M_bM_c)$, as described in the general introduction (Chapter I), is the total static relaxation term which is the amount by which the binding energy of the second electron in the Auger final state is reduced by the relaxation of the passive orbitals toward the hole left by the removal of the first electron. This "static relaxation" is different from the so-called "dynamic relaxation" that is associated with the ionization of the electrons $L_{2,3}$ and $M_{4,5}$ (or $L_{2,3}$ and $M_{2,3}$) in the analysis of the Auger process energies using the formation energy of the initial hole state (step (a) of equation IV-6) and step (b) of equation IV-6, an experimental measure of the formation of one of the holes created in the Auger process,

$$\begin{aligned} &\text{(a)}\quad L_{2,3} \rightarrow L_{2,3}^{+} + e^{-} \\ &\text{(b)}\quad M_{4,5} \rightarrow M_{4,5}^{+} + e^{-} \\ &\text{(c)}\quad M_{4,5}^{+} \rightarrow M_{4,5}^{++} + e^{-} \end{aligned} \qquad \text{IV-6}$$

and which is accounted for by the use of empirical binding energies. The static relaxation energy R_S^T, which arises in step (c) of equation IV-6 is usually split into two terms:

$$R_S^T(M_{4,5}M_{4,5}) = R_S^a(M_{4,5}M_{4,5}) + R_S^{ea}(M_{4,5}M_{4,5}) \quad \text{IV-7}$$

$R_S^a(M_{4,5}M_{4,5})$ is the static relaxation of a free atom and $R_S^{ea}(M_{4,5}M_{4,5})$ is the extraatomic relaxation energy that arises from electronic relaxation in the surrounding. The atomic term is set equal to twice the dynamic relaxation which accompanies photoemission,[58,59]

$$R_S^a(M_{4,5}M_{4,5}) = 2R_D(M_{4,5}) \quad \text{IV-8}$$

This dynamic term can be calculated from the optimized Hartree-Fock-Slater results of Rosen and Lindgren[60], from

$$R_D = \varepsilon_{HF} - \varepsilon_{\Delta SCF} \quad \text{IV-9}$$

where ε_{HF} is the orbital eigenvalue in the Hartree-Fock scheme and $\varepsilon_{\Delta SCF}$ is the difference in total energy of separate field calculations for the neutral atom and appropriate ion. Unfortunately, calculations have not been done for Germanium, however it is possible, with reasonable accuracy, to apply the binding energy calculations for Krypton, which gave $R_D(M_{4,5})_{Kr} = 8.9$ eV. Applying IV-8, gives therefore $R_S^a(M_{4,5}M_{4,5})_{Kr} = 17.8$ eV.

The corresponding quantity for Germanium was estimated by subtracting from $R_S^a(M_{4,5}M_{4,5})_{Kr}$ the contribution to the atomic relaxation arising from the four extra 4p electrons of Krypton. This last quantity may be calculated using a combination of Slater's integrals,[52] the equivalent cores approximation[30,31] and Mann's tables.[53] Therefore from the appropriate terms for Krypton the corresponding terms for Bromine were subtracted

$$\Delta R_{4p} = [F^0(3d4p) - \tfrac{1}{15} G^1(3d4p) - \tfrac{3}{70} G^3(3d4p)]_{Kr} - [F^0(3d4p) - \tfrac{1}{15} G^1(3d4p) - \tfrac{3}{70} G^3(3d4p)]_{Br} \qquad \text{IV-10}$$

The coefficients of the G^k integrals were obtained from standard multiplet theory.[52] The Slater integrals F^0 and G^k do not vary linearly with the atomic number so the equivalent cores approximation produced different values for the relaxation contribution of the 4p electrons when calculated for Br, Se, As, Ge; $\Delta R_{4p}(Br) = 1.22$ eV, $\Delta R_{4p}(Se) = 1.28$ eV, $\Delta R_{4p}(As) = 1.36$ eV, $\Delta R_{4p}(Ge) = 1.50$ eV. The average of the four was taken, multiplied by 4 and subtracted from $R_S^a(M_{4,5}M_{4,5})_{Kr}$ giving $R_S^a(M_{4,5}M_{4,5})_{Ge} = 12.5$ eV. The atomic relaxation calculated as described can be expressed as the sum of separate relaxation contributions from the various shells

$$R_S{}^a(M_{4,5}M_{4,5}) = R^{inner}(K \text{ and } L) + R^{intra}(M) + R^{outer}(N) \qquad \text{IV-11}$$

The inner-shell term has been found by Hedin and Johansson,[29] via the ΔE_{SCF} method, to be negligibly small compared to the intra and outer shell terms. As indicated in Chapter III, the relaxation energy is given by a combination of Coulomb and exchange integrals representing the electron interaction energy (equation III-2). Slater[52] has given the expression for the interaction energies between electrons of angular momenta ℓ and ℓ'. Shirley[39] obtained, on summing over the outer shells and using the "equivalent cores" approach, the following expression for the outer shell relaxation;

$$\langle n\ell|V_R|n'\ell'\rangle = \sum_{\ell'} \frac{N(n'\ell')}{4\ell' + 2}\{f(\ell\ell')\Delta[F^0(n\ell,n'\ell')] - \Delta \sum_k g_k[(\ell\ell')G^k(n\ell,n\ell')]\} \qquad \text{IV-12}$$

where

$$\Delta F^0(n\ell,n'\ell') \equiv F^0(n\ell,n'\ell';\ Z+1) - F^0(n\ell,n'\ell';\ Z) \qquad \text{IV-13a}$$

and

$$\Delta G^k(n\ell,n'\ell') \equiv G^k(n\ell,n'\ell';\ Z+1) - G^k(n\ell,n'\ell';\ Z)$$

IV-13b

$N(n'\ell')$ is the occupation number of the $n'\ell'$ subshell in the parent atom. The factors $f(\ell\ell')$ and $g_k(\ell\ell')$ were obtained from Slater's results[52] and they are listed by Shirley.[39] They apply rigorously to closed outer shells, but it has been observed[39] that only small errors arise if they are used for open shell atomic configurations. For Germanium, the outer shells are 4s and 4p with population of 2 each, and the expressions used in the equivalent cores approximation were:

$$\Delta F^0(3d4\ell') = F^0(3d4\ell';\ As) - F^0(3d4\ell';\ Ge) \qquad \text{IV-14(a)}$$

$$\Delta G_k(3d4\ell') = G^k(3d4\ell';\ As) - G^k(3d4\ell';\ Ge) \qquad \text{IV-14(b)}$$

Equation IV-12 becomes

$$R^{outer}(3d3d) = \frac{2}{6}[6\Delta F^0(3d4p) - \frac{2}{5}\Delta G^1(3d4p)] - \frac{9}{35}\Delta G^3(3d4p) + 2\Delta F^0(3d4s) + \frac{1}{5}\Delta G^2(3d4s) \qquad \text{IV-15}$$

Evaluation of IV-15 with F^0 and G^k integrals from Mann's tables[53] yielded $R^{outer}(3d3d)_{Ge} = 5.6$ eV. Subtracting

this value from the total atomic relaxation calculated above, yielded $R^{intra}(3d3d)_{Ge} = 6.9$ eV.

The values which have been obtained for R^{intra} and R^{outer} are only an approximate estimate but they are useful in providing insight into the magnitude of the orbital contributions to the total atomic relaxation. Differently from the inner core electron case, for which the outer shell relaxation is by far the largest contribution to the relaxation, in the case of a 3d electron in Germanium, the intra shell relaxation seems to be the largest term.

The calculation for the extraatomic relaxation (equation IV-7) is more difficult being very sensitive to the chemical environment in the molecule. A crude estimate, giving the order of magnitude, can be obtained on the basis of a model[59,61] postulated for metals. The model assumes that the extra unit of positive charge induced on one atom in the molecule by the appearance of a hole in the filled 3d orbital is screened by the outermost electrons in such a way that the outgoing Auger electron sees less of the positive charge and leaves with an increased kinetic energy. In the limit of completely local screening, the screening charge coming from outside the atom occupies the first unfilled atomic orbital. The

extraatomic relaxation, $R_S^{ea}(M_{4,5}M_{4,5})$, is then given by the two-electron interaction between this unfilled orbital, which is a 4p, and the 3d orbital expressed as a combination of Slater's integrals[52]

$$R_S^{ea}(3d3d) = F^0(3d4p) - \frac{1}{15}G^1(3d4p) - \frac{3}{70}G^3(3d4p) \qquad \text{IV-16}$$

Using the appropriate values for F^0 and G^k integrals, equation IV-16 yielded $R_S^{ea}(3d3d)$ = 11.2 eV. The total static relaxation for Ge metal therefore is $R_S^T(M_{4,5}M_{4,5})$ = 23.64 eV. Confirmation of the approach is provided by the reasonable agreement of our estimate with the value of 23.3 eV found by Antonides et al. for Germanium metal[62] who used an empirical approach to evaluate this term.

The intensities of various $L_{2,3}M_{4,5}M_{4,5}$ lines were calculated in the mixed coupling scheme with jj coupling in the initial state and LS coupling in the final state. The transition rates for LS coupling in the final state were obtained from the transition amplitudes as given by H. and S. Aksela[63] using the direct and exchange matrix elements[64] D and E defined in Chapter I by equations I-16 and I-17.

D. Results and Discussion

The binding energies of Ge 2p,3p,3d photoelectrons, and the kinetic energies of Ge $L_{2,3}M_{4,5}M_{4,5}(^1G_4)$ and $L_{2,3}M_{2,3}M_{4,5}(^1F^1P)$ Auger electrons are given in Table IV-1. For comparison purpose the Germanium metal energies from ref. 62 are included. Spin-orbit splittings are the same for each of the compounds within the experimental error. The spin-orbit splittings $\Delta 2p$ obtained from the difference between the measured Auger $L_2M_{4,5}M_{4,5}(^1G_4)$ and $L_3M_{4,5}M_{4,5}(^1G_4)$ lines agree with those obtained directly from the photoelectron measurements. The value of ~31 eV (the same for all compounds) agrees with the compilation by Sevier[54] and the value given by Antonides et al.[62] for Ge metal. The splittings obtained from the $L_{2,3}M_{2,3}M_{4,5}$ spectra are less reliable because of the poorer statistics of the experimental data. The Ge $L_{2,3}M_{4,5}M_{4,5}$ and $L_{2,3}M_{2,3}M_{4,5}$ spectra of the six compounds are shown in Figures IV-1 to IV-12. The band components obtained by curve fitting procedures[26] are shown under the experimental envelope. Due to the limited resolution of the spectra, only four peaks were fitted in each group L_2-$L_3M_{4,5}M_{4,5}$. For the fitting procedure a Lorentzian line shape with a constant tail[26] was used. A Gaussian line shape gave a larger least squares standard deviation

Table IV-1. Germanium Binding Energies (eV) and Auger Energies (eV) for Germanium Compounds

	Ge_{metal}[a]	$GeO_2(s)$[b]	$Ge(C_2H_5)_4(g)$	$Ge(CH_3)_4(g)$	$GeH_4(g)$	$GeCl_4(g)$	$GeF_4(g)$
E_B							
$2p_{1/2}$	1247.2	1251.21(10)[c]	1254.15(05)	1254.50(05)	1256.42(05)	1258.58(05)	1260.01(05)
$2p_{3/2}$	1216.2	1220.16(10)	1223.28(05)	1223.61(05)	1225.31(05)	1227.67(05)	1229.28(05)
$3p_{1/2}$	125.2	128.62(10)	131.81(05)	132.14(05)	133.65(05)	136.40(05)	137.94(05)
$3p_{3/2}$	121.4	124.55(10)	127.84(05)	128.06(05)	129.48(05)	132.08(05)	133.86(05)
3d	29.2	32.65(10)	35.70(05)	35.98(05)	37.43(05)	39.93(05)	42.16(05)
Auger							
$L_2M_{4,5}M_{4,5}$; $^1G_4$	1175.9	1169.63(10)	1164.45(05)	1163.00(05)	1160.60(05)	1159.89(05)	1155.16(05)
$L_3M_{4,5}M_{4,5}$; $^1G_4$	1144.9	1138.59(10)	1133.51(05)	1132.53(05)	1129.51(05)	1128.89(05)	1124.15(05)
$L_2M_{2,3}M_{4,5}$; $^1F^1P$	1074.3	1068.25(20)	1061.70(20)	1061.50(10)	1058.45(06)	1057.64(10)	1053.31(10)
$L_3M_{2,3}M_{4,5}$; $^1F^1P$	1043.3	1037.04(20)	1031.23(10)	1030.30(10)	1027.57(06)	1026.89(04)	1022.42(10)

a. Experimental values from Ref. 62.

b. The energies relative to $GeO_2(s)$ are obtained with respect to the Fermi level.

c. The values in brackets represent the maximum deviations from the average values for three different measurements.

Figure IV-1. Germanium $L_{2,3}M_{4,5}M_{4,5}$ Auger spectrum of solid GeO_2 excited by Al $K\alpha_{1,2}$ radiation. The solid lines indicate the experimental positions of the multiplet terms. The dashed lines indicate the LS calculated positions of the terms unresolved in the spectrum.

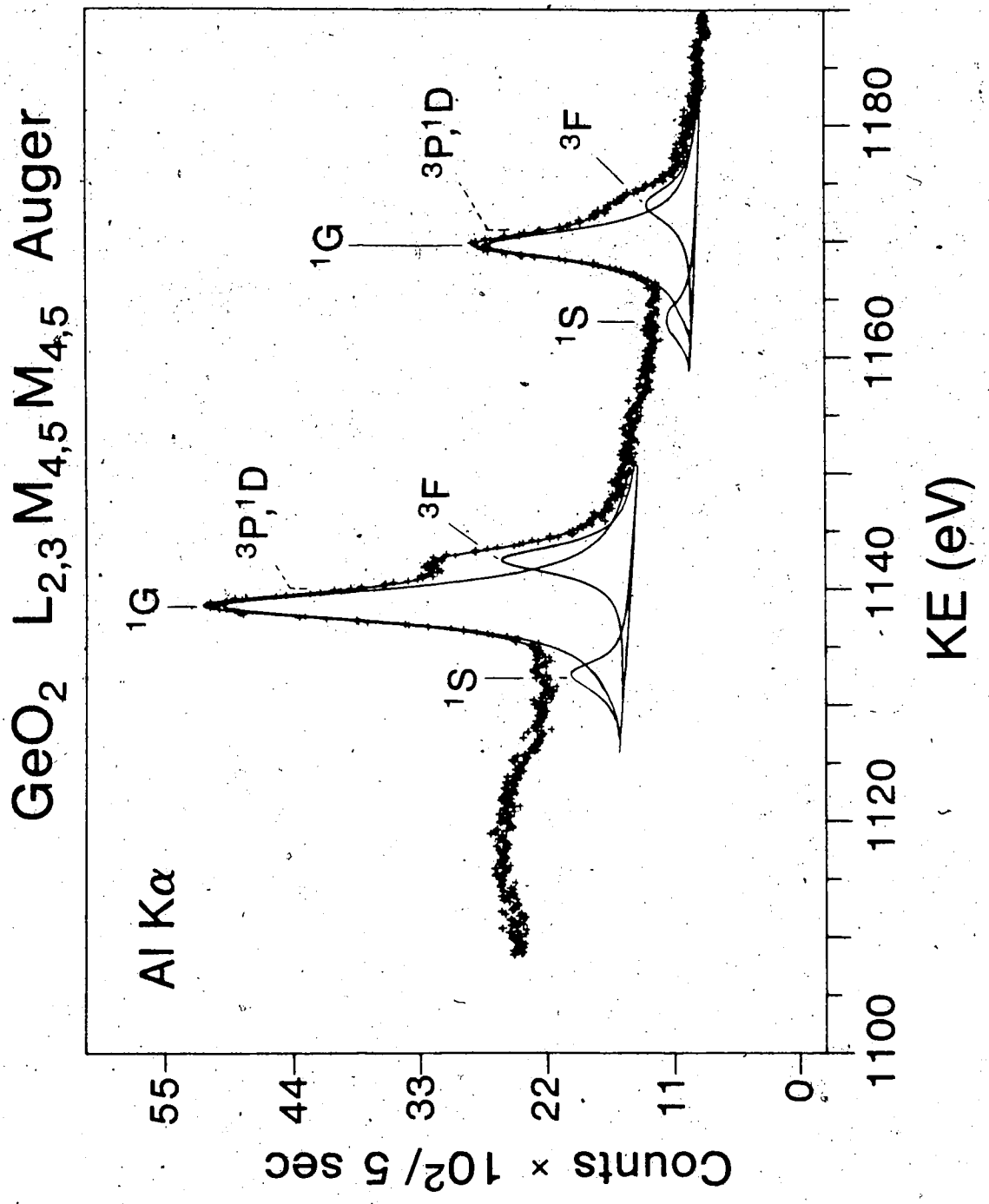
GeO2 L2,3 M4,5 M4,5 Auger
Al Kα
1G
3P,1D
3F
1S
1G
3P,1D
3F
1S
Counts × 10²/ 5 sec
0
11
22
33
44
55
1100
1120
1140
1160
1180
KE (eV)

Figure IV-2. Germanium $L_{2,3}M_{2,3}M_{4,5}$ Auger spectrum of solid GeO_2 excited by Al $K\alpha_{1,2}$ radiation. The solid lines indicate the experimental positions of the multiplet terms. The dashed lines indicate the LS calculated positions of the terms unresolved in the spectrum.

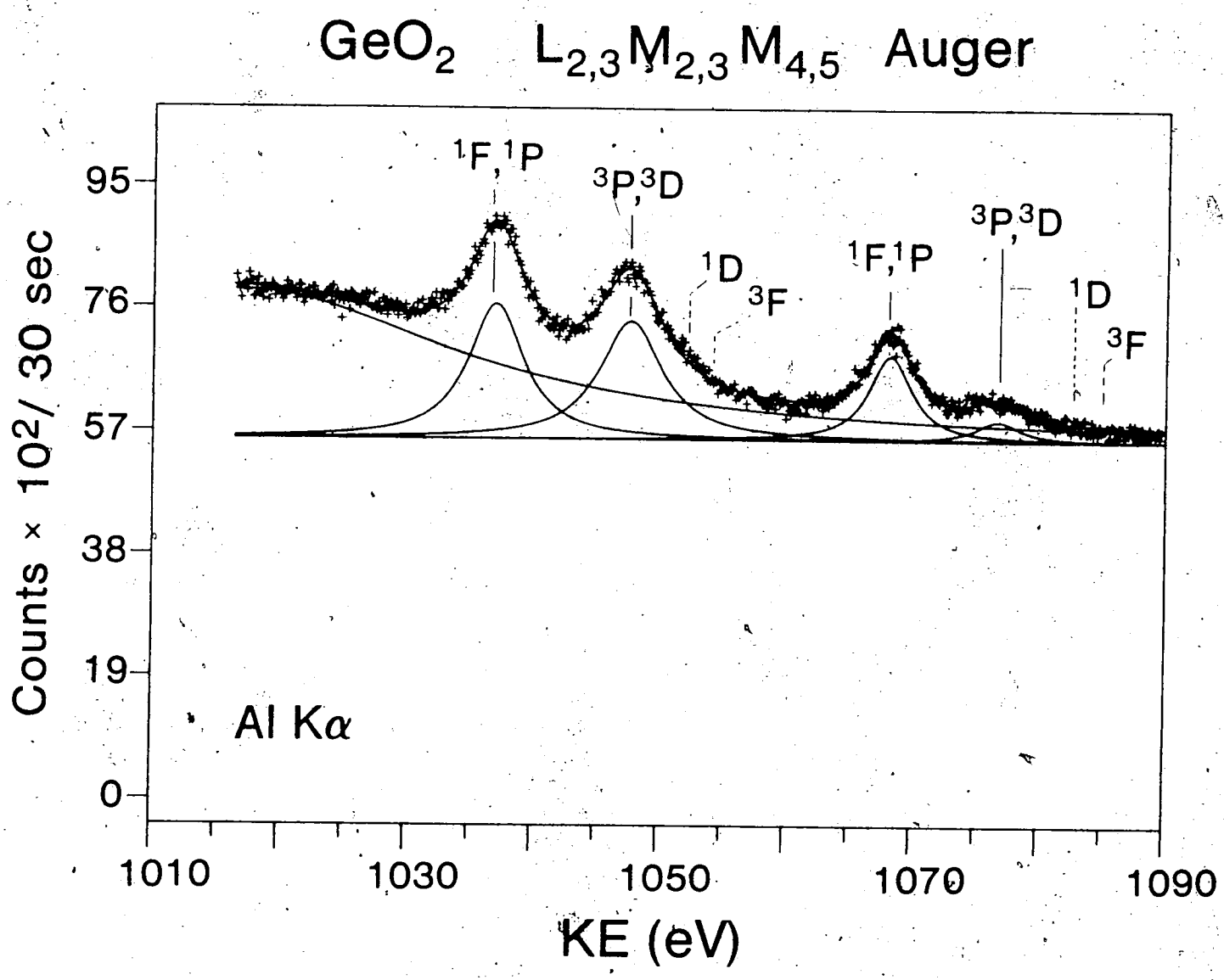
GeO2 L2,3M2,3M4,5 Auger
1F,1P
3P,3D
1D
3F
1F,1P
3P,3D
1D
3F
95
76
57
38
19
0
Counts × 10²/ 30 sec
Al Kα
1010
1030
1050
1070
1090
KE (eV)

Figure IV-3. Germanium $L_{2,3}M_{4,5}M_{4,5}$ Auger spectrum of $Ge(C_2H_5)_4$ vapor excited by Al $K\alpha_{1,2}$ radiation at a sample pressure of 200μ. s=satellite; α= Ge 3d photoelectron line excited by Ge Lα; β= Ge 3d photoelectron line excited by Ge Lβ.

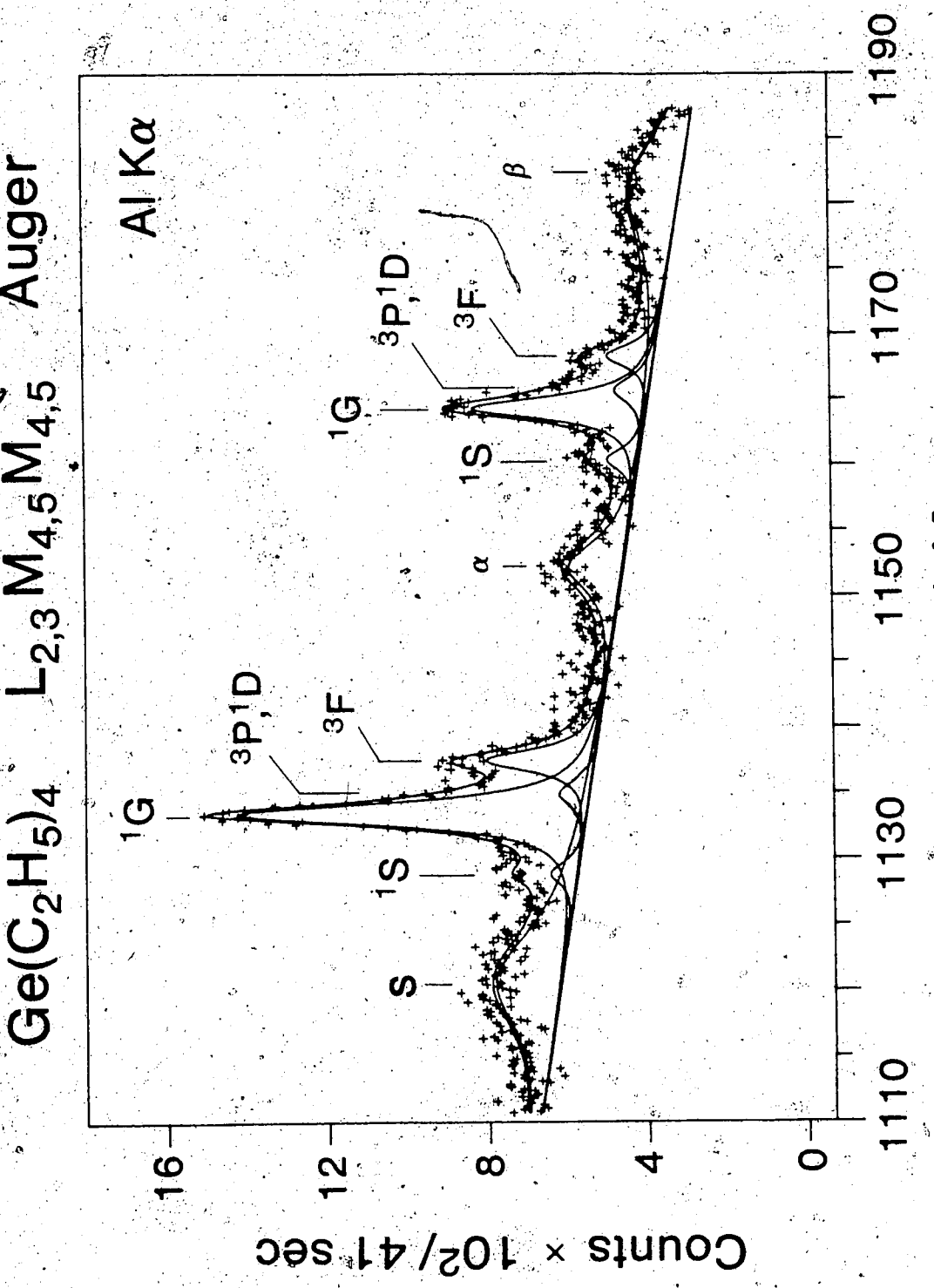
Ge(C2H5)4 L2,3M4,5M4,5 Auger
Al Kα
1G
3P,1D
3F
1S
S
α
β
Counts × 10²/41 sec
KE (eV)
0
4
8
12
16
1110
1130
1150
1170
1190

Figure IV-4. Germanium $L_{2,3}M_{2,3}M_{4,5}$ Auger spectrum of $Ge(C_2H_5)_4$ vapor excited by Al $K\alpha_{1,2}$ radiation at a sample pressure of 200μ. The solid lines indicate the experimental positions of the multiplet terms. The dashed lines indicate the LS calculated positions of the terms unresoved in the spectrum.s = satellite.

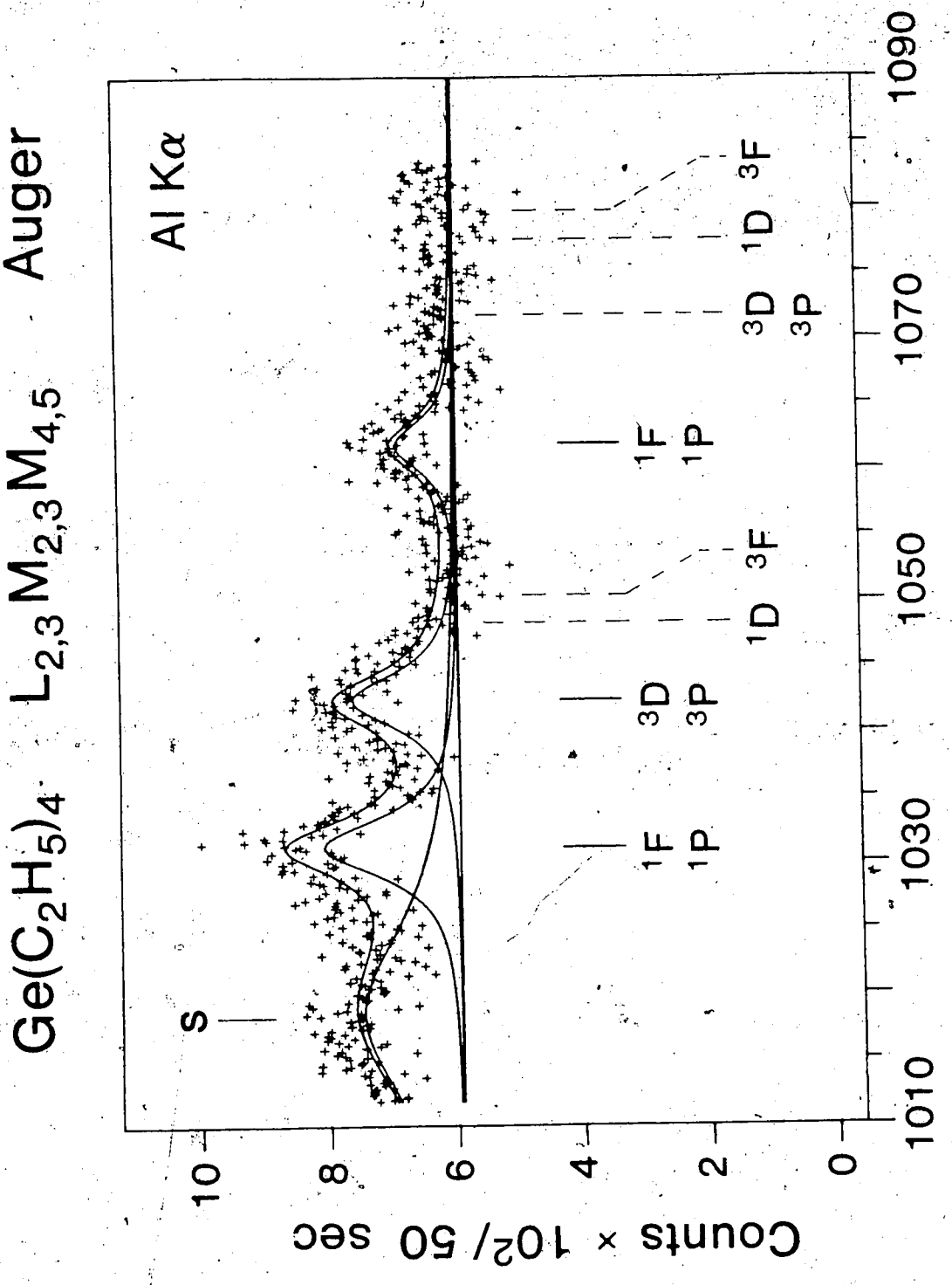
Ge(C2H5)4 L2,3M2,3M4,5 Auger
Al Kα
S
1F
1P
3D
3P
1D 3F
3D 3P
1D 1F
Counts x 10²/ 50 sec
KE (eV)
0
2
4
6
8
10
1010
1030
1050
1070
1090

Figure IV-5. Germanium $L_{2,3}M_{4,5}M_{4,5}$ Auger spectrum of $Ge(CH_3)_4$ vapor excited by Al $K\alpha_{1,2}$ radiation at a sample pressure of 200μ. s = satellite; α= Ge 3d photoelectron line excited by Ge Lα ; β= Ge 3d photoelectron line excited by Ge Lβ

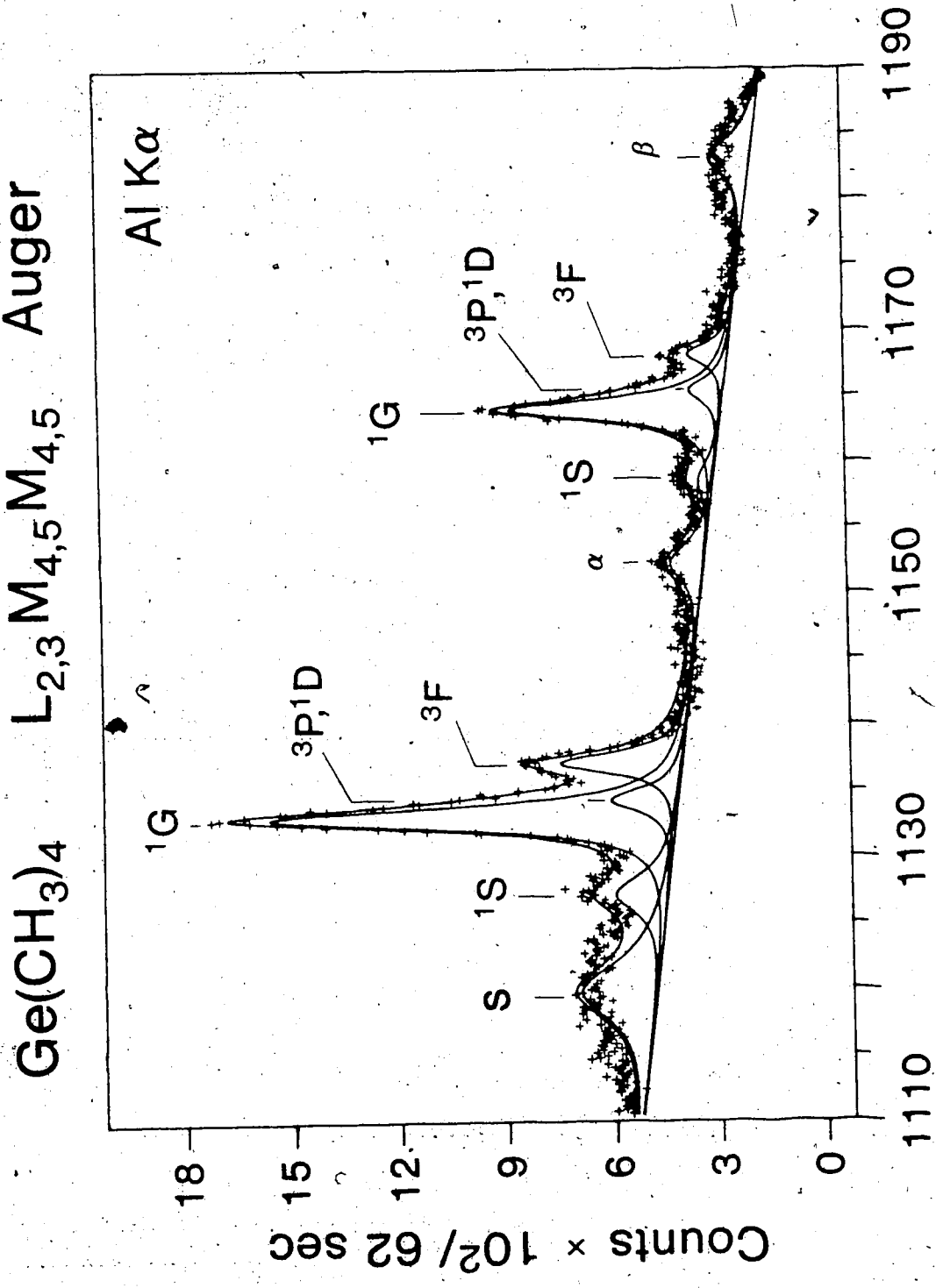
Ge(CH3)4 L2,3M4,5M4,5 Auger
Al Kα
1G
3P,1D
3F
1S
S
α
β
Counts × 10²/ 62 sec
KE (eV)
0
3
6
9
12
15
18
1110
1130
1150
1170
1190

Figure IV-6. Germanium $L_{2,3}M_{2,3}M_{4,5}$ Auger spectrum of $Ge(CH_3)_4$ vapor excited by Al $K\alpha_{1,2}$ radiation at a sample pressure of 200μ. The solid lines indicate the experimental positions of the multiplet terms. The dashed lines indicate the LS calculated positions of the terms unresolved in the spectrum. s = satellite; α= Ge 3p photoelectron line excited by Ge Lα.

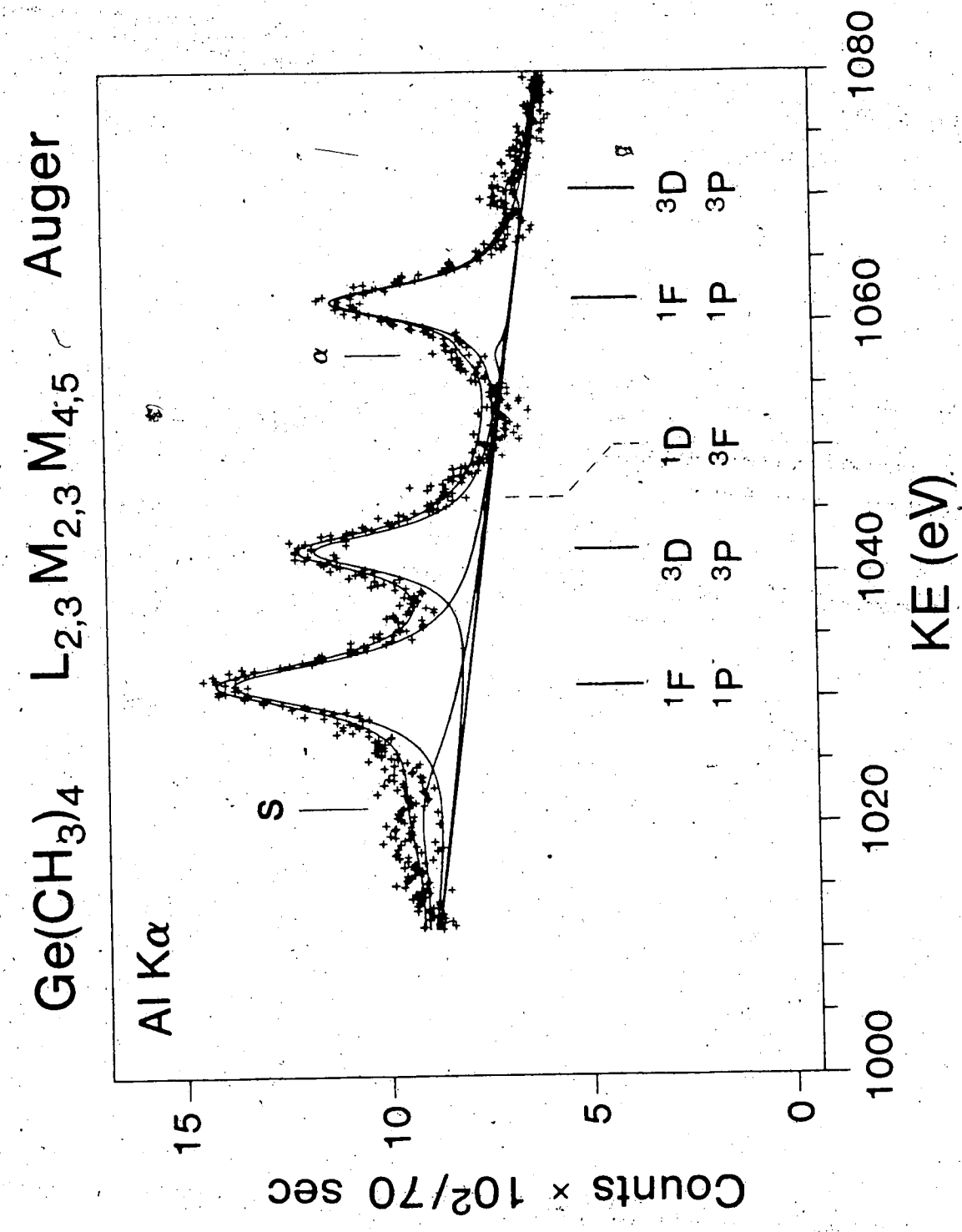
Ge(CH3)4 L2,3 M2,3 M4,5 Auger
Al Kα
S
α
β
1F 3D
1P 3P
3D 1D
3P 3F
1F 3D
1P 3P
Counts x 102/70 sec
KE (eV)
0
5
10
15
1000
1020
1040
1060
1080

Figure IV-7. Germanium $L_{2,3}M_{4,5}M_{4,5}$ Auger spectrum of gaseous GeH_4 excited by Al $K\alpha_{1,2}$ radiation at a sample pressure of 200μ. s = satellite; α= Ge 3d photoelectron line excited by Ge Lα; β= Ge 3d photoelectron line excited by Ge Lβ.

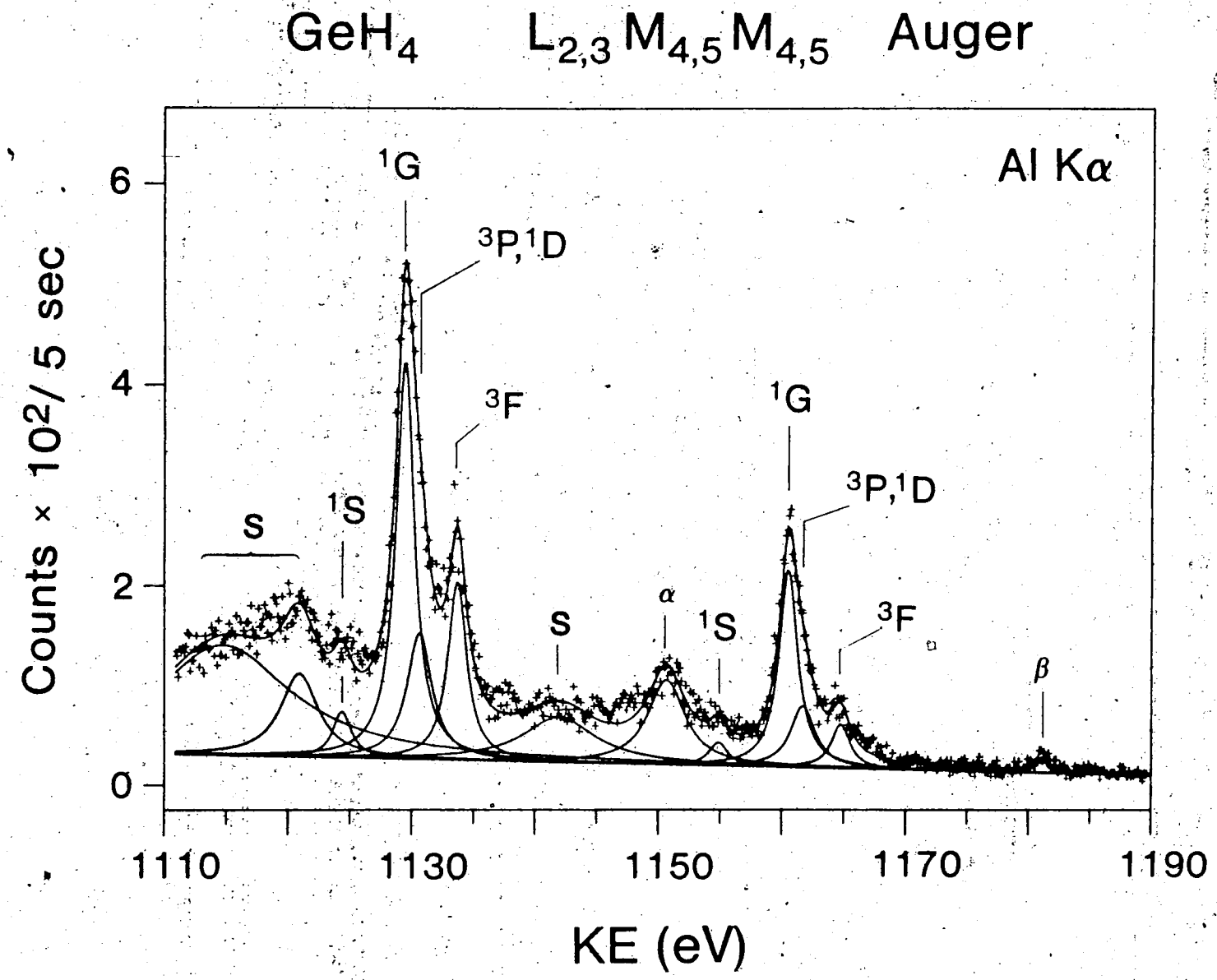
GeH4 L2,3 M4,5 M4,5 Auger
Al Kα
Counts × 10²/ 5 sec
KE (eV)
1G
3P,1D
3F
1S
S
α
β
0
2
4
6
1110
1130
1150
1170
1190

Figure IV-8. Germanium $L_{2,3}M_{2,3}M_{4,5}$ Auger spectrum of gaseous GeH_4 excited by Al $K\alpha_{1,2}$ radiation at a sample pressure of 200μ. The solid lines indicate the experimental positions of the multiplet terms. The dashed lines indicate the LS calculated positions of the terms unresolved in the spectrum. s = satellite.

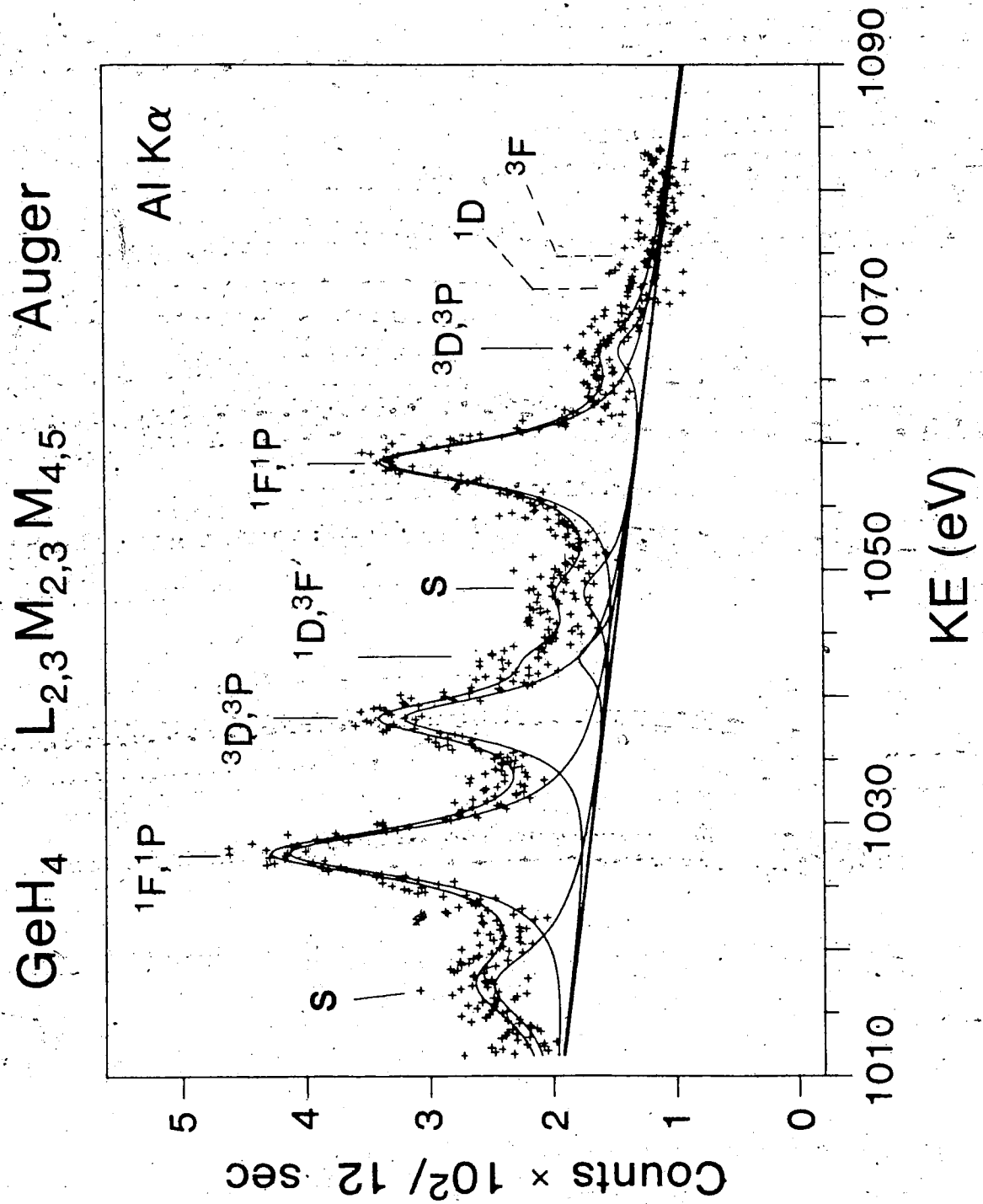
GeH4
L2,3M2,3M4,5 Auger
Al Kα
1F,1P
3D,3P
1D,3F'
S
1F,1P
3D,3P
1D
3F
S
Counts × 10²/ 12 sec
KE (eV)
0
1
2
3
4
5
1010
1030
1050
1070
1090

Figure IV-9. Germanium $L_{2,3}M_{4,5}M_{4,5}$ Auger spectrum of $GeCl_4$ vapor excited by Al $K\alpha_{1,2}$ radiation at a sample pressure of 200μ. s = satellite; α= Ge 3d photoelectron line excited by Ge Lα.

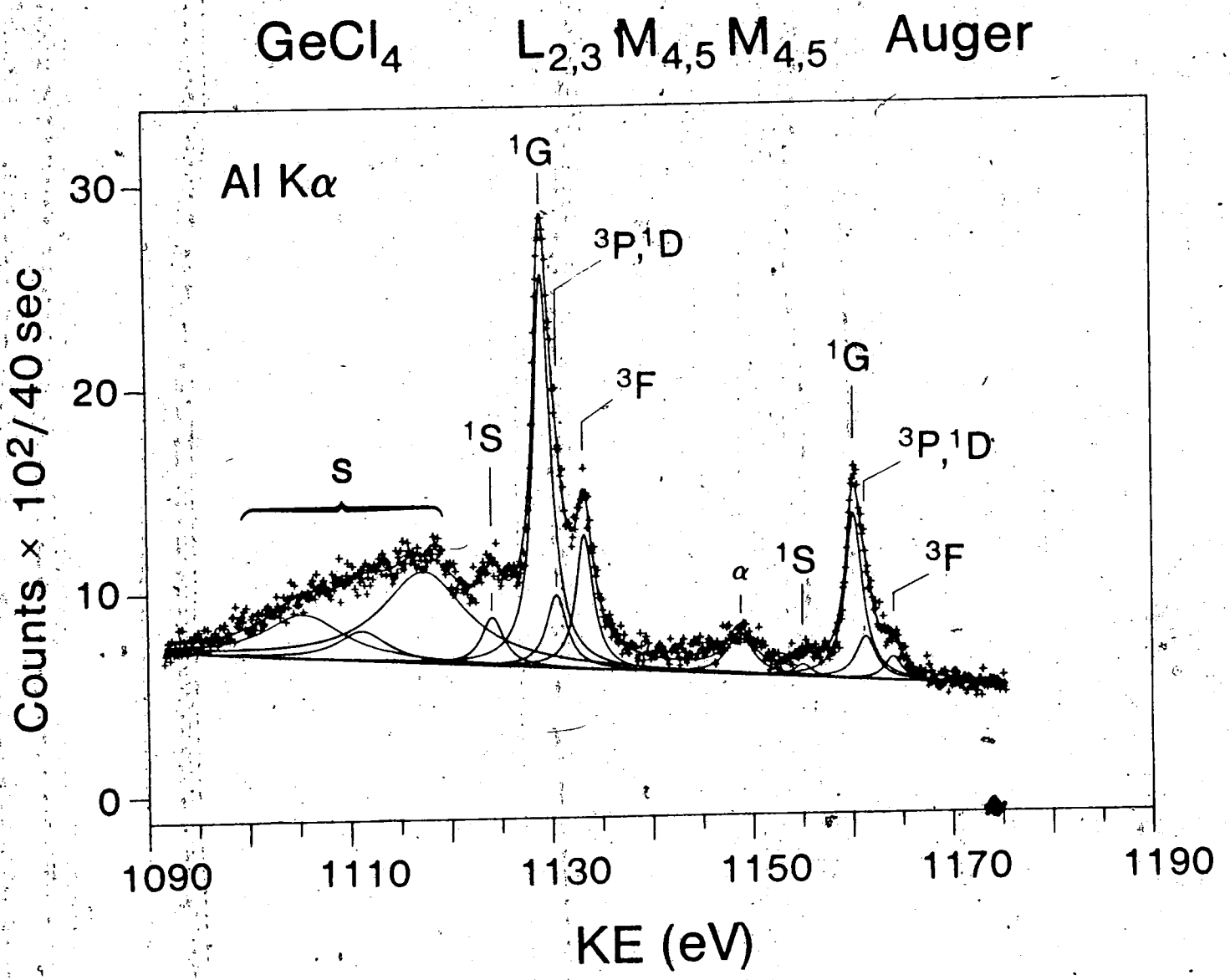
GeCl4 L2,3 M4,5 M4,5 Auger
Al Kα
1G
3P,1D
3F
1S
S
α
1G
3P,1D
1S
3F
Counts x 10²/40 sec
30
20
10
0
1090
1110
1130
1150
1170
1190
KE (eV)

Figure IV-10. Germanium $L_{2,3}M_{2,3}M_{4,5}$ Auger spectrum of $GeCl_4$ vapor excited by Al $K\alpha_{1,2}$ radiation at a sample pressure of 200μ. The solid lines indicate the experimental positions of the multiplet terms. The dashed lines indicate the LS calculated positions of the terms unresolved in the spectrum. s = satellite; β= Cl 2p photoelectron line excited by Ge Lβ.

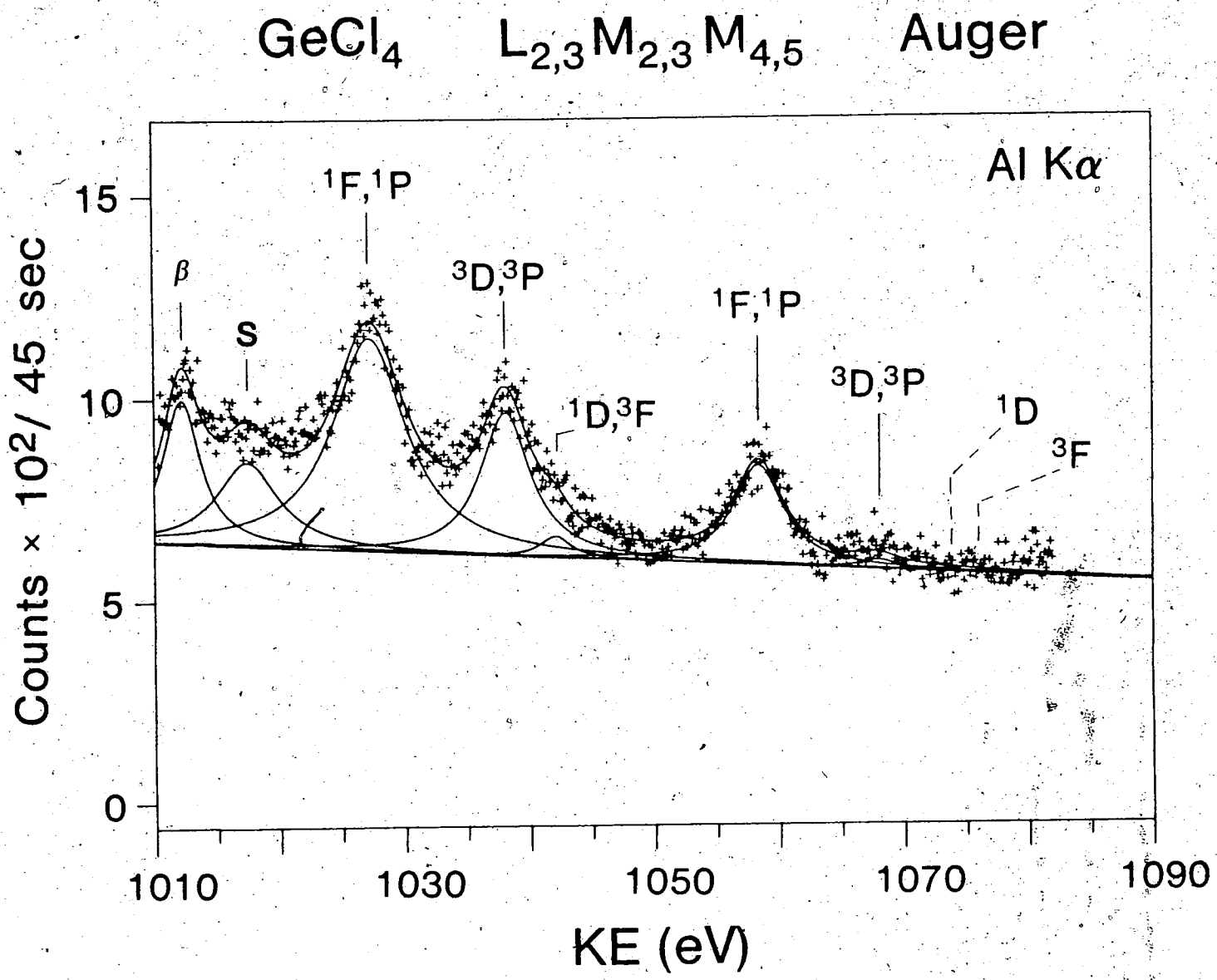
GeCl4 L2,3M2,3M4,5 Auger
Al Kα
Counts × 10²/ 45 sec
15
10
5
0
β
S
1F,1P
3D,3P
1D,3F
1F,1P
3D,3P
1D
3F
1010
1030
1050
1070
1090
KE (eV)

Figure IV-11. Germanium $L_{2,3}M_{4,5}M_{4,5}$ Auger spectrum of gaseous GeF_4 excited by Al $K\alpha_{1,2}$ radiation at a sample pressure of 200μ. s= satellite; α= Ge 3d photoelectron line excited by Ge Lα.

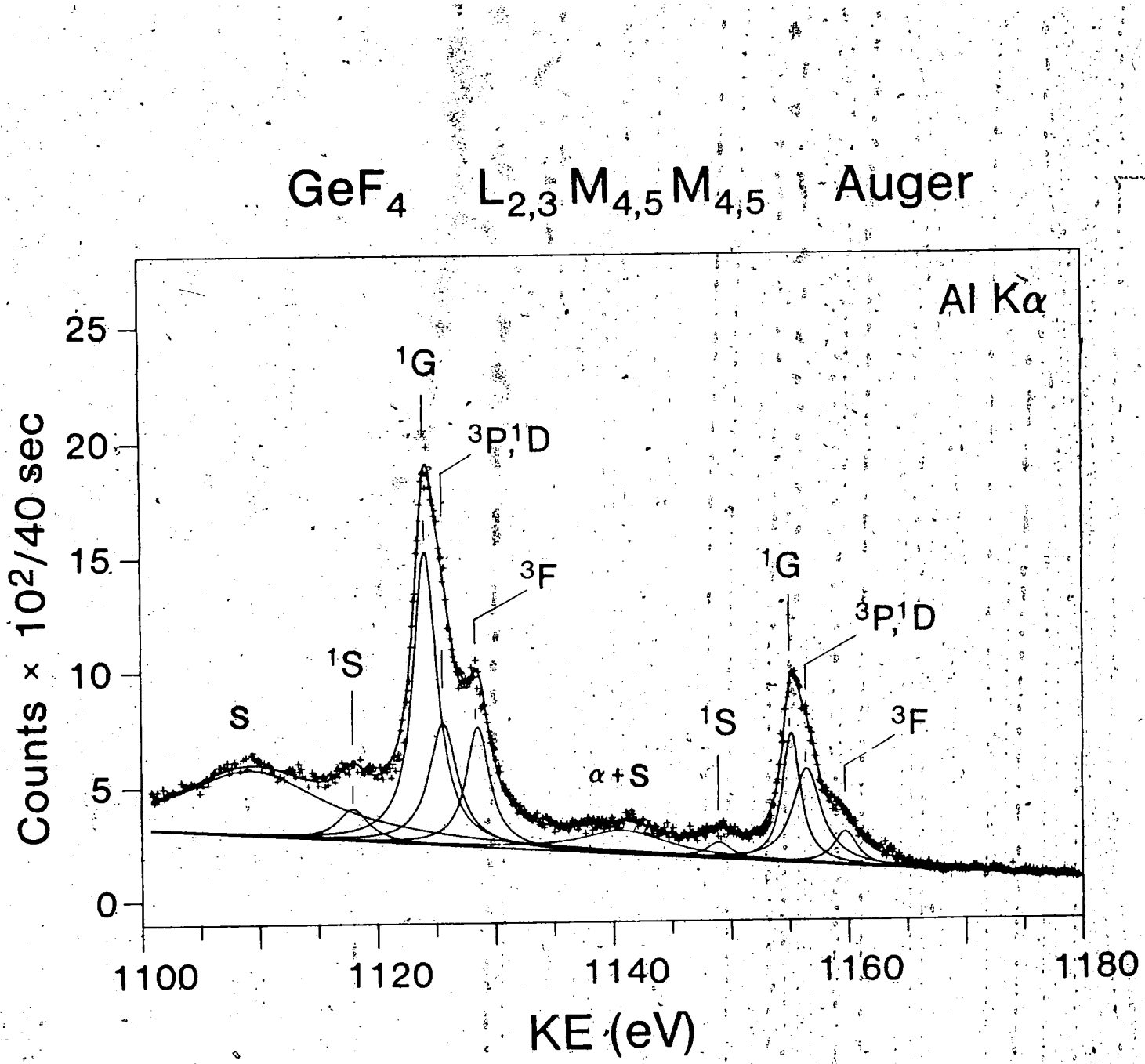
GeF4 L2,3M4,5M4,5 Auger
Al Kα
Counts × 10²/40 sec
25
20
15
10
5
0
1100
1120
1140
1160
1180
KE (eV)
1G
3P,1D
3F
1S
S
α+S
1G
3P,1D
1S
3F

Figure IV-12. Germanium $L_{2,3}M_{2,3}M_{4,5}$ Auger spectrum of gaseous GeF_4 excited by Al $K\alpha_{1,2}$ radiation at a sample pressure of 200μ. The solid lines indicate the experimental positions of the multiplet terms. The dashed lines indicate the LS calculated positions of the terms unresolved in the spectrum. s = satellite; α= Ge 3p photoelectron line excited by Ge Lα.

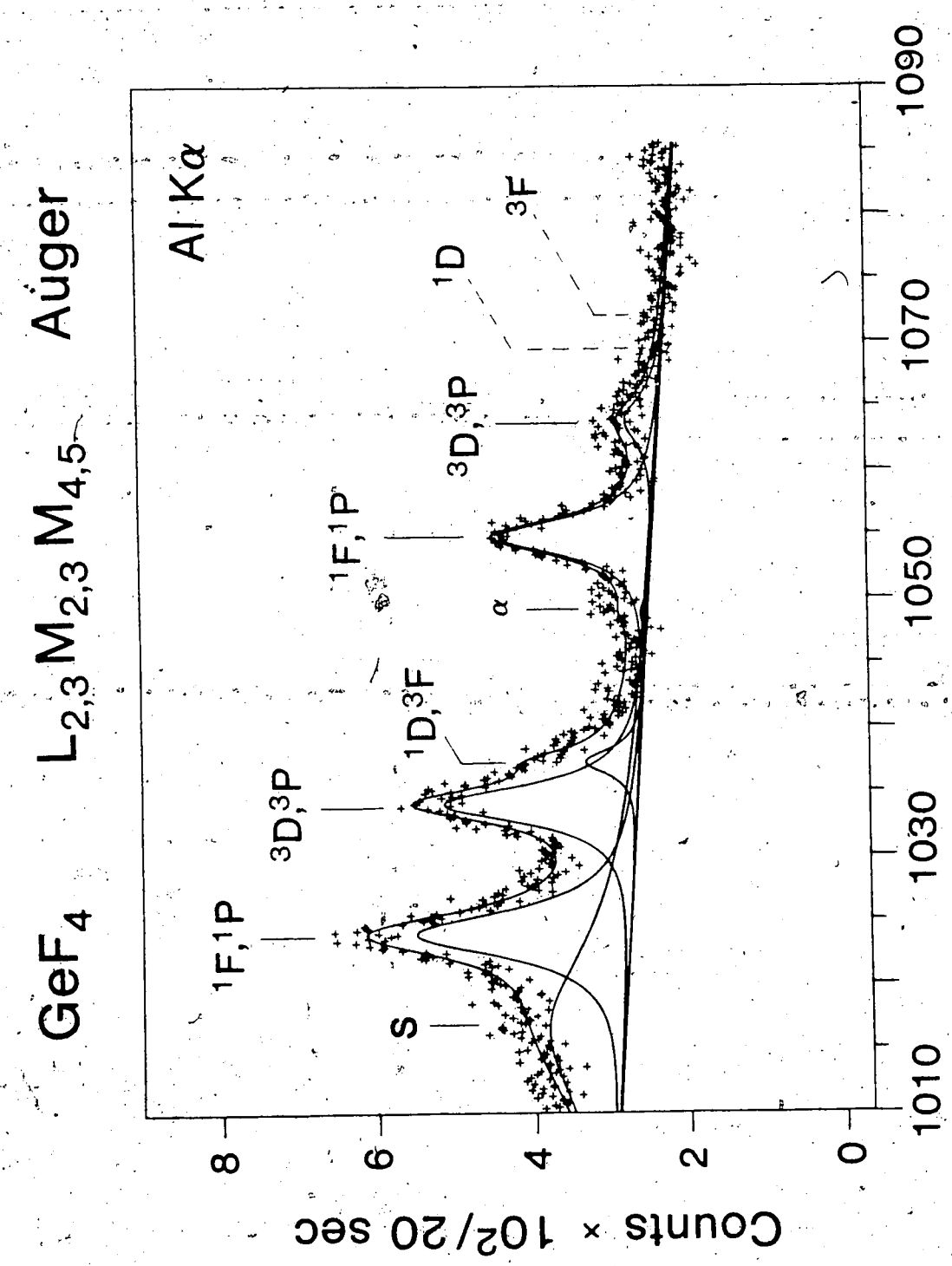
GeF4
L2,3M2,3M4,5 Auger
Al Kα
1F,1P
3D,3P
1D,3F
1F,1P
α
3D,3P
1D
3F
S
Counts × 102/20 sec
KE (eV)
0
2
4
6
8
1010
1030
1050
1070
1090

indicating a poorer fit of the data. The efficacy of Lorentzian analysis suggests that the Auger lineshapes are dominated by the natural lineshape characteristics and that the spectrometer contribution is minor. In order to perform a comparable fitting for all spectra, it was assumed that the line width of the diagram lines within the same final state configuration was constant. For certain cases this restriction prevented convergence of the programme so the widths were unconstrained. Table IV-2 lists the experimental Auger energies. The kinetic energies of the $L_{2,3}M_{4,5}M_{4,5}$ and $L_{2,3}M_{2,3}M_{4,5}$ diagram lines relative to $^1G_4$ and $(^1F\,^1P)$ terms respectively are given in Table IV-3. These data show a good overall agreement between the relative energies of the Auger lines of all compounds. The largest deviations are observed for the $L_{2,3}M_{4,5}M_{4,5}(^1S_0)$ final state. The experimental determination for this term may contain some uncertainty because of the presence of broad satellite peaks in this energy region. As shown in Figures IV-1 to IV-12, in most of the spectra there is also a high background on the low energy side. In some cases it was attempted to fix the slope of the background at zero, but this restriction created fictitious peaks. Allowing the slope to be a free parameter was a preferable procedure. Relatively high

Table IV-2. Ge $L_{2,3}M_{4,5}M_{4,5}$ and $L_{2,3}M_{2,3}M_{4,5}$ Auger Energies (eV) for Germanium Compounds

Transition	Final State Terms	GeO_2(s)[a]	$Ge(C_2H_5)_4$(g)	$Ge(CH_3)_4$(g)	GeH_4(g)	$GeCl_4$(g)	GeF_4(g)
$L_2M_{4,5}M_{4,5}$							
	$^1S_0$	1164.27(15)[b]	1160.49(15)	1158.08(15)	1154.92(15)	1154.78(15)	1149.11(15)
	$^1G_4$	1169.63(10)	1164.45(05)	1163.51(05)	1160.60(05)	1159.89(05)	1155.15(05)
	$^3P_{012}$ $^1D_2$		1165.82(10)	1164.93(10)	1161.77(10)	1161.01(10)	1156.47(10)
	$^3F_{234}$	1172.94(10)	1168.44(10)	1167.64(10)	1164.83(10)	1163.73(10)	1159.33(10)
$L_3M_{4,5}M_{4,5}$							
	$^1S_0$	1132.65(15)	1128.98(15)	1126.72(15)	1124.46(15)	1123.81(15)	1118.05(10)
	$^1G_4$	1138.59(10)	1133.51(05)	1132.53(05)	1129.51(05)	1128.89(05)	1124.15(05)
	$^3P_{012}$ $^1D_2$		1135.10(10)	1133.83(10)	1130.69(10)	1130.20(10)	1125.58(10)
	$^3F_{234}$	1142.47(10)	1137.61(10)	1136.67(10)	1133.78(10)	1133.05(10)	1128.50(10)

(Continued)

Table IV-2 (Continued)

Transition	Final State Terms	GeO_2(s)[a]	$Ge(C_2H_5)_4$(g)	$Ge(CH_3)_4$(g)	GeH_4(g)	$GeCl_4$(g)	GeF_4(g)
$L_2M_{2,3}M_{4,5}$				1057.34	1048.18		1047.39
	$^1F_3\ ^1P_0$	1068.20(10)	1061.81(20)	1061.50(20)	1058.45(10)	1058.02(10)	1053.31(10)
	$^3D_{123}\ ^3P_{012}$	1076.67(20)		1070.66(10)	1067.27(40)	1067.74(80)	1062.35(20)
	$^1D_2\ ^3F_{234}$						
$L_3M_{2,3}M_{4,5}$			1018.52	1021.37	1017.12	1011.84	1015.23
	$^1F_3\ ^1P_0$	1036.99(10)	1031.23(10)	1030.30(10)	1027.57(10)	1026.89(10)	1022.42(06)
	$^3D_{123}\ ^3P_{012}$	1047.67(10)	1042.47(10)	1041.69(10)	1038.23(10)	1037.74(10)	1032.54(06)
	$^1D_2\ ^3F_{234}$			1045.61(10)	1042.98(10)	1041.70(40)	1035.80(10)

a. The energies relative to GeO_2(s) are obtained with respect to the Fermi level.

b. The values in brackets represent the maximum deviations from the average values for three different measurements.

Table IV-3. Experimental Relative Energies (eV) of the Ge $L_{2,3}M_{4,5}M_{4,5}$ and $L_{2,3}M_{2,3}M_{4,5}$ Auger Spectra for Germanium Compounds

Transition	Final State Terms	GeO_2(s)[a]	$Ge(C_2H_5)_4$(g)	$Ge(CH_3)_4$	GeH_4(g)	$GeCl_4$	GeF_4(g)
$L_2M_{4,5}M_{4,5}$							
	$^1S_0$	-5.36	-3.96	-5.43	-5.68	-5.11	-6.14
	$^1G_4$	0.00	0.00	0.00	0.00	0.00	0.00
	$^3P_{012}$ $^1D_2$	3.31	1.37	1.42	1.17	1.12	1.32
	$^3F_{234}$		4.37	4.13	4.23	3.84	4.32
$L_3M_{4,5}M_{4,5}$							
	$^1S_0$	-5.94	-4.53	-5.80	-5.05	-5.08	-6.19
	$^1G_4$	0.00	0.00	0.00	0.00	0.00	0.00
	$^3P_{012}$ $^1D_2$	3.88	1.59	1.30	1.18	-1.31	1.47
	$^3F_{234}$		4.10	4.14	4.27	4.16	4.42

Continued.

Table IV-3 (Continued)

Transition	Final State Terms	$GeO_2(s)$[a]	$Ge(C_2H_5)_4(g)$	$Ge(CH_3)_4(g)$	$GeH_4(g)$	$GeCl_4(g)$	$GeF_4(g)$
$L_2M_{2,3}M_{4,5}$							
	$^1F_3\,^1P_0$	0.00	0.00	0.00	0.00	0.00	0.00
	$^3D_{123}\,^3P_{012}$	8.47		9.16	8.82	9.72	9.04
	$^1D_2,\ ^3F_{234}$						
$L_3M_{2,3}M_{4,5}$							
	$^1F_3\,^1P_0$	0.00	0.00	0.00	0.00	0.00	0.00
	$^3D_{123}\,^3P_{012}$	10.68	11.24	11.39	10.66	10.85	10.12
	$^1D_2,\ ^3F_{234}$			15.31	15.41	14.81	13.38

backgrounds are probably due to combinations of inelastically scattered Auger and other electrons in the sample volume with contribution from Auger line satellites of low intensity. The peaks of the $L_{2,3}M_{2,3}M_{4,5}$ spectra are due to overlap of many lines ($L_{2,3}M_2M_{4,5}$, $L_{2,3}M_3M_{4,5}$) and so they are quite broad. $L_3M_{2,3}M_{4,5}$ Auger group shows in all compounds two prominent peaks with a large width (FWHM ≈ 4-4.5 eV). According to the calculations the peak at lower energy is attributable to the sum of $^1F_3$ and $^1P_0$ terms and the second peak to the sum of $^3D_{123}$ and $^3P_{012}$. The weak peak in the same group is due to a combination of $^1D_2$ and $^3F_{234}$; it does not appear in the spectrum of GeO_2 which is very broad nor in the spectrum of $Ge(C_2H_5)_4$ for which poor statistics were achieved.

The attribution of the peaks in $L_2M_{2,3}M_{4,5}$ spectra is more difficult. In the spectra of all compounds there is only one dominant peak which is quite broad (FWHM = 4.5 eV). This peak is found about 31 eV to higher energy of the first strong peak in the $L_3M_{2,3}M_{4,5}$ group so it is reasonable to attribute it to a combination of $^1F_3$ and $^1P_0$ lines. On the high energy side of this peak, about 9 eV higher, there is a small peak due to the combination of

$^3P_{012}$, and $^3D_{321}$. The $^3F_{234}$ and $^1D_2$ final states are not observed, probably because their intensities are very low as shown by the theoretical calculations of Antonides et al.[62] for atomic Germanium. A detailed analysis of the intensities of each peak was not possible due to the poor statistics of the spectra. However from the sum of the areas enclosed by the Lorentzian curves, the intensity of the $L_3M_{2,3}M_{4,5}$ Auger group relative to the intensity of the $L_2M_{2,3}M_{4,5}$ group has been estimated to range between 2.2 and 2.5. This value, which is larger than the statistical distribution (2:1) of the initial state holes in the $2p_{3/2}$ and $2p_{1/2}$ levels (given by $2j+1/2j'+1$ with $j = 3/2$ and $j' = 1/2$) may be a consequence of the high background which increases the intensity of the low energy peaks belonging to the $L_3M_{2,3}M_{4,5}$ group as compared to those from the $L_2M_{2,3}M_{4,5}$ group.

In Figures IV-1 and IV-2 the $L_{2,3}M_{4,5}M_{4,5}$ and $L_{2,3}M_{2,3}M_{4,5}$ spectra of solid GeO_2 are shown. Both regions are quite broad, only the $^1S_0$, $^1G_4$ and $^3F_{234}$ components have been fitted in the $L_{2,3}M_{4,5}M_{4,5}$ spectrum. The $^3P_{012}$ and $^1D_2$ components were not resolved and they probably contribute to the intensity assigned to the highest peaks thus these intensity values are probably high.

The $L_{2,3}MM$ spectra of $Ge(C_2H_5)_4$ are shown in Figures IV-3 and IV-4. In the $L_{2,3}M_{4,5}M_{4,5}$ spectrum the two Auger groups with L_2 and L_3 as initial states show one more peak due to $^3P_{012}$ and $^1D_2$ lying too close in energy to be separated. In the spectrum there are also features that do not belong to the diagram Auger lines. The peaks at 1152.35 eV and at 1181.51 eV are due to photoionization of Ge3d by respectively Ge L_α (1188.0 eV)[65] and Ge L_β (1218.5 eV)[65] radiations, presumably arising from some Germanium deposition on the anode produced by the decomposition of the Germanium compounds in the open X-ray tube. This interpretation is supported by the fact that the intensities of these peaks increased during the analysis and the appearance of these peaks occurred to a large extent with those Germanium compounds with the lowest thermal stability. The position of these lines can not be accurate because of the uncertainty of the radiation emitted by unidentified Germanium decomposition products. Although sealing the cell to prevent such leakage with the resultant contamination of the spectrum was attempted, the requirement that there be a slit to allow electrons to enter the analyzer means that some of the Ge compounds will enter the pumping system and gain access to the open X-ray tube. Sealing the X-ray tube and

provision of more efficient differential pumping would probably solve the problem but resources were not available to do this prior to or during this study. In the region around 1181 eV the structure is quite broad probably because of contribution from other satellites. The $L_{2,3}M_{2,3}M_{4,5}$ spectrum shows a peak at about 1018 eV which is also quite broad and which could be due to a shake-off process accompanying the ionization of the L_3 level.

The $Ge(CH_3)_4$ spectra shown in Figures IV-5 and IV-6 are very similar to the $Ge(C_2H_5)_4$ spectra. Again the Ge3d photoelectron lines appear at about 1152 eV and 1181 eV in the $L_{2,3}M_{4,5}M_{4,5}$ spectrum of this compound. The $L_{2,3}M_{2,3}M_{4,5}$ spectrum shows a broad peak at 1021.37 eV which is attributed to shake-off processes, and a small peak at 1057.34 eV which could be due to Ge3p photoelectron lines excited by Ge L_α radiation. The Auger spectra of GeH_4 illustrated in Figures IV-7 and IV-8 show the normal Auger lines in the $L_{2,3}M_{4,5}M_{4,5}$ spectrum and again the Ge3d photoelectron lines appear at around 1151 eV and 1181 eV. There are also two satellite peaks at 1121 eV and 1142 eV. In the $L_3M_{2,3}M_{4,5}$ and $L_2M_{2,3}M_{4,5}$ regions, there are two peaks on the low energy side of $^1F_3$ $^1P_0$ terms at 1017.1 eV and 1048.2 eV

respectively. All of these structures could arise from shake-off processes.

In Figures IV-9 to IV-12 the Auger spectra of $GeCl_4$ and GeF_4 are illustrated.

The $L_{2,3}M_{4,5}M_{4,5}$ spectrum of $GeCl_4$ shows features which are similar to the above spectra of Germane and Alkylgermanes. The $L_{2,3}M_{2,3}M_{4,5}$ spectrum of $GeCl_4$ has one extra peak on the low energy side at 1011.8 eV, which is due to the Cl 2p photoelectron line excited by Ge L_β radiation.

The corresponding spectra in GeF_4 are generally broader than those for the other compounds. The reason for the increased breadth of the peaks could be a shorter lifetime of the hole state in this molecule which contributes to the broadening of the spectra. In the $L_{2,3}M_{4,5}M_{4,5}$ spectrum the Ge3d photoelectron peaks excited by Ge L_α and Ge L_β are not as strong as in the other compounds because GeF_4 is presumably more resistant to decomposition in the electron beam in the X-ray tube. In these spectra there is a broad feature centered at ≈1141 eV that could contain some contribution from the Ge 3d photoelectron line although the photoelectron line is not clearly resolved. The $L_{2,3}M_{2,3}M_{4,5}$ Auger spectrum of this compound also shows a small peak at ≈1050 eV which is

probably due to the Ge 3p photoelectron line excited by Ge L_α radiation.

As it is shown in Figures IV-1 to IV-12 the $L_{2,3}M_{4,5}M_{4,5}$ spectra of all compounds exhibit a quite broad band on the low energy side which in certain cases has been fitted with more than one Lorentzian and which may be due to multielectron processes.[66,67]

The calculations of the relative energies and intensities have been made in the two-hole representation (equation I-14). In the initial state the inner-shell hole is coupled to a hole in the continuum representing the missing Auger electron, and in the final state the two vacancies are coupled. For the calculations of the energies of the $L_{2,3}M_{4,5}M_{4,5}$ Auger spectra, the spin-orbit interaction has been taken into account. In Table IV-4 are listed the calculated energies of the $L_{2,3}M_{4,5}M_{4,5}$ and $L_{2,3}M_{2,3}M_{4,5}$ lines relative to $^1G_4$ and $(^1F_3\,^1P_0)$ terms respectively. In column (a) are listed the values obtained in the pure LS coupling scheme. In column (b) the values obtained by adding the diagonal elements of the spin-orbit matrices to the LS values are given. The values in column (c) were obtained from the solutions of the secular equations[16] corresponding to each term according to the intermediate coupling scheme. There is a

Table IV-4. Calculated Relative Energies (eV) of the $L_{2,3}M_{4,5}M_{4,5}$ and $L_{2,3}M_{2,3}M_{4,5}$ Auger Lines of Germanium

Transition	Final State Term	Pure LS (a)	LS + Diagonal Elements (b)	IC (c)
$L_{2,3}M_{4,5}M_{4,5}$				
	$^1S_0$	-6.28	-6.28	-5.72
	$^1G_4$	0.00	0.00	0.00
	$^3P_0$		0.62	1.34
	$^3P_1$	0.92	0.77	0.77
	$^3P_2$		1.07	1.68
	$^1D_2$	1.48	1.48	0.78
	$^3F_2$		3:59	3.98
	$^3F_3$	4.19	4.04	4.04
	$^3F_4$		4.64	4.66
$L_{2,3}M_{2,3}M_{4,5}$				
	$^1F_3$	0.00		
	$^1P_0$	1.51		
	$^3D_3$			
	$^3D_2$	10.01		
	$^3D_1$			
	$^3P_2$			
	$^3P_1$	10.97		
	$^3P_0$			
	$^1D_2$	16.23		
	$^3F_4$			
	$^3F_3$	18.38		
	$^3F_2$			

reasonably good agreement between the pure LS values in Table IV-4 and the experimental results given in Table IV-3 with the exception of the $^1S_0$ terms which, as was previously noted, are not experimentally well determined. It seems that the pure Russell-Saunders scheme is satisfactory for the analysis of these spectra given the small spin-orbit splitting of the 3d level in Germanium (0.7 eV)[54] which was not resolved experimentally. In the case of $L_{2,3}M_{2,3}M_{4,5}$ spectra, only the LS coupling scheme was applied.

The Auger parameter ξ for each compound was obtained from the experimental Auger energy of the strongest line ($^1G_4$) of the L_2 and L_3 groups and from the experimental binding energies. The values for all systems are listed in Table IV-5 along with the total relaxations obtained from the Auger parameters and the coulombic term $F(M_{4,5}M_{4,5};\ ^1G_4)$ (equation IV-4). The coulombic term $F(M_{4,5}M_{4,5};\ ^1G_4)$ was calculated for the neutral configuration $Ge(3d^{10}4s^24p^2)$ in the LS coupling scheme in terms of Slater's integrals from Mann's tables.[53] A value of 36.12 eV in agreement with the value of 36.2 eV given by Antonides et al. was obtained.[62] McGilp and Weightman[68] also evaluated $F(M_{4,5}M_{4,5};\ X)$ using electrostatic integrals determined for the $Ge^{2+}(3d^84s^24p^2)$

Table IV-5. The Auger Parameter and Relaxation for Germanium Compounds

	ξ^a $M_5(^1G_4)$	ξ^a $M_4(^1G_4)$	$R_S^T(M_{4,5}M_{4,5})^b$ $M_5(M_4)$	$R_S^{ea}(M_{4,5}M_{4,5})^c$ $M_5(M_4)$
Ge[d]	12.90	12.90	23.22 (23.22)	10.72 (10.72)
GeO_2	16.27	16.28	19.85 (19.84)	7.35 (7.34)
$Ge(C_2H_5)_4$	18.37	18.30	17.75 (17.82)	5.25 (5.32)
$Ge(CH_3)_4$	19.12	18.94	17.00 (17.18)	4.50 (4.68)
GeH_4	20.94	20.96	15.18 (15.16)	2.68 (2.66)
$GeCl_4$	18.92	18.83	17.20 (17.29)	4.70 (4.79)
GeF_4	20.81	20.53	15.31 (15.59)	2.81 (3.09)

a. Calculated from equation IV-3.

b. Calculated from equation IV-4 taking $F(M_{4,5}M_{4,5}; {}^1G_4)$ = 36.12 eV

c. Calculated from equation IV-7 taking $R_S^a(M_{4,5}M_{4,5})$ = 12.5 eV.

d. Experimental values from Ref. 62.

configuration from the Hartree-Fock programme of Froese-Fisher[69] obtaining a value of 39.1 eV, 3 eV larger than that obtained above. However their results for the multiplet splitting calculation of Ge $L_{2,3}M_{4,5}M_{4,5}$ spectra overestimated by 20% the measured separations $^1S_0$-$^1G_4$ and $^1G_4$-$^3F_0$. This was attributed to a neglect of relativistic effects which, by indirectly expanding the 3d orbital, reduce the electron-electron Coulomb repulsion. The values used above for the electrostatic integrals of the neutral atom configuration were about 10% smaller than those for the $Ge^{2+}(3d^8 4s^2 4p^2)$ configuration thus compensating in part for the relativistic effect.

Assuming that the atomic relaxation contribution is constant (independent of the environment of the atom), the extraatomic, environment sensitive, portion was extracted by subtracting the $R_S{}^a$ term evaluated above (12.5 eV) from the total relaxation terms, leaving the residuals $R_S{}^{ea}$ which are given in Table IV-5. For comparison purposes the corresponding values for Ge metal obtained using the experimental energies from ref. 62 have been included in the table. The relaxation term obtained in this way for the metal agrees quite well with the value of 23.64 eV calculated in part C of this chapter. The relaxation terms found for the other systems are considerably smaller

than the calculated value because the electrons on neighbouring atoms, being more attracted by their own nuclei, have a smaller screening effect on the charge on the central atom than is estimated by the atomic integrals (equation IV-16).

As shown in Table IV-5, GeH_4 and GeF_4 have approximately the same relaxation value. As it was pointed out in Chapter III, relaxation and polarizability are related to each other. The results for GeH_4 and GeF_4 agree with the results obtained by Aitken et al.[43] on a series of Chlorine compounds which showed that Hydrogen and Fluorine have the same polarizability. The substantially greater electronegativity of Fluorine relative to Hydrogen produces a large decrease in the electrostatic potential at the Germanium nucleus yielding larger Germanium binding energies in GeF_4 than in GeH_4.

It is interesting to compare the relaxation energies in GeH_4 and in the isoelectronic noble gas Krypton. The relaxation for Krypton was estimated from a comparison of the experimental energy of the $L_3M_{4,5}M_{4,5}$ ($^1G_4$) Auger term with a calculated value obtained according to equation IV-1 neglecting the R_S^T term. The experimental Auger and photoelectron energies were taken from ref. 8. A relaxation of 17.7 eV was obtained for Krypton in

agreement with the value of 17.8 eV obtained from the results of Rosen and Lindgren.[60] It is not however easy to explain why the value for Germane is smaller than the relaxation value for Krypton. Whereas Krypton has a smaller polarizability than a Germanium atom (average polarizability of Krypton and Germanium are respectively 2.48 and 6.07 in units of 10^{-24} cm^3),[70] the larger polarizability of Methane (2.60×10^{-24} cm^3),[71] relative to Neon (0.39×10^{-24} cm^3)[70], suggests that the polarizability of Krypton will be smaller than that of Germane and, consequently, Krypton would have a smaller relaxation than Germane. It would appear that effects other than the polarizability of the molecule controls the relaxation. In Krypton all the electrons and in particular the ones of interest, 3d and 4p, are localized in their orbitals and can fully contribute to the relaxation potential (equation III-2) which is a combination of Coulomb and exchange integrals. In GeH_4 the Hydrogen is slightly more electronegative than Germanium. When a positive charge is created in the Germanium atom, the electronegativity of Hydrogen may restrict the flow of the electron density, which is the source of the relaxation contribution, toward the positive hole in the central atom. So it seems that, in addition to the polarizability of the molecule itself which is

related to the size and to the charge in the molecule,[71] the amount of electronic charge which can be polarized on the atom of interest is also important. In $Ge(C_2H_5)_4$ the relaxation energy of 17.7 eV, very close to the Krypton value, suggests that the electrons from the Ethyl groups can flow more freely toward the Germanium hole creating an electronic environment analogous to that of the noble gas Krypton which has 6 electrons in the 4p orbital. Chlorine, due to its large atomic size, is more polarizable than Fluorine and produces a larger relaxation contribution to the Germanium Auger energies in $GeCl_4$ as compared to GeF_4. $Ge(CH_3)_4$ and $Ge(C_2H_5)_4$ show large relaxations which are comparable with that of $GeCl_4$, in agreement with the results by Smith and Thomas[48] on $CH_2ClCOOH$ and C_2H_5COOH which indicated that Chlorine and Methyl have about the same overall relaxation. The atomic size and the electronegativity of Chlorine act in such a way to produce in $GeCl_4$ the same relaxation energy as the alkyl groups in $Ge(CH_3)_4$ and $Ge(C_2H_5)_4$. In Chapter III it was observed that the relaxation effect created by a Chlorine atom was slightly larger than that of a Methyl group, however, in that case the probe atom was a terminal atom rather than the central atom. The response of the binding and Auger energies in the case of a terminal atom

to the chemical environment was smaller and somewhat constrained by the terminal atom character. Furthermore in that case, the analysis of the relaxation was based on the assumption that the chemical shifts in binding energies were the same for all core electrons, whereas in this case the appropriate experimental energies for each level involved in the Auger process are used in equation IV-1. The large relaxation shown by GeO_2 is attributed to the solid state where, in general, because of the presence of a large number of atoms in proximity, the relaxation effects are bigger than those in gas phase.[72]

Assuming a linear relationship between relaxation and polarizability of the substituents around the central atom, then, the above results (Table IV-5) produce an order of polarizability ($H \lesssim F < CH_3 \leq Cl < C_2H_5$) which is analogous to that given by Aitken et al.[43] and is consistent with optically determined polarizabilities.[70]

For metallic Germanium the extraatomic relaxation can be used to evaluate the solid vapor shift by noting that the Lang and Williams'[51] Auger parameter (equation IV-3) is independent of state. Writing equation IV-4 for solid or gaseous state gives

$$\varepsilon^{gas} = F(M_{4,5}M_{4,5}) - R_S^T(M_{4,5}M_{4,5})^{gas}$$

$$\xi^{solid} = F(M_{4,5}M_{4,5}) - R_S{}^T(M_{4,5}M_{4,5})^{solid}$$

and recalling that the solid state term can be divided into atomic and extraatomic components

$$R_S{}^T(M_{4,5}M_{4,5})^{solid} = R_S{}^a(M_{4,5}M_{4,5}) + R_S{}^{ea}(M_{4,5}M_{4,5})^{solid}$$

whereas in the case of atomic Germanium only the atomic term contributes:

$$R_S{}^T(M_{4,5}M_{4,5})^{gas} = R_S{}^a(M_{4,5}M_{4,5})$$

Hence

$$\Delta\xi = \xi^{solid} - \xi^{gas} = R_S{}^{ea}(M_{4,5}M_{4,5})^{solid} = 10.72 \text{ eV}$$

The Auger parameter has been shown by Thomas[38] to be approximately $2\Delta R_V$ (the outershell relaxation associated with the formation of a single core hole) therefore $\Delta R_V = 5.36$ eV.

The binding energy shift for solid to vapor Germanium is then given by

$$\Delta E_B{}^{solid\text{-}gas} = E_B{}^{solid} - E_B{}^{gas}$$

Applying the relation for binding energy in terms of core potentials and relaxation (from equation III-8)

$$E_B = -V - R \qquad \text{IV-17}$$

and assuming that the core potentials (V) are insensitive to the state (assumption suggested by the argument that the orbital energy differences between solid and vapor are small)[59] gives

$$\Delta E_B^{\text{solid-gas}} = -R^{\text{solid}} + R^{\text{gas}}$$
$$= -\Delta R^{\text{solid-gas}} = 5.36 \text{ eV}$$

and the binding energy should be higher in the vapor state by about 5.36 eV. The Auger energy in the same form (from equation III-17) is given by

$$E_{Au} = V + 3R \qquad \text{IV-18}$$

and the same arguments yield for the solid-gas shift

$$\Delta E_{Au}^{\text{solid-gas}} = 3R^{\text{solid}} - 3R^{\text{gas}}$$
$$= 3(\Delta R^{\text{solid-gas}}) = 16.08 \text{ eV}$$

with the Auger energy lower by 16.08 eV in the gaseous state. While the values are not known for Germanium, the solid-vapor shifts reported[73,74,75] for Ag, Zn and Cd show the electron binding energies to be ~3 eV higher in the vapor state and the Auger energies 12-13 eV lower in the vapor state in keeping with the above prediction. The estimated values of extraatomic relaxation given above seem to be acceptable in that these estimates yield reasonable shift predictions. Since the extraatomic contributions are reasonable for metallic Germanium it also seems reasonable to consider the corresponding terms for the Germanium molecules studied herein to be an evaluation of the relative contribution of molecular effects (i.e. the presence of adjacent electrons and atoms in the vicinity of the probe atom (Ge)). The value of 11.32 eV estimated for the extraatomic relaxation from equation IV-16 is close to the value (10.72 eV) obtained from the experimental energy analysis for the Germanium metal, but it is much larger than the values for the Germanium molecules. Equation IV-16 gives an upper limit for the extraatomic relaxation. This limit applies to the situation when the hole in the 3d level (as in the Ge $L_{2,3}M_{4,5}M_{4,5}$ case) is completely screened by one unit of

charge arising from outside the atom with the hole and localized in the 4p level. In the case of Germanium metal where the screening charge arises from the conduction band, the 4p orbital may be delocalized and therefore the atomic integrals used in equation IV-16 overestimate the electrostatic interaction between a 3d and a 4p electron yielding an extraatomic relaxation which is slightly larger than the value for Ge metal. In molecules the electrons able to screen the positive charge associated with the hole are fewer and delocalized on the whole molecule therefore it is perhaps not surprising that molecules suffer smaller relaxation effects than the metal.

In Table IV-6 the theoretical and experimental intensities of $L_{2,3}M_{4,5}M_{4,5}$ Auger spectra have been listed. The theoretical transition rates were calculated in the mixed coupling scheme,[55,56] treating the initial L shell and continuum hole in jj-coupling and the final two holes in LS coupling. The calculated spectrum for Germanium atom is shown in Figure IV-13. The spectrum was obtained by a curve simulation programme,[76] using relative energies as derived from the pure LS calculations, areas as required by the mixed coupling intensity results and widths from the deconvolution of the experimental

Table IV-6. Calculated and Experimental Intensities[a] of Ge $L_{2,3}M_{4,5}M_{4,5}$ Spectrum for Germanium Compounds

Transitions	Final State Terms	LS[b]		GeO_2(s)	$Ge(C_2H_5)_4$(g)	$Ge(CH_3)_4$(g)	GeH_4(g)	$GeCl_4$(g)	GeF_4(g)
$L_2M_{4,5}M_{4,5}$									
	$^1S_0$	1.8		7.9(7.0)	10.9(1.5)	8.9(1.4)	6.7(0.9)	4.5(0.8)	8.4(1.3)
	$^1G_4$	63.3		70.8(2.3)	58.6(4.5)	66.3(3.1)	57.2(5.8)	64.8(3.4)	38.5(2.9)
	$^3P_0$	0.4	2.0						
	$^3P_1$	1.0							
	$^3P_2$	0.6			14.1(4.5)	12.1(3.0)	23.4(6.0)	20.2(3.2)	29.6(5.3)
	$^1D_2$	10.4							
	$^3F_2$	7.2	22.5						
	$^3F_3$	8.1		21.3(3.1)	16.3(1.7)	12.6(1.1)	12.4(1.0)	10.5(1.3)	23.4(3.4)
	$^3F_4$	7.2							

(Continued)

Table IV-6 (Continued)

Transitions	Final State Terms	LS[b]		GeO_2(s)	$Ge(C_2H_5)_4$(g)	$Ge(CH_3)_4$(g)	GeH_4(g)	$GeCl_4$(g)	GeF_4(g)
$L_3M_{4,5}M_{4,5}$									
	$^1S_0$	1.8		7.3(1.2)	5.4(0.7)	14.0(0.9)	5.8(0.7)	10.2(0.9)	7.2(1.2)
	$^1G_4$	63.3		72.7(1.1)	68.3(2.4)	57.7(2.3)	50.2(3.4)	58.3(2.1)	49.0(1.6)
	$^3P_0$	0.1	2.0		7.3(2.3)	10.9(2.2)	21.4(3.6)	12.3(2.1)	19.3(1.5)
	$^3P_1$	0.5							
	$^3P_2$	1.4							
	$^1D_2$	10.4							
	$^3F_2$	4.6	22.5	20.5(0.9)	21.2(1.1)	17.0(0.7)	22.6(0.8)	19.1(1.7)	24.5(0.5)
	$^3F_3$	7.2							
	$^3F_4$	10.7							

a. Intensities for each component in each major Auger group (L_2 and L_3) are expressed as a % summing to 100% for the group. The numbers in parentheses are the standard deviations obtained from the least squares fit.

b. The values have been obtained from mixed coupling scheme using LS coupling for the final state.

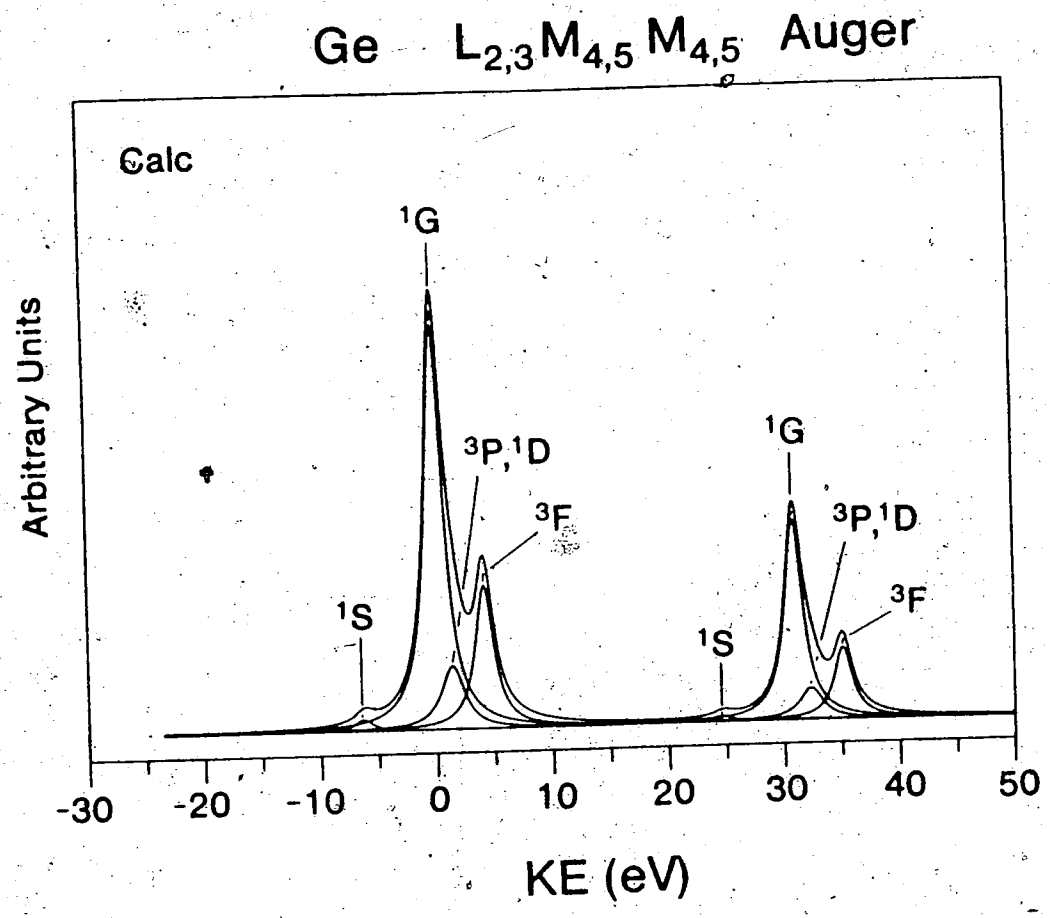

Figure IV-13. Calculated Germanium $L_{2,3}M_{4,5}M_{4,5}$ Auger spectrum. The relative positions of the multiplet terms were derived from pure LS calculations, the areas were derived from mixed coupling calculations using LS coupling for the final state.

spectra. The distance between the $L_2M_{4,5}M_{4,5}$ and $L_3M_{4,5}M_{4,5}$ Auger groups was taken equal to the Ge 2p spin-orbit splitting value which is 31 eV. The components ^1D and ^3P have been combined to obtain a spectrum comparable to the experimental spectra. The results of the intensity calculations show that the transition rates for $^1S_0$, $^1G_4$, and $^1D_2$ and the separate sums of ^3P and ^3F terms are independent of the j value of the initial 2p hole. However the distribution of the transition rate between the components of ^3P and ^3F is significantly different in the two groups. The calculated intensities are in quite good agreement with those obtained previously by Antonides et al,[62] who used the same coupling scheme. Even with the inaccuracy of the line decomposition procedure, it seems that the intensities of the different terms do not change much from one compound to the other. Poor resolution renders unreliable the individual intensities of $^1G_4$, $^3P_{012}$ and $^1D_2$ terms, but the sum of the three terms is reliable. The largest deviations from the calculated intensities are shown by the GeF_4 spectrum probably because of the difficulty in fitting the peaks due to a larger linewidth in this case. We have attributed the broadening to lifetime effects.

Table IV-7 gives the relative intensity ratio $I(L_3M_{4,5}M_{4,5}/L_2M_{4,5}M_{4,5})$ obtained from the calculated peak areas of the fitted curves. For most of the compounds the ratio of the total intensities of the two Auger groups reflects the statistical distribution of the hole states between the L_3 and L_2 levels of approximately 2 with an exception in the case of $GeCl_4$ which shows a substantially larger value, but the reason for the discrepancy is not clear. There is some difficulty arising in this case because of the relatively high background level in the spectrum.

E. Conclusions

The analysis of the Ge $L_{2,3}M_{2,3}M_{4,5}$ and $L_{2,3}M_{4,5}M_{4,5}$ Auger spectra of different Germanium compounds shows that the chemical environment does not change the general characteristics of the spectra. It affects the relaxation contributions accompanying the photoionization and the Auger processes, resulting in a constant energy shift for all components of the Auger spectrum. Complete theoretical reproduction of the absolute energies requires a comprehensive treatment of the relaxation contributions. However it is possible to obtain an understanding of the trends demonstrated in molecules from

Table IV-7. Experimental Intensity Ratio $I(L_3M_{4,5}M_{4,5})/I(L_2M_{4,5}M_{4,5})$

Compounds	$I(L_3M_{4,5}M_{4,5})/I(L_2M_{4,5}M_{4,5})$
GeO_2(s)	2.1
$Ge(C_2H_5)_4$(g)	1.8
$Ge(CH_3)_4$(g)	1.9
GeH_4(g)	1.8
$GeCl_4$(g)	2.6
GeF_4(g)	2.3

an empirical analysis based on the use of experimental binding energies and the assumption that the atomic terms can be adequately calculated from atomic theory leaving the residuals to be associated with the molecular environment effects.

The results indicate that the dependence of the relaxation energy on the chemical environment follows the same order as the polarizability of the group attached to the central atom.

The model used to estimate the extraatomic relaxation term is valid for metals, only in those cases where there is a complete screening of the positive charge associated with the hole. The model overemphasises the R_S^{ea} term in molecules.

The LS coupling scheme is adequate to predict the relative energies of the $L_{2,3}M_{4,5}M_{4,5}$ spectra. The mixed coupling scheme for the calculations of the intensities seems to reproduce the experimental values within the uncertainty of the curve decomposition procedure.

CHAPTER V

NEAR THRESHOLD IONIZATION EFFECTS IN AUGER SPECTRA OF GERMANIUM COMPOUNDS

A. Introduction

In the previous chapter the Al $K\alpha_{1,2}$ excited $L_{2,3}MM$ Auger spectra of Germanium in a series of Germanium compounds were described. The many features of these spectra were those normally expected for the system. Considering the proximity of the Magnesium $K\alpha_{1,2}$ radiation to the ionization energy of the Germanium $2p_{1/2}$ (L_2) energy level it appeared that it might be instructive to compare the Mg $K\alpha_{1,2}$ excited $L_{2,3}MM$ Auger spectra with the corresponding Al $K\alpha_{1,2}$ excited spectra. Having only the fixed Mg $K\alpha_{1,2}$ radiation energy at our disposal, the same approach as was used by Bahl et al.[77] for Selenium was used. The difference between the Ge L_2 binding energy and the Mg $K\alpha_{1,2}$ excitation energy was changed by selecting Germanium compounds with different L_2 chemical shifts (chemical tuning) so that the threshold ionization effects could be scanned by XAES (X-ray Auger electron

spectroscopy). Because the L_3 binding energy is significantly smaller than the energy of the Mg $K\alpha_{1,2}$ radiation, no threshold effects are expected in the L_3MM spectra. In all compounds, pronounced Post Collision Interaction (PCI) effects were observed. Also, for the first time, a pronounced effect of the Auger final state configuration was observed by means of a comparison of the behavior of the $L_{2,3}M_{4,5}M_{4,5}$ with the $L_{2,3}M_{2,3}M_{4,5}$ Auger spectra, the two strongest diagram Auger transition groups in Germanium compounds.

B. Experimental

The details of the experimental procedure have been given in Chapter IV except for the use of a Mg $K\alpha_{1,2}$ X-ray source (1253.64 eV)[21] to excite the spectra. The same compounds as in Chapter IV were analyzed; gaseous GeH_4, $Ge(CH_3)_4$, $Ge(C_2H_5)_4$, $GeCl_4$, GeF_4 and solid GeO_2.

C. Theory

The Auger decay, following inner shell photoionization, is not usually affected by the energy of the incident photon. However, when the photon energy is very close to the ionization threshold of the primary

electron being ejected, the emission of an Auger electron may occur while the slowly receding photoelectron is still in the vicinity of the excited atom. In such a situation, the Auger spectrum is expected to be influenced by what is called Post Collision Interaction (PCI).[78,79] This term was first used for the autoionization of an atom which, under certain conditions, may be influenced by the Coulomb field of a slowly receding particle. Much experimental data on PCI has been reported for autoionization following electron impact

$$e^- + B \rightarrow B^* + e^-(1)\ (\text{slow}) \qquad B^* \rightarrow B^+ + e^-(2)\ (\text{fast}) \qquad \text{V-1}$$

where the slowly receding particle is the inelastically scattered electron $e^-(1)$. At impact energies slightly above the threshold for excitation of the autoionizing state the ejected electron $e^-(2)$ peaks were found to be shifted towards higher energies and broadened.[80] Experimentally it appeared that the PCI led to an energy loss for the slow electron e^- (1) and an energy gain for the autoionization electron e^- (2). PCI phenomena have also been observed[81] for the process of inner shell ionization by X-ray followed by Auger ejection of a fast electron

$$h\nu + B \rightarrow B^{+} + e^{-} \text{ (slow)}$$
$$\qquad\qquad \rightarrow B^{2+} + e^{-} \text{ (fast)} \qquad \text{V-2}$$

When the energy of the photon is very close to the ionization energy of B, then the PCI spectrum is observed. The main features in a PCI spectrum, shift in the Auger energy, line broadening and line asymmetry, are explained with a semiclassical theory due to Niehaus[78] in terms of pure energy exchange between the fast and the slow electrons.

According to this model, the slowness of the receding electron, compared to the other bound electrons and to the fast ejected Auger electron, allows the separation of the motion of the slow electron from the motion of the other electrons. Its behavior may be described in terms of potential curves representing a pure Coulomb potential (-1/R) in the initial state before the Auger decay and a Coulomb potential (-2/R) thereafter for the system of the ion plus a slow electron. The model provides an analytic expression for the energy distribution of the energy gain ε of the Auger electron (energy loss $-\varepsilon$ for the photoelectron). The distribution depends on the excess energy ΔE which is the difference between the energy of

the incident photon and the ionization energy of the atom, and on the lifetime of the inner shell ionization process. The results predict an asymmetric Auger peak having a high energy tail. The most probable energy shift is determined as the position at the maximum of the energy distribution which satisfies the following relationship

$$[2(\xi + \delta)^{1/2} - \xi(5\xi + 4\delta)] = 0 \qquad \text{V-3}$$

where the reduced energies δ and ξ are related to the excess energy ΔE and to the Auger peak energy shift (ε) by the lifetime (τ) of the core level according to the equations

$$\xi = \varepsilon\tau^{2/3}$$

$$\delta = \Delta E\tau^{2/3} \qquad \text{V-4}$$

with all quantities in atomic units. The use of reduced energies in equations V-4 allows the energy shifts to be expressed independently of the lifetime (τ).

From equations V-3 and V-4 it follows that: a) for $\delta \to 0$ (at threshold) the Auger peak energy shift is equal to

$(\sqrt{2}/5\tau)^{2/3}$; b) the peak position varies smoothly across the threshold. When $\varepsilon << \Delta E$ equation V-3 reduces to the classical result obtained by Barker and Berry[82]

$$\xi = \frac{1}{2\sqrt{2\delta}} \qquad \text{V-5}$$

according to which for $\delta \to 0$, $\xi \to \infty$ and also $\varepsilon \to \infty$. In the absence of PCI, the probability for ionization and so the subsequent Auger effect would be a step function rising abruptly at $\Delta E = 0$ from zero to one. As it is shown in the Niehaus[78] theory and confirmed experimentally,[82] the probability for ionization increases smoothly through the threshold in a rather wide energy range whose width increases as the lifetime of the hole state decreases.

Another phenomenon arising at the threshold is the so called Auger Resonant Raman effect[83,84] by analogy with the X-ray Resonant Raman effect. In the X-ray Resonant Raman effect, absorption of a photon $h\omega_1$ promotes an atomic inner shell electron to an excited bound state. The inner shell vacancy is simultaneously filled by another atomic electron under emission of a characteristic X-ray photon $h\omega_2$ ($< h\omega_1$). For the Auger Resonant Raman effect, an Auger electron is emitted in place of the X-

ray. The resonantly emitted Auger electron (or X-ray line) is different from the normal Auger electron in that it reflects the width of the exciting radiation as well as the natural lifetime width Γ of the inner shell hole state. If excitation is accomplished with a sharp line, then the energy of the Auger electron (or emitted photon) will vary with the energy of the incident photon $h\omega_1$ over a range of Γ. The linear dispersion and the narrowing of the emitted Auger electron line (or the emitted radiation linewidth) are the identifying characteristics of the Auger Resonant Raman process. Two possible spectral appearances arise depending on whether the electron placed in the excited state acts as a spectator while an Auger process takes place with two of the more tightly bound electrons, or whether the electron in the excited state is directly involved in the filling of the hole. Both cases result in Auger electron energies which are higher than the normal Auger lines, with the latter having the higher energy.

D. Results and Discussion

The Ge $L_{2,3}M_{4,5}M_{4,5}$ and $L_{2,3}M_{2,3}M_{4,5}$ Auger spectra of the six compounds excited by Mg $K\alpha_{1,2}$ X-radiation are shown in Figures V-1 to V-12. The figures corresponding

Figure V-1. Germanium $L_{2,3}M_{4,5}M_{4,5}$ Auger spectrum of solid GeO_2 excited by Mg $K\alpha_{1,2}$ radiation. In the insert is shown the $L_2M_{4,5}M_{4,5}$ region excited by Al $K\alpha_{1,2}$ radiation from Figure IV-1. I_2 and I_3 are the intensities of the $^1G_4$ lines in the L_2- and L_3-$M_{4,5}M_{4,5}$ groups respectively in Figure IV-1.

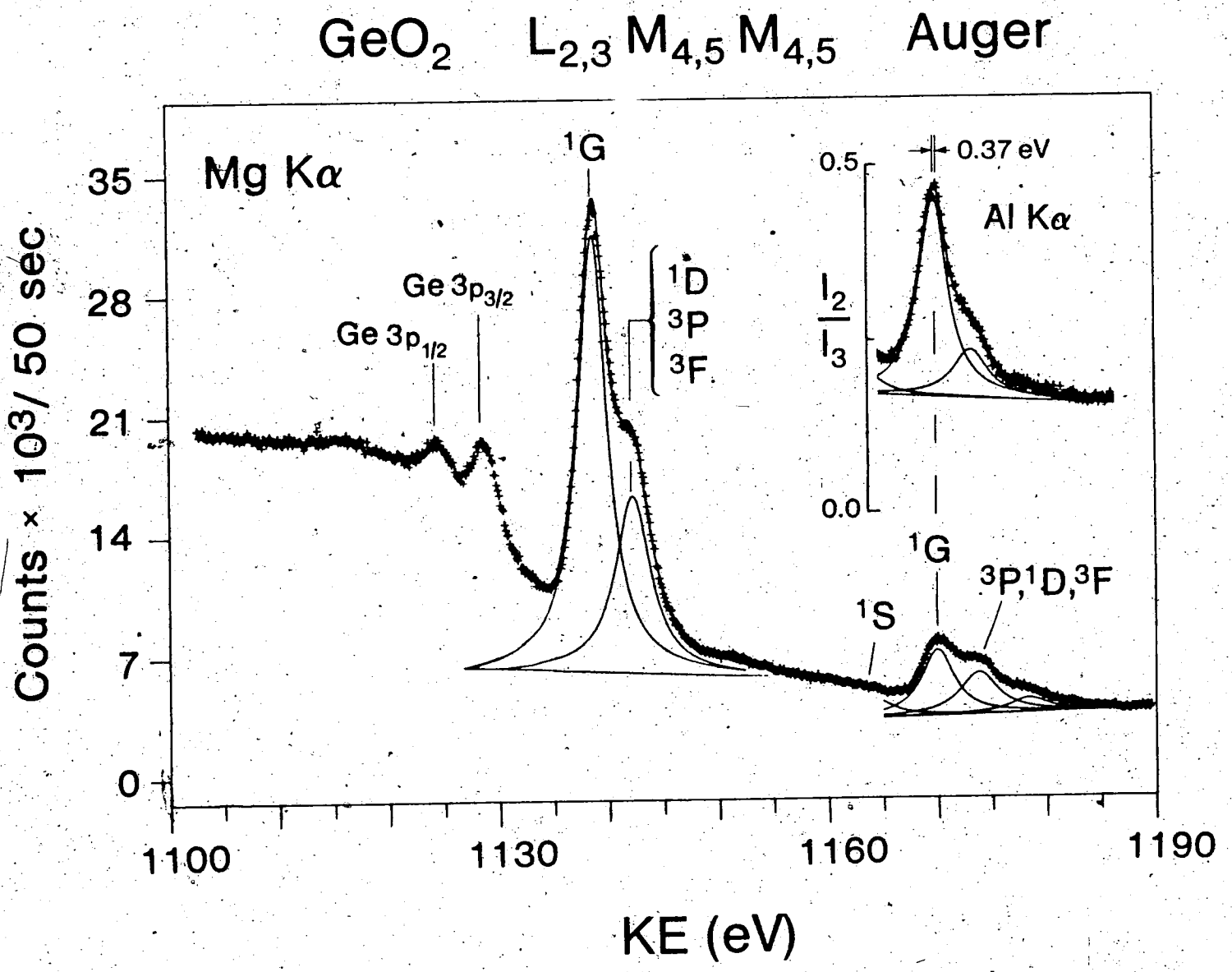
GeO2 L2,3 M4,5 M4,5 Auger
Mg Kα
Al Kα
0.37 eV
1G
1D
3P
3F
Ge 3p3/2
Ge 3p1/2
1S
3P,1D,3F
I2/I3
0.5
0.0
Counts × 10³/ 50 sec
35
28
21
14
7
0
1100
1130
1160
1190
KE (eV)

Figure V-2. Germanium $L_{2,3}M_{2,3}M_{4,5}$ Auger spectrum of solid GeO_2 excited by Mg $K\alpha_{1,2}$ radiation. The solid lines indicate the experimental position of the multiplet terms. The dashed lines indicate the LS calculated positions of the terms unresolved in the spectrum.

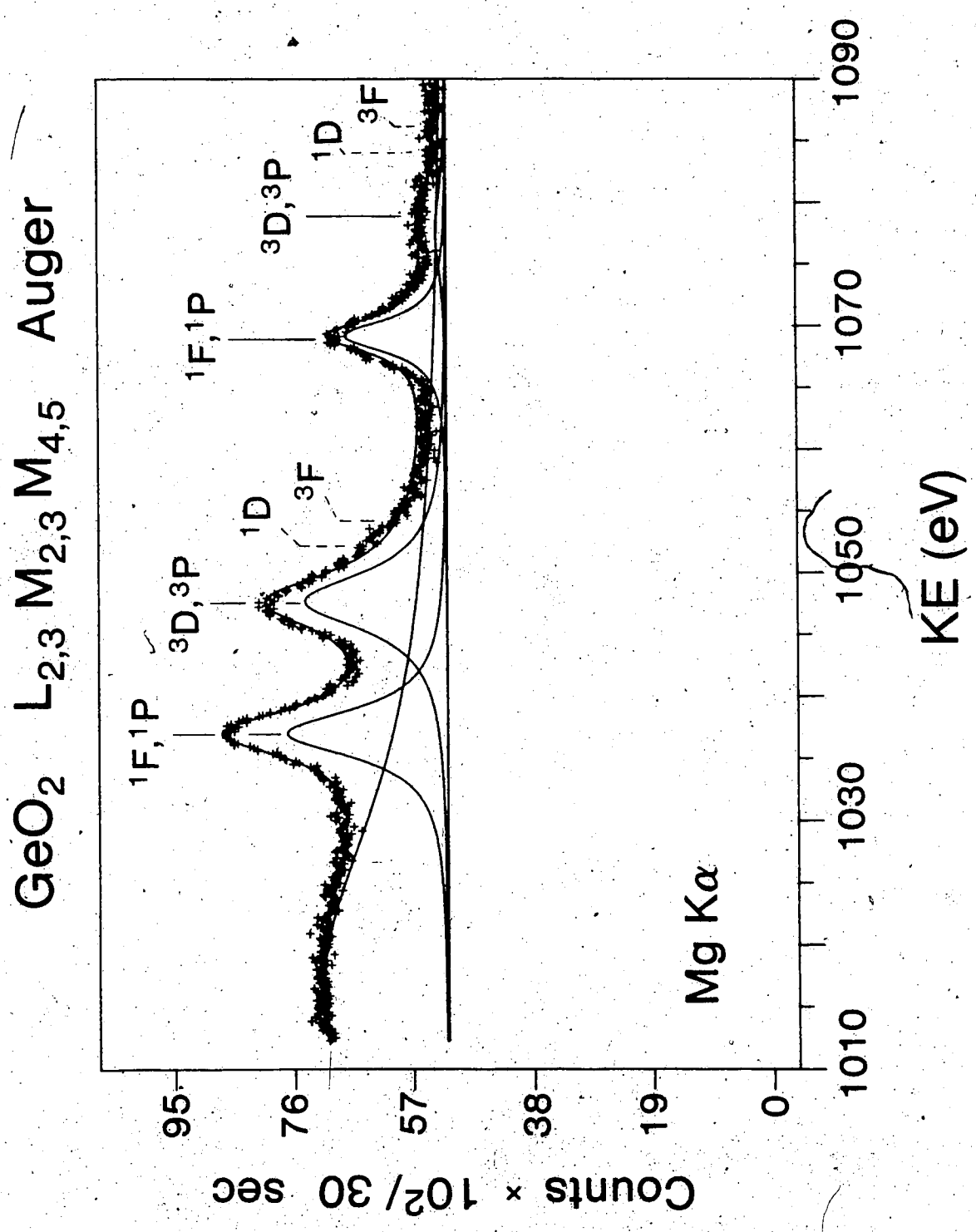
GeO2 L2,3 M2,3 M4,5 Auger
1F,1P
3D,3P
1D
3F
1F,1P
3D,3P
1D
3F
Mg Kα
Counts × 10²/ 30 sec
0
19
38
57
76
95
1010
1030
1050
1070
1090
KE (eV)

Figure V-3. Germanium $L_{2,3}M_{4,5}M_{4,5}$ Auger spectrum of $Ge(C_2H_5)_4$ vapor excited by Mg $K\alpha_{1,2}$ radiation at a sample pressure of 200μ. In the insert is shown the $L_2M_{4,5}M_{4,5}$ region excited by Al $K\alpha_{1,2}$ radiation from Figure IV-3. I_2 and I_3 are the intensities of the $^1G_4$ line in the L_2- and L_3- $M_{4,5}M_{4,5}$ groups respectively in Figure IV-3. s = satellite; α= Ge 3d photoelectron line excited by Ge Lα; PCI = Post Collision structure; s.s. = spectator satellite.

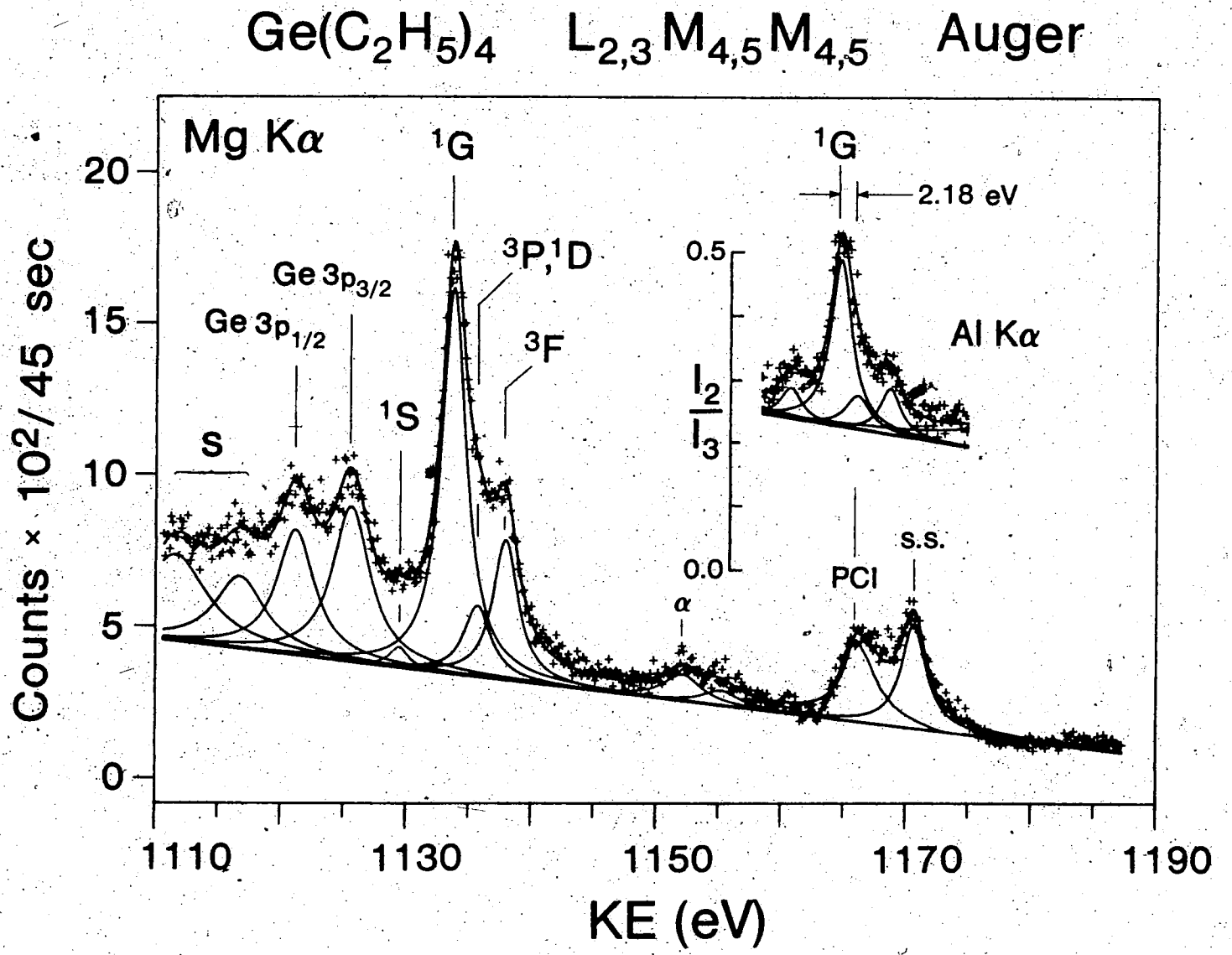
Ge(C2H5)4 L2,3M4,5M4,5 Auger
Mg Kα
1G
3P,1D
3F
1S
Ge 3p3/2
Ge 3p1/2
s
α
PCI
s.s.
1G
2.18 eV
Al Kα
I2/I3
0.5
0.0
Counts × 10²/ 45 sec
0
5
10
15
20
1110
1130
1150
1170
1190
KE (eV)

Figure V-4. Germanium $L_{2,3}M_{2,3}M_{4,5}$ Auger spectrum of $Ge(C_2H_5)_4$ vapor excited by Mg $K\alpha_{1,2}$ radiation at a sample pressure of 200μ . The solid lines indicate the experimental positions of the multiplet terms. The dashed lines indicate the LS calculated positions of the terms unresolved in the spectrum. s= satellite.

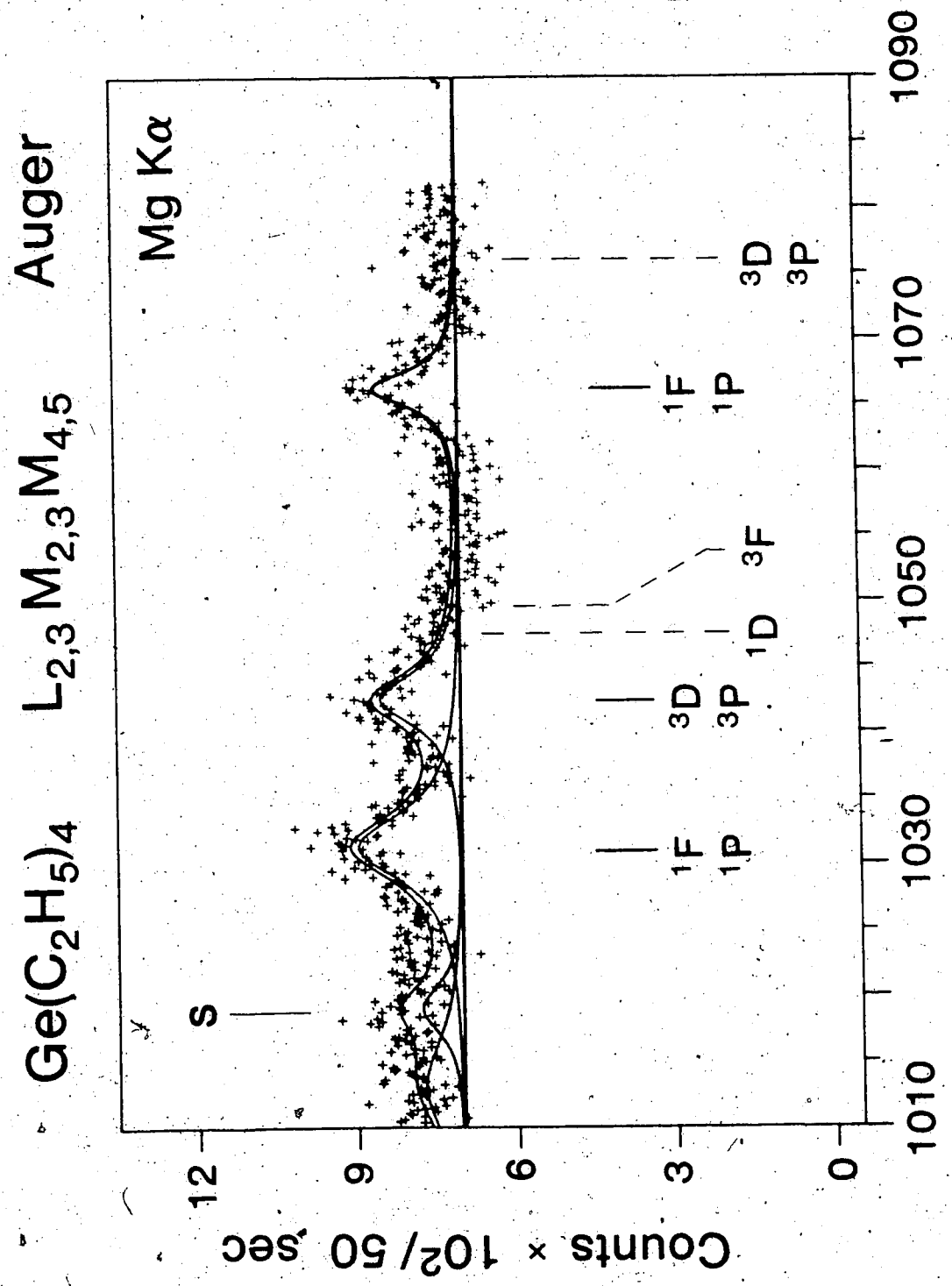
Ge(C2H5)4
L2,3M2,3M4,5 Auger
Mg Kα
S
1F
1P
3D
3P
1D
3F
Counts × 102/50 sec
KE (eV)
0
3
6
9
12
1010
1030
1050
1070
1090

Figure V-5. Germanium $L_{2,3}M_{4,5}M_{4,5}$ Auger spectrum of $Ge(CH_3)_4$ vapor excited by Mg $K\alpha_{1,2}$ radiation at a sample pressure of 200μ. In the insert is shown the $L_2M_{4,5}M_{4,5}$ region excited by Al $K\alpha_{1,2}$ radiation from Figure IV-5. I_2 and I_3 are the intensities of the $^1G_4$ lines in the L_2- and L_3- $M_{4,5}M_{4,5}$ groups respectively in Figure IV-5. s = satellite; α= Ge 3d photoelectron line excited by Ge Lα; β= Ge 3d photoelectron line excited by Ge Lβ; PCI = Post Collision structure; s.s.= spectator satellite.

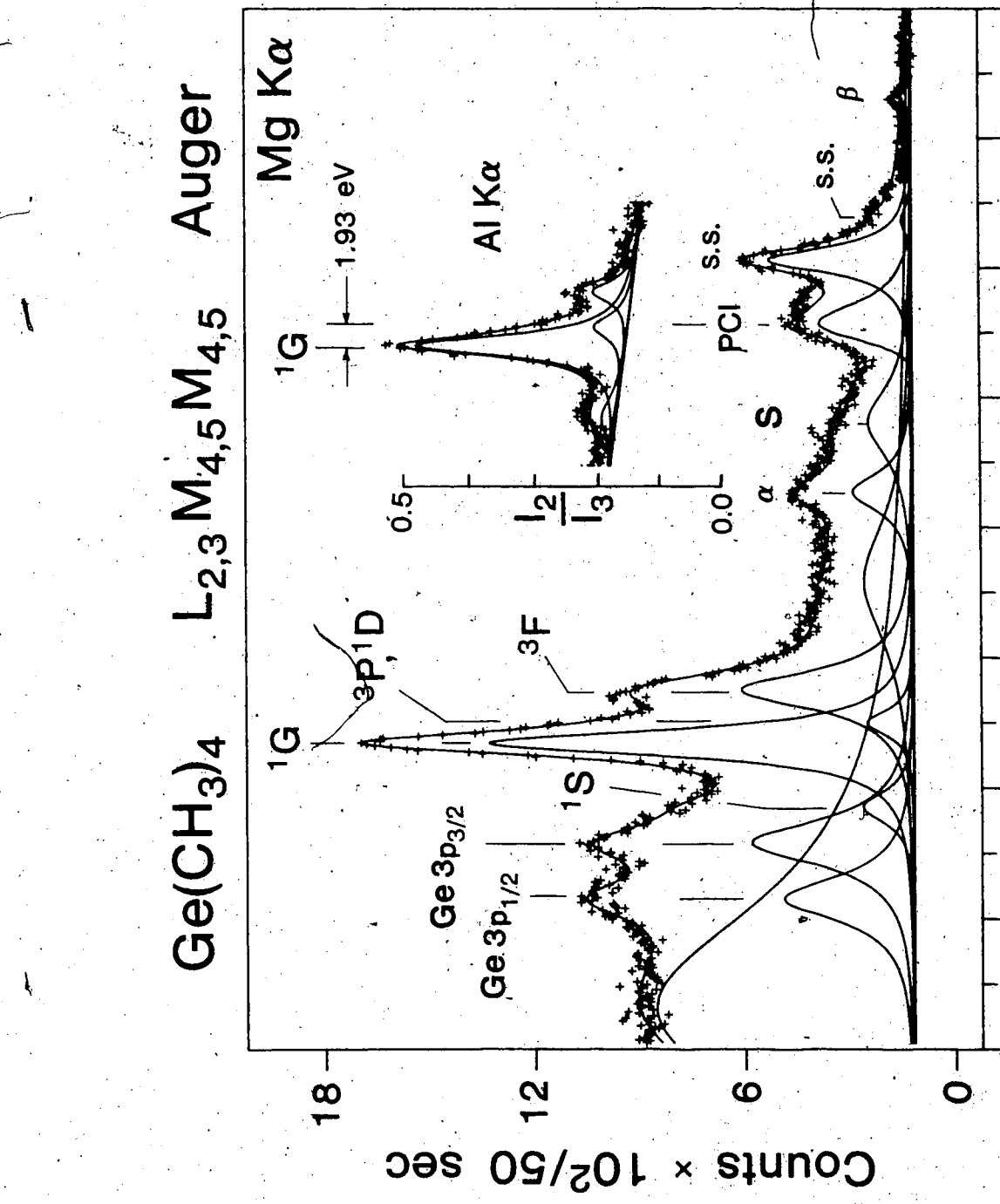
Ge(CH3)4
L2,3M4,5M4,5 Auger
Mg Kα
1G
3P,1D
3F
1S
Ge 3p3/2
Ge 3p1/2
1G
1.93 eV
Al Kα
I2/I3
0.5
0.0
PCI
s.s.
S
α
β
Counts × 102/50 sec
KE (eV)
0
6
12
18
1110
1130
1150
1170
1190

Figure V-6. Germanium $L_{2,3}M_{2,3}M_{4,5}$ Auger spectrum of $Ge(CH_3)_4$ vapor excited by Mg $K\alpha_{1,2}$ radiation at a sample pressure of 200μ. s = satellite.

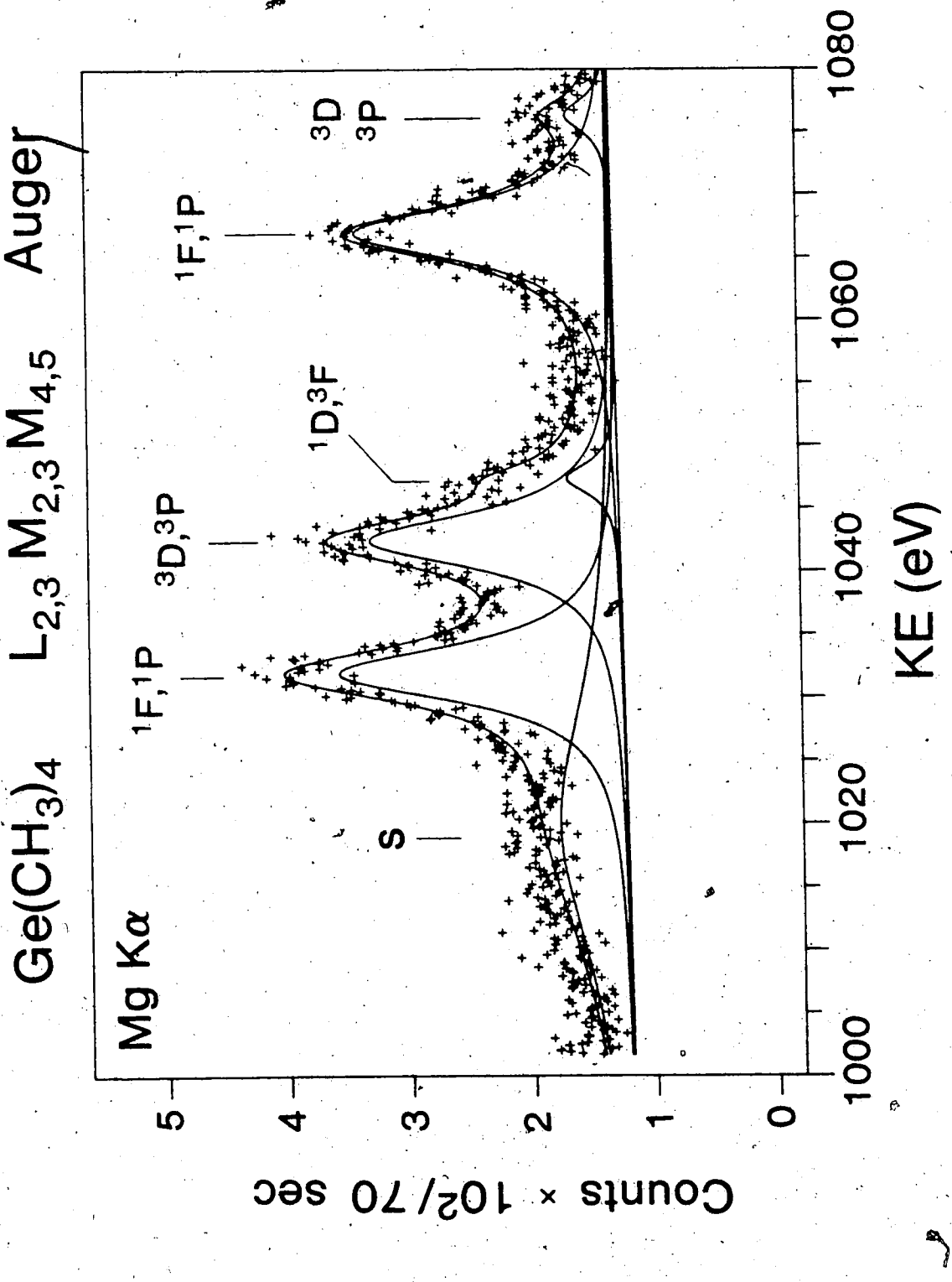
Ge(CH3)4 L2,3 M2,3 M4,5 Auger
Mg Kα
1F,1P
3D,3P
1D,3F
1F,1P
3D
3P
S
Counts × 102/70 sec
KE (eV)
0
1
2
3
4
5
1000
1020
1040
1060
1080

Figure V-7. Germanium $L_{2,3}M_{4,5}M_{4,5}$ Auger spectrum of gaseous GeH_4 excited by Mg $K\alpha_{1,2}$ radiation at a sample pressure of 200μ . In the insert is shown the $L_2M_{4,5}M_{4,5}$ region excited by Al $K\alpha_{1,2}$ radiation from Figure IV-7. I_2 and I_3 are the intensities of the $^1G_4$ lines in the L_2- and L_3- $M_{4,5}M_{4,5}$ groups respectively in Figure IV-7. PCI= Post Collision Structure; s.s.= spectator satellite.

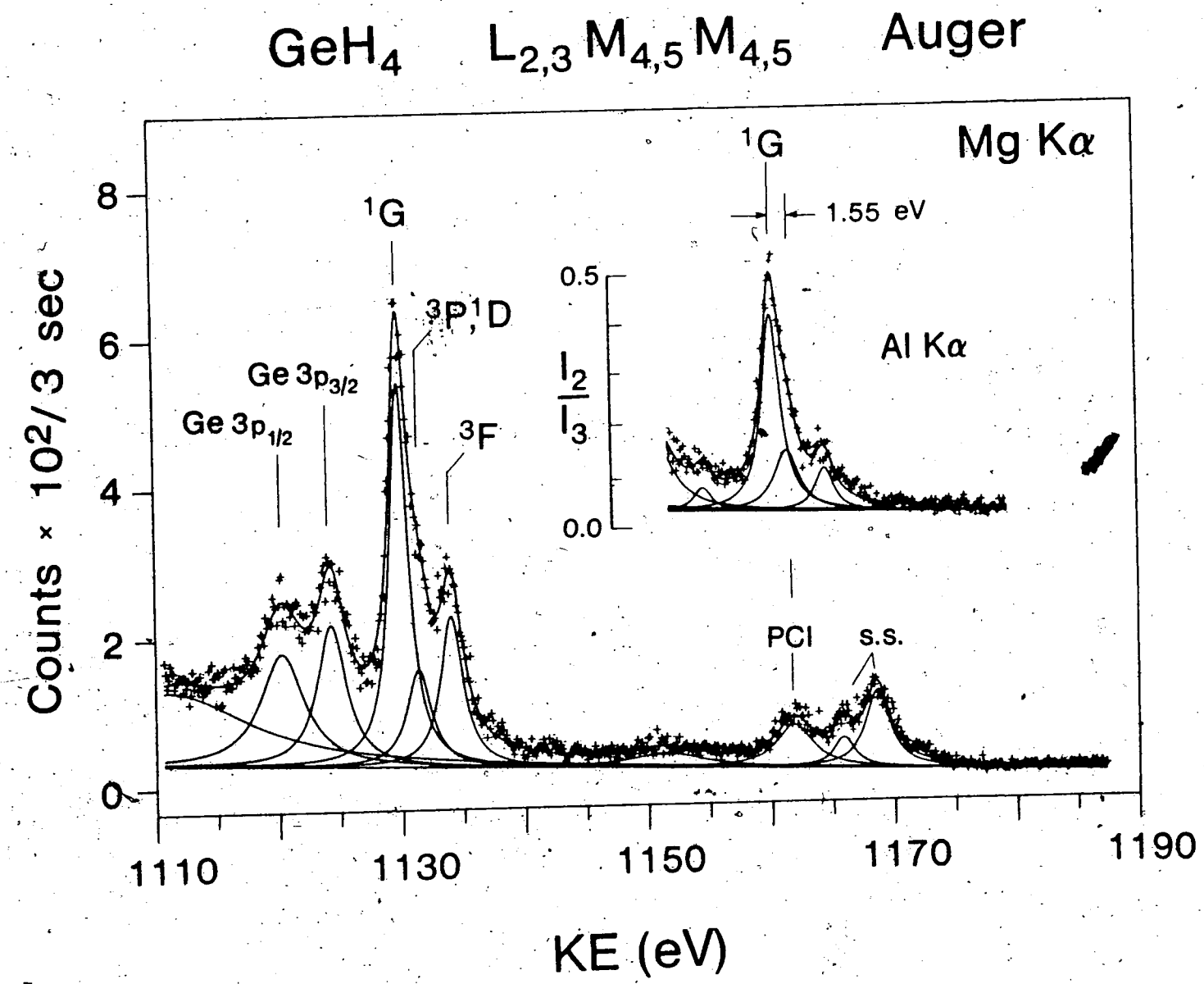
GeH4 L2,3 M4,5 M4,5 Auger
Mg Kα
1G
1.55 eV
Al Kα
I2/I3
0.5
0.0
Ge 3p1/2
Ge 3p3/2
3P,1D
3F
PCI
s.s.
Counts × 10²/3 sec
KE (eV)
0
2
4
6
8
1110
1130
1150
1170
1190

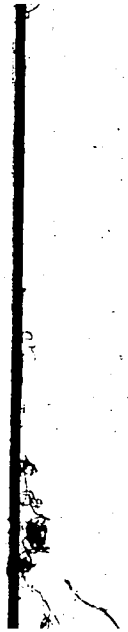

Figure V-8. Germanium $L_{2,3}M_{2,3}M_{4,5}$ Auger spectrum of gaseous GeH_4 excited by Mg $K\alpha_{1,2}$ radiation at a sample pressure of 200μ.s = satellite; α= Ge 3p photoelectron line excited by Ge Lα.

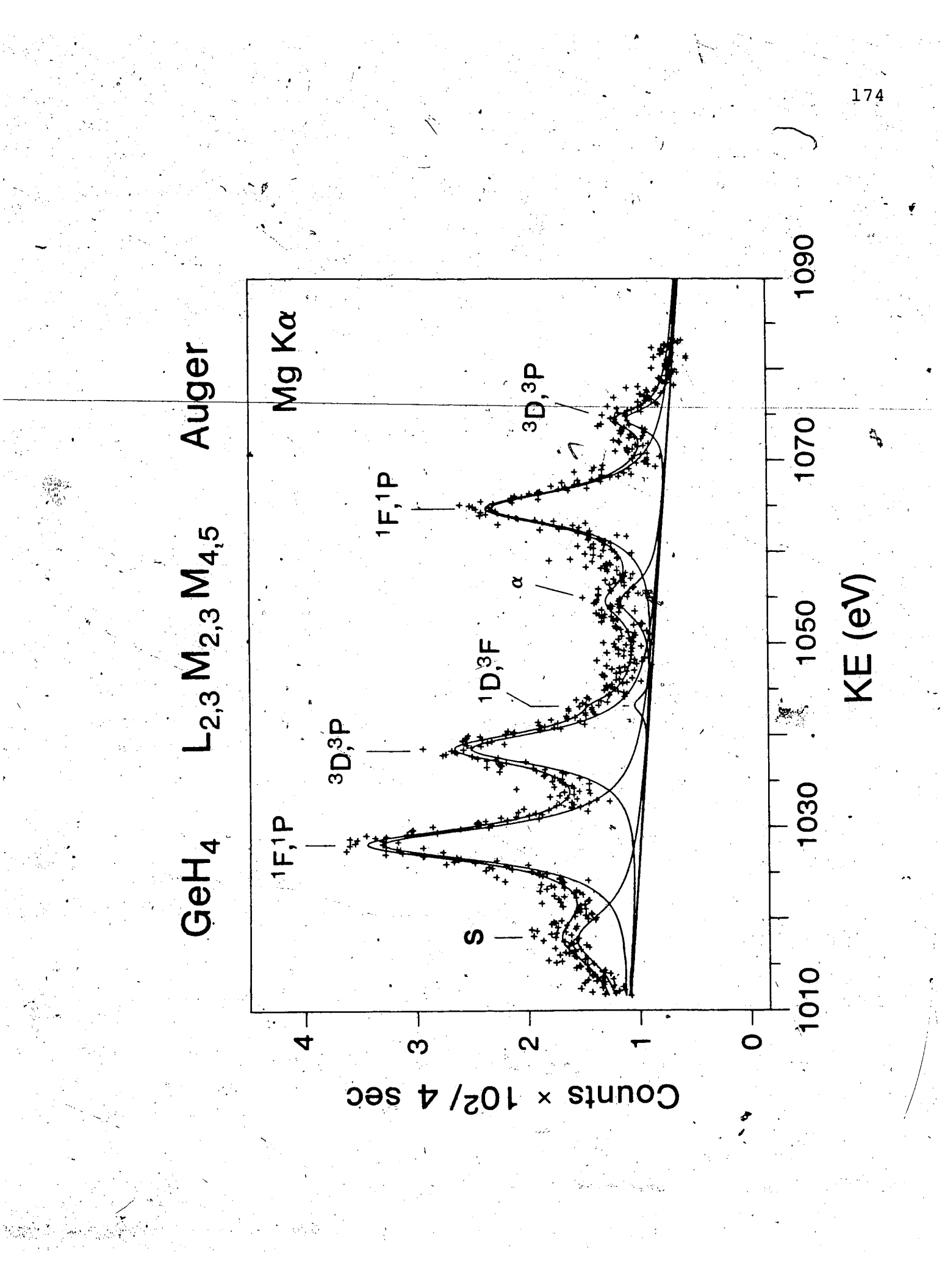
GeH4
L2,3 M2,3 M4,5 Auger
Mg Kα
1F,1P
3D,3P
S
1D,3F
α
1F,1P
3D,3P
Counts x 10²/ 4 sec
KE (eV)
0
1
2
3
4
1010
1030
1050
1070
1090

Figure V-9. Germanium $L_{2,3}M_{4,5}M_{4,5}$ Auger spectrum of $GeCl_4$ vapor excited by Mg $K\alpha_{1,2}$ radiation at a sample pressure of 200μ . In the insert is shown the $L_2M_{4,5}M_{4,5}$ region excited by Al $K\alpha_{1,2}$ radiation from Figure IV-9. I_2 and I_3 are the intensities of the $^1G_4$ lines in the L_2- and L_3- $M_{4,5}M_{4,5}$ groups respectively in Figure IV-9. s= satellite; α= Ge 3d photoelectron line excited by Ge Lα; PCI= Post Collision Structure in this case excited by Mg $K\alpha_{3,4}$ radiation component; s.s.= spectator satellite.

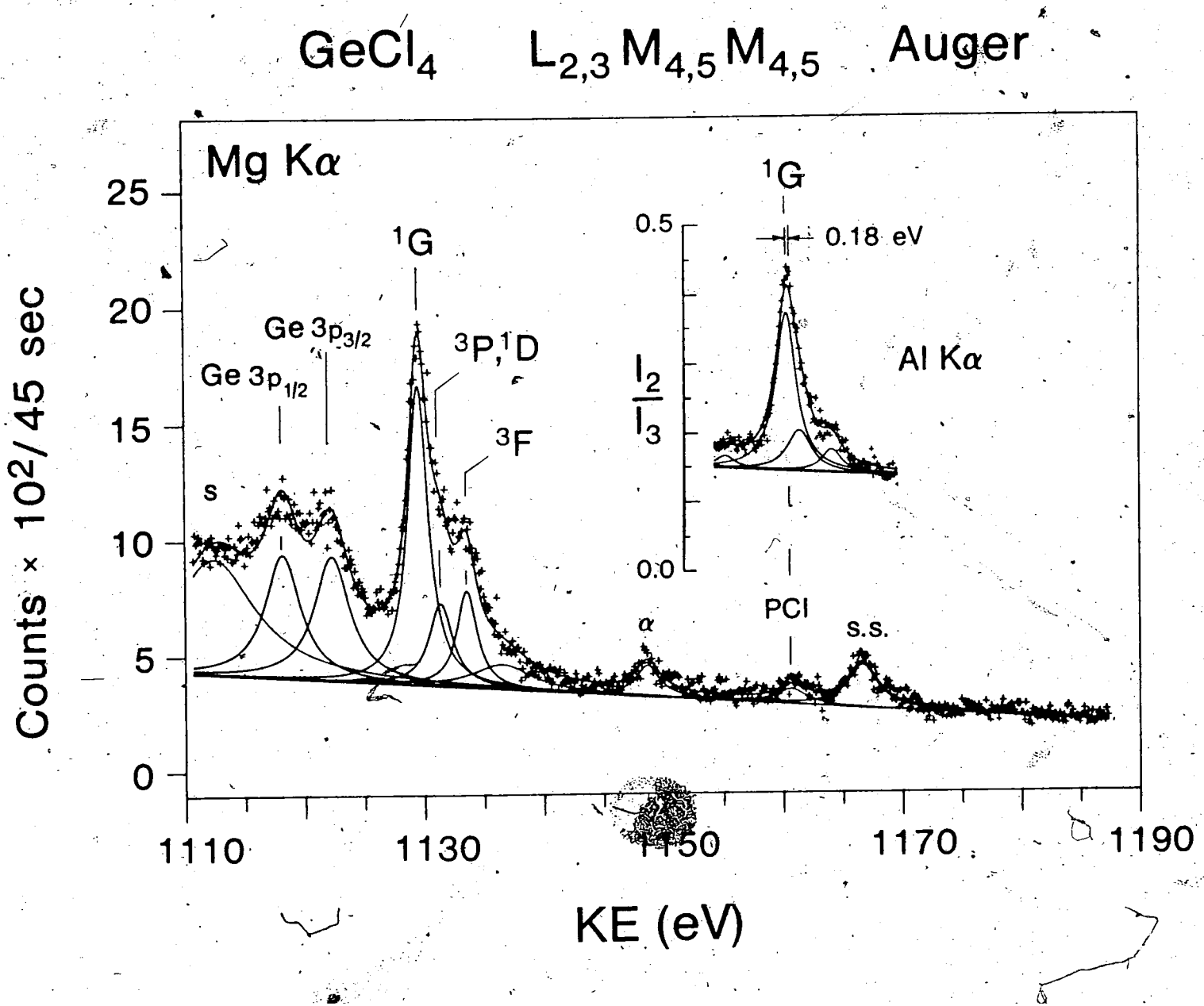
GeCl4 L2,3 M4,5 M4,5 Auger
Mg Kα
Counts × 10²/45 sec
25
20
15
10
5
0
1110
1130
1150
1170
1190
KE (eV)
1G
Ge 3p3/2
Ge 3p1/2
3P,1D
3F
s
0.5
0.0
I2/I3
0.18 eV
Al Kα
PCI
α
s.s.

Figure V-10. Germanium $L_{2,3}M_{4,5}M_{4,5}$ Auger spectrum of gaseous GeF_4 excited by Mg $K\alpha_{1,2}$ radiation at a sample pressure of 200μ. In the insert is shown the $L_2M_{4,5}M_{4,5}$ region excited by Al $K\alpha_{1,2}$ radiation from Figure IV-11. I_2 and I_3 are the intensities of the $^1G_4$ lines in the L_2- and L_3- $M_{4,5}M_{4,5}$ groups respectively in Figure IV-11. s = satellite; α= Ge 3d photoelectron line excited by Ge Lα; PCI = Post Collision structure; s.s. = spectator satellite.

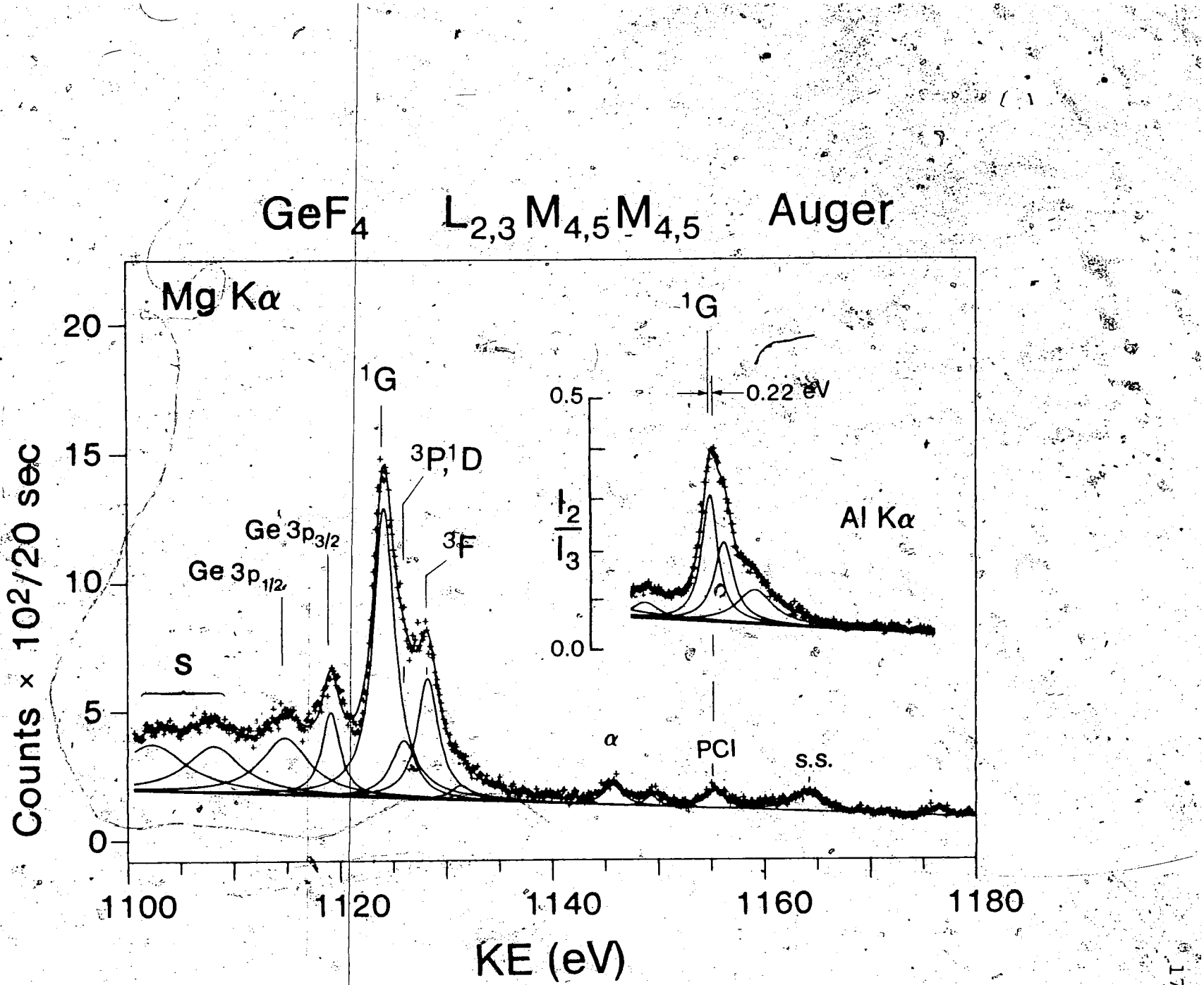
GeF4 L2,3 M4,5 M4,5 Auger
Mg Kα
Counts × 10²/20 sec
KE (eV)
1G
3P,1D
3F
Ge 3p3/2
Ge 3p1/2
S
α
PCI
s.s.
0.22 eV
I2/I3
Al Kα

Figure V-11. Germanium $L_{2,3}M_{2,3}M_{4,5}$ Auger spectrum of $GeCl_4$ vapor excited by Mg $K\alpha_{1,2}$ radiation at a sample pressure of 200μ . s= satellite; β= Cl 2p photoelectron line excited by Ge Lβ .

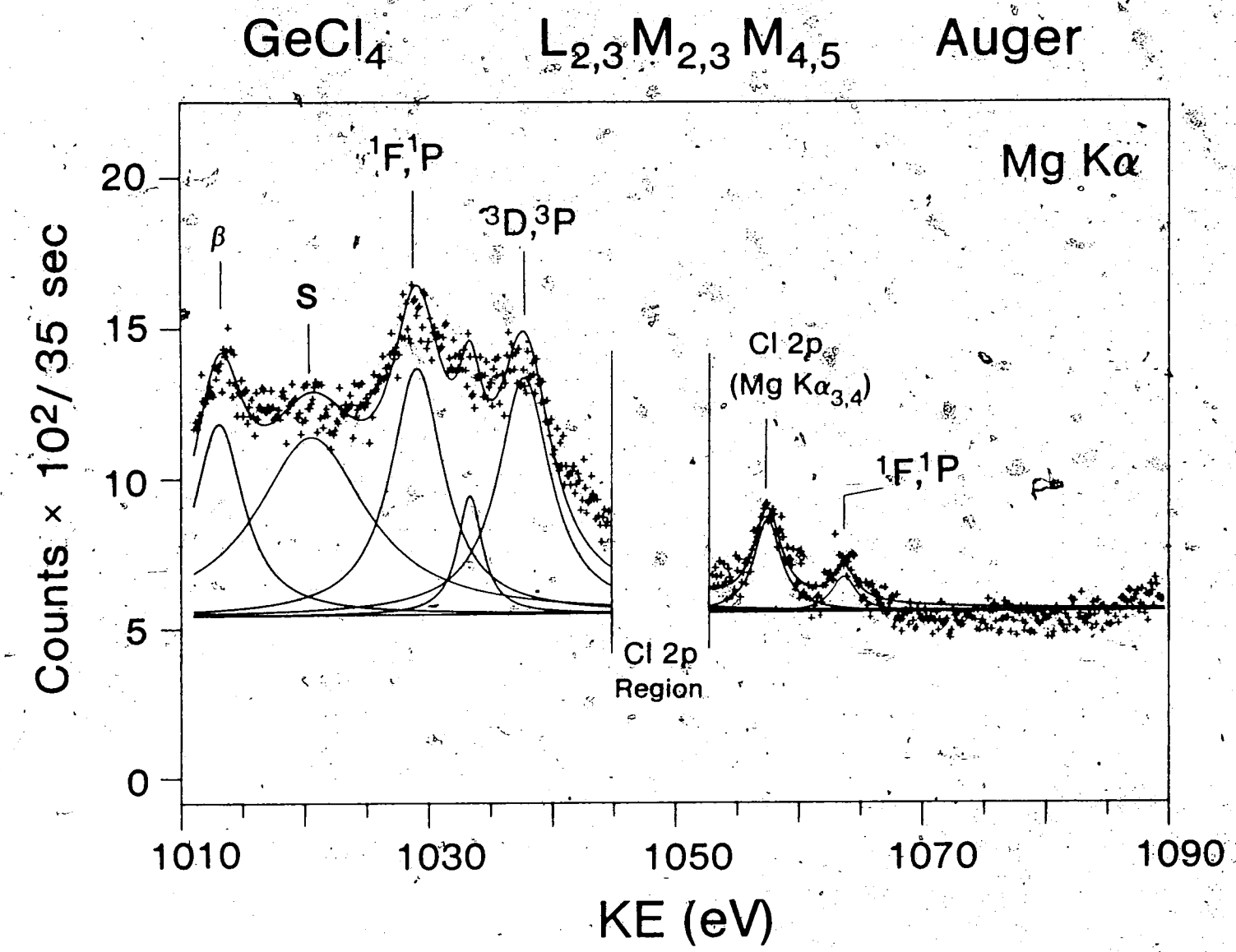
GeCl4
L2,3M2,3M4,5
Auger
Mg Kα
1F,1P
3D,3P
β
S
Cl 2p
(Mg Kα3,4)
1F,1P
Cl 2p
Region
Counts × 10²/35 sec
0
5
10
15
20
1010
1030
1050
1070
1090
KE (eV)

Figure V-12. Germanium $L_{2,3}M_{2,3}M_{4,5}$ Auger spectrum of gaseous GeF_4 excited by Mg $K\alpha_{1,2}$ radiation at a sample pressure of 200μ . The solid lines indicate the experimental positions of the multiplet terms. The dashed lines indicate the calculated positions of the terms unresolved in the spectrum. α= Ge $3p_{1/2}$ and $3p_{3/2}$ photoelectron lines excited by Ge Lα.

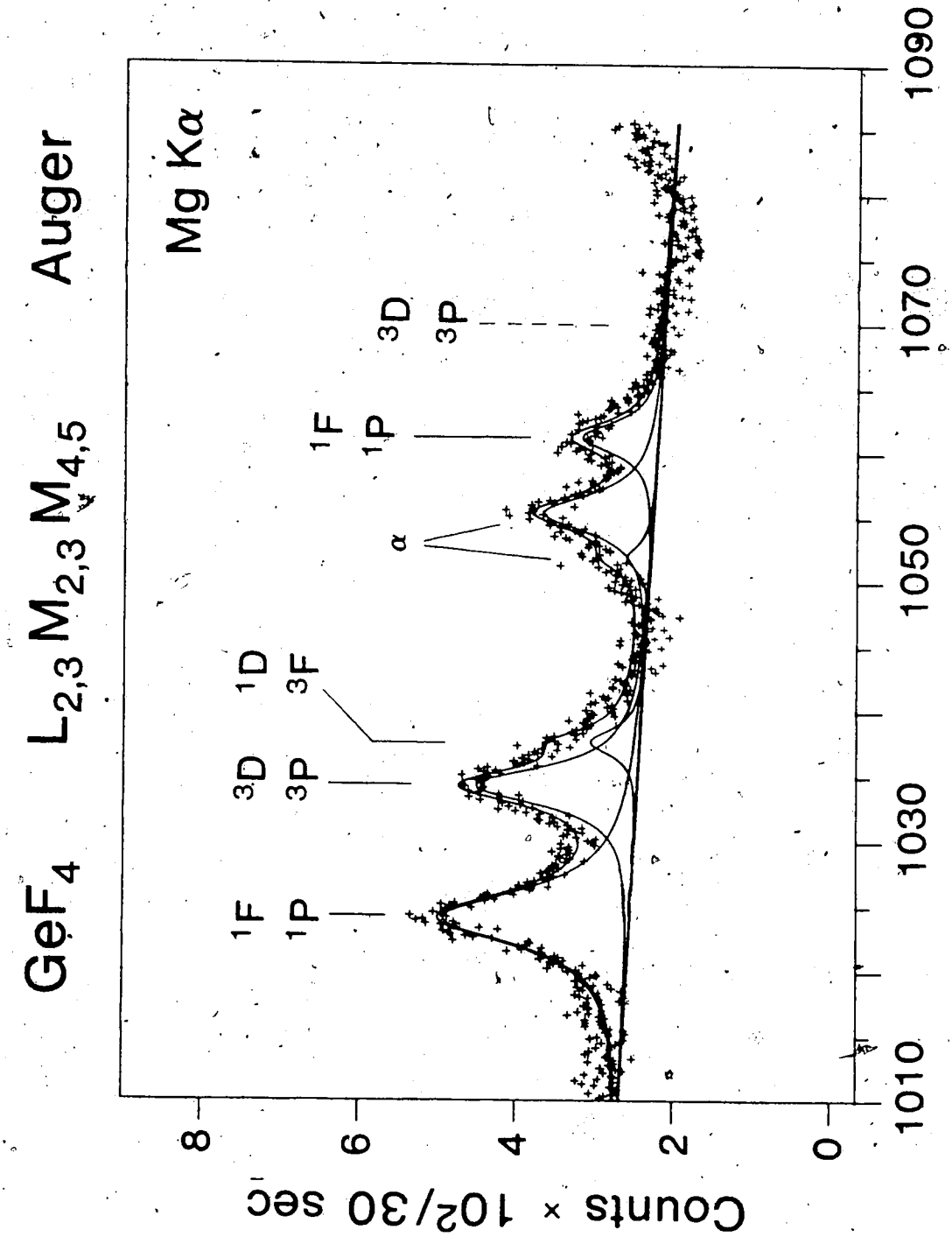
GeF4
L2,3 M2,3 M4,5 Auger
Mg Kα
1F
1P
3D
3P
1D
3F
α
Counts × 102/30 sec
KE (eV)
0
2
4
6
8
1010
1030
1050
1070
1090

to the $L_{2,3}M_{4,5}M_{4,5}$ Auger spectra contain an insert with the $L_2M_{4,5}M_{4,5}$ region taken from the complete $L_{2,3}M_{4,5}M_{4,5}$ spectra excited with Al $K\alpha_{1,2}$ radiation which were discussed in Chapter IV. The band components were obtained by the curve fitting procedure described in Chapter IV. All the $L_{2,3}M_{4,5}M_{4,5}$ spectra excited with Mg $K\alpha_{1,2}$ radiation contain the photoelectron lines arising from excitation of Ge $3p_{1/2}$ and Ge $3p_{3/2}$ levels (E_B ~ 130 eV) and this feature appears in the region of 1110-1120 eV obscuring the $^1S_0$ term. As with the Al $K\alpha_{1,2}$ excited spectra, the Mg $K\alpha$ excited spectra show the Ge 3d photoelectron line excited by Ge $L\alpha$ and Ge $L\beta$ radiations generated from some Germanium deposition on the anode. The L_3MM group of the Auger spectra excited by Mg $K\alpha_{1,2}$ is essentially the same as that excited by Al $K\alpha_{1,2}$ as expected because the $2p_{3/2}$ (L_3) binding energy is substantially smaller than the Mg $K\alpha_{1,2}$ radiation energy in all chemical environments of Ge, thus no threshold effects arise in this group.

GeO_2 which has a $2p_{1/2}$ binding energy 2.43 eV smaller than the Mg $K\alpha_{1,2}$ radiation energy shows an L_2MM spectrum (Figure V-1) with some pronounced differences compared to the spectrum obtained with Al $K\alpha_{1,2}$ radiation. The $L_2M_{4,5}M_{4,5}$ group is shifted by 0.37 eV to higher energy in

the Mg $K\alpha_{1,2}$ spectrum relative to the group position in the spectrum excited by Al $K\alpha_{1,2}$ radiation. Also noticeable is a dramatic decrease in the $L_2M_{4,5}M_{4,5}/L_3M_{4,5}M_{4,5}$ intensity ratio, changing from 0.5 with Aluminum excitation to 0.2 with Magnesium excitation. This behavior reflects the variation of the $2p_{1/2}$ photoionization cross-section near the threshold. It seems that there is also an alteration of the relative intensities within the $L_2M_{4,5}M_{4,5}$ group. The peak previously attributed to a sum of the ^3P, ^1D, ^3F final states (Chapter IV) is increased in intensity relative to the $^1G_4$ final state in comparison with the Al $K\alpha_{1,2}$ spectrum. Also in the spectrum excited with Magnesium radiation there is a structure at high energy, about 8.5 eV away from the $^1G_4$ lines which does not seem to belong to any of the diagram Auger transitions. The origin of this feature is unkhown. The $L_{2,3}M_{2,3}M_{4,5}$ spectrum shown in Figure V-2 has the same features as the Al $K\alpha_{1,2}$ excited spectrum. The only difference is a shift of about 0.97 eV of the $L_2M_{2,3}M_{4,5}$ group to higher kinetic energy in the spectrum excited with Mg $K\alpha_{1,2}$ radiation respect to that excited by Al $K\alpha_{1,2}$ radiation. No change in the $L_2M_{2,3}M_{4,5}/L_3M_{2,3}M_{4,5}$ intensity ratio is observed.

In Figure V-3 the $L_{2,3}M_{4,5}M_{4,5}$ spectrum of $Ge(C_2H_5)_4$ is shown. For this compound the Germanium $2p_{1/2}$ binding

energy is 0.51 eV larger than the Mg $K\alpha_{1,2}$ radiation energy. The $L_2M_{4,5}M_{4,5}$ Auger group excited by Mg $K\alpha_{1,2}$ differs markedly from the Aluminum excited spectrum, which is the normal Auger spectrum because of the threshold ionization phenomena. Because of the limitations of the curve fitting procedure which allows only the use of either Gaussians or Lorentzians, the asymmetric shape found in this region could only be fitted with two Lorentzians centered at 1166.63 eV. This feature is shifted by 2.18 eV to higher energy with respect to the normal Auger line $^1G_4$ ($L_2M_{4,5}M_{4,5}$) in the Aluminum excited spectrum. The two Lorentzians were then replaced by the PCI asymmetric shape calculated by Dr. J. Väyrynen of this laboratory according to the theory of Niehaus.[78] As the result shown in Figure V-3 indicates, the PCI function reproduces reasonably well the structure in the experimental spectrum. At about 6 eV above the normal $^1G_4$ ($L_2M_{4,5}M_{4,5}$) another structure similar in appearance to the diagram Auger line appears. This line can be explained as a spectator satellite Auger line. The spectator satellite Auger process may consist of a $2p_{1/2} \rightarrow$ kd excitation, followed by the Auger decay with the kd electron acting as a spectator. In the case of a participation of the kd electron in the Auger decay, the

process would have appeared as a structure at even higher energy.[7a] The intensity ratio, as derived from the areas obtained from the least square fitting procedure, of the PCI and satellite structure over the $L_3M_{4,5}M_{4,5}$ region in the Mg $K\alpha_{1,2}$ excited spectrum was compared to the $L_2M_{4,5}M_{4,5}/L_3M_{4,5}M_{4,5}$ intensity ratio obtained in the spectrum excited with Aluminum radiation. A 38% decrease of the total intensity of PCI and satellite peaks with respect to the normal $L_2M_{4,5}M_{4,5}$ Auger transition was observed. The $L_{2,3}M_{2,3}M_{4,5}$ spectrum of $Ge(C_2H_5)_4$ shown in Figure V-4 is very much like that of the spectrum excited with Aluminum radiation, there being only a rather large shift of the $L_2M_{2,3}M_{4,5}$ group by 4.5 eV to higher energy. No change in the $L_2M_{2,3}M_{4,5}/L_3M_{2,3}M_{4,5}$ intensity ratio was observed.

In Figure V-5 is shown the $L_{2,3}M_{4,5}M_{4,5}$ Auger spectrum of $Ge(CH_3)_4$. For this compound the energy of the Ge $2p_{1/2}$ is 0.86 eV above the Mg $K\alpha_{1,2}$ radiation. The $L_2M_{4,5}M_{4,5}$ spectrum shows the PCI effect consisting of a broadened, asymmetric lineshape shifted by 1.93 eV to higher energy relative to the normal $^1G_4(L_2M_{4,5}M_{4,5})$ Auger line and with a diagram Auger-like line shifted by 6.2 eV to higher kinetic energy relative to the normal

$^1G_4(L_2M_{4,5}M_{4,5})$ Auger line. The asymmetric structure is matched quite well by the calculated PCI function. The latter part of the spectrum is again explained as a spectator satellite Auger line. The intensity of the entire structure (PCI and satellite) relative to the intensity of the $L_3M_{4,5}M_{4,5}$ group is about 25% less than the $L_2M_{4,5}M_{4,5}/L_3M_{4,5}M_{4,5}$ intensity ratio in the Aluminum excited spectrum. In Figure V-6 the $L_{2,3}M_{2,3}M_{4,5}$ spectrum of $Ge(CH_3)_4$ excited by Mg $K\alpha_{1,2}$ radiation is illustrated. The $L_2M_{2,3}M_{4,5}$ group is shifted by 4.62 eV to higher kinetic energy relative to the Aluminum excited $L_2M_{2,3}M_{4,5}$ group. The statistics of the spectral data obtained with Mg $K\alpha$ excitation were poorer than that of the spectrum excited with Aluminum radiation, however an approximate estimate of the intensities revealed no change in the $L_2M_{2,3}M_{4,5}/L_3M_{2,3}M_{4,5}$ intensity ratio.

The $L_{2,3}M_{4,5}M_{4,5}$ spectrum of GeH_4 is shown in Figure V-7. The binding energy of Ge $2p_{1/2}$ is 2.78 eV larger than the Mg $K\alpha_{1,2}$ radiation energy. Even this far below the threshold, the $L_2M_{4,5}M_{4,5}$ spectrum excited by the Magnesium anode shows some PCI effect with a structure which is shifted by 1.55 eV to higher kinetic energy relative to the normal $^1G_4(L_2M_{4,5}M_{4,5})$ Auger line. The intensity of this peak is quite low and it is not possible

to discern an asymmetric shape. A satellite peak is present at 6.11 eV above the diagram $^1G_4$ ($L_2M_{4,5}M_{4,5}$) Auger line. The small peak between the PCI and the satellite structure may be due to another spectator satellite involving a different orbital. The combined intensity of PCI and satellites relative to the intensity of the $L_3M_{4,5}M_{4,5}$ group of the same spectrum is only 40% of the $L_2M_{4,5}M_{4,5}/L_3M_{4,5}M_{4,5}$ intensity ratio obtained in the spectrum excited by Aluminum radiation. The $L_{2,3}M_{2,3}M_{4,5}$ spectrum shown in Figure V-8 is similar to the spectrum excited with Aluminum radiation, the only notable difference being the shift of the $L_2M_{2,3}M_{4,5}$ group by 5.74 eV to higher energy. The structure near 1054 eV, whose intensity increased during the measurement, may be due to the Ge $3p_{1/2}$ and Ge $3p_{3/2}$ photoelectron lines excited by Ge $L\alpha$ radiation, again due to Germanium deposition on the anode.

Different features from the ones described above are shown by the Ge $L_{2,3}M_{4,5}M_{4,5}$ Auger spectra of $GeCl_4$ and GeF_4 illustrated in Figures V-9 and V-10.

The Ge $2p_{1/2}$ binding energy in $GeCl_4$ is 4.94 eV larger than the Mg $K\alpha_{1,2}$ radiation energy. In the $L_2M_{4,5}M_{4,5}$ region of the Magnesium excited spectrum there is a weak structure shifted by 0.18 eV to higher kinetic

energy with respect to the normal $^1G_4$ line in the $L_2M_{4,5}M_{4,5}$ spectrum excited by Aluminum radiation, and a weak satellite peak shifted by 6.11 eV to higher kinetic energy again with respect to the normal $^1G_4$ transition. The combined intensity of PCI and satellite relative to the intensity of the $L_3M_{4,5}M_{4,5}$ group is only 22% of the $L_2M_{4,5}M_{4,5}/L_3M_{4,5}M_{4,5}$ intensity ratio in the Aluminum excited spectrum.

In GeF_4 the Ge $2p_{1/2}$ binding energy is 6.37 eV larger than the Mg $K\alpha_{1,2}$ radiation energy. The $L_2M_{4,5}M_{4,5}$ region of the $L_{2,3}M_{4,5}M_{4,5}$ spectrum shows a peak shifted by 0.22 eV and a satellite shifted by 8.81 eV to higher kinetic energy both with respect to the normal $^1G_4(L_2M_{4,5}M_{4,5})$ diagram line. The combined intensity of the two structures relative to the $L_3M_{4,5}M_{4,5}$ group is only 18% of the $L_2M_{4,5}M_{4,5}/L_3M_{4,5}M_{4,5}$ intensity ratio in the spectrum excited with Al $K\alpha_{1,2}$ radiation.

In Figures V-11 and V-12 the $L_{2,3}M_{2,3}M_{4,5}$ spectra of $GeCl_4$ and GeF_4 respectively are shown. In the region of the $L_{2,3}M_{2,3}M_{4,5}$ spectrum of $GeCl_4$ there was also a strong Cl 2p photoelectron line (the deleted portion of the data in the figure) with the corresponding satellite due to the Mg $K\alpha_{3,4}$ radiation. In the $L_{2,3}M_{2,3}M_{4,5}$ spectrum of GeF_4 there is some structure near 1053 eV which increased

during the measurement, suggesting that it was due to the Ge $3p_{1/2}$ and Ge $3p_{3/2}$ photoelectron lines excited by Ge $L\alpha$ radiation arising from anode contamination. These lines appear to be quite strong in comparison to the $L_2M_{2,3}M_{4,5}$ Auger group. The shift of the $L_2M_{2,3}M_{4,5}$ groups relative to the $L_2M_{2,3}M_{4,5}$ spectra excited by Aluminum radiation is 3.84 eV for $GeCl_4$ and 6.21 eV for GeF_4, both to higher kinetic energy. For both compounds the $L_2M_{2,3}M_{4,5}/L_3M_{2,3}M_{4,5}$ intensity ratios, in contrast to the other systems, are much smaller in the Mg $K\alpha_{1,2}$ than in the Al $K\alpha_{1,2}$ excited spectra.

In Tables V-1 and V-2 are listed results for all compounds. In Table V-1 the Ge $2p_{1/2}$ binding energies relative to Mg $K\alpha_{1,2}$ radiation are given along with the PCI shifts and the satellite shifts. In Table V-2 the PCI/$L_3M_{4,5}M_{4,5}$ intensity ratios are given, excluding the intensities of the satellites. As shown in this table, the peaks in the $GeCl_4$ and GeF_4 $L_{2,3}M_{4,5}M_{4,5}$ spectra, which are shifted only by 0.18 eV and 0.22 eV respectively from the diagram $^1G_4$ ($L_2M_{4,5}M_{4,5}$) Auger line (Table V-1), have only 4% and 3% of the intensity of the unshifted $L_3M_{4,5}M_{4,5}$ diagram line. If it is considered that in a diagram Auger transition the $L_2M_{4,5}M_{4,5}/L_3M_{4,5}M_{4,5}$ intensity ratio is approximately 1:2, as has been observed

Table V-1. Ge $2p_{1/2}$ Binding Energies Relative to Mg $K\alpha_{1,2}$ Radiation, PCI shifts, and Satellite Shifts for Germanium Compounds

Compound	(Mg $K\alpha_{1,2}$-Ge $2p_{1/2}$) (eV)	PCI[a]-$^1G_4$[b]($L_2M_{4,5}M_{4,5}$) (eV)	Satellite-$^1F^1P$[b]($L_2M_{2,3}M_{4,5}$) (eV)	Satellite-$^1G_4$($L_2M_{4,5}M_{4,5}$) (eV)
GeO_2(s)	2.43	0.37	0.97	-
$Ge(C_2H_5)_4$(g)	-0.51	2.18	4.29	5.97
$Ge(CH_3)_4$(g)	-0.86	1.93	4.62	6.23
GeH_4(g)	-2.78	1.55	5.74	8.34
$GeCl_4$(g)	-4.94	0.18	3.84	6.11
GeF_4(g)	-6.37	0.22	6.21	8.81

a. These values have been obtained from the spectra excited with Mg $K\alpha_{1,2}$ radiation.

b. These values have been obtained from the spectra excited with Al $K\alpha_{1,2}$ radiation.

Table V-2. $PCI/L_3M_{4,5}M_{4,5}$ Intensity Ratio for Germanium Compounds

Compound	$PCI/L_3M_{4,5}M_{4,5}$
GeO_2 (s)	0.20
$Ge(C_2H_5)_4$(g)	0.18
$Ge(CH_3)_4$(g)	0.17
GeH_4(g)	0.13
$GeCl_4$(g)	0.04
GeF_4(g)	0.03

for the Aluminum excited spectra, it follows that the intensities of these small peaks are about 8% of the normal $L_2M_{4,5}M_{4,5}$ Auger group. Therefore, it seems reasonable to attribute these peaks to the Mg $K\alpha_{3,4}$ high energy satellite in the unfiltered X-radiation, which lies about 10 eV above the Mg $K\alpha_{1,2}$ line, and possesses an intensity of approximately 8% of the principal Mg $K\alpha_{1,2}$ radiation. The weak peaks are also slightly shifted because of the proximity of the radiation energy (approximately 1263.6 eV) to the threshold of the Ge $2p_{1/2}$ binding energies.

In Figures V-13 and V-14 plots of ξ and δ as defined by equation V-4 using Γ = 0.95 eV[85] are shown for the $M_{4,5}M_{4,5}$ and $M_{2,3}M_{4,5}$ final states. The PCI shift of the diagram Auger ($M_{4,5}M_{4,5}$) final state (Figure V-13) shows a behavior similar to that reported by Brown et al.[83] for Xe $L_3M_4M_5(^1G_4)$. The PCI shift passes through a maximum value near the threshold, and the shift decreases when the excess energy has larger positive or negative value. The two points relative to $GeCl_4$ and GeF_4, for the reasons given above, represent a different situation in that the slightly shifted $L_2M_{4,5}M_{4,5}$ transitions are those apparently excited by the Mg $K\alpha_{3,4}$ satellite. However a small contribution from some PCI shifted diagram Auger

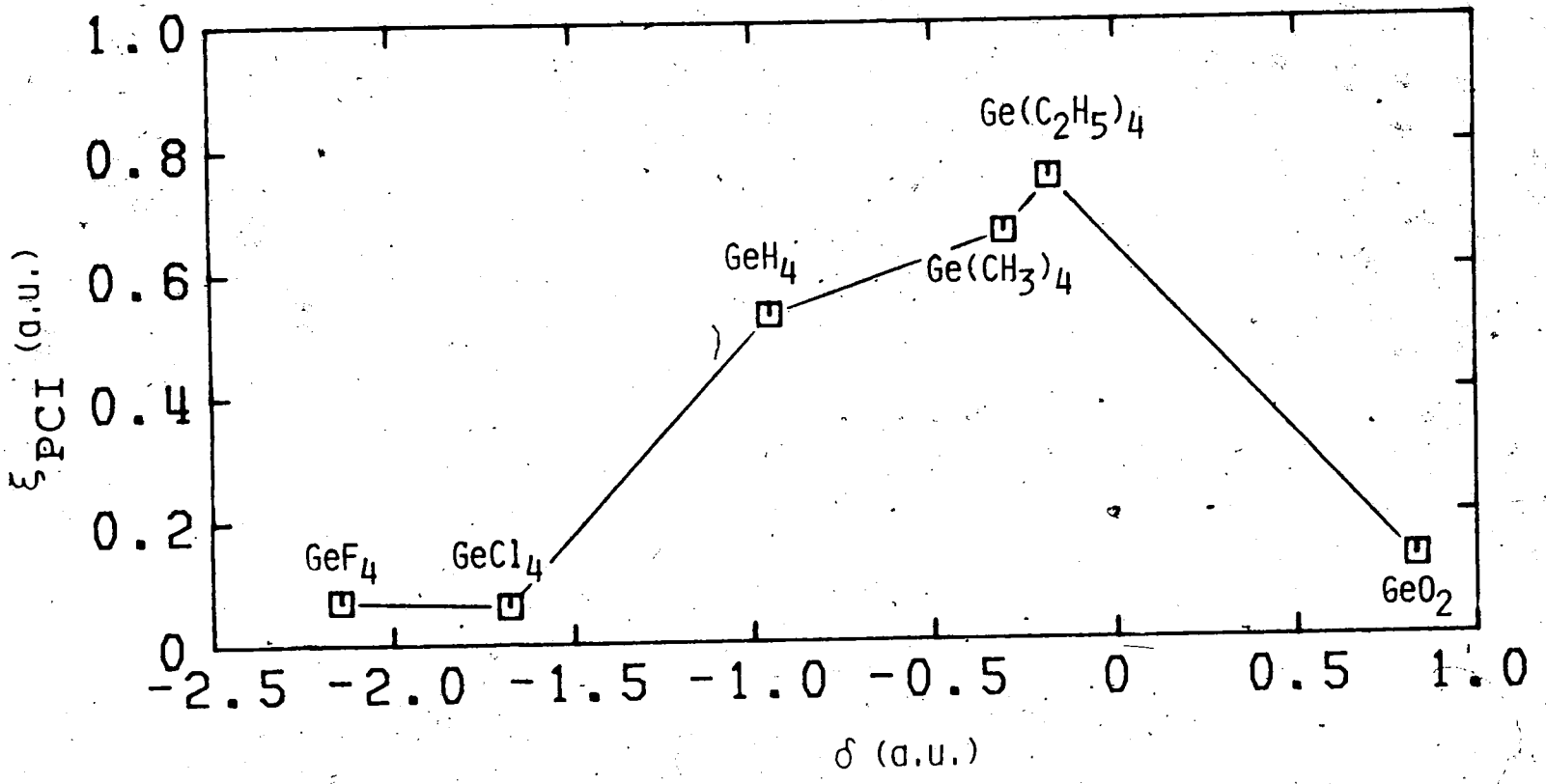

Figure V-13. Reduced Germanium $L_2M_{4,5}M_{4,5}$ Auger shifts, ξ_{PCI}, versus reduced excess energy, δ.

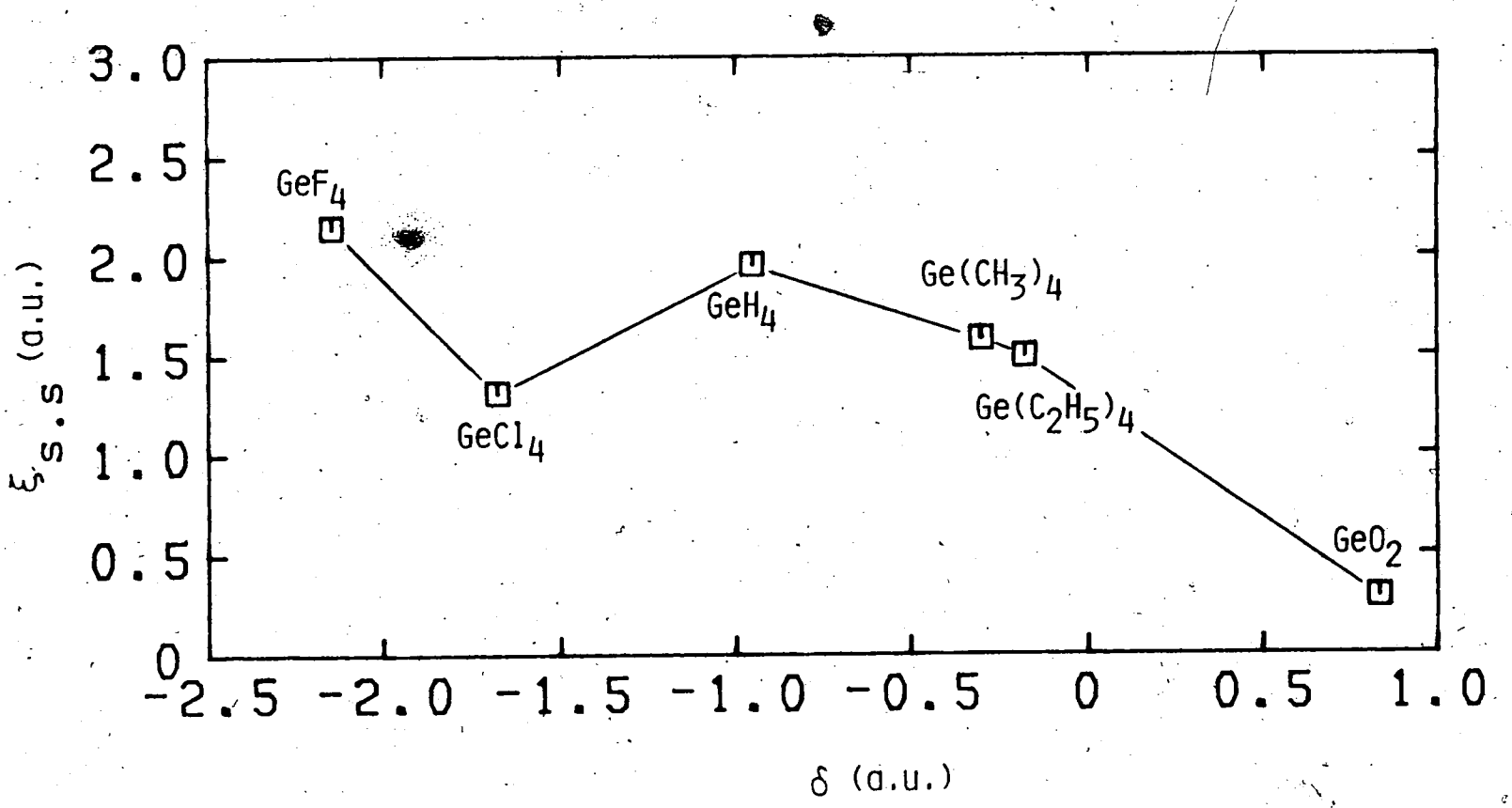

Figure V-14. Reduced Germanium $L_2M_{2,3}M_{4,5}$ Auger spectator satellite shifts, $\xi_{s.s.}$, versus reduced excess energy, δ.

transitions can not be excluded. A different behavior is observed for the $L_2M_{2,3}M_{4,5}$ shifts. From Figure V-14 it appears that the shift increases when the excess energy becomes more negative, with exception of $GeCl_4$ for which a decrease in the shift is observed. From both sets of experimental data, $L_2M_{4,5}M_{4,5}$ and $L_2M_{2,3}M_{4,5}$ spectra, ξ values larger than those predicted by equation V-3 are obtained. Only GeO_2 has a PCI Shift (ξ = 0.28 au) of the diagram Auger transition to the final state $M_{4,5}M_{4,5}$ which agrees reasonably with the value of ξ = 0.32 au given by the theory. Figure V-15 shows the plot of the spectator satellite peak corresponding to the $M_{4,5}M_{4,5}$ final state relative to the unshifted $^1G_4$ ($L_2M_{4,5}M_{4,5}$) Auger line versus the excess energy. It does not show the linear dispersion that was observed by Brown et al.[83] The behavior of the shift is very similar to the shift observed for the Auger transition to the $M_{2,3}M_{4,5}$ final state suggesting, then, that in both cases the processes may be quite similar.

The appearance of PCI effects and of the spectator Auger satellites in $Ge(CH_3)_4$, $Ge(C_2H_5)_4$ and GeH_4 can be explained as follows. The energy of the incident radiation ($h\nu$ = 1253.64 eV) is less than the threshold value of the L_2 binding energy therefore it is reasonable

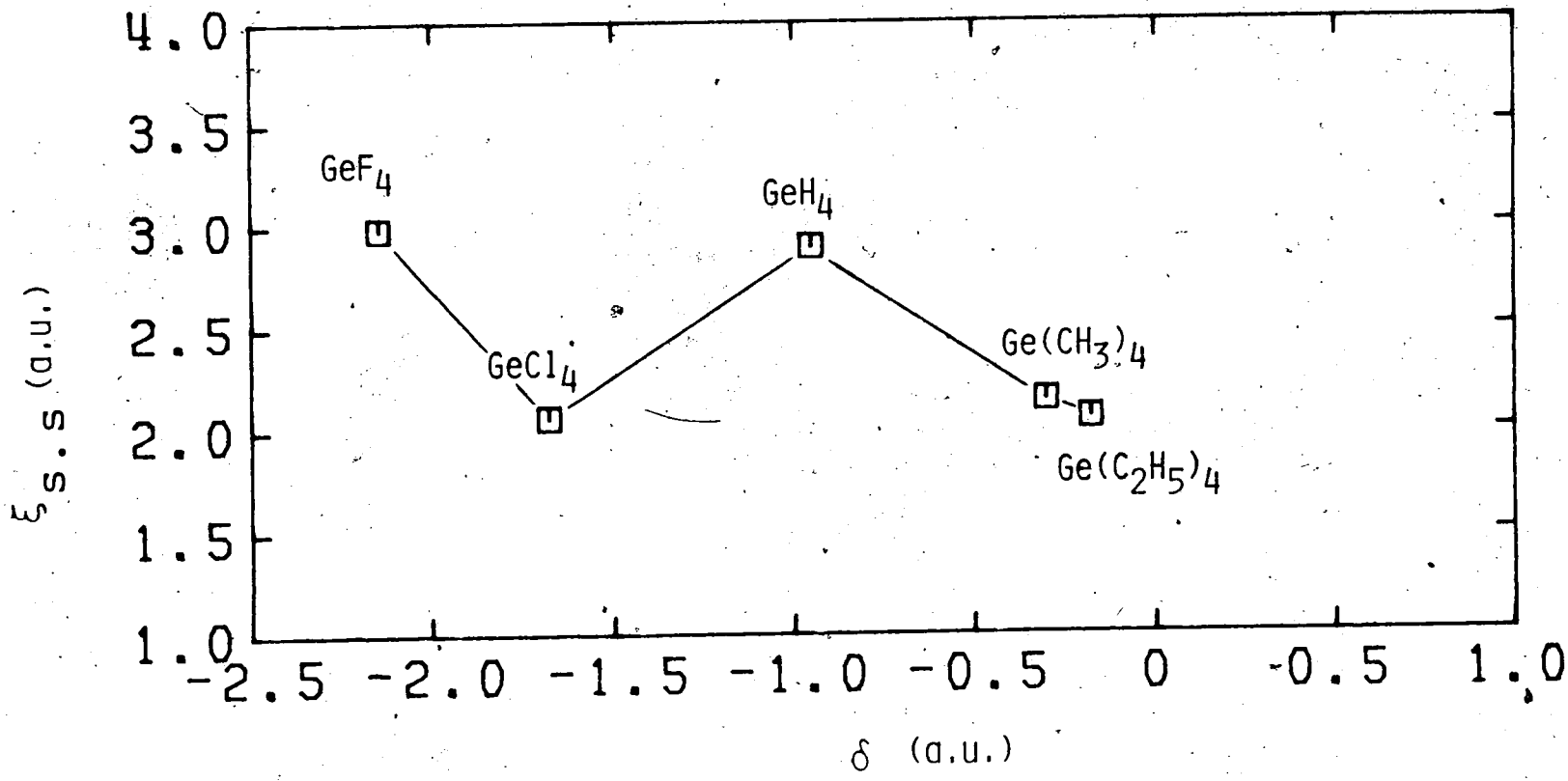

Figure V-15. Reduced Germanium $L_2M_{4,5}M_{4,5}$ Auger spectator satellite shifts, $\xi_{s.s.}$, versus reduced excess energy, δ.

to presume that the L_2 electron has been excited to a Rydberg or antibonding molecular orbital, which is an unoccupied bound level. This excited state decays through a radiationless process following, say, two channels of comparable probability. Both channels consist of an Auger process. It is possible that when an electron from a $M_{4,5}$ level fills the hole in the L_2 level with emission of an Auger electron, the change in the nuclear potential felt by the Rydberg electron (the nuclear charge becomes more screened by the additional L_2 electron) causes this excited and loosely bound electron to move slowly out of the molecule (the process can be considered analogous to a relaxation process). The Auger electron, therefore, interacts with the slow electron gaining kinetic energy with an asymmetric probability distribution which is typical of PCI effect. The feature present at higher kinetic energy, and which resembles a normal Auger transition, is the so-called spectator-Auger satellite wherein the atomic core vacancy becomes filled through an Auger transition, and the excited electron is undisturbed in its excited level. In effect, an excited neutral species is undergoing an Auger transition with a characteristic energy which is different from that of the normal ionic precursor state to the Auger process. The

two decay modes are illustrated in Figure V-16. When the energy of the incident photons, hν, is very much below the L_2 threshold, as in the case of GeF_4 and $GeCl_4$, the excited state reached by the L_2 electron will be of lower energy. This state is a more stable state with a longer lifetime. It is then possible that the excited state will not be affected by the fast change in potential produced by the Auger process, and that, as a consequence, the probability for the PCI interaction becomes very small, so only the spectator Auger satellite is observed.

When the final state of the Auger process changes from $M_{4,5}M_{4,5}$ to $M_{2,3}M_{4,5}$, a different relaxation may be felt by the Rydberg electron. The process giving rise to a PCI effect, shown in Figure V-16 for the $M_{4,5}M_{4,5}$ final state, may not occur for the $M_{2,3}M_{4,5}$ final state and only the satellite structure due to the Auger process in presence of a spectator electron in an excited state is observed. The process in the two different final states is illustrated in Figure V-17. It seems possible that the relative probability of the PCI and spectator satellite processes depends on the lifetime of the excited state and on the incident energy which selects the excited state.

The results in Figures V-14 and V-15 can be explained by screening effects. Increasing negatively the excess

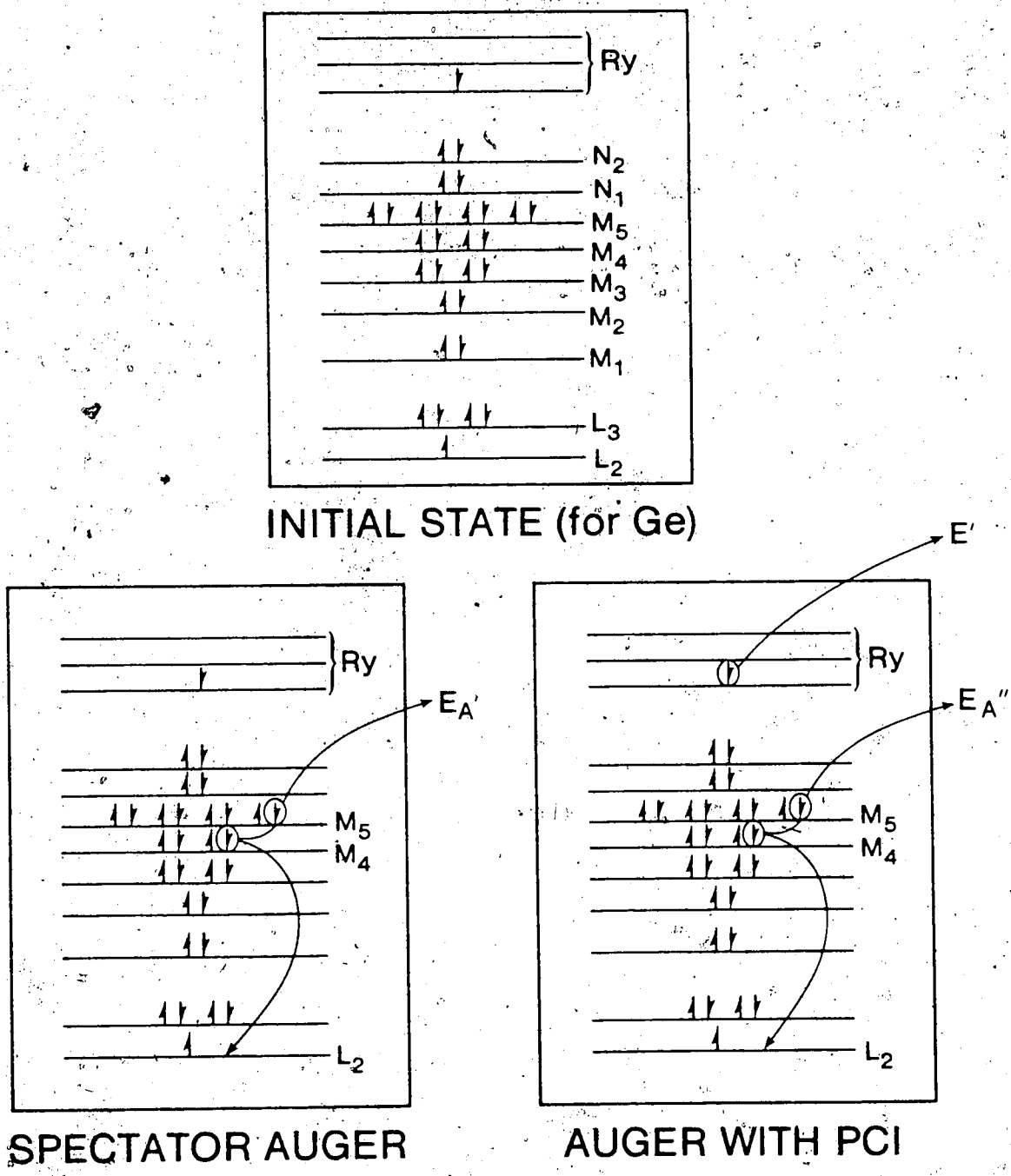

Figure V-16. Spectator Auger satellite and Post Collision Interaction (PCI) processes associated with the final state $M_{4,5}\ M_{4,5}$.

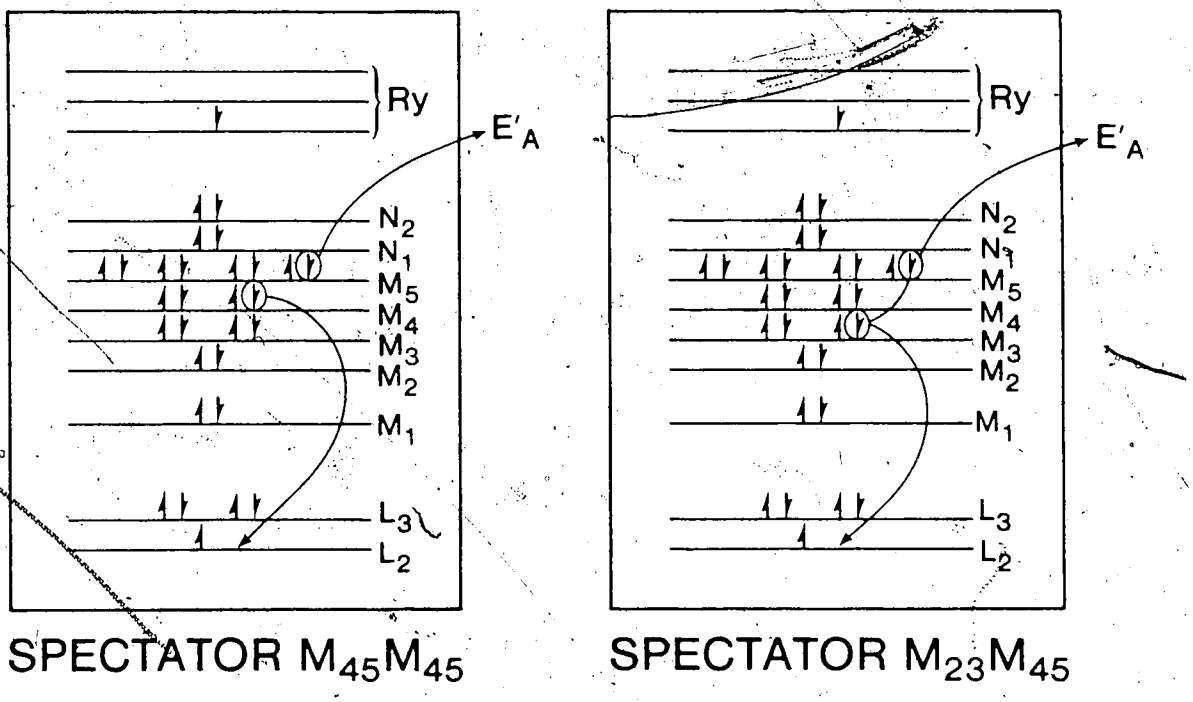

Figure V-17. Spectator Auger satellite process associated with final states $M_{4,5}\,M_{4,5}$ and $M_{2,3}\,M_{4,5}$.

energy, that is, increasing chemically the binding energy of Ge $2p_{1/2}$, the L_2 electron is actually excited to a lower unoccupied Rydberg level, Ry, (Figure V-17). As a consequence, the spectator electron will more effectively "screen" the Auger electron yielding a greater increase in the kinetic energy of the outgoing Auger electron. The peculiar behavior of $GeCl_4$ in both cases, $M_{2,3}M_{4,5}$ and $M_{4,5}M_{4,5}$ spectator satellites, could be attributed to its large relaxation energy (Chapter IV) which strongly determines the kinetic energy of the Auger electron. It is possible that the effect of the spectator electron on the kinetic energy of the Auger electron is small compared to the relaxation process and so the extent of the shift is decreased. A complication for this argument is that $Ge(C_2H_5)_4$ also has a large relaxation energy and should behave similarly to $GeCl_4$. However in this case, because of the small excess energy, the L_2 electron will be excited to a higher unoccupied level producing less screening and consequently smaller shift.

E. Conclusions

In agreement with what observed by Brown et al.[83] this work has shown that, as the incident photon energy varies through the threshold region, the $^1G_4$ diagram line

of the $M_{4,5}M_{4,5}$ final state is shifted to higher energy, and it assumes an asymmetric shape indicative of a PCI effect. Above this shifted diagram line a spectator satellite appears, which persists even after the intensity of the diagram line has vanished, which occurs about 5 eV below the threshold as illustrated by the behavior of $GeCl_4$ and GeF_4. Previously unobserved is the evidence shown here of the different behavior exhibited for the $M_{2,3}M_{4,5}$ and $M_{4,5}M_{4,5}$ final states. In the case of the $M_{2,3}M_{4,5}$ final state it seems that only the Auger spectator satellite effect occurs as is suggested from a comparison of the shifts obtained for the $L_2M_{2,3}M_{4,5}$ Auger spectra and the spectator satellites in the $L_2M_{4,5}M_{4,5}$ Auger spectra. In both cases the excess of energy is quite large and greater than the natural line width of the inner shell $2p_{1/2}$ (Γ = 0.95 eV) level. Therefore the conditions necessary for the observation of the Raman linear dispersion,[83] which requires that the change in photon energy is of the order of Γ, are not fulfilled. When the excess of energy ε is changed by more than Γ, the electron in the L_2 level may be excited to different unoccupied levels lying close to each other, yielding different spectator satellite shifts (see Table V-1). Also, because different molecules are being studied, the

unoccupied levels reached by each of the transitions are different. The screening effect of the excited electron is different and dependent on the excited orbital in which it has been placed. The concept of "screening" can also be used to explain the different shifts obtained for the $M_{2,3}M_{4,5}$ and for the $M_{4,5}M_{4,5}$ spectator satellites.

An interesting question which arises from the above results is why the Auger transition to the $M_{2,3}M_{4,5}$ final state does not show any PCI effect as compared to the $M_{4,5}M_{4,5}$ Auger transition. This observation contradicts the generally accepted belief that the PCI effects are determined only by the slow electron (photoelectron in this case) and are not influenced by the fast electron which means that only the initial state is important in such effects.

It would be interesting to compare these results obtained by "chemical tuning" of the threshold energy, with results obtained by changing smoothly the ionization energy across a fixed threshold energy, using for example, synchrotron radiation. With this technique the relaxation effects would not vary through the experiment because the same molecule would be probed with different excitation energies.

CHAPTER VI

TIN $M_{4,5}N_{4,5}N_{4,5}$ AUGER SPECTRA OF $Sn(CH_3)_4$ AND $[Sn(CH_3)_3]_2$

A. Introduction

The MNN spectra of Tin compounds have many similarities with the LMM spectra discussed above for Germanium compounds. The $M_{4,5}N_{2,3}N_{2,3}$ peaks are extremely broad because of the $N_{2,3}N_{4,5}N_{4,5}$ "super-Coster-Kronig" Auger transitions in which the initial state hole and both final state holes are in the same shell.[7] These transitions cause $N_{2,3}$ lifetime broadening of up to 20 eV.[86] Except for the $M_{4,5}N_{4,5}N_{4,5}$ transitions all the other MNN spectra are quite weak and broad, so only the $M_{4,5}N_{4,5}N_{4,5}$ Auger transitions which have sharp peaks will be analyzed in this work.

The $M_{4,5}N_{4,5}N_{4,5}$ spectra are more complicated than the $L_{2,3}M_{4,5}M_{4,5}$ spectra because the M_4-M_5 separation is smaller than the L_2-L_3 separation so the M_4 and M_5 groups partly overlap. Also in contrast to the $L_{2,3}M_{4,5}M_{4,5}$ spectra, which showed the same appearance for the two

groups L_2- and L_3-, here the corresponding M_4- and M_5-$N_{4,5}N_{4,5}$ spectra, even if the final states for the transitions are the same, have different shapes because the matrix elements for the transitions from different initial states to the same final states are different.

The Sn $M_{4,5}N_{4,5}N_{4,5}$ inner shell Auger spectra of $Sn(CH_3)_4$ and $[Sn(CH_3)_3]_2$ were obtained and analyzed with comparison to the spectrum of Tin metal reported by Pessa et al.[87] With the same approximations used for Germanium compounds, the relative energies and intensities were calculated and compared to the experimental data. The energy calculations were based on both Russell-Saunders (LS) and intermediate coupling (IC) of final hole states. The intensity calculations were based on a mixed coupling scheme. Relaxation contributions were deduced from a comparison of Auger and core level measurements.

B. Experimental

Tin compounds, $Sn(CH_3)_4$ and $[Sn(CH_3)_3]_2$, were obtained from ALFA Products and used without further purification. The Auger spectra of the vapors were excited by incident electrons with energy of 2.5 KeV produced by an electron gun. The spectra were calibrated with reference to the Argon $L_3M_{2,3}M_{2,3}(^1D_2)$ Auger line

203.49(05) eV kinetic energy)[25] and Neon $KL_{2,3}L_{2,3}(^1D_2)$ Auger line (804.557(17) eV kinetic energy).[24] The Sn 3d and 4d photoelectron lines were excited by Al $K\alpha_{1,2}$ radiation (1486.6 eV).[21] The 3d lines were calibrated with respect to Ne $KL_{2,3}L_{2,3}(^1D_2)$ Auger line and Ne 1s photoelectron line (870.312(17) eV binding energy).[24] The Tin 4d lines were calibrated with respect to the Ne 2s (48.42(5) eV binding energy)[8] and the Ne 2p (21.59 eV binding energy)[8] photoelectron lines.

C. Theory

The kinetic energy of the $M_{4,5}N_{4,5}N_{4,5}$ Auger electrons is given by an expression[50] similar to equation IV-1.

$$E(M_{4,5}N_{4,5}N_{4,5}; X) = E(M_{4,5}) - E(N_{4,5}) - E(N_{4,5}) - F(N_{4,5}N_{4,5}; X) + R_S^T(N_{4,5}N_{4,5}) \quad \text{VI-1}$$

where $E(M_{4,5})$, $E(N_{4,5})$ are the core level binding energies directly measurable by XPS. $F(N_{4,5}N_{4,5}; X)$ describes the interaction energy betwen the two $N_{4,5}$ holes in the final state X. $R_S^T(N_{4,5}N_{4,5})$ is the total static relaxation energy. $F(N_{4,5}N_{4,5}; X)$ can be calculated using standard

multiplet coupling theory.[52] Because the final state $N_{4,5}N_{4,5}$ has an electronic configuration d^{-2}, the same as for a $M_{4,5}M_{4,5}$ final state, the number of terms arising in pure LS coupling are again five; ^1S, ^1G, ^3P, ^1D, and ^3F. The general expressions for the energy of each term[52] are the ones already given in IV-5. In intermediate coupling (IC) the five levels split into nine states. Guided by successful results on Xenon[88] and Cadmium[73], which are close to Tin in the periodic table, the mixed coupling scheme[55,56] applying jj coupling for the initial state, and intermediate coupling for the final state, was used to calculate the relative intensities of the line components. In the calculations of the energies of the final state levels in intermediate coupling, the expressions in equation IV-5 were used together with the spin-orbit matrix element from Condon and Shortley.[16] Numerical values of the spin-orbit parameters were taken from the theoretical calculations of Huang et al.[57] Solutions of the corresponding secular equations yielded the interaction energy $F(N_{4,5}N_{4,5}; X)$ of the various levels in intermediate coupling and also, corresponding to each of those energy values, the mixing coefficients. These coefficients were used to obtain the intensities for the transitions to the different levels in intermediate

coupling, in terms of the umperturbed Russell-Saunders amplitudes[89] ((amplitude)^2 = intensity). The relaxation term $R_S^T(N_{4,5}N_{4,5})$ was calculated in the same way as for the Germanium spectra. It was divided into atomic $R_S^a(N_{4,5}N_{4,5})$ and extraatomic $R_S^{ea}(N_{4,5}N_{4,5})$ contributions[39]

$$R_S^T(N_{4,5}N_{4,5}) = R_S^a(N_{4,5}N_{4,5}) + R_S^{ea}(N_{4,5}N_{4,5}) \quad \text{VI-2}$$

The atomic term was set equal to twice the dynamic relaxation which accompanies photoemission[58,59] and which can be obtained from the optimized Hartree-Fock-Slater results of Rosen and Lindgren.[60] Because calculations were not available for Tin, the results for Iodine[60] were used which gave $R_S^a(N_{4,5}N_{4,5})_I$ = 9.24 eV. The corresponding quantity for Tin was estimated by subtracting from $R_S^a(N_{4,5}N_{4,5})_I$ the contribution to the atomic relaxation arising from the three extra 5p electrons for Iodine. This correction was estimated in the way described in Chapter IV for Germanium, using the equivalent cores approximation[30,31,58] and Mann's tables.[53] From the appropriate terms for Iodine, the corresponding terms for the equivalent core atom Te were subtracted

$$\Delta R_{5p} = [F^0(4d5p) - \tfrac{1}{15}G^1(4d5p) - \tfrac{3}{70}G^3(4d5p)]_I - [F^0(4d5p) - \tfrac{1}{15}G^1(4d5p) - \tfrac{3}{70}G^3(4d5p)]_{Te} \quad \text{VI-3}$$

Because of the non-linearity of the Slater's integrals F^0 and G^k with the atomic number, equation VI-3 gave three different values for the relaxation contribution of the 5p electrons when calculated for Te, Sb and Sn; ($\Delta R_{5p}(Te)$ = 0.82 eV, $\Delta R_{5p}(Sb)$ = 0.93 eV, $\Delta R_{5p}(Sn)$ = 1.02 eV). The average of the three was taken, multiplied by 3 and subtracted from the above value for $R_S^a(N_{4,5}N_{4,5})_I$ giving $R_S^a(N_{4,5}N_{4,5})_{Sn}$ = 6.47 eV. Using equation IV-9 with the appropriate factors $f(\ell\ell')$ and $g_k(\ell\ell')$[39] and the appropriate Slater's integrals,[53] an outer shell contribution of 3.9 eV and an intrashell contribution of 3.6 eV to the atomic relaxation were obtained. Differently from Germanium, the intrashell electrons 4d and the outer shell electrons 5s and 5p produced almost the same relaxation contribution.

Following the same approach used for Germanium in Chapter IV, the extraatomic relaxation was given by the two-electron interaction between a 5p and a 4d electron expressed as a combination of Slater's integrals[52]

$$R_S^{ea}(N_{4,5}N_{4,5}) = F^0(4d5p) - \frac{1}{15}G^1(4d5p) - \frac{3}{70}G^3(4d5p) \qquad \text{VI-4}$$

The use of Slater's integrals, given in Mann's tables,[53] yielded $R_S^{ea}(N_{4,5}N_{4,5}) = 9.57$ eV. Combining the two contributions $R_S^{a}(N_{4,5}N_{4,5})$ and $R_S^{ea}(N_{4,5}N_{4,5})$, the calculated total static relaxation for Tin is

$$R_S^{T}(N_{4,5}N_{4,5}) = 16.04 \text{ eV}$$

The intensities of various $M_{4,5}N_{4,5}N_{4,5}$ lines were calculated in the mixed coupling scheme with jj coupling for the initial state and with both LS coupling and intermediate coupling for the final state. The transition rates for LS coupling in the final state were obtained directly from the expression given by El Ibyari et al.[89] using the direct and exchange matrix element calculated by McGuire.[64] The transition rates for intermediate coupling in the final state were calculated following the procedure outlined by Hagmann et al.[88] using the mixing coefficients obtained from the energy matrices and the amplitudes in LS coupling.

D. Results and Discussion

The binding energies of 3d and 4d photoelectrons and the kinetic energies of the $M_{4,5}N_{4,5}N_{4,5}$ ($^1G_4$, $^1D_2$) Auger lines are given in Table VI-1 along with the corresponding values for Tin metal.[87] Spin-orbit splittings are the same for each system within the experimental error. The spin-orbit splitting Δ_{3d} obtained from the measured Auger $M_5N_{4,5}N_{4,5}$ ($^1G_4$, $^1D_2$) and $M_4N_{4,5}N_{4,5}$ ($^1G_4$, $^1D_2$) lines (Δ_{3d} = 8.52 eV) is slightly larger than that obtained directly from the photoelectron measurements (Δ_{3d} = 8.39 eV). The disagreement could be due to the lack of resolution of the $^1D_2$ and $^1G_4$ lines and concomitant fitting errors. For the spin-orbit splitting Δ_{4d} a value of 1.18 eV was obtained. Both splittings Δ_{3d} and Δ_{4d} agree with the compilation by Sevier.[54] Experimental and calculated spectra of $Sn(CH_3)_4$ and $[Sn(CH_3)_3]_2$ are shown in Figures VI-1 and VI-2 respectively. The calculated spectra were obtained by a curve simulation programme[75] using widths as derived from the deconvolution of the experimental data and positions and areas as required by the calculated mixed coupling intensity results. Each Auger group in the experimental spectra was decomposed into six component lines by means of the least squares programme[26] employing a Lorentzian line shape with a constant tail. As for the

Table VI-1. Absolute Tin 3d and 4d Binding Energies (E_B) and Tin $M_{4,5}N_{4,5}N_{4,5}(^1G_4, {}^1D_2)$ Auger Energies of Tin Compounds

		$Sn(CH_3)_4$ (eV)	$[Sn(CH_3)_3]_2$ (eV)	Sn(Metal)[a] (eV)
E_B	$3d_{3/2}$	500.01(05)[b]	499.64(05)	493.32(15)
	$3d_{5/2}$	491.59(05)	491.27(05)	484.87(15)
		491.55[c]	491.2[c]	-
	$4d_{3/2}$	31.74(05)	31.49(05)	24.76(10)
	$4d_{5/2}$	30.61(05)	30.25(05)	23.68(10)
Auger	$M_5N_{4,5}N_{4,5}(^1G_4, {}^1D_2)$	415.88(05)	416.88(05)	428.85(15)
	$M_4N_{4,5}N_{4,5}(^1G_4, {}^1D_2)$	424.39(05)	425.42(05)	437.27(15)

a. Relative to the Fermi Level. Ref. 87.

b. 0.05 is the maximum deviations from the average values for three different measurements.

c. Ref. 101.

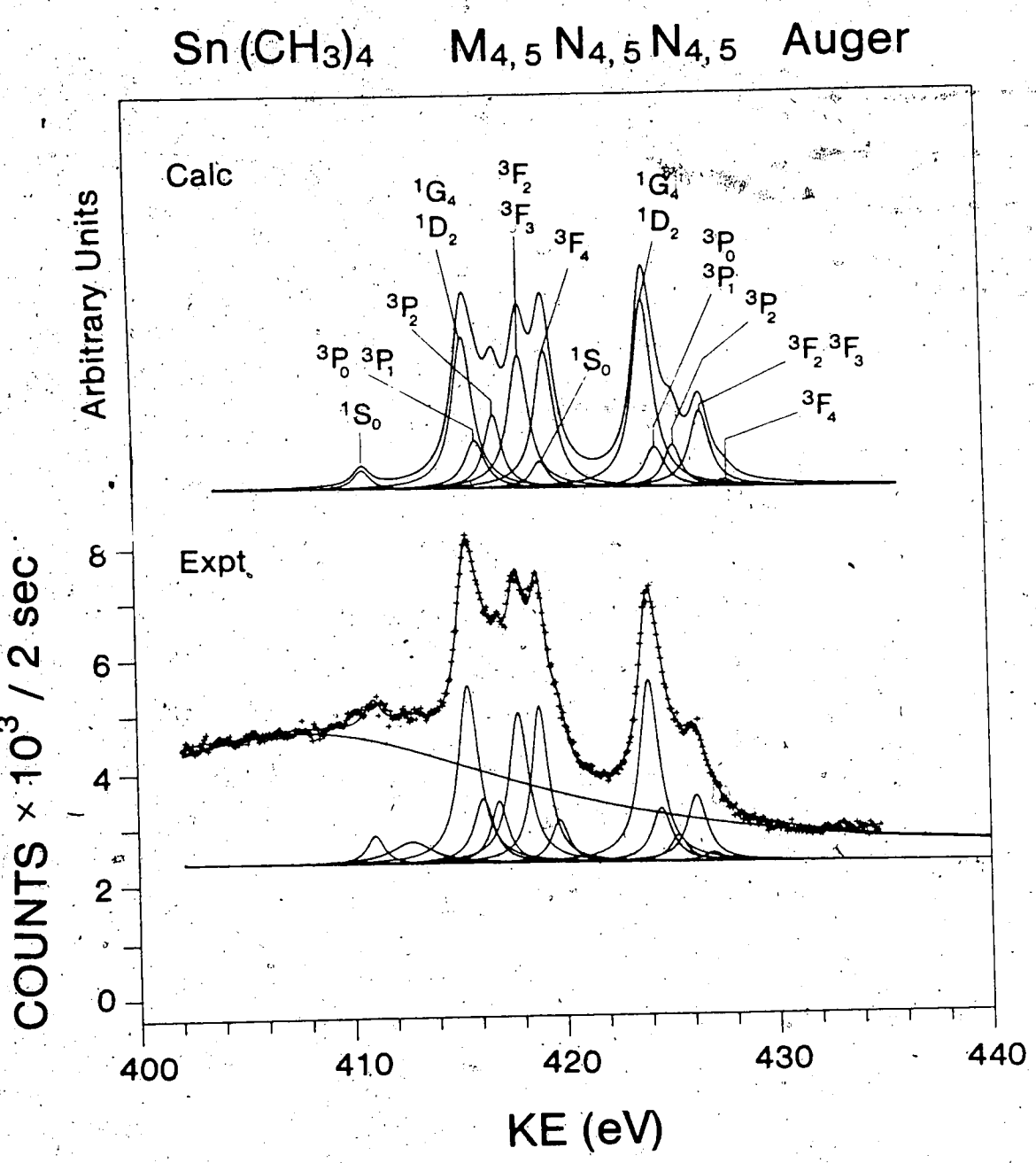

Figure VI-1. Experimental and calculated (IC) $M_{4,5}N_{4,5}N_{4,5}$ Auger spectra of $Sn(CH_3)_4$ vapor. The experimental spectrum was excited with 2.5 keV electrons at a sample pressure of 1μ. The $M_5(^1G_4)$ peak of the calculated spectrum has been arbitrarily aligned with the experimental energy.

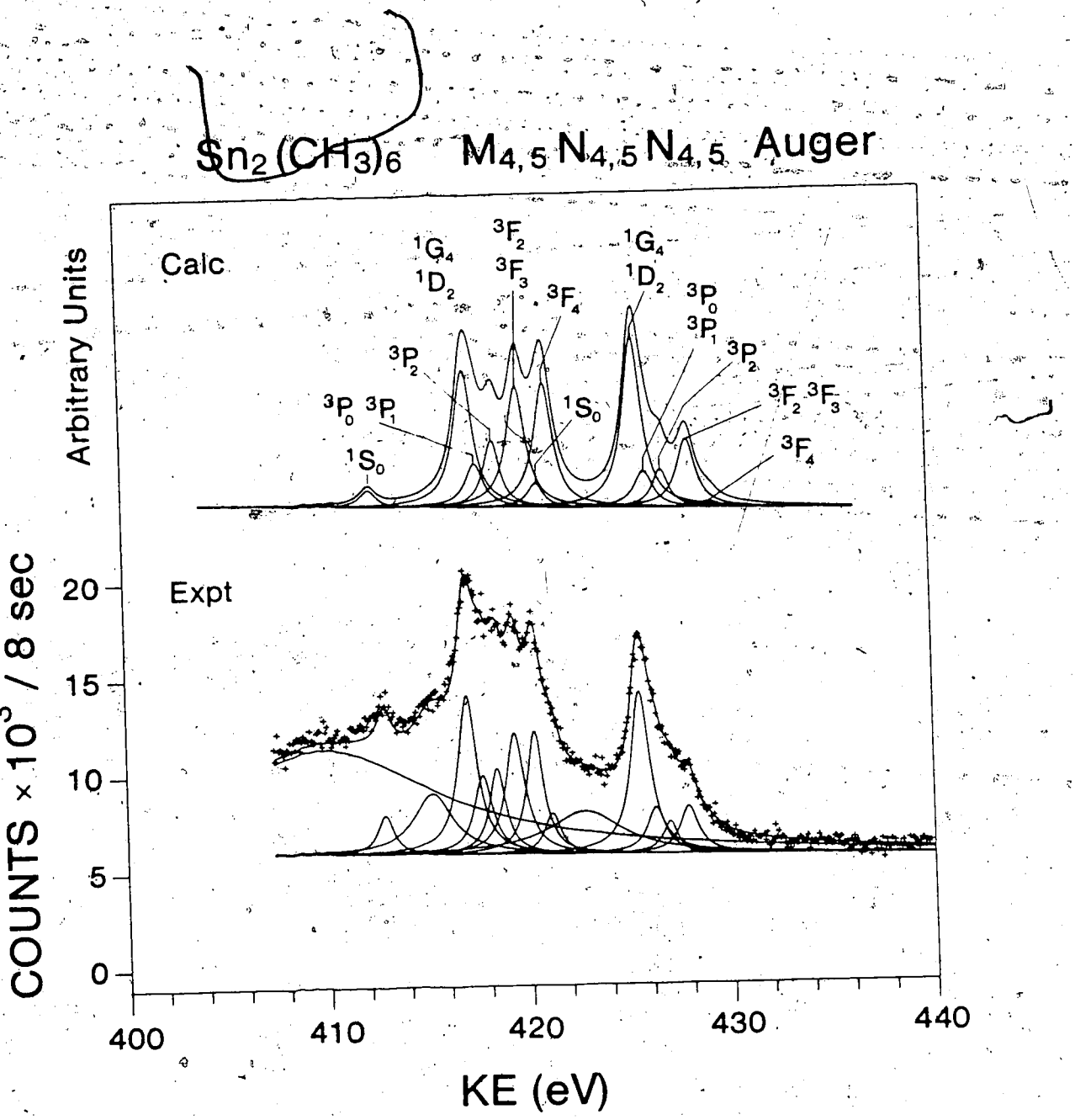

Figure VI-2. Experimental and calculated (IC) $M_{4,5}N_{4,5}N_{4,5}$ Auger spectra of $[Sn(CH_3)_3]_2$ vapor. The experimental spectrum was excited with 2.5 keV electrons at a sample pressure of 1μ. The $M_5(^1G_4)$ peak of the calculated spectrum has been arbitrarily aligned with the experimental energy.

Germanium compounds the Gaussian lineshape gave a poorer fit of the data. A FWHM value of 0.96 eV was used for the single peaks and a slightly larger value of 1.12 eV, obtained for the $M_5N_{4,5}N_{4,5}$ ($^1G_4$, $^1D_2$) line in the $Sn(CH_3)_4$ spectrum, was used for all the other unresolved double peaks. For the experimental spectrum of $Sn(CH_3)_4$ (Figure VI-1) the two broad peaks centered at 408.17 eV (FWHM = 25 eV) and 413.16 eV (FWHM = 2.4 eV), which are necessary to give a good fit, can be associated with indetermined shake-off which becomes part of the background. For the same reason it has been necessary to include three broad peaks in the spectrum of $[Sn(CH_3)_3]_2$ shown in Figure VI-2. In this case they are centered at 409.79 eV (FWHM = 13.5 eV), 415.14 eV (FWHM = 2.4 eV)and 422.66 eV. (FWHM = 4.4 eV). Similar features were also observed in some KLL Auger spectra.[90] The arbitrary location of these extra peaks could affect the ratios of the diagram lines. They also could account for the observation that the $I(M_5N_{4,5}N_{4,5})/I(M_4N_{4,5}N_{4,5})$ intensity ratios of 1.64 and 1.77 for $Sn(CH_3)_4$ and $[Sn(CH_3)_3]_2$ respectively are both greater than the statistical value of 1.5. The relative kinetic energies of the Auger lines are given in Table VI-2. These data show a good overall agreement between the relative energies of the Auger

Table VI-2. Experimental Relative Kinetic Energies of the Tin $M_{4,5}N_{4,5}N_{4,5}$ Auger Lines for Tin Compounds

Transition	Final State Terms	$Sn(CH_3)_4$ (eV)	$[Sn(CH_3)_3]_2$ (eV)	Sn(Metal)[a] (eV)
$M_4N_{4,5}N_{4,5}$	$^1S_0$	-4.25	-4.38	-4.08
	$^1G_4$, $^1D_2$	0.00	0.00	0.00
	$^3P_0$, $^3P_1$	0.53	0.74	0.41
	$^3P_2$	1.32	1.46	1.31
	$^3F_2$, $^3F_3$	2.19	2.35	2.34
	$^3F_4$	2.98	3.42	2.84
$M_5N_{4,5}N_{4,5}$	$^1S_0$	-4.46	-4.15	-4.48
	$^1G_4$, $^1D_2$	0.00	0.00	0.00
	$^3P_0$, $^3P_1$	0.66	0.75	0.77
	$^3P_2$	1.42	1.47	1.53
	$^3F_2$, $^3F_3$	2.36	2.35	2.30
	$^3F_4$	3.38	3.33	3.34

a. Relative to Fermi level. Ref. 87.

components for the three different systems. The largest deviations are observed for the $^1S_0$ ($M_{4,5}N_{4,5}N_{4,5}$) and the $^3F_4$ ($M_4N_{4,5}N_{4,5}$) components. Although the energy shifts between different terms should be the same in the M_4 and M_5 groups, the differences observed here are due to the limited resolution of certain lines and to the inability of the decomposition procedure to separate closely spaced lines. Therefore it is assumed that these differences do not have any physical significance. The calculated energies relative to the $^1G_4$ level of the $N_{4,5}N_{4,5}$ final state configuration are given in Table VI-3 in LS and in intermediate coupling (IC). In the LS coupling scheme, the spin-orbit diagonal elements have been included in the calculations. From a comparison of Table VI-2 with Table VI-3, it appears that there is a good agreement between the experimental and calculated values in intermediate coupling, except for the $^1S_0$ and the $^3F_4$ states which were quite poorly resolved in the spectra. Absolute transition energies were calculated semiempirically from equation VI-1 using the experimental core level binding energies given in Table VI-1 and the relation

$$E_{N_{4,5}} = E_{N_4} - \xi_{4d} \qquad \text{VI-5}$$

Table VI-3. Calculated Relative Kinetic Energies of the $M_{4,5}N_{4,5}N_{4,5}$ Auger Lines of Tin

Final State Terms	LS[a] (eV)	IC[b]
$^1S_0$	-4.45	-4.78
$^1G_4$	0.00	0.00
$^1D_2$	1.04	0.13
$^3P_0$	0.25	0.60
$^3P_1$	0.51	0.54
$^3P_2$	1.01	1.43
$^3F_2$	1.97	2.56
$^3F_3$	2.74	2.77
$^3F_4$	3.76	3.86

a. LS coupling plus diagonal contributions from the spin-orbit interaction.

b. Intermediate coupling.

where ξ_{4d} is the spin-orbit parameter. The $F(N_{4,5}N_{4,5}; X)$ terms obtained in the intermediate coupling scheme were used, the $R_S^T(N_{4,5}N_{4,5})$ term was neglected. The values obtained in this way are listed in Table VI-4 and VI-5 along with the experimental energies. The average deviation of experimental from calculated values is 10.46 (±0.60) eV for $Sn(CH_3)_4$ and 11.41 (±0.65) eV for $[Sn(CH_3)_3]_2$. These large differences arise from the neglect of the $R_S^T(N_{4,5}N_{4,5})$ term in equation IV-1 and these differences can be considered equal to the "static relaxation" contribution. The static relaxation term found in this way is smaller than the theoretical value calculated above by 5.5 eV for $Sn(CH_3)_4$ and 4.6 eV for $[Sn(CH_3)_3]_2$.

In the case of Tin metal the average static relaxation of 16.27 eV obtained by the same analysis of each line agrees well with the theoretical value of 16.04 eV calculated above. It is notable that this static relaxation term is consistent throughout the various multiplets for any one molecule indicating that the multiplet state effect contributions are adequately described by the coupling term. Furthermore the M_4 and M_5 sets gave the same results so the contributions are independent of the initial state.

Table VI-4. Calculated and Experimental Tin $M_{4,5}N_{4,5}N_{4,5}$ Auger Energies for $Sn(CH_3)_4$

Transition	Final State Terms	Calculated Energies (eV)	Experimental Values (eV)
$M_4N_{4,5}N_{4,5}$			
	$^1S_0$	408.96	420.14
	$^1G_4$	413.76	424.39
	$^1D_2$	413.89	
	$^3P_0$	414.36	424.92
	$^3P_1$	414.30	
	$^3P_2$	415.19	425.71
	$^3F_2$	416.32	426.58
	$^3F_3$	416.52	
	$^3F_4$	417.62	427.37
$M_5N_{4,5}N_{4,5}$			
	$^1S_0$	400.56	411.42
	$^1G_4$	405.34	415.88
	$^1D_2$	405.47	
	$^3P_0$	405.94	416.54
	$^3P_1$	405.88	
	$^3P_2$	406.77	417.30
	$^3F_2$	407.90	418.24
	$^3F_3$	408.10	
	$^3F_4$	409.20	419.26

Table VI-5. Calculated and Experimental Tin $M_{4,5}N_{4,5}N_{4,5}$ Auger Energies for $[Sn(CH_3)_3]_2$

Transition	Final State Terms	Calculated Energies (eV)	Experimental Values (eV)
$M_4N_{4,5}N_{4,5}$	$^1S_0$	409.11	421.03
	$^1G_4$	413.89	425.41
	$^1D_2$	414.02	
	$^3P_0$	414.49	426.15
	$^3P_1$	414.43	
	$^3P_2$	415.32	426.87
	$^3F_2$	416.45	427.78
	$^3F_3$	416.65	
	$^3F_4$	417.75	428.83
$M_5N_{4,5}N_{4,5}$	$^1S_0$	400.74	412.73
	$^1G_4$	405.52	416.88
	$^1D_2$	405.65	
	$^3P_0$	406.12	417.63
	$^3P_1$	406.06	
	$^3P_2$	406.95	418.35
	$^3F_2$	408.08	419.30
	$^3F_3$	408.28	
	$^3F_4$	409.52	420.21

The approach used above to obtain the relaxation terms is equivalent to the use of the Auger parameter as defined by Lang and Williams[51] and described in Chapter IV

$$\xi = E(M_a) - E(N_b) - E(N_c) - E(M_aN_bN_c; X) \qquad VI-6$$

and also

$$\xi = F(N_{4,5}N_{4,5}; X) - R_S{}^T(N_{4,5}N_{4,5}) \qquad VI-7$$

Focussing only on the strongest feature in the Auger spectrum, the principal line $^1G_4$ of the $M_5N_{4,5}N_{4,5}$ group, the position of which is better defined, and using the experimental $E(3d_{5/2})$ energy for $E(M_a)$, the experimental $E(4d_{3/2})$ energy minus the spin-orbit parameter ξ for $E(N_b)$ and $E(N_c)$, and the coulombic term $F(N_{4,5}N_{4,5}; {}^1G_4)$ obtained in the IC scheme, the total relaxation values of 11.14 eV in the case of $[Sn(CH_3)_3]_2$ and 10.43 eV in the case of $Sn(CH_3)_4$ (Table VI-6) were obtained. The data of Pessa et al.[87] for Sn metal gave $R_S{}^T(N_{4,5}N_{4,5}) = 16.18$ eV for the same analysis. Similar analysis of the $^1G_4$ line of the M_4 group using $E(3d_{3/2})$ gave results in good agreement with those derived from the M_4 set. Assuming now that the atomic relaxation contribution is constant,

Table VI-6. The Auger Parameter and Relaxation Terms for Tin Species

		$Sn(CH_3)_4$ (eV)	$[Sn(CH_3)_3]_2$ (eV)	Sn[a] metal (eV)
ξ[b] $M_5(^1G_4)$		13.36	12.65	7.61
ξ $M_4(^1G_4)$		13.27	12.48	7.61
$R^T{}_S(N_{4,5}N_{4,5})$[c]	M_5	10.43	11.14	16.18
	M_4	10.52	11.31	16.18
$R^{ea}{}_S(N_{4,5}N_{4,5})$[d]	M_5	3.96	4.67	9.71
	M_4	4.05	4.84	9.71
$\Delta\xi = 2\Delta R_v$	M_5	0	0.71	-
	M_4	-	0.79	-
ΔR_v		-	0.36	-

(a) Experimental values from Ref. 87.
(b) Calculated from equation VI-6.
(c) Calculated from equation VI-7, taking $F(N_{4,5}N_{4,5}; {}^1G_4)$ = 23.79 eV.
(d) Calculated from equation VI-2, taking $R^a{}_S(N_{4,5}N_{4,5})$ = 6.47 eV.

(independent of the environment of the atom) the extraatomic, environment sensitive, portion can be extracted by subtracting the R_S^a term evaluated above (6.47 eV) from the R_S^T terms leaving the residuals which are given as R_S^{ea} in Table VI-6. For metallic Tin this residual (extraatomic relaxation) value of 9.71 eV is in good agreement with the theoretical estimate of 9.57 eV derived in Section C. This extraatomic relaxation value permits the prediction of the solid-vapor shifts in binding energy and Auger energy by noting that Lang and Williams'[51] Auger parameter (equation VI-6) is independent of the physical state. By the same analysis done in Chapter IV for Germanium, the solid-vapor difference in the Auger parameter is given by:

$$\Delta\xi = \xi^{solid} - \xi^{gas} = R_S^{ea}(N_{4,5}N_{4,5}) = 9.71 \text{ eV}$$

which is approximately $2\Delta R_v$[38] (the outer shell relaxation shift associated with the formation of a single core hole) therefore $\Delta R_v = 4.85$ eV. Applying the relation[38]

$$E_B = -V - R \qquad \text{IV-14}$$

and assuming that the core potentials (V) are insensitive to the state,[59b] gives for the binding energy solid-vapor shifts

$$\Delta E_B^{\text{solid-gas}} = -R^{\text{solid}} + R^{\text{gas}}$$

$$= -\Delta R^{\text{solid-gas}} = -4.85 \text{ eV}$$

and the binding energy should be higher in the vapor state by about 4.85 eV.

Parallel arguments yield for the Auger solid-vapor shifts

$$\Delta E_{Au}^{\text{solid-gas}} = 3R^{\text{solid}} - 3R^{\text{gas}}$$

$$= 3(\Delta R^{\text{solid-gas}}) = 14.55 \text{ eV}$$

with the Auger energy lower by 14.55 eV in the gaseous state. These estimated shifts seem to be quite reasonable being in the same energy range of shifts observed for Ag, Zn and Cd.[73,74,75] These results suggest that the estimated values of the extraatomic relaxation are reasonable. It seems plausible to consider also the corresponding terms for $Sn(CH_3)_4$ and $[Sn(CH_3)_3]_2$ to be an evaluation of the contributions of molecular effects.

The values in Table VI-6 show the expected trend; the total static relaxation contribution increases from $Sn(CH_3)_4$ through $[Sn(CH_3)_3]_2$ to metallic Tin, in the order of increasing complexity of the environment. The difference between $Sn(CH_3)_4$ and $[Sn(CH_3)_3]_2$ can be related to the molecular effects arising from the replacement of a CH_3 group with a $(CH_3)_3Sn$ group. It may be due to the difference in the delocalization of the Tin 4d and 5p as a result of chemical bonding with the Carbon and/or Tin. The extraatomic relaxation terms (Table VI-6) of 3.96 eV in $Sn(CH_3)_4$ and 4.67 in $[Sn(CH_3)_3]_2$ can then be attributed to the contribution of the electrostatic interaction of the additional valence shell electrons, provided by the substituents bonded to the atom of interest, with the 4d electrons. The largest contribution arises from metallic Tin in which the conduction band provides a mobile supply of electrons which can respond to the increased effective core charge. The supply of electrons is more restricted in the two molecules relative to metallic Tin presumably because of the effective electronegativity of the substituents. It can then be concluded that the $Sn(CH_3)_3$ group has a lower effective electronegativity than CH_3 probably because Tin has a lower electronegativity than Carbon. The model as it stands does not recognize the

effects of redistribution of the 5p electrons (two from the atomic configuration and extra charge from the surrounding). For this reason the atomic and especially the extraatomic relaxations are overestimated by the calculations. If a proper detailed analysis can be performed, the relaxation term could provide insight into electron distributions in molecular systems.

The calculated relative intensities of the Auger components in the M_4 and M_5 groups are given in Table VI-7 along with the experimental values. The IC results are in better agreement with experiment in all cases except that the calculated (IC) intensity of the peak due to the sum of the $^3P_0$ and $^3P_1$ terms is slightly lower than the experimental values for the combined unresolved peaks whereas the calculated (IC) intensity of the $^3P_2$ term is slightly larger than the experimental intensity in both the M_4 and the M_5 Auger groups and for both compounds. The sum of all ^3P terms is however well predicted by the IC method. Within the accuracy of the spectral decomposition procedure it seems that the intermediate coupling calculation reproduces satisfactorily the experimental intensities for all three systems whereas the LS coupling is inadequate.

Table VI-7. Calculated and Experimental Relative Intensities of the Tin $M_{4,5}N_{4,5}N_{4,5}$ Auger Lines.[a]

Transition	Final State Terms	LS[b]		IC[c]		$Sn(CH_3)_4$	$[Sn(CH_3)_3]_2$	Sn(Metal)
$M_4N_{4,5}N_{4,5}$								
	$^1S_0$	4.4		6.2		9.9 (0.7)	10.8 (1.9)	5.0
	$^1G_4$	25.9	38.4	28.5	51.1	49.4 (3.5)	50.3 (1.7)	
	$^1D_2$	12.5		22.6				64.6
	$^3P_0$	9.1	12.6	9.1	10.7	14.5 (3.1)	14.3 (2.0)	
	$^3P_1$	3.5		1.6				
	$^3P_2$	9.0		9.9		6.1 (1.1)	8.6 (1.3)	11.9
	$^3F_2$	16.6	31.5	5.5	20.4	17.9 (0.9)	14.7 (1.1)	17.2
	$^3F_3$	14.9		14.9				
	$^3F_4$	4.0		1.6		2.1 (0.8)	1.2 (0.8)	1.3

(Continued)

Table VI-7 (Continued)

Transition	Final State Terms	LS[b]		IC[c]		$Sn(CH_3)_4$	$[Sn(CH_3)_3]_2$	Sn(Metal)
$M_5N_{4,5}N_{4,5}$								
	$^1S_0$	4.4		2.9		4.0 (0.3)	5.8 (0.6)	5
	$^1G_4$	25.7	38.1	23.5	27.6	29.5 (1.3)	27.9 (1.5)	39.9
	$^1D_2$	12.4		4.1				
	$^3P_0$	1.6	7.4	2.9	8.7	10.6 (0.9)	13.8 (1.6)	
	$^3P_1$	5.8		5.8				
	$^3P_2$	13.9		11.5		8.8 (1.0)	12.8 (1.3)	10.3
	$^3F_2$	4.1	13.9	14.4	24.2	24.9 (0.6)	21.2 (1.1)	22.1
	$^3F_3$	9.8		9.8				
	$^3F_4$	22.3		25		22.2 (0.5)	18.4 (1.1)	22.7

a. Intensities for each component in each major Auger group (M_4 and M_5) are expressed as a % summing to 100%. The numbers in parentheses are the standard deviations obtained from the least squares fit.
b. LS coupling for final state.
c. Intermediate coupling for final state.

E. Conclusions

The above results indicate that present intermediate coupling theory gives good agreement with experiment for the intensities of the peaks. However, in order to reproduce the absolute energies, a better treatment of the relaxation effect is necessary. This refinement should account for the redistribution of the valence electrons in the molecular environment.

It would be useful to have a comparison spectrum of atomic Tin in order to evaluate more reliably the contributions arising from chemical environmental effects.

CHAPTER VII

KVV VALENCE AUGER SPECTRA IN SIMPLE MOLECULES: OF_2, BF_3

A. Introduction

The Auger spectra which have been analyzed in the preceding chapters involved only transitions between core levels. Those spectra revealed essentially atomic character and therefore could be interpreted by means of atomic theory according to the appropriate coupling scheme. Core type spectra have an internal invariance with respect to both energies and intensities, in that they respond to different chemical environment with a uniform energy shift. Another group of Auger spectra, which only recently has received some experimental and theoretical attention, involves transitions to final states wherein both final state vacancies are distributed among the valence molecular orbitals. These spectra usually show quite broad features due to the presence of a large number of states, and also because the valence double-hole transitions produce in general a considerable vibrational and dissociative broadening. In addition, the

analysis of valence Auger spectra are complicated by the interference of other processes,[91] the most important of which are the "shake-off" and "shake-up" transitions associated with multielectron core level excitation, double Auger transitions, autoionization (especially using electron impact) and inelastic scattering.[91] In this work, valence level Auger spectra, the O(KVV) and F(KVV) Auger spectra of OF_2 and the B(KVV) and F(KVV) Auger spectra of BF_3 have been investigated. These spectra are due to an Auger transition from an initial state with a hole in the core level K to a final state with two holes in the valence shell V. The initial core hole vacancy was produced by electron impact excitation. Energies have been compared with the corresponding calculated values.

B. Experimental

OF_2 gas was used directly from a cylinder supplied by the Ozark Mahoning Chemical Company. The absence of air in the cylinder was ascertained by scanning the Nitrogen (N_2) and Oxygen (O_2) core line regions with negative results. BF_3 gas was used as supplied by Matheson. The spectra were excited by incident electrons with energy of 2.5 KeV produced by the electron gun described earlier (Chapter II). The beam current was 700 μA. The spectra

were calibrated with respect to the Argon $L_3M_{2,3}M_{2,3}$ ($^1D_2$) Auger line (203.49(5) eV kinetic energy)[25] and the Neon $KL_{2,3}L_{2,3}$ ($^1D_2$) Auger line (804.557(17) eV kinetic energy).[24] The B 1s, F 1s and O 1s photoelectron lines were excited by Al $K\alpha_{1,2}$ radiation (1486.6 eV).[21] F 1s, O 1s lines were calibrated with respect to the Ne $KL_{2,3}L_{2,3}$ ($^1D_2$) Auger line and the Ne 1s photoelectron line (870.312(17) eV binding energy).[24] Boron 1s was calibrated with respect to Ar $2p_{3/2}$ photoelectron line (248.62(8) eV binding energy).[25]

C. Theory

The same expression[50] used previously for inner shell Auger processes can be applied to the case of valence Auger spectra

$$E_{KYZ} = E^{\circ}_{KYZ} - \mathbf{F}(YZ) + R(YZ) \qquad \text{VII-1}$$

where E°_{KYZ} is the transition energy deduced from the one-electron binding energies E(K), E(Y), E(Z) (equation I-23); $\mathbf{F}(YZ)$ is the coulombic two-electron interaction energy describing the coupling of the final state holes in levels Y and Z and R(YZ) is the relaxation energy

associated with the two-hole final state. In this case the two electron interaction energy **F**(YZ) and the relaxation energy R(YZ) are defined within the context of the MO model.[92] The expression used for the coulombic term is:

$$\mathbf{F}(YZ) = \sum_{n,m} c_{yn}^2 \, c_{zm}^2 \, F^0(nm) \qquad \text{VII-2}$$

where the c_{yn}^2 and c_{zn}^2 are the atomic orbital populations in the Y and Z molecular orbitals respectively, and $F^0(nm)$ are the atomic Slater's integrals between the atomic orbitals n and m. The sum in equation VII-2 includes all atomic orbital contributions to the molecular orbitals, i.e. orbitals of the central atom as well as those of the ligands, and includes both one-center and two-center terms. All the one center integrals were obtained from Mann's tables.[53] Integrals involving two centers are calculated using an approximation by Mataga and Nishimoto[93]

$$F^0(nm) = e^2\left[R_{nm} + \frac{2e^2}{f_n + f_m}\right] \qquad \text{VII-3}$$

R_{nm} is the internuclear distance between the two centers, e is the charge on the electron, and f_n, f_m are the one

center Slater integrals. This approximation takes an appropriate average of two extrema; for large R_{nm}, $F^0(nm) = e^2/R_{nm}$, and for very small R_{nm}, $F^0(nm) = (f_n + f_m)/2$. The relaxation energy in the inner shell Auger processes, as described in Chapter IV, is divided into four components; inner, intra and outer shell components of the central atom, and an extraatomic component due to electrons on the other atoms. Considering that the O(KVV), F(KVV) and B(KVV) Auger processes create two holes in the outermost orbitals distributed in principle over the whole molecule, the previously employed concepts of outer shell relaxation and extraatomic relaxation contributions lose their meaning. A better model for the relaxation energy for valence Auger processes consists in evaluating the intrashell contribution arising from those molecular orbitals which contain the final holes. Inner shell relaxation contributions can be assumed to be negligibly small in analogy to the atomic case.[29,50] The relaxation term in equation VII-1 is then given[92] by the average of the relaxation energies R_Y and R_Z associated with each of the molecular orbitals Y and Z which contribute a final state hole

$$R(YZ) = \frac{1}{2}(R_Y + R_Z) \qquad \text{VII-4}$$

Within the context of the MO model, these relaxation terms R_Y and R_Z are obtained by a sum of atomic relaxation energies R_n^a weighted by the atomic orbital populations c_Y^2 and c_Z^2 respectively, associated with the atomic orbitals n that contribute to the molecular orbitals involved in the Auger process

$$R_Y = \sum_n c_{yn}^2 R_n^a \qquad \text{VII-5}$$

Calculations are not available for the intraatomic relaxation R_n^a. However, the term R(YZ) can be obtained by subtraction of the coulombic interaction F(YZ) from the Auger parameter ξ which, as described in Chapter III, is given by the difference between experimental binding energies and the Auger energy (equations IV-3 and IV-4).

The transition intensities are calculated from the equation[92,94]

$$I_{KYZ} = \sum_{n,m} c_{yn}^2 \, c_{zm}^2 \, P_{Knm} \qquad \text{VII-6}$$

where c_{yn}^2 and c_{zm}^2 are the populations of the n, m atomic orbitals on the central atom in the Y and Z molecular orbitals respectively. P_{Knm} is the Auger transition

probability given by the appropriate atomic Auger matrix element expressed as

$$P_{Knm} = \sum_{\ell'} |\langle \phi_K E\ell' | r_{12}^{-1} | \phi_n \phi_m \rangle|^2 \qquad \text{VII-7}$$

where ϕ_K and $E\ell'$ are the core and continuum orbitals respectively. Since several values of the orbital angular momentum quantum number ℓ' of the continuum hole $(E\ell')^{-1}$ may couple with the quantum number ℓ of the initial vacancy to give $L_{initial} = L_{final}$, the summation must be carried out over all possible values of ℓ'. For the Auger processes which involve an initial s vacancy (ℓ=0), ℓ' has only one value $\ell' = L_f$. In the KVV transitions of Oxygen, Boron and Fluorine in the molecules investigated, the initial vacancy is in an s level and the two final state holes are in molecular orbitals formed from atomic orbitals belonging to the level L, therefore in equation VII-6 the KLL transition probabilities are appropriate. In Table VII-1 are listed the analytic expressions for the KLL transition probabilities[12] in terms of direct and exchange Slater's integrals.

$R^k(n_b\ell_b n_c\ell_c, n_a\ell_a E\ell')$ represents the radial part of the Direct and Exchange matrix elements defined in Chapter I (equations I-16, I-17); n_b, n_c and ℓ_b, ℓ_c are

Table VII-1. Analytic Expressions for the KLL Transition Probabilities

Transition	Final vacancies		ℓ'	Transition Probability
$KL_1L_1(^1S_0)$	$2s^{-2}$	$^1S_0$	0	$2\pi\|R^0(2020, 10E0)\|^2$
$KL_1L_{2,3}(^1P_1)$	$(2s2p)^{-1}$	$^1P_1$	1	$3\pi\|R^0(2021,10E1) + \frac{1}{3}R^1(2120,10E1)\|^2$
		^3P_j	1	$(2j+1)\pi\|R^0(2021, 10E1) - \frac{1}{3} R^1(2120,10E1)\|^2$
$KL_{2,3}L_{2,3}(^1S_0)$	$2p^{-2}$	$^1S_0$	0	$\frac{2\pi}{3}\|R^1(2121,10E0)\|^2$
$(^1D_2)$		$^1D_2$	2	$\frac{4\pi}{3}\|R^1(2121,10E2)\|^2$

respectively the principal and orbital quantum numbers of the two electrons missing in the Auger final state; n_a,E and ℓ_a,ℓ' are the corresponding numbers for the emitted electron in the initial state and the Auger electron in the continuum.

Summing over all the terms arising from the same configuration and using the radial integrals R^k, calculated by Walters and Bhalla[95] within the HFS SCF method, the transition probabilities listed in Table VII-2 for Boron, Oxygen and Fluorine, expressed in atomic units of time τ_o (2.42×10^{-7} sec) were obtained.

There is no clear agreement about the orbital populations to be used in equation VII-6, the local or the Mulliken. Both are defined by the MO overlap equation[96]

$$\sum_{n,m} c_n c_m S_{nm} = \sum_n (c_n^2 + \sum_{m \neq n} c_n c_m S_{nm}) = 1 \qquad \text{VII-8}$$

where c_n, c_m are the orbital coefficients and S_{nm} is the overlap integral between the orbitals n and m. The Mulliken populations include the bonding charge such that

$$P_n^M = c_n^2 + \frac{1}{2} \sum_{m \neq n} c_n c_m S_{nm} \qquad \text{VII-9}$$

and satisfy the sum rule

Table VII-2. KLL Auger Transition Probabilities for Boron, Oxygen and Fluorine

Transitions	Transition Probability (a.u.)/π
B KL_1L_1	2.663×10^{-3}
B $KL_1L_{2,3}$	7.653×10^{-3}
O KL_1L_1	2.656×10^{-3}
O $KL_1L_{2,3}$	7.871×10^{-3}
O $KL_{2,3}L_{2,3}$	18.254×10^{-3}
F KL_1L_1	2.631×10^{-3}
F $KL_1L_{2,3}$	7.803×10^{-3}
F $KL_{2,3}L_{2,3}$	18.029×10^{-3}

$$\sum_n P_n^M = 1 \qquad \text{VII-10}$$

The local populations include only the diagonal terms $P_n^L = c_n^2$. It is now becoming generally accepted that the Auger process samples the populations only on the atom with the core hole. The interatomic Auger matrix elements $P_{Kab} = \langle \phi_K \phi_{E\ell'} | r_{12}^{-1} | \phi_a \phi_b \rangle$ for a system of two atoms a and b with core hole K in the atom a, have been found[97] to be much smaller than the intraatomic elements $P_{Kaa} = \langle \phi_K \phi_{E\ell'} | r_{12}^{-1} | \phi_a \phi_a \rangle$. However the extent of the radial wave function sampled by the Auger process is not clear. So a valid question which remains is whether the Auger process probes only the electron density on the atom with the core hole, or also the bonding charge. So far comparisons with experiments have been inconclusive. There are examples of good agreement obtained with either the local or the Mulliken populations in different problems,[98,99] depending on the more or less localized nature of the electron density. In the following analysis the orbital coefficients, as given by CNDO calculations, have been used. These values reflect the local contribution of each atomic orbital to the molecular orbitals.

D. Results and Discussion

In Table VII-3 and VII-4 the core level binding energies and the experimental ionization potential of some of the molecular orbitals as found by others[100,102] are listed for OF_2 and BF_3 respectively. The electronic configuration of neutral OF_2 in the ground electronic state is $(3a_1)^2(2b_2)^2(4a_1)^2(1b_1)^2(5a_1)^2(3b_2)^2(1a_2)^2(4b_2)^2-(6a_1)^2(2b_1)^2$.[35] The electronic configuration of BF_3 in the ground state is $(3a'_1)^2(2e')^4(1a_2'')^2(4a_1')^2(3e')^4-(1a_2')^2(1e'')^4(4e')^4$. The orbital eigenvalues obtained from CNDO/2[35] calculations are also given. It has been found[104] that approximate LCAO SCF calculations such as CNDO/2 give energies differing from experiment by ~4 eV. To obtain "corrected" binding energies this value was subtracted from each CNDO orbital energy and the corrected values were used as Koopmans' theorem ionization potentials in subsequent calculations wherein. The results given in Tables VII-3 and VII-4 show that CNDO calculations gave generally larger values than experimental for the ionization potentials, the largest discrepancy from the experimental value being of the order of 2 eV.

Before considering the detailed analysis of the spectra, it is appropriate to describe the general feature

Table VII-3. Experimental Core Level and Experimental and Calculated Molecular Orbital Ionization Energies (eV) of OF_2

Experimental[a]	CNDO/2
13.26	15.23 $2b_1$
16.17	16.63 $6a_1$
16.47	17.30 $4b_2$
18.68	19.12 $1a_2$
19.50	20.70 $3b_2$
20.9	21.06 $5a_1$
	21.92 $1b_1$
	32.15 $4a_1$
	41.43 $2b_2$
	45.85 $3a_1$

$E_{O\ 1s}$ = 545.32[b], 545.33[c]

$E_{F\ 1s}$ = 695.13[b], 695.07[c]

a. The values are taken from ref. 100.

b. This study.

c. Ref. 101.

Table VII-4. Experimental Core Level and Experimental and Calculated Molecular Orbital Ionization Energies (eV) of BF_3

Experimental[a]	CNDO/2
15.95	15.9 (4e')
16.63	16.7 (1e")
17.13	17.2 ($1a'_2$)
19.06	21.2 (3e')
20.14	21.5 ($4a'_1$)
21.40	22.0 ($1a"_2$)
	44.0 (2e')
	45.8 ($3a'_1$)

$E_{B\ 1s}$ = 202.74[b], 202.8[c]

$E_{F\ 1s}$ = 694.77[b], 694.8[c]

a. Values given in ref. 102.

b. This study.

c. Ref. 103

of these valence Auger spectra. The molecular orbitals of the first row elements may be partitioned into inner and outer valence orbitals. The former being mainly of 2s character, are tightly bound, whereas the latter which are essentially of 2p character are less tightly bound. This leads to a natural division of the double hole Auger states into three classes, comprising outer-outer, outer-inner, and inner-inner vacancies. These three groups of states will represent non-overlapping energy regions in the Auger spectrum. Most of the intensity is found in the first energy interval corresponding to the outer-outer group of states of the high kinetic energy part, as will be seen in the spectra of OF_2 and BF_3. On the low kinetic energy side of the spectrum, the bands become weaker and broader, and the background increases further obscuring the discrete transitions. The analysis of the bands occurring in this part of the spectrum, i.e. the second and the third energy regions, is arduous due to the presence of different satellite processes. A complete classification of different types of satellite processes in Auger spectra has been given by Moddeman et al.[105]

The O(KVV) and F(KVV) Auger spectra of OF_2 are shown in Figures VII-1 and VII-2. The B(KVV) and F(KVV) Auger spectra of BF_3 are shown in Figures VII-3 and VII-4

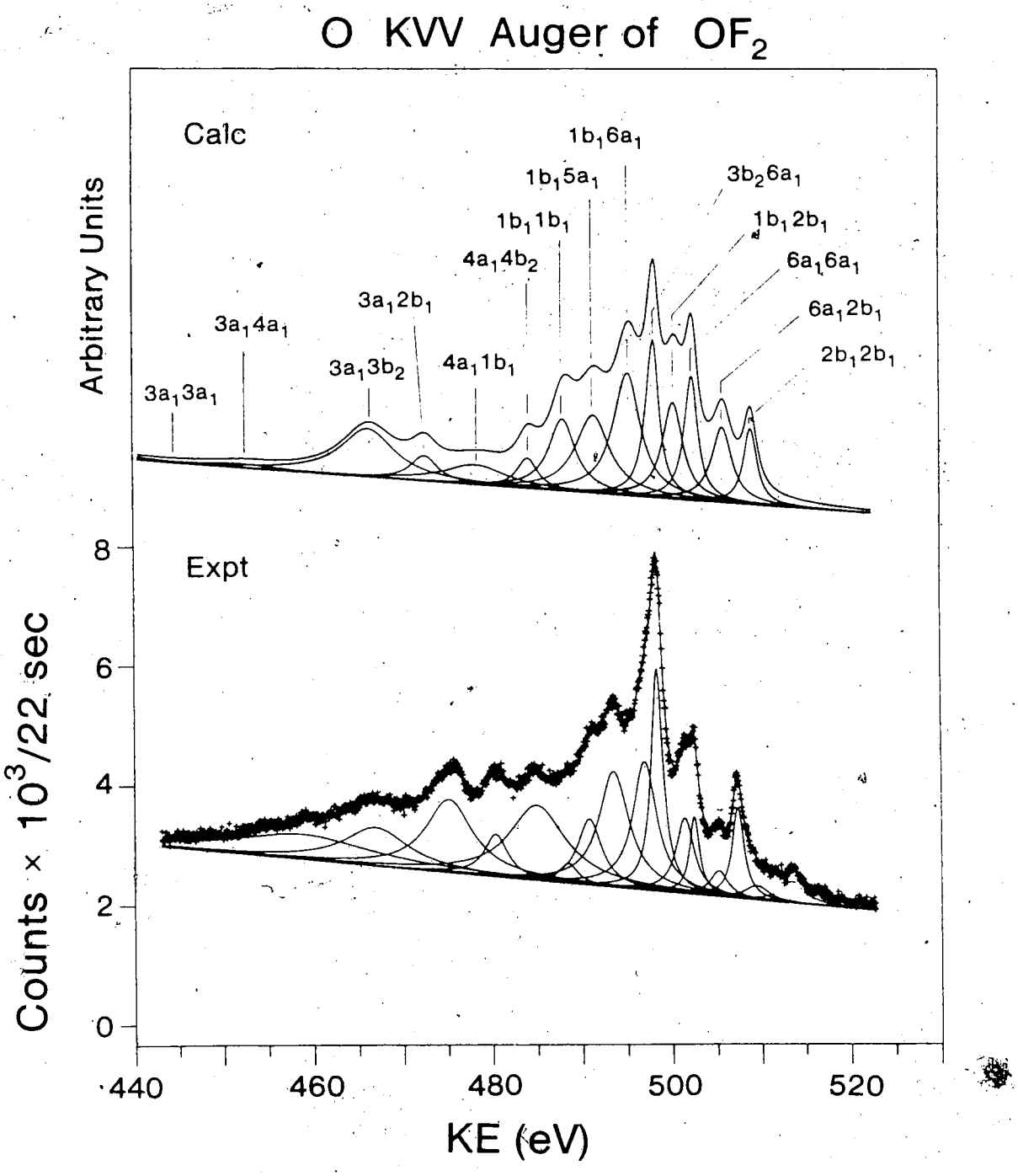

Figure VII-1. Calculated and experimental O(KVV) Auger spectra of gaseous OF_2. The experimental spectrum was excited with 2.5 keV electrons at a sample pressure of 1μ.

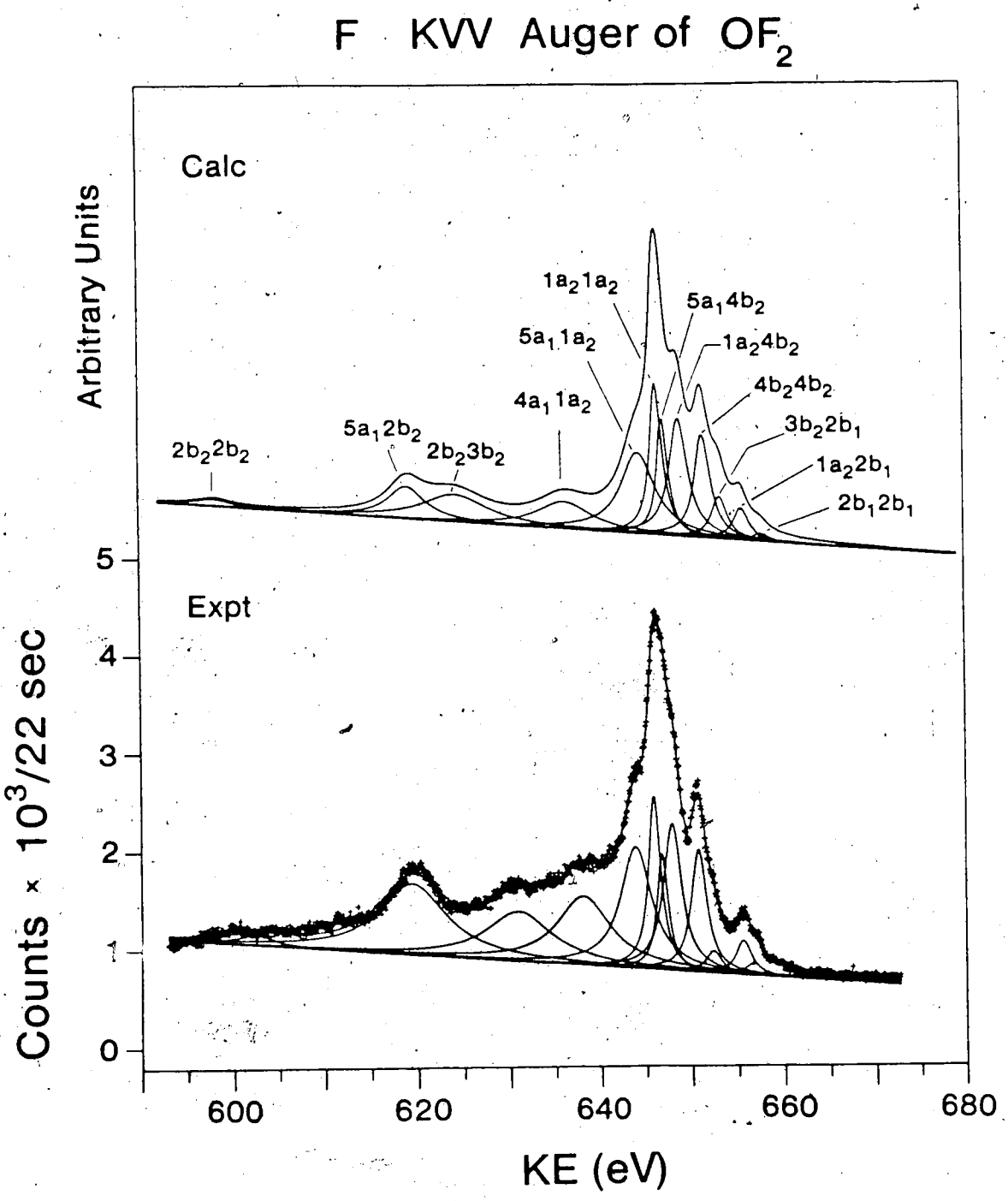

Figure VII-2. Calculated and experimental F(KVV) Auger spectra of gaseous OF_2. The experimental spectrum was excited with 2.5 keV electrons at a sample pressure of 1μ.

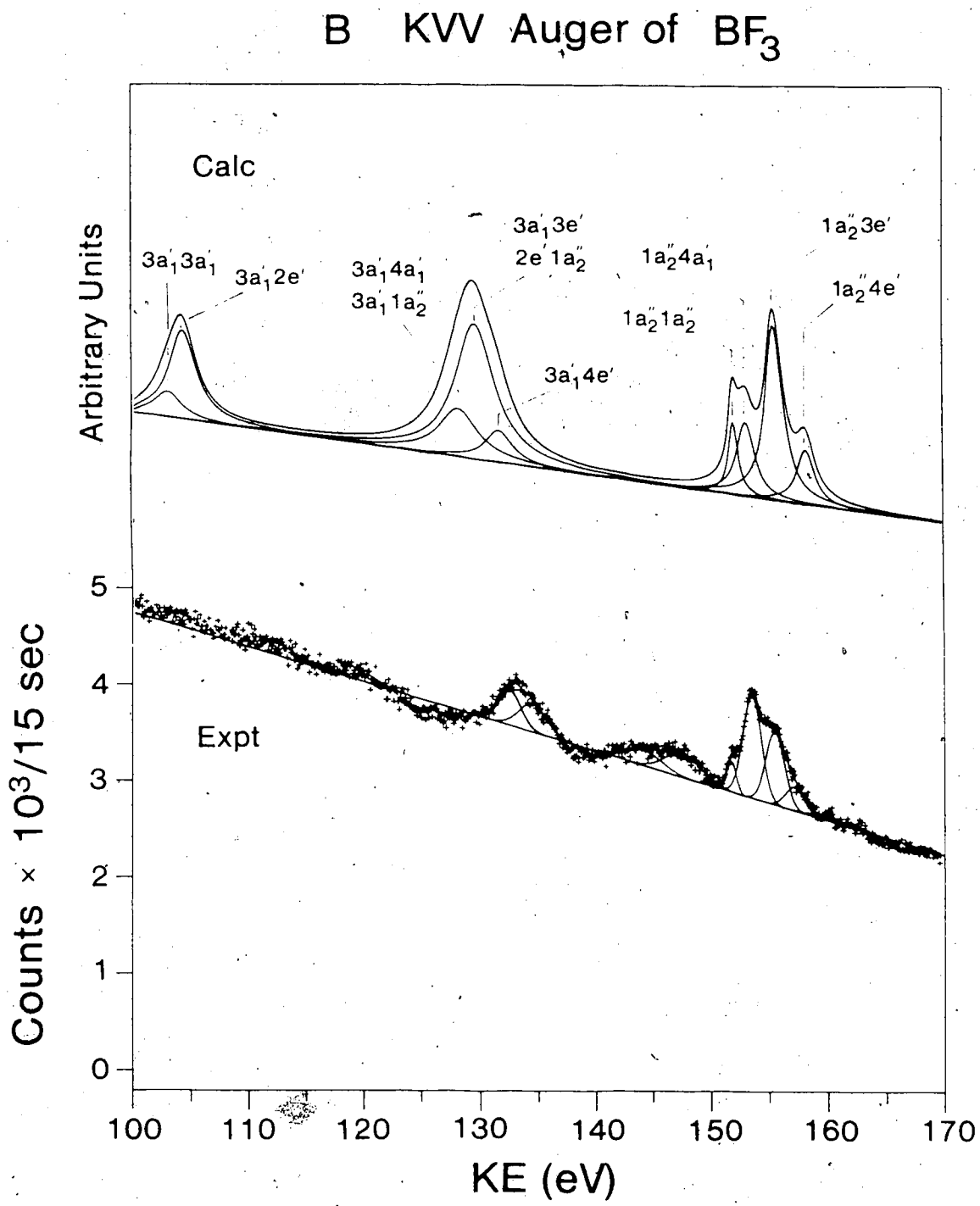

Figure VII-4. Calculated and experimental B(KVV) Auger spectra of gaseous BF_3. The experimental spectrum was excited with 2.5 keV electrons at a sample pressure of 1μ.

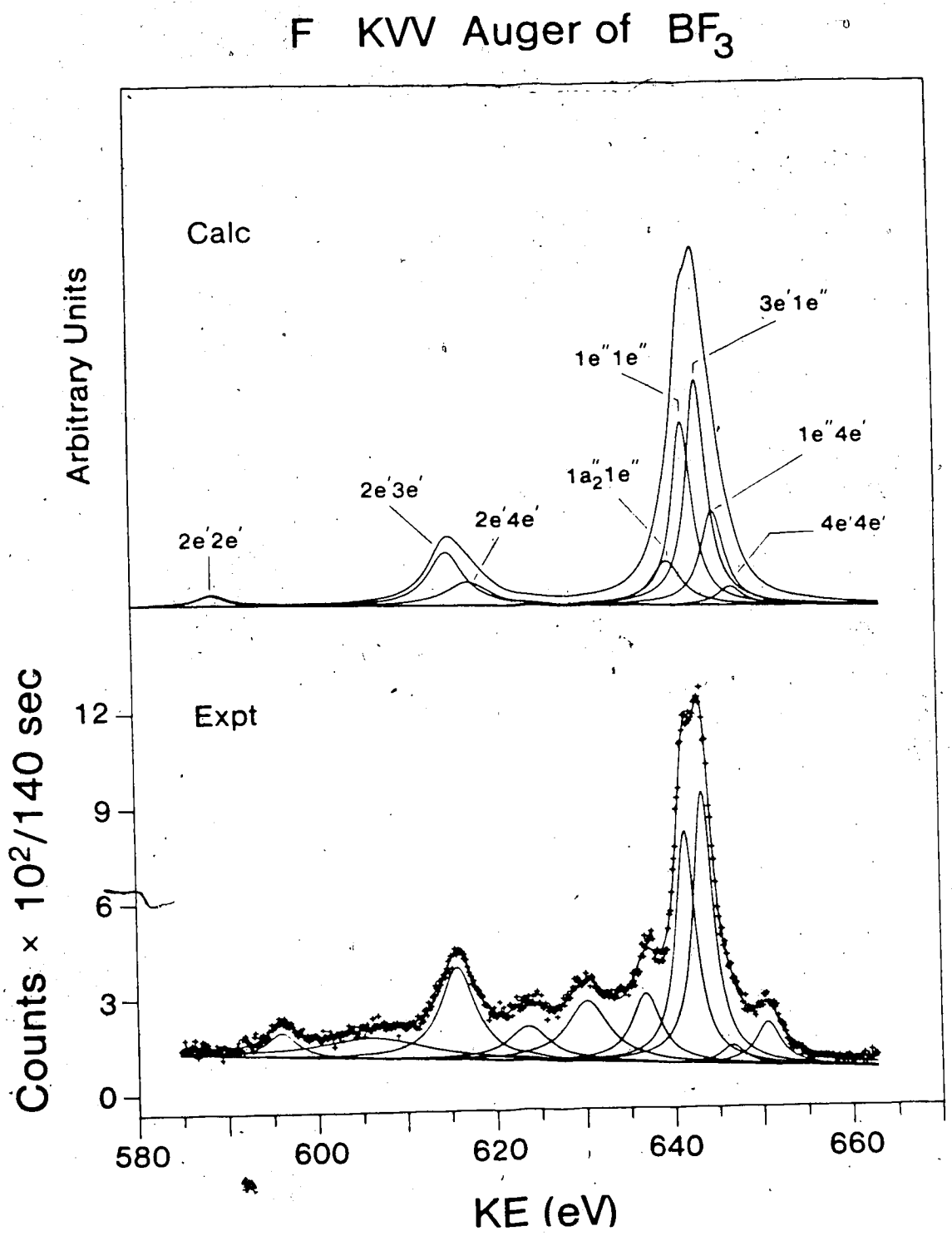

Figure VII-4. Calculated and experimental F(KVV) Auger spectra of gaseous BF_3. The experimental spectrum was excited with 2.5 keV electrons at a sample pressure of 1μ.

respectively along with the corresponding calculated spectra. Even if the Auger processes of the two elements in both compounds (Oxygen and Fluorine in OF_2, Boron and Fluorine in BF_3) involve the same final states, the appearance of the spectra is quite different. This indicates that the transition probability for a given final state is determined by the location of the initial K hole. The experimental line shapes were decomposed into component Lorentzian curves by means of a least square line fit programme.[26] The linewidths were allowed to be free parameters in order to achieve the best fit. The calculated spectra have been obtained by a curve simulation programme[76] using positions estimated from equation VII-1, neglecting the relaxation term, widths as derived from the deconvolution of the experimental data and areas as required by the intensity values derived from the molecular orbital intensity model (equation VII-6). Lorentzian functions have been computed for each peak and these have been summed to give the total envelope. The coulombic terms **F**(YZ) required in equation VII-1 were calculated from equation VII-2 using the atomic orbital coefficients given by the CNDO/2 calculations performed on the neutral molecules. The experimental energies, widths, intensities, and for comparison, corresponding calculated

values are given in Tables VII-5 to VII-8 along with the coulombic terms obtained as above. In the tables are also given the final state configurations which are the major contributors to the intensity of the peaks. On the basis of the atomic character of the molecular orbitals, assuming that only transitions to molecular orbitals with atomic contributions from the element with the core hole produce the Auger spectrum, and on the basis of the atomic Auger matrix elements, it was possible to deduce the number of possible final state configurations in each spectrum. For the O(KVV) and F(KVV) Auger spectra of OF_2 there are 45 and 55 final state configurations respectively. The B(KVV) and F(KVV) Auger spectra of BF_3 involve 10 and 36 final state configurations respectively. In order to have comparable calculated and experimental spectra, many of the lines arising from different final states were grouped by energy in such a way as to yield approximately the same number of peaks as observed in the experimental spectra. Linewidths were not calculated, the values used in the simulated spectra were taken from the experimental results, except in those cases when the attribution of the peak was uncertain and an arbitrary width, suggested by the number of final state contributions, was used. The relaxation terms R(YZ)

Table VII-5. O(KVV) Auger Transitions of OF_2

Peak Number	Principal Final State Configuration[a]	Other Final States[b]	Calculated E_{KYZ}[c] (eV)	Calculated F(YZ)[d] (eV)	Calculated FWHM[e] (eV)	Calculated Area[f]	Calculated R(YZ)[g] (eV)	Experimental E_{KYZ}[h] (eV)	Experimental FWHM (eV)	Experimental Area[h]
1	$(3a_1 3a_1)$	$(3a_1 2b_2)(2b_2 1b_1)$	443.00	-11.4	11.0	122	15.74	458.74(60)	18.3	1120(251)
2	$(3a_1 4a_1)$	$(2b_1 4a_1)$	456.96	-11.8	6.4	113	9.92	466.88(10)	6.4	830 (56)
3	$(3a_1 3b_2)$	$(3a_1 6a_1)(3a_1 4b_2)$	469.40	-11.1	6.4	1154	5.69	475.09(05)	6.4	1150 (17)
4	$(3a_1 2b_1)$	$(2b_2 4b_2)(2b_2 6a_1)$	474.96	-11.6	3.2	313	5.41	480.37(05)	3.2	330 (11)
5	$(4a_1 1b_1)$	$(4a_1 5a_1)$	480.18	-11.7	7.6	563	4.82	485.00(09)	7.6	1400 (20)
6	$(4a_1 4b_2)$		485.29	-11.6	2.4	285	3.18	488.47(10)	2.4	120 (13)
7	$(1b_1 1b_1)$	$(4a_1 2b_1)$	488.81	-11.3	3.2	888	2.00	490.81(06)	3.2	520 (17)
8	$(1b_1 5a_1)$	$(3b_2 2b_1)5a_1 3b_2)$	491.76	-12.1	4.0	1197	1.75	493.51(04)	4.0	1140 (19)
9	$(1b_1 6a_1)$	$(1b_1 4b_2)(3b_2 3b_2)$	495.18	-10.6	3.2	1516	1.75	496.93(04)	3.2	1010 (23)
10	$(3b_2 6a_1)$	$(5a_1 6a_1)(3b_2 4b_2)$	497.61	-11.2	1.6	985	0.72	498.33(01)	1.6	880 (19)
11	$(1b_1 2b_1)$	$(5a_1 2b_1)$	499.71	-10.8	2.4	899	1.67	501.38(09)	2.4	450 (19)
12	$(6a_1 6a_1)$	$(4b_2 6a_1)(4b_2 4b_2)$	501.46	-11.3	1.6	780	0.97	502.43(02)	1.6	260 (16)

(Continued)

Table VII-5 (Continued)

Peak Number	Principal Final State Configuration[a]	Other Final States[b]	Calculated E_{KYZ}[c] (eV)	Calculated F(YZ)[d] (eV)	Calculated FWHM[e] (eV)	Calculated Area[f]	Calculated R(YZ)[g] (eV)	Experimental E_{KYZ}[h] (eV)	Experimental FWHM (eV)	Experimental Area[h]
13	$(6a_1 2b_1)$	$(4b_2 2b_1)$	504.57	-11.2	2.4	700	0.56	505.13(07)	2.4	150(7)
14	$(2b_1 2b_1)$		507.38	-11.4	1.6	475	0.09	507.29(02)	1.6	360(8)
15								509.41(20)	3.2	110(9)
16								513.39(08)	3.2	170(8)

a. These final state configurations are responsible for the largest portion of the intensity of the peak.

b. These final state configurations contribute minor portions of peak intensity.

c. Energies obtained from equation VII-1 neglecting R(YZ).

d. Coulombic terms calculated from equation VII-2.

e. Full widths at half maximum taken from the experimental spectrum.

f. Areas calculated from equation VII-6.

g. Relaxation terms calculated as $E_{KYZ}(exp) - E_{KYZ}(calc)$.

h. The numbers in parentheses are the standard deviations obtained from the least squares fit.

Table VII-6. F(KVV) Auger Transitions of OF_2

Peak Number	Principal Final State Configuration[a]	Other Final States[b]	Calculated E_{KYZ}[c] (eV)	Calculated F(YZ)[d] (eV)	Calculated FWHM[e] (eV)	Calculated Area[f]	Calculated R(YZ)[g] (eV)	Experimental E_{KYZ}[h] (eV)	Experimental FWHM (eV)	Experimental Area[h]
1	$(2b_2 2b_2)$	$(3a_1 3a_1)(3a_1 2b_2)$	596.23	-12.6	4.8	151	6.2	602.43(23)	4.8	148(15)
2	$(2b_2 5a_1)$	$(3a_1 1a_2)(3a_1 3b_2)$	617.29	-11.8	4.8	749	2.14	619.43(07)	8.7	1891(57)
3	$(2b_2 3b_2)$	$(2b_1 1b_1)(3a_1 4b_2)$	622.59	-12.3	8.5	1096	8.35	630.94(12)	8.7	1326(93)
4	$(4a_1 1a_2)$	$(4a_1 3b_2)(4a_1 4b_2)$	634.41	-11.0	7.2	930	3.69	638.10(10)	7.2	1515(49)
5	$(5a_1 1a_2)$	$(1b_1 1a_2)(5a_1 5a_1)$ $(1b_1 3b_2)$	642.65	-11.7	4.5	1781	1.26	643.91(07)	4.5	1517(98)
6	$(1a_2 1a_2)$	$(3b_2 3b_2)(3b_2 1a_2)$	644.74	-12.7	1.6	1214	1.21	645.95(02)	1.6	846(27)
7	$(5a_1 4b_2)$	$(1b_1 4b_2)(1b_1 6a_1)$	645.35	-11.7	1.4	824	1.46	646.81(03)	1.4	511(44)
8	$(1a_2 4b_2)$	$(3b_2 4b_2)(5a_1 6a_1)$ $(1b_2 2b_1)$	647.15	-12.1	2.4	1407	0.77	647.92(03)	2.4	1079(33)

(Continued)

Table VII-7. B(KVV) Auger Transitions of BF_3

Peak Number	Principal Final State Configuration[a]	Other Final States[b]	Calculated E_{KYZ}[c] (eV)	Calculated F(YZ)[d] (eV)	Calculated FWHM[e] (eV)	Calculated Area[f]	Calculated R(YZ)[g] (eV)	Experimental E_{KYZ}[h] (eV)	Experimental FWHM (eV)	Experimental Area[h]
1	$(3a'_1 3a'_1)$		102.45	-8.7	2.8	354		120.28(30)	2.8	296(62)
2	$(3a'_1 2e')$		103.75	-9.2	2.8	1305				
3	$(3a'_1 1a''_2)$	$(3a_1 4a'_1)$	127.50	-9.5	4.0	1099	5.55	132.50(10)	2.3	1109(110)
4	$(3a'_1 3e')$	$(2e'1a''_2)$	128.94	-9.5	4.0	3109				
5	$(3a'_1 4e')$		130.90	-9.2	2.8	517	3.59	134.49(20)	2.8	1069(111)
								144.13(30)[i]	3.7	749 (93)
								147.55(30)[i]	3.7	1188 (94)
6	$(1a''_2 1a''_2)$		151.25	-8.7	1.0	428	0.51	151.76(05)	1.0	397 (52)

(Continued)

Table VII-7 (Continued)

Peak Number	Principal Final State Configuration[a]	Other Final States[b]	Calculated E_{KYZ}[c] (eV)	Calculated F(YZ)[d] (eV)	Calculated FWHM[e] (eV)	Calculated Area[f]	Calculated R(YZ)[g] (eV)	Experimental E_{KYZ}[h] (eV)	Experimental FWHM (eV)	Experimental Area[h]
7	$(1a''_2 4a'_1)$		152.31	-8.9	1.8	780	1.22	153.53(04)	1.8	2566(65)
8	$(1a''_2 3e')$		154.79	-7.5	1.8	1837	0.69	155.48(07)	1.8	1843(74)
9	$(1a''_2 4e')$		157.40	-8.2	1.8	569	-0.24	157.16(16)	1.8	603(78)
								160.11(97)[i]	3.7	178(71)

a. These final state configurations are responsible for the largest portion of the intensity of the peak.

b. These final state configurations contribute minor portions of peak intensity.

c. Energies obtained from equation VII-1 neglecting R(YZ).

d. Coulombic terms calculated from equation VII-2.

e. Full widths at half maximum taken from the experimental spectrum.

f. Areas calculated from equation VII-6.

g. Relaxation terms calculated as $E_{KYZ}(exp) - E_{KYZ}(calc)$.

h. The numbers in parentheses are the standard deviations from the least squares fit.

i. Values not predicted by theory, probably due to satellites.

Table VII-8. F(KVV) Auger Transitions of BF_3

Peak Number	Principal Final State Configuration[a]	Other Final States[b]	Calculated E_{KYZ}[c] (eV)	Calculated F(YZ)[d] (eV)	Calculated FWHM[e] (eV)	Calculated Area[f]	R(YZ)[g] (eV)	Experimental E_{KYZ}[h] (eV)	Experimental FWHM (eV)	Experimental Area[h]
1	(2e'2e')	($3a'_1 3a'_1$)($3a'_1 2e'$)	594.92	-11.2	4.0	190	1.02	595.94(13)	4.0	300(18)
								606.25(40)	14.8	960(45)
2	(2e'3e')	($2e'1a''_2$)($2e'4a'_1$)	621.24	-10.7	4.8	1228	-5.49	615.75(05)	4.8	1360(26)
3	(2e'4e')	($2e'1a'_2$)($3a'_1 2e''$)	623.74	-9.1	6.0	668	0.90	624.64(14)	6.0	1153(48)
								630.19(09)	5.7	1070(26)
4	($1a''_2 1e''$)	($1a''_2 3e''$)($1a''_2 2a'_2$) ($1a''_2 1a''_2$)	645.84	-9.2	4.0	842	-9.05	636.79(07)	4.0	850(24)
5	(1e''1e'')	($1a''_2 4e''$)($4a'_1 3e'$)	647.72	-12.7	2.7	2396	-6.27	641.45(04)	2.7	1951(57)

(Continued)

Table VII-6 (Continued)

Peak Number	Principal Final State Configuration[a]	Other Final States[b]	Calculated E_{KYZ}[c] (eV)	Calculated F(YZ)[d] (eV)	Calculated FWHM[e] (eV)	Calculated Area[f]	Calculated R(YZ)[g] (eV)	Experimental E_{KYZ}[h] (eV)	Experimental FWHM (eV)	Experimental Area[h]
9	$(4b_2 4b_2)$	$(1a_2 6a_1)(5a_2 2b_1)$	649.69	-11.7	2.0	1030	1.10	650.79(03)	2.0	749(18)
10	$(3b_2 2b_1)$	$(6a_1 6a_1)(4b_2 2b_1)$	651.46	-12.4	2.0	420	0.86	652.32(12)	2.0	135(17)
11	$(1a_2 2b_1)$	$(6a_1 2b_1)$	653.74	-10.4	2.0	318	1.80	655.54(10)	2.0	208(27)
12	$(2b_1 2b_1)$		655.82	-12.8	2.0	78	0.80	656.62(22)	2.0	72(28)

a. These final state configurations are responsible for the largest portion of the intensity of the peak.

b. These final state configurations contribute minor portions of peak intensity.

c. Energies obtained from equation VII-1 neglecting R(YZ).

d. Coulombic terms calculated from equation VII-2.

e. Full widths at half maximum taken from the experimental spectrum.

f. Areas calculated from equation VII-6.

g. Relaxation terms calculated as $E_{KYZ}(exp) - E_{KYZ}(calc)$.

h. The numbers in parentheses are the standard deviations obtained from the least squares fit.

Table VII-8 (Continued)

Peak Number	Principal Final State Configuration[a]	Other Final States[b]	Calculated E_{KYZ}[c] (eV)	Calculated F(YZ)[d] (eV)	Calculated FWHM[e] (eV)	Calculated Area[f]	Calculated R(YZ)[g] (eV)	Experimental E_{KYZ}[h] (eV)	Experimental FWHM (eV)	Experimental Area[h]
6	(3e'1e")	(3e'4e')(3e'3e')	649.38	-10.5	2.7	2938	-5.94	643.44(04)	2.7	2280(57)
7	(1e"4e')		651.08	-10.8	3.2	1438	-4.53	646.55(26)	3.2	190(25)
8	(4e'4e")		653.00	-8.4	3.3	294	-2.41	650.59(08)	3.3	440(18)

a. These final state configurations are responsible for the largest portion of the intensity of the peak.

b. These final state configurations contribute minor portions of peak intensity.

c. Energies obtained from equation VII-1 neglecting R(YZ).

d. Coulombic terms calculated from equation VII-2.

e. Full widths at half maximum taken from the experimental spectrum.

f. Areas calculated from equation VII-6.

g. Relaxation terms calculated as $E_{KYZ}(exp) - E_{KYZ}(calc)$.

h. The numbers in parentheses are the standard deviations obtained from the least squares fit.

listed in the tables were obtained from the Auger parameter as described in Section C, and they are equal to the difference between the experimental and calculated Auger energies listed in Tables VII-5 to VII-8. In contrast to the inner shell Auger spectra and assuming that the coulombic interaction terms used in our analysis are correctly estimated, the relaxation contribution for valence Auger spectra is different for each line. The calculated intensities, given in the tables as areas of the peaks, were obtained from equation VII-6 using the coefficients from Tables VII-9 and VII-10 and the transition probabilities from Table VII-2. The coefficients listed in Tables VII-9 and VII-10 for OF_2 and BF_3 molecules respectively were obtained from two different CNDO/2 calculations performed on both molecules. The values referring to Oxygen and Boron were obtained from calculations performed on molecular ions with a nuclear charge of Z+1 for Oxygen and Boron atoms. This procedure was followed to take into account the alteration of the population in response to the introduction of a core hole in the initial state of the Auger process.[106] The coefficients relative to Fluorine in both compounds were obtained from calculations performed on the neutral molecules. It was observed that

Table VII-9. Atomic Populations from CNDO/2 for OF_2 Used for the Intensity Calculations

		$3a_1$	$2b_2$	$4a_1$	$1b_1$	$5a_1$	$3b_2$	$1a_2$	$4b_2$	$6a_1$	$2b_1$
O	2s	0.5111		0.4283							
	$2p_x$		0.0536				0.3296		0.2690		
	$2p_y$			0.0321		0.3095				0.3982	
	$2p_z$				0.5473						0.4527
F[b]	2s	0.3388	0.4698	0.1388			0.0105				
	$2p_x$			0.0286		0.2947			0.3902		
	$2p_y$			0.0272		0.0947	0.3689		0.0320	0.3146	
	$2p_z$				0.3077			0.5000			0.1923
F	2s	0.3388	0.4698	0.1388			0.0105				
	$2p_x$			0.0286		0.2947			0.3902		
	$2p_y$			0.0272		0.0947	0.3689		0.0320	0.3146	
	$2p_z$				0.3077			0.5000			0.1923

a. The populations used for O(KVV) spectrum intensity calculations are obtained from CNDO/2 calculations performed on the molecular ion with a nuclear charge of Z+1 for Oxygen atom.

b. The populations used for F(KVV) spectrum intensity calculations are obtained from CNDO/2 calculations performed on the neutral molecule.

Table VII-10. Atomic Populations from CNDO/2 Calculations in BF_3 Used for the Intensity Calculations

		$3a'_1$	2e'	2e'	$1a''_2$	3e'	3e'	$4a'_1$	$1a'_2$	1e"	1e"	4e'	4e'
B[a]	2s	0.2457			0.2704								
	$2p_x$			0.1580		0.1715							
	$2p_y$		0.1580				0.1715						
	$2p_z$							0.2329					
F[b]	2s	0.2639		0.5526									
	$2p_x$					0.2355		0.2509					0.3327
	$2p_y$						0.3171		0.3323			0.3168	
	$2p_z$				0.2631						0.6668		
F	2s	0.2644	0.4141	0.1380		0.0103	0.0310	0.0301					
	$2p_x$					0.0909	0.2060	0.0627	0.2500				0.3205
	$2p_y$					0.2056	0.0497	0.1889	0.0834			0.3285	
	$2p_z$				0.2632					0.5003	0.1664		

(Continued)

Table VII-10 (Continued)

		$3a'_1$	2e'	2e'	$1a''_2$	3e'	3e'	$4a'_1$	$1a'_2$	1e"	1e"	4e'	4e'
F	2s	0.2644	0.4143	0.1380		0.0103	0.0310	0.0301					
	$2p_x$					0.0903	0.2060	0.0627	0.2500				0.3205
	$2p_y$					0.2056	0.0497	0.1889	0.0834			0.3285	
	$2p_z$				0.2632					0.4997	0.1669		

a. The populations used for B(KVV) spectrum intensity calculations are obtained from CNDO/2 calculations performed on the molecular ion with a nuclear charge of Z+1 for Boron atom.

b. The populations used for F(KVV) spectrum intensity calculations are obtained from CNDO/2 calculations performed on neutral molecule.

in the case of Oxygen and Boron spectra, the coefficients obtained from CNDO calculations performed with a nuclear charge of Z+1 for the central atom produced better agreement between experimental and calculated intensities than the coefficients obtained from the calculations on the neutral molecules. For the Fluorine spectra of both compounds, the coefficients from the neutral molecule calculations gave better results.

Tables VII-5 and VII-6, together with Figures VII-1 and VII-2 referring to O(KVV) and F(KVV) in OF_2 show a general agreement between the calculated and the experimental spectra. However, at the low energy side of both spectra, the calculations underestimate the intensity of the peaks. The experimental Auger energy scales for the Oxygen KVV and Fluorine KVV differ approximately by 150 eV which is the difference between the O 1s and F 1s binding energies in agreement with the fact that the final states are the same in both spectra. The experimental spectrum of O(KVV) in OF_2 is very much different from the one obtained for water vapor,[107] which exhibited some similarity with the normal atom-like KLL Auger spectrum of the isoelectronic Ne species[108] shown for comparison in Figure VII-5. The resemblance was attributed to the domination of Oxygen character in the molecular orbitals

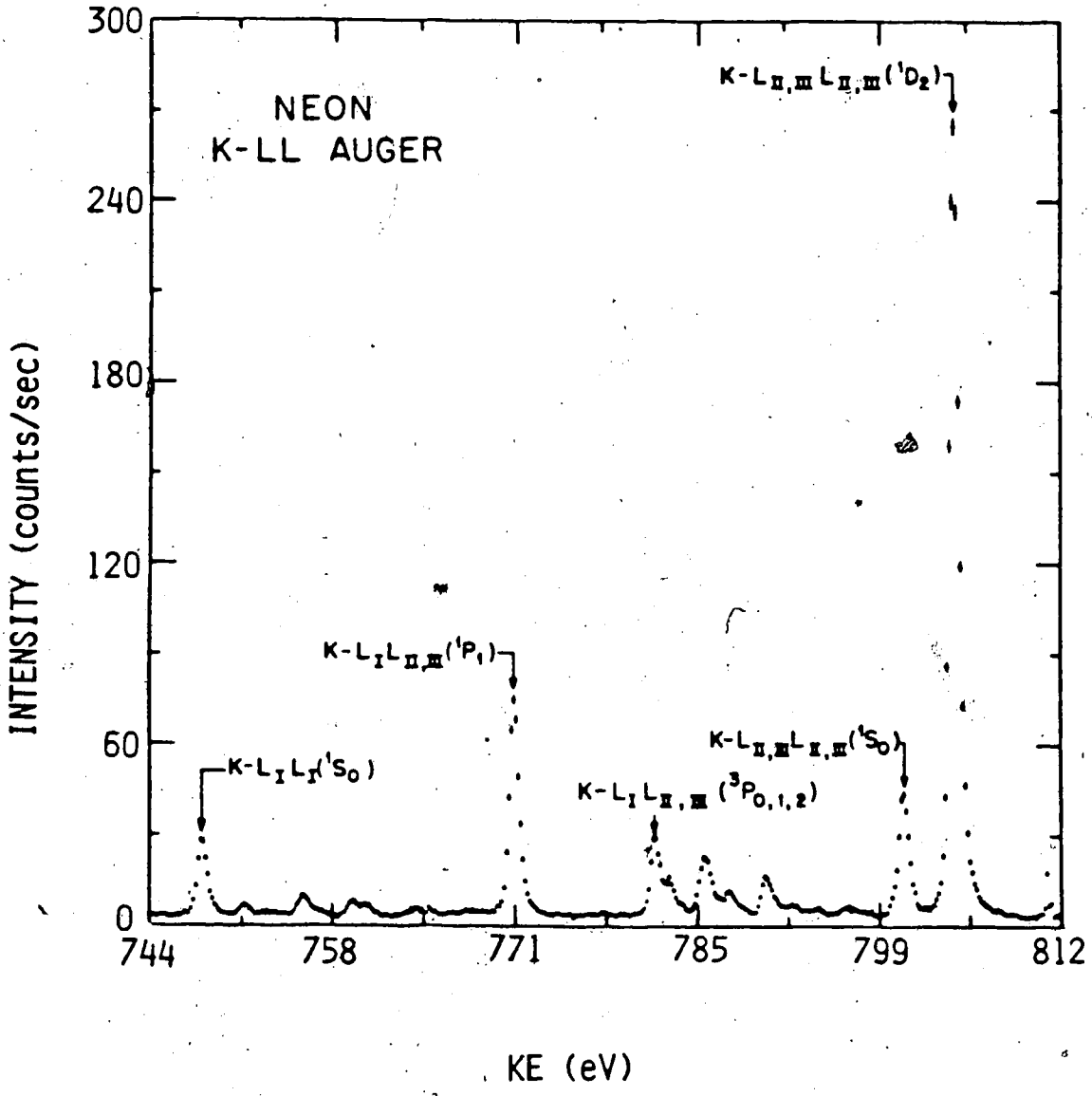

108

Figure VII-5. KLL Auger spectrum of Neon.

of water. In OF_2 the large amount of Fluorine character in the molecular orbitals (Table VII-9) alters the O(KVV) spectrum of this molecule so that it is quite different from that of the isoelectronic relative of the central atom, Neon. The experimental spectrum of F(KVV) in OF_2 (Figure VII-2) shows some similarity with the atomic KLL spectrum of Ne, however the contribution of the Oxygen orbitals to the molecular orbitals is also large enough to alter the atomic shape of the spectrum.

The experimental O(KVV) (Figure VII-1) spectrum shows two structures on the high energy side, which are not predicted by the theory. These structures can be due to autoionization or formation of excited state showing as high energy satellite.[105] The autoionization process is usually verified by comparing the electron excited spectrum with an X-ray excited spectrum. For this purpose a Mg $K\alpha_{1,2}$ excited O(KVV) spectrum was also obtained, however the intensity was so low that it was not possible to verify the presence of these high energy peaks. In the electron excited F(KVV) spectrum of the same compound, there is no evidence of high energy satellite peaks. For atoms which are surrounded, in molecules, by highly electronegative species it has been postulated the presence of a "potential barrier"[109] to explain certain X-

ray absorbtion features. This potential barrier arises from the following situation: an electron, when it is within the cage of electronegative atoms and near the electropositive atom, will experience a net attraction due to the partially screened nucleus of the central atom; this region of space is defined as the "inner well" potential. An electron will also experience a net attraction when it is at larger distance and sees only the Coulomb attraction by the molecular ion; this region of space is defined as the "outer-well" potential. At intermediate distances the potential may not be attractive and may constitute a "barrier" due to the electronegative atoms located there. If the barrier is high (10-20 eV), quasistationary states above the K shell edge can exist. Whether or not transitions from an initial state to these states can occur depends also upon the relative symmetry of initial and excited states, i.e. these states must have opposite parity for a non-vanishing dipole transition. It is possible, then, that in a molecule like OF_2 the potential barrier created by the two Fluorine atoms gives rise to excited states that may be reached by the O 1s electron and not by the F 1s electron, explaining the absence of high energy satellites in the F(KVV) spectrum.

The energies of the Auger lines, estimated excluding R(YZ), are generally smaller than the experimental values. The differences are an estimate of the relaxation contribution. In the O(KVV) spectrum (Table VII-5) the relaxation seems to decrease with increasing energy of the Auger electron. However, because orbital energies from CNDO calculations for the high valence ionization energies which were not experimentally accessible were used, the relaxation contribution extracted for transitions involving these innermost valence orbitals are not reliable. As it is shown in Table VII-3 from a comparison of the available experimental ionization energies with the CNDO values, the latter are generally larger than the experimental energies. For O(KVV) and F(KVV) spectra of OF_2, the intensities of the peaks at high energy are overestimated by the calculations, whereas the low energy peak intensities are underestimated. The discrepancies may be due to the use of inadequate values of the atomic matrix elements (Walters and Bhalla[95] obtained these matrix elements without allowing for the relaxation of the electrons and using neutral-atom ground state orbitals) or to the inadequacy of the atomic orbital populations from CNDO calculation.

In the O(KVV) spectrum (Figure VII-1 and Table VII-5) peak 11 at 501.38 eV has the main contribution from the transition to the final state ($1b_1 2b_1$), peak 12 at 502.43 eV is due to a combination of transitions to the final states ($6a_1 6a_1$), ($4b_2 6a_1$) and ($4b_2 4b_2$). Peak 13 at 505.13 eV is due to a combination of transitions to the final states ($6a_1 2b_1$), ($4b_2 2b_1$). All the orbitals involved in these transitions, as we can see from the atomic populations in Table VII-9, have a large Oxygen 2p character. The peaks at lower enegies are due to transitions involving mostly the molecular orbitals $3a_1$ and $4a_1$, which have Oxygen 2s character.

In the F(KVV) spectrum (Figure VII-2 and Table VII-6) peak 6 at 645.95 eV gets most of the intensity from the transition to the $1a_2 1a_2$ final state and peak 7 at 646.81 eV is due to a combination of transitions to $5a_1 4b_2$, $1b_1 4b_2$, $1b_1 6a_1$ final states which involve orbitals with large Fluorine 2p character whereas the peaks at lower energy are due to transition involving $2b_2$, $4a_1$, $3a_1$ orbitals which have large Fluorine 2s character. Others have suggested[106] that the screening charge is mainly s like, thus the screening increases the ss and sp Auger contributions relative to the pp. As it was previously noted, the matrix elements[95] were obtained without

considering relaxation of the electrons so they do not account for the increased ss or sp contributions. Another possibility for the observed discrepancies between calculated and experimental intensities could arise from the background contributions which are difficult to account for properly.

The experimental spectra of B(KVV) and F(KVV) in BF_3 compared to the simulated spectra are shown in Figures VII-3 and VII-4 respectively. The parameters of the spectra are listed in Table VII-7 and VII-8. The energy scales of B(KVV) and F(KVV) differ by ~490 eV which is the difference between the B 1s and F 1s binding energies.

The experimental B(KVV) spectrum has a simple structure in agreement with little Boron orbital character for the molecular orbitals (Table VII-10). In the calculated spectrum a quite strong peak at 103 eV is predicted by the theory which is not seen in the experimental spectrum. The structure present at ~132-134 eV in the experimental spectrum is less pronounced than in the calculated spectrum where it is predicted to occur at ~126-129 eV. The group of lines at 151-157 eV in the experimental spectrum is predicted by the theory, however there are discrepancies in the relative intensities. In the experimental spectrum at 160.11 eV there is a weak

peak not given by the theory, it may be due to autoionization or formation of excited states. In contrast to the O(KVV) case, here the peaks at higher energy are underestimated by the calculations. Peak 7 at 153.53 eV and peak 8 at 155.48 eV have been attributed to Auger transitions to the $1a''_2 4a'_1$ and $1a''_2 3e'$ final states respectively. From the atomic orbital populations given in Table VII-10 it is seen that the major contributions from Boron to these molecular orbitals come from s and p atomic orbitals, therefore the transition rates for the corresponding Auger lines must be proportional to the sp matrix elements.

The similarity of the experimental F(KVV) spectrum (Figure VII-4) with the atom-like Ne KLL spectrum (Figure VII-5) in this case is due to the large Fluorine orbital contribution to the molecular orbitals in BF_3 (Table VII-10). The calculated and experimental F(KVV) Auger spectra illustrated in Figure VII-4 show the same overall shape. However, the calculated peaks, values for which are given in Table VII-8, occur at higher energies than the experimental values. Considering that no relaxation has been included, which would further increase the energies, the coulombic interaction term must have been substantially underestimated. Comparing the most intense

and narrow peaks in the experimental or calculated spectra, it appears that the coulombic term F(YZ) should be at least 3-9 eV larger (more negative) if a relaxation zero is assumed. If the relaxation is non-zero, then the coulombic term must be even larger. Fluorine is much more electronegative than Boron and its contribution to the molecular orbitals, as expressed by the atomic coefficients, is larger than the contribution from Boron. Considering that Fluorine in BF_3 is more like F^-, calculations of the coulombic term have also been attempted using negative ion one center integrals[111] instead of the neutral atomic integrals. However, because the ion integrals were slightly smaller (<10%) than the atomic ones, the coulombic terms derived from these integrals were smaller than those obtained from atomic integrals yielding larger discrepancies. It is possible, then, that the atomic orbital coefficients representing local populations were not adequate. In the experimental spectrum of F(KVV), there are two bands on the low energy side at around 606 eV and 630 eV which are not predicted by the theory. These two features could be attributed to shake-off satellites associated with the strong peaks at 615.75 eV and at 641.45 eV respectively.

In the same spectrum, the peaks at higher energy, between 641 eV and 650 eV are overestimated by the calculations. From the analysis of the spectrum followed that peak 5 at 641.45 eV is due mainly to a combination of transitions to $le"le"$, $la"_2 4e'$, $4a'_1 3e'$ final states and peak 6 at 643.44 eV is due to a combination of transitions to $3e'le"$, $3e'4e'$, $3e'3e'$ final states. Peak 7 at 646.55 eV is due to the transition to the $le"4e'$ final state.

As shown from the populations listed in Table VII-10 all the orbitals involved in these Auger transitions have a strong Fluorine 2p character, therefore, the Auger transition rates are best expressed by the pp Auger matrix elements. The peaks at lower energies which are due mainly to transitions to $2e'2e'$, $2e'3e'$, $2e'4e'$, $3a'_1 3a'_1$ final states, are underestimated. From Table VII-10 it is shown that the orbitals involved in these final states have either both Fluorine 2s or one has Fluorine 2s and the other has Fluorine 2p character, so the Auger transition rates are dependent on the ss and sp matrix elements. Because of the s screening effect,[106] which has been mentioned above, the matrix elements may exaggerate the pp/ss and pp/sp ratios, resulting in the observed discrepancies.

The highest energy normal Auger line in a valence Auger spectrum is of particular interest because from this value one can obtain the minimum energy for double electron removal, $E_{II}(min)$, from the relationship:[105]

$$E_{II}(min) = E(K) - E_A \qquad \text{VII-12}$$

where E(K) is the binding energy of the K shell and E_A is the measured Auger energy for the highest energy normal Auger line. The value obtained in this way is the vertical ionization potential which is the energy required for the formation of an ion in a vibrational state different from the ground vibrational state. Taking the onset of the Auger line, the adiabatic ionization potential is obtained. This corresponds to the energy required for the formation of a molecular ion in its lowest vibrational state. As it was noted before, the probability for reaching a given final Auger state will depend on whether the orbitals involved in the transition are strongly associated with the atom having the K vacancy. It is expected, therefore, that different values for the energy of the doubly charged molecular ions are obtained from the Auger spectra of two different elements in the molecule, the smallest value represents $E_{II}(min)$.

Table VII-11 lists the E_{II}(min) values obtained from O(KVV) and F(KVV) in OF_2 and B(KVV) and F(KVV) in BF_3. To obtain the adiabatic ionization potentials, the onset of the peak was taken as the intersection of the tangent to the experimental peak with the baseline of the spectrum.

E. Conclusions

The analysis of valence Auger spectra showed that the general shape of the spectra can be reproduced using a molecular orbital treatment. In some cases, for example O(KVV) and B(KVV) Auger spectra, improved agreement between experimental and calculated intensities resulted from the use of atomic populations calculated for a nuclear charge of Z+1 in the atom with the core hole, thus taking into account the alterations of the population in response to the introduction of a core hole in the initial state of the Auger process.[106] For Fluorine in both compounds, it seemed that this effect was not important and the populations from the neutral molecule gave better results, at least insofar as intensities were concerned. Perhaps the Auger process is faster in the Fluorine atom than the eventual rearrangement of the electronic charge. The reasons for this peculiarity are not clear, and more studies on Fluorine containing molecules should be done.

Table VII-11. Minimum Energy Required for Producing Doubly Charged Molecular Ions, as Obtained from the Auger Spectra of Both Elements in OF_2 and BF_3

Ion	$E(min)_{vert}$[a] (eV)	$E(min)_{adiab}$[b] (eV)
$(OF_2)^{2+}$	38.03(O), 38.51(F)	36.22(O), 36.70(F)
$(BF_3)^{2+}$	45.58(B), 44.18 (F)	43.78(B), 42.38(F)

a. Values obtained from the position of the highest energy normal Auger peak.

b. Values obtained from the onset of the highest energy normal Auger peak.

The relaxation terms for O(KVV) and F(KVV) in OF_2 are small and of comparable magnitude, especially for the peaks at high energy for which experimental ionization energies were used. This result suggests that the main effect to the relaxation is due to the final state which is the same in both spectra. A different result arises for B(KVV) and F(KVV) in BF_3. F(KVV), even considering the all approximations used to calculate the energies of each term, appears to have a significantly larger coulombic term (negative) than that which has been estimated, and a very small relaxation term.

CHAPTER VIII

CONCLUSIONS

The original goal of the work described in this thesis was to elucidate chemical effects on molecular Auger spectra. It has been shown that the absolute energies of the Auger spectra depend mostly on the so-called "final state effect" which is associated with the relaxation process suffered by the molecule as the result of the removal of electrons. This effect also contributes significantly to photoelectron shifts with, however, reduced magnitude.

The inner shell Auger spectra of Ge and Sn exhibited an energy shift which was constant through all the diagram lines while maintaining a general atomic shape with essentially unchanged intensity ratios. Therefore atomic theory can be used to adequately describe such spectra both in terms of the relative energies and the intensities within a group of Auger lines. The theoretical estimate of the extraatomic relaxation energy is close to the experimental value for a metal, but it is larger than the experimental relaxation for molecular systems. A

different approach to the estimation of this "extra atomic" contribution is required which takes into account the chemical environment of the atom of interest.

In the case of the valence Auger spectra, the energies as well as the intensities were very dependent on the molecular environment, and a theoretical estimate of both was accomplished using a molecular orbital model with semiempirical calculations. This approach seemed to be reasonably successful allowing the reproduction of the main features of these spectra. However, relative intensities of some peaks were not well predicted, possibly because of the inadequacies of semiempirical (CNDO) atomic coefficients. The relaxation term obtained from a comparison of experimental and calculated spectra was, in general, lower than that found for the inner shell Auger spectra. The reason for this is attributable to the nature of the electrons involved in the final state of the Auger process. They are valence electrons which belong to the outermost orbitals in the molecule and therefore there can not be outer shell and extraatomic relaxation contributions to the relaxation term. The energies of the doubly charged ions were also obtained from the valence Auger spectra.

Using chemical "tuning" of the inner shell ionization energy, required to provide the initial vacancy of the Auger process, the effect of the excitation energy near the threshold photoionization energy on the inner Auger spectra was studied for Germanium. Post Collision Interaction effects and spectator satellite Auger peaks were observed. A dependence of the PCI effects on the final state of the Auger decay, not previously noticed, was also observed. Also in this study, extraatomic relaxation effects seemed to play an important role, yielding deviations from the purely atomic post-collision behavior.

REFERENCES

1. A. Einstein, Ann. Physik, **17**, 132 (1905).
2. P. Auger, Compt. Rend., **177**, 169 (1923).
3. K. Siegbahn, C. Nordling, E. Sokolowski, "Chemical Shifts of Photo and Auger Electron Lines" in Proc. Rehovoth Conf. on Nuclear Structure 1957, ed. by H.J. Lipkin, North-Holland, Amsterdam (1958), p. 291.
4. D.W. Turner, M.L. Al-Jobury, J. Chem. Phys., **37**, 3007 (1962).
5. J.W. Rabelais, "Principles of Ultraviolet Spectroscopy", Wiley-Interscience, New York (1977), p. 50.
6. S.T. Manson, J.W. Cooper, Phys. Rev., **165**, 126 (1968).
7. See for example:
   a. T.A. Carlson, "Photoelectron and Auger Spectroscopy", Plenum Press, New York (1975).
   b. K.D. Sevier, "Low Energy Electron Spectrometry", Wiley-Interscience (1972).
8. K. Siegbahn et al. "ESCA Applied to Free Molecules", North-Holland (1969).

9. T.A. Carlson, Phys. Rev., **156**, 142 (1967).

10. M.O. Krause, T.A. Carlson, Phys. Rev., **158**, 18 (1967).

11. R.L. Martin, D.A. Shirley, J. Chem. Phys., **64**, 3685 (1976).

12. W. Melhorn, Unpublished lecture notes: "Electron Spectroscopy of Auger and Autoionizing States: Experiment and Theory". From Lectures held during the summer of 1978 at the Institute of Physics, University of Aarhus, Denmark.

13. D. Coster, R.de L. Kronig, Physica, **2**, 13 (1935).

14. W. Bambynek, B. Crasemann, R.W. Fink, H.U. Freund, H. Mark, C.D. Swift, R.E. Price, P.V. Rao, Rev. Mod. Phys., **44**, 716 (1972).

15. G. Wentzel, Z. Physik, **43**, 524 (1927).

16. E.U. Condon, G.H. Shortley, "Theory of Atomic Spectra", Cambridge University Press (1959), p. 174.

17. W.N. Asaad, E.H.S. Burhop, Proc. Phys. Soc., **72**, 369 (1958).

18. J.C. Slater, "Quantum Theory of Atomic Structure, Vol. I", McGraw Hill, New York (1960).

19. H.A. Bethe, R. Jackiw, "Intermediate Quantum Mechanics", W.A. Benjamin Inc. (1968), p. 135.

20. K. Faegri Jr., O. Keski-Rahkonen, J. Electr. Spectr. Relat. Phenom., **11**, 275 (1977).

21. E. Källne, T. Aberg, X-ray Spectr., **4**, 26 (1975).

22. M.O. Krause, J.G. Ferreira, J. Phys., B**8**, 2077 (1975).

23. O. Keski-Rahkonen, M.O. Krause, J, Electr. Spectr. Relat. Phenom., **9**, 391 (1976).

24. T.D. Thomas, R.W. Shaw Jr., J. Electr. Spectr. Relat. Phenom., **5**, 1081 (1974).

25. G. Johannson, J. Hedman, A. Berndtsson, M. Klasson, R. Nilsson, J. Electr. Spectr. Relat. Phenom., **2**, 295 (1973).

26. The lineshape programme is a locally established version of the programme by C.S. Fadley and C. Lederer (Lawrence Berkeley Laboratory) which is described in C.S. Fadley Thesis (University of California 1970) UCRL 19535.

27. D.B. Adams, D.T. Clark, Theor. Chim. Acta, **31**, 171 (1973).

28. T. Koopmans, Physica, **1**, 104 (1934).

29. L. Hedin, A. Johansson, J. Phys., B**2**, 1336 (1969).

30. J.M. Hollander, W.L. Jolly, Acc. Chem. Res., **3**, 193 (1970).

31. W.L. Jolly, D.N. Hendrickson, J. Am. Chem. Soc., **92**, 1863 (1970)

32. D.W. Davis, D.A. Shirley, J. Electr. Spectr. Relat. Phenom., **3**, 137 (1974).

33. H. Basch, Chem. Phys. Lett., **5**, 337 (1970).

34. M.E. Schwartz, Chem. Phys. Lett., **6**, 631 (1970).

35. J.A. Pople, D.L. Beveridge, "Approximate Molecular Orbital Theories", McGraw Hill, New York (1970).

36. G. Howart, O. Goscinski, Chem. Phys. Lett., **30**, 87 (1975).

37. D.B. Adams, J. Electr. Spectr. Relat. Phenom., **10**, 247 (1977).

38. T.D. Thomas, J. Electr. Spectr. Relat. Phenom., **20**, 117 (1980).

39. D.A. Shirley, Chem. Phys. Lett., **16**, 220 (1972).

40. C.D. Wagner, P. Biloen, Surf. Science, **35**, 82 (1973).

41. N.F. Mott, R.W. Gurney, "Electronic Processes in Ionic Crystals", Clarendon, Oxford (1948).

42. C.D. Wagner, Faraday Discuss. Chem. Soc., **60**, 291 (1975).

43. E.J. Aitken, M.K. Bahl, K.D. Bomben, J.K. Gimzewski, G.S. Nolan, T.D. Thomas, J. Am. Chem. Soc., **102**, 4873 (1980).

44. T.D. Thomas, J. Am. Chem. Soc., **92**, 4184 (1970).

45. K. Siegbahn, D. Hammond, H. Fellner-Feldegg, E.F. Barnett, Science, **176**, 245 (1972).

46. P. Kelfve, B. Blomster, H. Siegbahn, K. Siegbahn, Phys. Scripta, **21**, 75 (1980).

47. H. Siegbahn, R. Medeiros, O. Goscinski, J. Electr. Spectr. Relat. Phenom., **8**, 149 (1976).

48. S.R. Smith, T.D. Thomas, J. Am. Chem. Soc., **100**, 5459 (1978).

49. L.I. Yin, I. Addler, T. Tsang, M.H. Chen, D.A. Ringers, B. Crasemann, Phys. Rev., A**9**, 1070 (1974).; A**17**, 1556 (1978).

50. D.A. Shirley, Chem. Phys. Lett., **17**, 312 (1972).

51. N.D. Lang, A.R. Williams, Phys. Rev., B**20**, 1369 (1979).

52. J.C.Slater, "Quantum Theory of Atomic Structure, Vol. II", McGraw Hill, New York (1960), pp. 286-294.

53. J.B. Mann, "Atomic Structure Calculations. I, Hartree-Fock Energy Results for the Elements Hydrogen to Lawrencium", Los Alamos Scientific Laboratory Report No. LASL-3690 (1967), unpublished

54. K.D. Sevier, At. Data and Nucl. Data Tables, **24**, 323 (1979).

55. W.N. Asaad, Nucl. Phys., **44**, 399 (1963).

56. W.N. Asaad, Nucl. Phys., **66**, 494 (1965).

57. K.M. Huang, M. Aoyagi, M.M. Chen, B. Crasemann, H. Mark, At. Data Nucl. Data Tables, **18**, 243 (1976).

58. D.A. Shirley, Phys. Rev., A**7**, 1520 (1973).

59. a. S.P. Kowalczyk, R.A. Pollak, F.R. McFeely, L. Ley, D.A. Shirley, Phys. Rev., B**8**, 2387 (1973);
b. Phys. Rev., B**8**, 2392 (1973).

60. A. Rosen, I. Lindgren, Phys. Rev., **176**, 114 (1968).

61. S.P. Kowalczyk, L. Ley, F.R. McFeely, R.A. Pollak, D.A. Shirley, Phys. Rev., B**9**, 381 (1974).

62. E. Antonides, E.C. Janse, G.A. Sawatzky, Phys. Rev., B**15**, 1669 (1977).

63. H. Aksela, S. Aksela, University of Oulu, Finland, Rep. No. 41, ISBN 951-42-0164-7 (1974), unpublished.

64. E.J. McGuire, Sandia Research Laboratories Research Report No. SC-RR710835 , unpublished.

65. J.A. Bearden, Rev. Mod. Phys., **39**, 78 (1967).

66. M.O. Krause, M.L. Vestal, W.H. Johnston, T.A. Carlson, Phys. Rev., **133**, A385 (1965).

67. T.A. Carlson, M.O. Krause, Phys. Rev., **137**, A1655 (1965).

68. J.F. McGilp, P. Weightman, J. Phys., C**9**, 3541 (1976).

69. C. Frose-Fisher, Comp. Phys. Comm., **4**, 107 (1972).

70. T.M. Miller, B. Bederson, in "Advances in Atomic and Molecular Physics, eds. D.R. Bates, B. Bederson, Academic Press, **13**, 1 (1977).

71. O.E. Frivold, O. Hassel, E. Hetland, Physik. Z., **40**, 29 (1939).

72. J.C. Fuggle in "Electron Spectroscopy", eds. Brundle, Baker, Academic Press, **4**, 85 (1982).

73. H. Aksela, S. Aksela, J. Phys., B**7**, 1262 (1974).

74. R. Kumpula, J. Väyrynen, T. Rantala, S. Aksela, J. Phys. C., **12**, L809 (1979).

75. J. Väyrynen, S. Aksela, M. Kellokumpu, H. Aksela, Phys. Rev., A**22**, 1610 (1980).

76. Written by Dr. C. Pua of this laboratory.

77. M.K. Bahl, R.L. Watson, K.J. Irgolic, Phys. Rev. Lett., **42**, 162 (1979).

78. A. Niehaus, J. Phys., B**10**, 1845 (1977).

79. R. Morgenstern, A. Niehaus, U. Thielmann, J. Phys., B**10**, 1039 (1977).

80. A.J. Smith, P.J. Hicks, F.H. Read, S. Cvejanovic, G.C.M. King, J. Comer, J.M. Sharp, J. Phys., B**7**, L496 (1974).

81. V. Schmidt, N. Sandner, W. Mehlhorn, M.Y. Adam, F. Wuilleumier, Phys. Rev. Lett., **38**, 63 (1977).

82. R.B. Barker, H.W. Berry, Phys. Rev., **151**, 14 (1966).

83. G.S. Brown, M.H. Chen, B. Crasemann, G.E. Ice, Phys. Rev. Lett., **45**, 1937 (1980).

84. P. Eisenberger, P.M. Platzman, H. Winick, Phys. Rev. Lett., **45**, 1937 (1980).

85. M.O. Krause, J.H. Oliver, J. Phys. Chem. Ref. Data, **8**, 329 (1979).

86. M.S. Chen, B. Crasemann, L.J. Yin, T. Tsang, I. Adler, Phys. Rev., A**13**, 1435 (1976).

87. M. Pessa, A. Vuoristo, M. Vulli, S. Aksela, J. Väyrynen, T. Rantala, H. Aksela, Phys. Rev., B**20**, 3115 (1979).

88. S. Hagmann, G. Hermann, W. Melhorn, Z. Phys., **266**, 189 (1974).

89. S.V. El Ibyari, W.W. Asaad, E.J. McGuire, Phys. Rev., A**5**, 1048 (1972).

90. J. Väyrynen, R.N. Sodhi, R.G. Cavell, J. Chem. Phys., **79**, 5329 (1983).

91. H. Agren, J. Chem. Phys., **75**, 1267 (1981).

92. D.E. Ramaker, J.S. Murday, N.H. Turner, G. Moore, M.G. Lagally, J. Huston, Phys. Rev., B**19**, 5375 (1979).

93. N. Mataga, K. Nishimoto, Z. Phys. Chem. (N.F.), **13**, 140 (1957).

94. D.E. Ramaker, Phys. Rev., B**21**, 4608 (1980).

95. D.L. Walters, C.P. Bhalla, Phys. Rev., A**4**, 2164 (1971).

96. F.L. Hutson, D.E. Ramaker, B.I. Dunlap, J.D. Ganjei, J.S. Murday, J. Chem. Phys., **76**, 2181 (1982).

97. J.A.D. Matthews, W. Kominos, Surf. Sci., **53**, 716 (1975).

98. S.D. Bader, L. Richter, M.B. Brodsky, Solid State Commun., **37**, 729 (1981).

99. D.R. Jennison, Phys. Rev. Lett., **40**, 807 (1978).

100. A.B. Cornford, D.C. Frost, F.G. Herring, C.A. McDowell, J. Chem. Phys., **55**, 2820 (1971).

101. A.A. Bakke, H.-W. Chen, W.L. Jolly, J. Elect. Spectr. Relat. Phenom., **20**, 333 (1980)

102. T.E.H. Walker, J.A. Horsley, Molec. Phys., **21**, 939 (1971).

103. D.A. Allison, G. Johansson, C.J. Allan, U. Gelins, H. Siegbahn, J. Allison, K. Siegbahn, J. Electr. Spectr. Relat. Phenom., **1**, 269 (1972).

104. D.W. Davies, Chem. Phys. Lett., **2**, 173 (1968).

105. W.E. Moddeman, T.A. Carlson, M.O. Krause, B.P. Pullen, W.E. Bull, G.K. Schweitzer, J. Chem. Phys., **55**, 2317 (1971).

106. D.E. Ramaker, Phys. Rev., B**25**, 7341 (1982).

107. H. Siegbahm, L. Asplund, P. Kelfve, Chem. Phys. Lett., 35, 330 (1975).

108. W.E. Moddeman, "Auger Spectroscopy of Simple Gaseous Molecules", Ph.D. Thesis, Oak Ridge National Laboratory and University of Tennessee, ORNL-TM-3012 (1970).

109. J.L. Dehmer, J. Chem. Phys.; 56, 4496 (1972).

110. R.R. Rye, J. Houston, J. Chem. Phys., 78, 4321 (1983).

111. C. Fisk, S. Fraga, Can. J. Phys., 46, 1140 (1968).